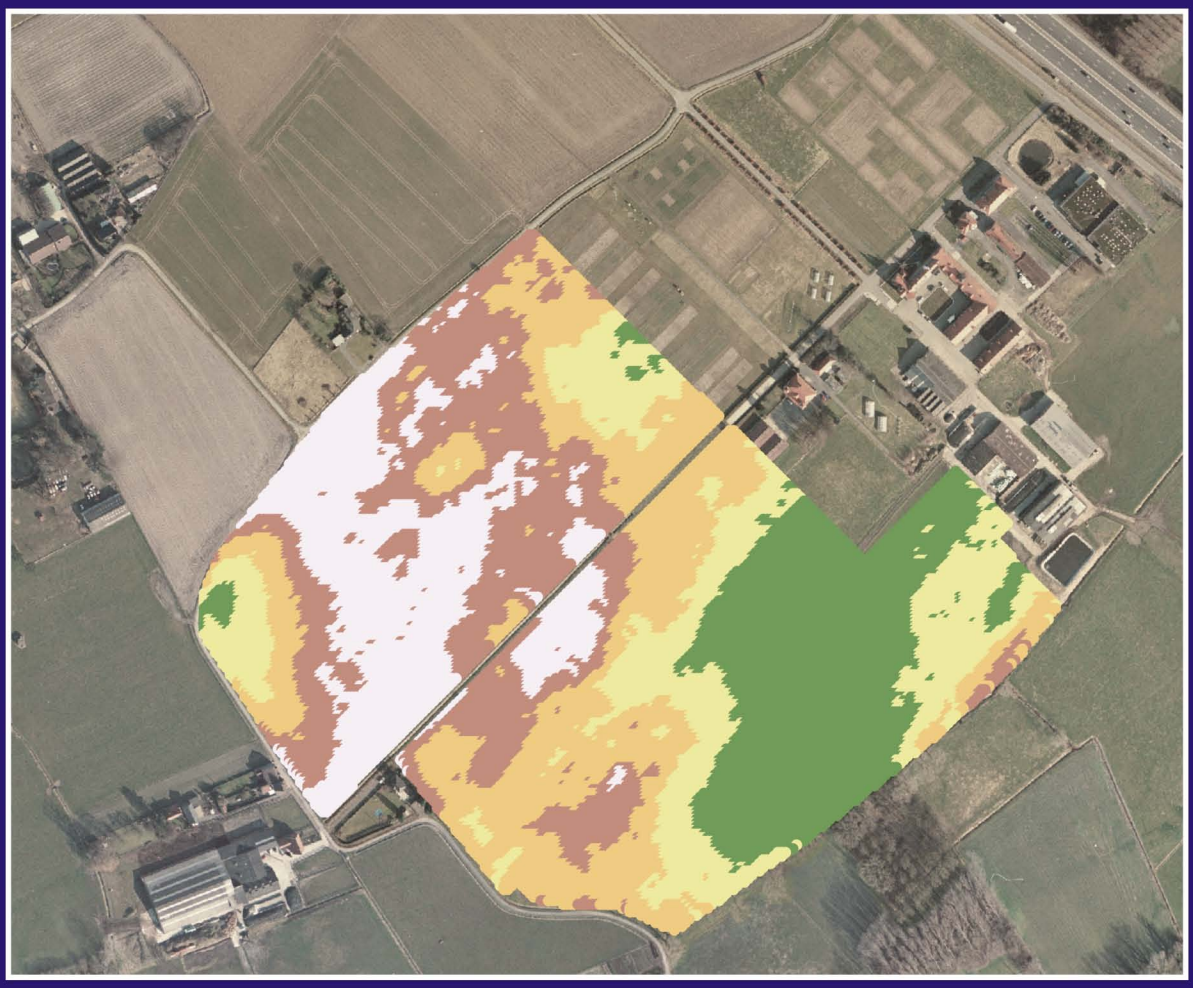

Spatial Inventory Techniques in Support of Site-specific Soil Management

Wellewatte Arachchige Udayakantha Vitharana

UNIVERSITEIT GENT

Spatial Inventory Techniques in Support of Site specific Soil Management W.A.U. Vitharana 2008

Promoter	Prof. dr. ir. Marc Van Meirvenne Department of Soil Management, Faculty of Bioscience Engineering, Ghent University
Dean	Prof. dr. ir. Guido Van Huylenbroeck
Rector	Prof. dr. Paul Van Cauwenberge

Wellewatte Arachchige Udayakantha Vitharana

SPATIAL INVENTORY TECHNIQUES IN SUPPORT OF SITE-SPECIFIC SOIL MANAGEMENT

Thesis submitted in fulfilment of the requirements for the degree of Doctor (PhD)
in Applied Biological Sciences: Land and Forest Management

Dutch translation of the title:

RUIMTELIJKE INVENTARISATIETECHNIEKEN TER ONDERSTEUNING VAN PLAATSSPECIFIEK BODEMBEHEER

Illustrations on the cover: Proximal sensed soil apparent electrical conductivity overlaid on an aerial photograph of Melle site (Chapter 4).

Citation: Vitharana U.W.A. 2008. Spatial inventory techniques in support of site-specific soil management, PhD thesis, Ghent University.

ISBN-number: 978-90-5989-262-0

The author and the promoter give the authorization to consult and to copy parts of this work for personal use only. Every other use is subject to the copyright laws. Permission to reproduce any material contained in this work should be obtained from the author.

Acknowledgement

This dissertation is dedicated to my loving parents: Dr. W.A.J. Vitharana and Mrs. Lokumenike Vitharana, for the enormous sacrifices they made to educate me.

A PhD dissertation is rarely written alone. This work contains efforts of many wonderful individuals who genuinely supported in many different ways. First and the foremost, I would like to acknowledge and extend my heartfelt gratitude to my promoter, Prof. dr. ir. Marc Van Meirvenne, for accepting me as a PhD student. Throughout the four years, he inspired me with his passion for the scientific research and reporting the findings in a concise and an attractive way. Without the genuine guidance, valuable discussions and consistent encouragements offered by him, I never would have come this far. The members of my dissertation committee: Prof. Dr. ir. Marc Verloo, Prof. Dr. Peter Finke, Dr. Abdul Mounem Mouazen and Prof. Dr. ir. Wim Cornelis have generously given their time and expertise to improve my work. I thank them for their contribution and constructive support.

I am very fortunate to associate myself with the research group on soil spatial inventory techniques (ORBit). All the past and present orbiters are acknowledged for their support and advices offered during the last four years. Especially, I need to express my gratitude and appreciation to ir. Liesbet Cockx, whose friendship, hospitality and wisdom supported me tremendously to improve this work. My thanks and appreciation to ir. David Simpson and ir. Timothy Saey for their helpful comments about my work, assistance given to field sampling and analyse of data. I cannot forget the kind assistance given by ing. Hans Vermeersch. He was not only instrumental for field sampling and laboratory analysis but also for generating some figures included in my dissertation. For their assistance and comments on my work, I thank MSc. Meklit Tariku, ir. Jo Bonroy and ir. Samuel Verstraete. Former Master of Science students, MSc. Kabindra Adhikari and MSc. Amakor Xystus also made use of the data collected during last four years. I thank them for their collaboration and contributions for field sampling and data analysis.

My thanks go also to the academic and technical staff members of the Department of Soil Management for providing me a pleasant working environment. The assistance given by Mr. Luc Deboosere and Mr. Mathieu Schatteman for field sampling is highly appreciated. I am thankful to Mrs. Tina Coddens and Mrs. Sophie Schepens for their support for the laboratory analysis. I also extend my gratitude to emeritus Prof. Dr. ir. G. Hofman for his suggestions and explanations

to improve the results presented in the part two of chapter 6. I am also grateful to Dr. Steven Sleutel for his support for the preparation of the dissertation.

This is also an opportunity for me to acknowledge the generosity of few individuals who provided the access to their agricultural fields for my research. I am thankful to Mr. Etienne Van Der Schueren, who did not hesitate to allow the access to the field in Watervliet even during the growing season. Prof. Josse De Baerdemaeker of the Laboratory for Agricultural Machinery and Processing, K.U. Leuven, is also appreciated for the support given by him to find out the Leefdaal study field. I am also thankful to Dr. Mieke Reyniers of the Flemish Land Agency (VLM) for providing pre-processed yield data. Further I would like to extend my thanks to ir. Lydia Bommelé, the coordinator of the Biocentrum Agri-Vet of the Ghent University for granting the access to the Melle study site. I am grateful to Prof. E. Van Ranst for providing access to the Belgian soil survey reports. Also I am indebted to Mr. Ronald Demuynck at the former Iscal sugar factory in Moerbeke for the analyses of the sugar yield parameters.

My deep appreciation goes to the Ghent University, Belgium for providing a scholarship through the Special Research Fund of Ghent University (BOF) to pursue my doctoral study. I also thank my employer, the University of Peradeniya, Sri Lanka for providing a study leave to carry out my research.

My gratitude to Dr. Christian Kersebaum of the Leibniz-Center of Agricultural Landscape Research (ZALF), Germany for providing me a training on the HERMES model. I thank the Scientific Research Committee (CWO) of the Faculty of Bioscience Engineering for the financial support for this training. I am immensely grateful to Dr. Janaka Thennakoon for proof reading some parts of my thesis. I am thankful to Prof. Colin Peiris and Prof. Sriyani Peiris for their true encouragements and support for my education. My gratitude and sincere thanks to Nimal, Kumari, Asanka, Marlon, Mulin Munasinghe, Frans Van der Linden, Liesbet, Jan and little Marit for their hospitality, which make our stay in Belgium enjoyable.

I extend my heartiest appreciation to my mother, brother and sister for their encouragements. I always grateful to my loving wife, Wajira for her love, patience and understanding. She contributed in various ways to improve this dissertation and always stood behind me to lift my spirit whenever I felt down. My life has been graced with a beautiful daughter, Yoshini. Her love and affection provided my most important source of strength and determination to complete this work.

Udaya, December 2008.

Contents

Acknowledgement i
Contents iii
List of figures vii
List of tables xi
List of abbreviations xii
Summary xv
Samenvatting xix

1. General Introduction 1
1.1. Overview 2
1.2. Research problem and objectives 3
1.3. Structure of the dissertation 5

2. Site-Specific soil management: Literature review 9
2.1. Introduction 10
2.2. Site-specific soil management 10
2.2.1. Benefits of site-specific soil management 12
2.3. Site-specific soil management cycle 14
2.3.1. Monitoring of the soil spatial and temporal variation 16
2.3.1.1. Invasive and non invasive soil sensors 17
2.3.1.2. Yield monitoring 23
2.3.1.3. Remote sensing 24
2.3.1.4. Crop sensors 25
2.3.2. Analysis of spatial data 26
2.3.3. Managing variation 26
2.4. Conclusions 31

3. Materials and methods 33
3.1. Introduction 34
3.2. Spatial sampling 34
3.3. Selection of soil variables and laboratory analysis 37
3.3.1. Analysis of soil texture, organic carbon and $CaCO_3$ content 38
3.3.2. pH-KCl 39
3.4. Ancillary information 39
3.4.1. Apparent electrical conductivity measurement with EM38DD sensor 39
3.4.2. Digital Elevation Model 45
3.4.2.1. Interpolation and removal of pits 46
3.4.2.2. Delineation of catchment area 46
3.4.2.3. Calculation of primary and secondary topographic attributes 47
3.5. Methodology of spatial data analysis 50
3.5.1. Exploratory data analysis 50
3.5.2. Geostatistical analysis 52

3.5.2.1. Characterizing the spatial variation by the variogram 53
3.5.2.2. Spatial prediction with kriging 57
3.5.3. Fuzzy *k*-means classification 62
3.6. Geology and soils of Flanders 66
3.7. Study area selection 70
3.8. The national soil map of Belgium 71

4. Utility of Choropleth soil maps for site-specific soil management and map upgrading using proximal soil sensing 75
4.1. Introduction 76
4.2. Materials and methods 78
4.2.1. Study area and soils 78
4.2.1.1. National soil map (1:20,000) 79
4.2.1.2. Detailed soil map (1:5000) 80
4.3. Soil sampling and laboratory analysis 81
4.4. Electrical conductivity measurements 83
4.5. Data analysis 84
4.5.1. Spatial analysis 84
4.5.2. Assessment of predictive quality of polygon maps 85
4.6. Results and discussion 87
4.6.1. Spatial variability of soil properties 87
4.6.1.1. Descriptive statistics 87
4.6.1.2. Spatial variability of topsoil properties 90
4.6.1.3. Spatial variability of subsoil properties 95
4.6.1.4. Spatial variability of depth to the Tertiary clay substratum 99
4.6.2. Predictive quality assessment of polygon soil maps 100
4.6.2.1. Predictive quality of the 1:20,000 map 100
4.6.2.2. Predictive quality of 1:5000 soil map 102
4.6.3. Upgrading the Belgian national soil map using a EC_a data 104
4.6.3.1. Spatial distribution of EC_a and its relationship with EC_a 105
4.6.3.2. Spatial prediction techniques 108
4.6.3.3. Performance of different prediction techniques 112
4.6.3.4. Upgrading the 1:20,000 soil map 116
4.6.3.5. Evaluation of the accuracy of the upgraded map 118
4.7. Conclusions 120

5. Key soil and topographic properties to delineate potential management zones in the European loess area 123
5.1. Introduction 124
5.2. Materials and methods 126
5.2.1. Study field 126
5.2.2. Acquisition of spatial data layers 127
5.2.2.1. Soil sampling and EC_a measurements 127
5.2.2.2. DEM generation and topographic attributes calculation 128
5.2.3. Identification of key information layers and delineation of management zones 130
5.2.3.1. Principal component analysis 130

5.2.3.2. Fuzzy *k*-means classification 133
5.2.4. Crop productivity among potential management classes 133
5.3. Results and discussion 134
5.3.1. Spatial distribution of topographic attributes 134
5.3.2. Spatial distribution of soil attributes 136
5.3.2.1. Exploratory data analysis 136
5.3.2.2. Top and subsoil properties 137
5.3.2.3. Apparent electrical conductivity 142
5.4. Identification of key variables 143
5.5. Delineation of potential management zones 146
5.6. Crop productivity and potential management classes 149
5.7. Conclusions 152

6. Delineation of potential management zones in a polder area and investigation of their agronomi relevance 153
Part 1: Delineation of potential management zones in polder area 152
6.1. Introduction 154
6.2. Materials and Methods 156
6.2.1. Study area 156
6.2.2. Apparent electrical conductivity mapping and soil analysis 158
6.2.3. Soil sampling and analysis 158
6.2.4. Spatial prediction of soil texture using ordinary co-kriging 159
6.2.5. Management zones delineation 163
6.3. Results and discussion 163
6.3.1. EC_a measurements 163
6.3.2. Soil textural variation and its relationship with EC_aGM 165
6.3.3. Mapping of topsoil clay content 169
6.3.4. Mapping of subsoil clay content 171
6.3.5. Delineation of potential management zones 175
6.4. Conclusions 179

Part 2: Agronomic relevance of potential management classes delineated in the polder area 180
6.5. Introduction 182
6.6. Materials and methods 183
6.6.1. Land management practices 183
6.6.2. Field sampling scheme 184
6.6.3. Measurements of nitrogen and moisture 185
6.6.4. Measurement of sugar beet yield 186
6.6.4.1. Leaves and roots biomass 186
6.6.4.2. Income analysis 186
6.6.4.3. Data analysis 187
6.7. Results and discussion 188
6.7.1. Textural composition of monitoring points and soil moisture retention curves 188
6.7.2. Nitrogen and moisture dynamics across management classes 191
6.7.3. Crop yield and farm income across management classes 195

6.8. Conclusions 198

7. General conclusions and future research 201
7.1. Introduction 202
7.2. General conclusions 202
7.3. Future research issues 204

References 207

Curriculum Vitae 227

List of figures

Figure 2.1. Site-specific soil management versus traditional soil management. 12

Figure 2.2. The components of site-specific soil management cycle. 15

Figure 2.3. Soil information needs for site-specific soil management. 17

Figure 2.4. Soil sensors for site-specific soil management 22

Figure 2.5. The sensor based and map based approaches for managing within-field soil variation. 28

Figure 3.1. Simple random sampling scheme and grid sampling configuration with added couple random sample located within each grid cell. 36

Figure 3.2. Diagram showing the operation of electromagnetic induction based EM38 sensor. 40

Figure 3.3. Comparison of depth sensitivity of the vertical and horizontal dipole modes of EM38 sensor. 42

Figure 3.4. EM38DD sensor showing the vertical and horizontal dipole units. 43

Figure 3.5. Mobile EC_a measurement system. 44

Figure 3.6. A 3 x 3 moving window for estimating the primary and secondary topographic attributes 47

Figure 3.7. Omnidirectional experimental variogram and directional experimental variograms. 54

Figure 3.8. Spherical, exponential and Gaussian models with an identical nugget effect. 56

Figure 3.9. A map of Belgium showing the Flanders region. 66

Figure 3.10. Tertiary materials exposed on the north facing slopes of southern Flanders. 68

Figure 3.11. General soil map of Flanders and the locations of the three study areas. 70

Figure 3.12. Belgian and USDA soil texture triangles. 72

Figure 4.1. Localisation of the Melle study area. 79

Figure 4.2. The 1:20,000 soil map of the Melle study area. 80

Figure 4.3. The 1:5000 soil map of the Melle study area. 81

Figure 4.4. The grid plus random sampling scheme showing 135 locations and a depth observation showing the boundary between loess material and the underlying Tertiary clay substratum. 82

Figure 4.5. Scatter plot between the nearest neighbourhood observations of EC_aV of the surveying day 1 and day 2 and the fitted linear regression relationship. 83

Figure 4.6. The distribution of topsoil and subsoil textural data of the Melle study area on the Belgian textural triangle. 89

Figure 4.7. Histograms of topsoil and subsoil organic C (%) contents. 89

Figure 4.8. Directional experimental variogram and fitted models for topsoil clay and omnidirectional experimental variograms and fitted models for sand organic C content and pH. 91

Figure 4.9. Kriged estimates of topsoil sand (%), clay (%), texture classes, organic C (%) and pH. 92

Figure 4.10. Box plots showing the variation of organic C and pH in arable and pasture fields. 94

Figure 4.11. Omni directional experimental variograms and fitted models for subsoil clay, sand, organic C and pH. 95

Figure 4.12. Kriged estimates of subsoil sand (%), clay (%), texture classes, organic C (%) and pH. 97

Figure 4.13. Experimental variogram calculated for D_{ts} and fitted exponential model and kriged estimates of depth to the Tertiary substratum (m). 99

Figure 4.14. Mapping units of the 1:5000 soil map showing the variations of topsoil and subsoil texture and depth to the Tertiary clay substratum (m). 103

Figure 4.15. Kriged estimates of EC_aV (mS m^{-1}) 106

Figure 4.16. Schematic presentation showing the response of the EM38 sensor in vertical dipole mode when the Tertiary clay substratum occurs at shallower and at deeper depths. 107

Figure 4.17. Cumulative response function of EM38 sensor for measurements taken in the vertical dipole mode in a homogenous material. 110

Figure 4.18. Depth to the Tertiary clay substratum (D_{ts}) as a function of apparent electrical conductivity in the vertical dipole mode (EC_aV) with fitted empirical exponential regression and depth sensitivity function calibrated with 20 samples. 112

Figure 4.19. Experimental variogram calculated for residuals of D_{ts} and fitted spherical model. 113

Figure 4.20. Predictions of D_{ts} made with regression kriging and the model based on the depth sensitivity function calibrated with 20 depth observations. 113

Figure 4.21. Scatter plots of observed depth versus predicted depth by regression kriging and the depth sensitivity function using 60, 40 and 20 calibration samples. 115

Figure 4.22. Predicted D_{ts} classified according to the legend of the 1:20,000 Belgian national soil map and the upgraded 1:20,000 soil map. The inner thick boundary separates the two soil series Lcc and Ldc. 117

Figure 4.23. Original 1:5000 field report of the Belgian national soil survey indicating the soil auger observations conducted in the study area. 119

Figure 5.1. The location of the study field in the Belgian loess belt and the study field boundary demarcated on a satellite image. 126

Figure 5.2. The grid plus random sampling scheme showing 110 locations. 128

Figure 5.3. Perspective view of the DEMof the catchment area, contour map of the catchment area and the DEM of the study field. 129

Figure 5.4. Panoramic view of the Leefdaal study field indicating the topographic discontinuity. 130

Figure 5.5. Data analysis procedure for the selection of key variables and delineation of management zones. 131

Figure 5.6. Spatial distribution of topographic attributes: slope (%), wetness index (*WI*) and stream power index (*SPI*). 135

Figure 5.7. Omnidirectional experimental variogram and fitted models for topsoil clay subsoil organic C and directional experimental variograms and fitted models of topsoil pH. 140

Figure 5.8. Maps of kriged estimates for topsoil clay content (%), subsoil organic C (%) and topsoil pH. 141

Figure 5.9. Experimental variogram with the fitted exponential model and the map of kriged estimates for EC_aV. 143

Figure 5.10. Scree plot for soil and topographic data. 144

Figure 5.11. Rotated loading plots of the first and second PC and first and third PC. 146

Figure 5.12. Fuzziness performance index (*FPI*) and normalized classification entropy (*NCE*) corresponding to different numbers of classes. 147

Figure 5.13. Potential management classes delineated using topsoil pH, EC_aV and elevation, elevation along A-B with indication of the potential management zones and classes draped on the DEM. 148

Figure 5.14. Three-year average standardized yield map of grain and straw. 151

Figure 6.1. The polder area of northwest East-Flanders in Belgium, the location of study field within this area and an aerial image of the study field. 156

Figure 6.2. Digital elevation model of the study field. 157

Figure 6.3. Interpolated values in mS m^{-1} for EC_aH and EC_aV with the 63 sampling locations shown as dots. 164

Figure 6.4. The distribution of top and subsoil texture according to the Belgian textural triangle. 166

Figure 6.5. Experimental cross-variograms between topsoil clay and organic C and subsoil clay and organic C. 167

Figure 6.6. Experimental direct-variograms of topsoil clay, $\theta g_{(-1.5\ MPa)}$ and the cross-variogram fitted with the linear model of coregionalization. 170

Figure 6.7. Predicted clay contents in % by standardized ordinary co-kriging for topsoil subsoil. 172

Figure 6.8. Experimental direct variograms of subsoil clay, EC_aGM and cross-variogram with the fitted linear model of coregionalization. 173

Figure 6.9. Unburied creek network in the Schelder estuary and a close view of a creek. 175

Figure 6.10. Fuzziness performance index (*FPI*) and normalized classification entropy (*NCE*) correspond to different number of classes. 176

Figure 6.11. (a) Classes (1 to 3) obtained with Fuzzy *k*-means classification of top and subsoil clay contents and generalized potential management classes. 177

Figure 6.12. Oblique aerial image of the study field in July 1989 (© Dept. Archaeology and Ancient History of Europe, Ghent University, Belgium, Photo: J. Semey). 179

Figure 6.13. Ten monitoring points posted on the management class map. 184

Figure 6.14. Soil water retention curves for soil depth intervals: 0 – 30 cm and 30 – 60 cm of three management classes. 191

Figure 6.15. Average NO_3-N content in soil depth intervals: 0 – 30 cm and 30 – 60 cm for each monitoring date across potential management classes. 192

Figure 6.16. Average gravimetric moisture content in soil depth intervals: 0 –30 cm and 30 – 60 cm for each monitoring date across potential management classes. 195

Figure 6.17. Response of sugar beet to increasing nitrogen fertilizer amounts. Example for a 120 kg N ha^{-1} optimum application. 197

List of tables

Table 3.1. International geological time scale of the Tertiary and the Quaternary periods. 67

Table 4.1. Minimum legible areas for some common map scales. 77

Table 4.2. Descriptive statistics of sampled soil properties. 88

Table 4.3. Model parameters of the fitted variogram models for the topsoil properties 91

Table 4.4. Model parameters of the fitted variogram models for the subsoil properties. 96

Table 4.5. Within-class variances (s_W^2) and intra-class correlation values (R_i^2) of the 1:20,000 soil map. 101

Table 4.6. Within-class variances (s_W^2) and intra-class correlation values (R_i^2) of the 1:5000 soil map. 104

Table 4.7. Validation results of regression kriging (RK) and predictions based on the depth sensitivity function. (TM-60, TM-40 and TM-20 denote the models based on depth sensitivity function parameterized using 60, 40 and 20 calibration samples). 114

Table 4.8. Electrical conductivities (mS m^{-1}) of loess and clay layer calculated using the depth sensitivity function with varying number of calibration samples and coefficient of determination (R^2) values of the models. 115

Table 5.1. Summary statistics of sampled soil properties (n = 110) and EC_a (n = 5534). 137

Table 5.2. Pearson and sperman rank correlation (in brackets) between top (T) and subsoil (S) properties 139

Table 5.3. Model parameters of the fitted variogram models for the topsoil clay, pH, subsoil organic C and EC_aV. 140

Table 5.4. Factor loading of the rotated first three PC with labels (inside parenthesis) used in Figure 5.11. 145

Table 5.5. Mean values of soil properties and yield data for each potential management class (with standard deviations between brackets). 150

Table 6.1. Summary statistics of EC_a (mS m^{-1}) measurements (n = 4048). 163

Table 6.2. Declustered and non-declustered means of top and subsoil properties. 165

Table 6.3. Summary statistics for topsoil and subsoil clay, silt, organic C (n = 63) and topsoil $\theta g_{(-1.5\ MPa)}$ (n = 117). 166

Table 6.4. Pearson correlation between top- and subsoil clay and EC_a and $\theta g_{(-1.5\ MPa)}$ (n = 63). 168

Table 6.5. Model parameters of the direct- variogram models for the topsoil clay and $\theta g_{(-1.5\ MPa)}$ and the cross-variogram. 170

Table 6.6. Cross-validation indices between predicted and actual values of topsoil clay. 171

Table 6.7. Model parameters of the direct-variogram models for the subsoil clay and EC_aGM and the cross-variogram. 173

Table 6.8. Cross-validation indices between predicted and actual values of topsoil clay. 174

Table 6.9. Mean values of soil textural fractions and organic C for each potential management class (with standard deviations between brackets). 178

Table 6.10. Percentage of standard price (45 euro) added or deducted on the basis of sugar content. 187

Table 6.11. Average values of the textural fractions and standard error of the mean (in brackets) per management class on the basis of 10 monitoring points. 188

Table 6.12. Volumetric water contents at different pressure heads of soil samples taken in three management classes at two depth intervals. 189

Table 6.13. Parameters and coefficient of determination (R^2) of the fitted Van Genuchten equation of the soil moisture retention curves. 190

Table 6.14. Mean values of crop yield (sugar beets) variables per management class and, between brackets, the standard error of the mean. 196

Table 6.15. Results of the ANOVA on the crop yield (sugar beets) variables based on the 3 management classes. 197

List of abbreviations

A	Upslope contributing area
ALR	Additive log-ratio transformation
ANOVA	Analysis of variance
As	Specific catchment area
ATV	All terrain vehicle
BLUE	Best linear unbiased estimate
CV	Coefficient of variation
DEM	Digital elevation model
D_{ts}	Depth to the Tertiary clay substratum
EC_a	Apparent electrical conductivity
EC_aV	Apparent electrical conductivity measured in the vertical dipole orientation
EC_aH	Apparent electrical conductivity in the horizontal dipole orientation
EC_aGM	Geometric mean of EC_aV and EC_aH
EGNOS	European geostationary navigation overlay service
EMI	Electromagnetic induction
ER	Electrical resistivity
Exp	Exponential model
FPI	Fuzziness performance index
GIS	Geographical information systems
GPS	Global positioning system
ISODATA	Iterative self-organizing data analysis technique
LiDAR	Light detection and ranging
LMC	Linear model of coregionalization
Max	Maximum
MEE	Mean estimation error
MFD	Multiple flow direction algorithm

Min	Minimum
MSAS	Multi-functional satellite augmentation system
NCE	Normalized classification entropy
NIR	Near-infrared
PCA	Principal component analysis
RI	Relative improvement of predictions
RMSEE	Root mean squared estimation error
RNE	Relative nugget effect
SA	Selective availability
SFD	single flow direction algorithm
Sl	Slope
Sph	Spherical model
SPI	Stream power index
SSSM	Site-specific soil management
TIN	Triangulated irregular network
USDA	United states department of agriculture
WAAS	Wide area augmentation system
WI	Wetness index
WRB	World Reference Base for Soil Resources
WSS	Weighted sum of squares

Summary

Site-specific soil management seeks to address the within-field soil variability to guide soil management decisions. Detailed soil information is a prime requirement, but most of the currently available soil survey information does not satisfy this sufficiently. Therefore, this gap of soil information has been indicated as one of the major obstacles that prevent the progress of site-specific soil management. There is a need for cost effective, accurate and quantitative soil spatial inventory techniques to create detailed maps of key soil properties. This research was conducted to evaluate the potential of two ancillary information sources, namely soil apparent electrical conductivity (EC_a) measured with an EM38DD sensor and elevation data obtained by airborne laser scanning to provide detailed soil information needed for site-specific soil management. Within this broad objective, case studies were conducted in three different study sites in Flanders, Belgium.

Despite their shortcomings, choropleth soil maps remain the most widespread source of information on soil resources. Since most nationwide soil surveys were conducted in the second half of the previous century, a need for upgrading emerges to provide the current soil information needs. We evaluated the utility of detailed EC_a observations to upgrade a part of the 1:20,000 choropleth soil map of Belgium. This study was conducted on a 14 ha area in the sandy silt region near Melle, which had been mapped twice in the 1950s: first, during the national soil survey yielding a 1:20,000 soil map, and second, during a detailed investigation of a research farm resulting in a 1:5000 map. The first map failed to identify the within-field variability of soil properties: top and subsoil textural fractions, organic C, pH and depth to a Tertiary clay substratum (D_{ts}). This clearly emphasized the need for upgrading to provide soil information at a within-field scale. The detailed 1:5000 map was able to provide information on the within-field variation of D_{ts} with a sufficient accuracy. But it failed to characterize the within-field variation of the remaining soil properties. The EC_a survey provided 9192 measurements of EC_a

within the study area and these data were used as a covariate to predict D_{ts}. The accuracy of two prediction techniques was evaluated: predictions based on the depth sensitivity function and regression kriging. The predictions were validated using 46 independent observations of D_{ts}. A depth sensitivity function, which was calibrated using 20 D_{ts} observations showed a high accuracy of prediction with a mean estimation error (*MEE*) of 0.08 m and a correlation coefficient (r) of 0.91. However, it was also shown that these predictions can be further improved by employing regression kriging with some extra D_{ts} observations (n = 60): *MEE* = 0.02 m and r = 0.95. The 1:20,000 soil map was upgraded by incorporating the predictions of D_{ts} made using regression kriging. An assessment of the map accuracy indicated that even after classification, the D_{ts} classes were better predicted by the sensor data than the 1:5000 map which was based on 210 auger observations.

Recent advances in proximal soil sensing, terrain modelling and yield mapping have made available large quantities of information about the within-field variability of soil and crop properties. But the selection of the key variables for the identification of management zones which are required for site-specific soil management is not straightforward. We investigated a procedure for this selection. An 8 ha agricultural field near Leefdaal in the Loess belt of Belgium was considered for this study. The available information consisted of: (i) top- and subsoil samples taken at 110 locations, on which soil properties namely, textural fractions, organic C, $CaCO_3$ and pH were analysed, (ii) EC_a obtained through an EM38DD sensor, and (iii) wetness index, stream power index and slope angle derived from a detailed digital elevation model. A principal component analysis, involving 12 soil and topographic properties and two EC_a variables, identified three components explaining 70.1 % of the total variability. These three components were best represented by pH, EC_a which was strongly associated with texture, and organic C. However, organic C was closely related to some more readily obtainable topographic properties, and therefore elevation was preferred. A fuzzy *k*-means classification of these three key variables produced four potential

management classes. Three-year average standardized yield maps of grain and straw showed productivity differences across these classes, but mainly linked to their landscape position.

Variability in soil texture has a profound effect on soil management, especially in texturally complex soils such as polder soils. The conventional approach of point sampling requires a high sampling intensity in order to take into account such spatial variation. We investigated the use of two ancillary variables for the detailed mapping of soil texture and subsequent delineation of potential management zones. In an 11.5 ha arable field in the polder area near Watervliet, the geometric mean of the EC_a measured in both vertical and horizontal orientations strongly correlated with the heterogeneous subsoil clay content (r = 0.83), but the correlation was weaker with the homogenous topsoil clay content (r = 0.40). The topsoil gravimetric water content at wilting point ($\theta g_{(-1.5\ MPa)}$) correlated strongly (r = 0.96) with the topsoil clay content. Thus maps of topsoil and subsoil clay contents were obtained from 63 clay analyses supplemented with 117 $\theta g_{(-1.5\ MPa)}$ and 4048 EC_a measurements, using standardized ordinary cokriging. Three potential management classes were identified based on the spatial variation of both top and subsoil clay contents. The influence of subsoil textural variation on the behaviour of crop was illustrated by an aerial image of the sugar beet crop, confirming the reliability of the results.

The ability to delineate potential management classes is not sufficient to implement site-specific soil management. The agronomic relevance of these classes should also be validated. Thus we investigated the relevance of the potential management classes of the Watervliet field for site-specific water and nitrogen management. During the growing season of 2005, we monitored the top- and subsoil NO_3-N and moisture content and found strong differences among zones. The crop biomass at harvest (roots plus leaves) was markedly variable between classes (ranging from 106 to 150 Mg ha^{-1}), as well as sugar content (ranging from 15.7 to 17.2 %). But due to a compensation effect between the crop biomass and sugar accumulation, differences in sugar yield and financial income

between classes were relatively small (the income ranged from 3958 to 4245 € ha^{-1}). These results clearly emphasized that potential management zones delineated on the basis of the variation in soil texture are highly suitable for the site-specific management of soil nitrogen and water.

The three case studies presented in this dissertation consistently showed that proximal soil sensing of EC_a is a very satisfactory method for elucidating the soil variability at a within-field scale while economizing on invasive soil samples.

Samenvatting

Plaatsspecifiek bodembeheer is gericht op de binnenin-perceels bodemvariabiliteit om bodembeheersbeslissingen te vergemakkelijken. Een eerste vereiste hiervoor is nauwkeurige bodeminformatie, maar de huidige beschikbare bodeminformatie vervult deze conditie echter onvoldoende. Dit tekort is één van de grootste hindernissen die de ontwikkeling van plaatsspecifiek bodembeheer in de weg staan. Er is nood aan kost-effectieve, nauwkeurige en kwantitatieve ruimtelijke bodeminventarisatietechnieken die toelaten gedetailleerde kaarten van bodemeigenschappen te maken. Dit onderzoek evalueerde de mogelijkheden van twee secundaire informatiebronnen om gedetailleerde bodeminformatie nodig voor plaatsspecifiek bodembeheer te verschaffen. Deze twee bronnen waren bodem elektrische geleidbaarheid (EC_a) opgemeten met een EM38DD sensor en hoogtemetingen bekomen met een luchtgebaseerde laserscanner. Binnen deze brede doelstelling werden gevalstudies uitgevoerd in drie verschillende studiegebieden in Vlaanderen, België.

Ondanks hun gebreken blijven chloropleth bodemkaarten nog steeds de meest aanvaarde vorm van bodeminformatie. Aangezien de meeste nationale bodemsurveys uitgevoerd werden in de tweede helft van de vorige eeuw, is er een behoefte ontstaan om deze informatie op te waarderen zodat kan voldaan worden aan de huidige bodeminformatie vereisten. We evalueerden de bruikbaarheid van gedetailleerde EC_a observaties, bekomen met een EM38DD bodemsensor, om een deel van de 1:20,000 chloropleth bodemkaart van België op te waarderen. Deze studie werd uitgevoerd op een gebied van 14 ha in de zandige leemstreek nabij Melle. Het gebied werd twee keer gekarteerd in de jaren `50: eerst gedurende de nationale bodemsurvey wat resulteerde in een 1:20,000 bodemkaart en een tweede maal tijdens een gedetailleerd onderzoek van de proefhoeve wat een 1:5000 bodemkaart opleverde. De eerste kaart slaagde er niet in de binnenin-perceelsvariabiliteit van volgende bodemeigenschappen te identificeren**:**

textuurfracties van de boven- en ondergrond, organische C, pH en diepte tot een Tertiar kleisubstraat (D_{ts}). Dit toonde duidelijk de nood tot opwaardering aan zodat binnenin-perceels bodeminformatie beschikbaar zou zijn. De gedetailleerde 1:5000 kaart verschafte voldoende nauwkeurige informatie over de binnenin- perceels D_{ts} variabiliteit. De binnenin-perceelsvariatie van de overige bodemeigenschappen kon echter niet gekarakteriseerd worden. Binnen het studiegebied werden 9192 EC_a metingen gebruikt als een co-variabele om D_{ts} te voorspellen. De nauwkeurigheid van twee voorspellingstechnieken werd geëvalueerd: voorspellingen gebaseerd op de diepte-gevoeligheidscurve en regressie kriging. De voorspellingen werden gevalideerd op basis van 46 onafhankelijke D_{ts} observaties. Een diepte-gevoeligheidsfunctie, opgesteld aan de hand van 20 D_{ts} observaties vertoonde een hoge voorspellingsnauwkeurigheid met een gemiddelde schattingsfout (*MEE*) van 0.08 m en een correlatiecoefficient (r) van 0.91. Deze voorspellingen konden echter nog verbeterd worden met de regressie kriging techniek op basis van 60 extra stalen: *MEE* = 0.02 m en r = 0.95. De 1:20,000 bodemkaart werd opgewaardeerd door integratie van de D_{ts} voorspellingen bekomen met regressie kriging. Zelfs na classificatie werden de D_{ts} klassen beter voorspeld door de sensorgegevens dan door de 1:5000 bodemkaart die gebaseerd was op 210 boringen.

Recente vorderingen in de beschikbaarheid van proximale bodemsensoren, terrein modellering en opbrengstkartering verschaffen een grote hoeveelheid informatie over de binnenin-perceelsvariabiliteit van bodem- en gewaseigenschappen. De selectie van sleutelvariabelen voor de identificatie van beheerszones nodig voor plaatsspecifiek bodembeheer is echter geen eenduidige taak. Een procedure voor deze selectie werd ontwikkeld voor een 8 ha landbouwperceel in de leemstreek van België. De beschikbare informatie bestond uit: (i) stalen van de boven- en ondergrond op 110 locaties, geanalyseerd op textuur, organische C, $CaCO_3$ en pH, (ii) EC_a metingen, en (iii) topografische indices bekomen op basis van een digitaal terrein model. Een principale componenten analyse op basis van deze gegegevens identificeerde drie componenten die samen 70.1 % van de totale variabiliteit

verklaarde. Deze drie componenten werden best vertegenwoordigd door pH, EC_a dat sterk gerelateerd is met textuur en organische C. Omdat organische C sterk gecorreleerd is met gemakkelijk te bekomen topografische eigenschappen werd hoogte als derde sleutelvariabele verkozen. Een fuzzy *k*-means classificatie van deze drie variabelen resulteerde in vier mogelijke beheersklassen. Op basis van gestandardiseerde opbrengskaarten van graan en stro, uitgemiddeld over drie jaar, werden productiviteitsverschillen tussen deze klassen aangetoond die echter de grootste relatie vertoonden met hun landschapspositie.

Variabiliteit in bodemtextuur heeft een grote invloed op het bodembeheer, zeker in complex texturele bodems zoals in de polders. De klassieke aanpak om zulke variabiliteit in rekening te brengen is een puntbemonstering met een intensieve staalname. Het gebruik van twee secundaire variabelen voor het gedetailleerd karteren van bodemtextuur en vervolgens het afbakenen van potentiële beheerszones werd onderzocht. In een 11.5 ha landbouwperceel in de polderstreek nabij Watervliet werd de EC_a opgemeten in zowel de horizontale als verticale oriëntatie. Het geometrisch gemiddelde van de beide EC_a metingen was sterk gecorreleerd met de heterogene kleiconcentratie in de ondergrond (r = 0.83), terwijl de correlatie met de homogene kleiconcentratie in de bovengrond slechts zwak was (r = 0.40). Het gravimetrisch vochtgehalte bij het verwelkingspunt ($\theta g_{(-1.5\ MPa)}$) was echter zeer goed gecorreleerd met het kleigehalte van de bovengrond (r = 0.96). Kaarten van het boven- en ondergronds kleigehalte werden bekomen met gestandardiseerde ordinaire cokriging op basis van 63 klei analyses aangevuld met respectievelijk 117 $\theta g_{(-1.5\ MPa)}$ en 4048 EC_a metingen. Op basis van de ruimtelijke variatie in het boven-en ondergronds kleigehalte werden drie potentiële beheerszones afgebakend. De invloed van de ondergrondse texturele variabiliteit op het gedrag van het gewas werd aangetoond aan de hand een luchtfoto van het suikerbietgewas op dit veld en bevestigde de betrouwbaarheid van deze resultaten.

De mogelijkheid om potentiële beheerszones af te bakenen is echter niet voldoende om plaatsspecifiek bodembeheer toe te passen. De landbouwkundige

relevantie van deze zones moet ook gevalideerd worden. In een laatste gevalstudie werd de relevantie van de potentiële beheerszones onderzocht voor plaatsspecifiek water- en stikstofbeheer. Tijdens het groeiseizoen van 2005 werd het NO_3-N- en vochtgehalte van de boven- en ondergrond opgevolgd en sterke verschillen tussen de zones werden gevonden. Bovendien varieerde niet alleen de suikerbietbiomassa bij oogst (wortels plus bladeren) tussen de klassen (gaande van 106 tot 150 Mg ha $^{-1}$), ook het suikergehalte vertoonde sterke verschillen (variërend van 15.7 tot 17.2 %). Echter door een compensatie-effect tussen de gewasbiomassa en de suikeraccumulatie waren de verschillen in suikeropbrengst en financiële inkomsten tussen de klassen relatief klein(de inkomsten varieerden tussen 3958 en 4245 € ha^{-1}). Deze resultaten bewezen duidelijk dat potentiële beheerszones afgebakend op basis van bodemtextuur zeer geschikt zijn voor het plaatsspecifiek beheer van bodemstikstof en bodemvocht.

De drie gevalstudies voorgesteld in dit werk toonden consistent aan dat proximale EC_a bodemsensoren een geschikt middel zijn om bodemvariabiliteit op een binnenin-perceelsschaal te identificeren en dat ze toelaten te besparen op invasieve bodemstalen.

Chapter 1

General introduction

1.1. Overview

The world's food demand is steadily increasing as the world's population crosses the six billion mark and is expected to increase by another three billion over the next three decades. This is further aggravated by the higher food demand for a richer diet by those ascending the economic ladder. As a consequence, the global demand for food is projected to double within the first three decades of this century (Daily et al., 1998). The world's food crisis already became evident as a steady increase in food prices and public unrest can be seen in different parts of the world demanding the access to food. Therefore, humankind has to face the onerous challenge of meeting the increasing world's food demand. From the perspective of soil management, two options are available to boost the global food production: increase the total cultivated land area or increase the productivity of existing arable lands. The first option has become difficult to realize as per capita availability of arable lands has markedly depleted during the last decades and is projected to decline from about 0.23 ha in 2000 to about 0.15 ha by 2050 (Lal, 1991). This suggest that an increase of the productivity of existing arable lands through better soil management is the most appropriate means of meeting the ever increasing food demands.

Volatility in the cost of agricultural inputs, fuel and the income generated from farm products has lead to instability in the farm economy (Seelan et al., 2003). This has caused gradual shift of the work force attached to the agriculture sector into other industrial sectors. Therefore, this scenario has called for the introduction of modern technologies to improve crop yield, provide information to enable better in-field management decisions, reduce chemical and fertilizer costs through more efficient application, permit more accurate farm records and finally to increase the profit margin.

The pressure to increase the food production from limited available lands has lead to an excessive use of inorganic and organic fertilizers. This has resulted in a widespread nitrogen and phosphorous contamination in water supplies, related largely to agriculture (Baligar et al., 2001; Carpenter et al., 1998). Nevertheless, by

1990, agricultural practices like poor soil water management on irrigated crop lands has contributed to the degradation of 38 % of the approximately 1.5 billion crop land world wide and since then the losses have continued at a rate of 5 – 6 million hectares annually (World Resources Institute, 1998). These evidences have emphasized the need of improved better soil management practices in order to preserve the environmental quality and finite natural resources for the future generations.

Site-specific soil management is viewed as one of the most viable means of increasing the productivity of existing arable lands while minimizing the over utilization of finite natural resources and the detrimental environmental impacts of associated agrochemical pollutants (Corwin and Lesch, 2005a; Robert, 1993). Through efficient use of soil inputs, this strategy has the potential to improve the agricultural producer's net income (Lambert and Lowenberg-DeBoer, 2000). Site-specific soil management implies the concept of managing soils based upon the spatial variation within a field (Larson and Robert, 1991). By applying this simple concept, the management practices such as plant nutrient, soil water applications and tillage practices are fine tuned at a within-field scale with the aim of cost effectively maximizing crop production and making efficient use of agro-chemicals to minimize detrimental environmental impacts (Larson et al., 1997; Mulla and Schepers, 1997).

1.2. Research problem and objectives

To implement site-specific soil management practices, within field areas called management zones displaying similar behaviour with respect to specified characteristics (e.g. yield potential, leaching potential, moisture supply capacity, trafficability, workability and root penetration) should be identified (Dobermann et al., 2004). This, in turn demands detailed quantitative information about the variation of soil properties. Traditional small-scale soil maps, which were made for regional land use planning, are not capable of providing soil information in a sufficient detail to support site-specific soil management (Robert, 1993). This

deficiency of soil information has been emphasized as one of the obstacles that prevents the progress of site-specific soil management (Johnson and Robert, 1998; Robert, 2002). Therefore, in most countries, there is a need for acquiring detailed soil information or upgrading the existing soil maps by incorporating new information (Visschers et al., 2007). Traditionally, within-field soil variation is identified and mapped by analyzing soil samples taken from many evenly spaced augerings throughout the field (Wollenhaupt et al., 1997). However, the cost and time constraints have restricted the viability of this approach (Plant, 2001). Thus there is a need for cost effective, accurate and quantitative soil spatial inventory techniques to create detailed soil maps (Bouma et al., 1999; Cook et al., 1996; Dobermann et al., 2004; Sylvester-Bradley et al., 1999). Soil spatial inventory techniques involve the procedures of determining the pattern of soil cover, characterizing it, and presenting it in an understandable and interpretable form to various users (Rossiter, 2005)

Recent advances in proximal and remote sensing and on-the-go soil measurements have made several types of potential ancillary information available for spatial characterization of soil properties (Adamchuk et al., 2004). However, their utility for predicting soil variation in different soil-scapes combined with appropriate pedometrical techniques is yet to be explored.

The overall objective of this research was to investigate spatial inventory techniques in support of site-specific soil management. More specifically, two types of ancillary information, apparent electrical conductivity measured with an EM38DD sensor and elevation data obtained by airborne laser scanning were evaluated for their potentials to accurately map soil variability with a minimum effort of invasive field sampling. Through this, attempts were made to bridge the soil information gap that slows down the progress of site-specific soil management. Within the frame work of this broad objective, case studies were conducted in three different study sites in Flanders, Belgium. Each of case studies highlights more specific objectives which are reported in chapters four through six.

1.3. Structure of the dissertation

This dissertation is structured in seven chapters. The first chapter presents the research problem and the overall objective of this study. The next chapter further extends the theoretical and research backgrounds of this work through a literature review on site-specific soil management.

The materials and methods shared by the three studies reported in this dissertation are described in chapter three. Special attention is given to the introduction of sampling strategies and techniques used for spatial data analysis. Further, this chapter details the pedogenesis of the soils of Flanders to facilitate the reader to understand the results and discussions presented in chapters four through six.

Chapter four is based on the publication:

U.W.A. Vitharana, T. Saey, L. Cockx, D. Simpson, H. Vermeersch and M. Van Meirvenne. 2008. Upgrading a 1/20,000 soil map with an apparent electrical conductivity survey. Geoderma 148:107-112.

The choropleth soil maps constructed at a detail level can be useful to provide the spatial information needed for site-specific soil management. Identification of this potential is essential to understand the requirement of upgrading of these maps. In line of this problem setting, the first part of this chapter evaluated the potentials of two scales of choropleth soil maps (i.e. 1:20,000 and 1:5000) to predict variation of soil properties at a within-field scale. The focus of the subsequent sections of this chapter was to evaluate the potency of EM38DD sensor to upgrade the Belgian national soil map (scale 1:20,000) by incorporating accurate information on the depth to a clayey substratum. In relation to this objective, the challenge of using a minimum number of invasive soil samples while gaining maximum prediction accuracy was also addressed.

Chapter five is based on the publication:

U.W.A. Vitharana, M. Van Meirvenne, D. Simpson, L. Cockx, and J. De Baerdemaeker. 2008. Key soil and topographic properties to delineate potential management classes for precision agriculture in the European loess area. Geoderma 143:206-215.

In some situations, a variety of ancillary information is available to support detailed soil mapping. However, selecting of the key variables for an identification of potential management zones is not straight forward. The study reported in this chapter was conducted in a loess soil to formulate a procedure for this selection of variables to delineate potential management classes.

Chapter six is presented as two parts. Part I is based on the publication:

U.W.A. Vitharana, M. Van Meirvenne, L. Cockx and J. Bourgeois. 2006. Identifying potential management zones in a layered soil using multiple sources of ancillary information. Soil Use and Management 22: 405-413.

Variation in soil texture has a profound effect on soil management, especially in texturally complex soils such as the polder soils of Belgium. In contrast to the study presented in the preceding chapter, topographic attributes derived from elevation data were of little use for soil prediction in the flat polder landscape. Thus, this research addressed the potentials and weaknesses of EM38DD sensor for the detailed mapping of soil texture and subsequent delineation of potential management zones.

Part II is based on the publication:

U.W.A. Vitharana, M. Van Meirvenne, D. Simpson, L. Cockx and G. Hofman. 2008. Agronomic consequences of potential management zones delineated on the basis of EM38DD measurements. Near Surface Geophysics 6(5): 289-296.

Delineation of potential management zones itself is not adequate to implement site-specific soil management. The agronomic relevance of these zones should also be validated. Thus, in this part, the relevance of the potential management zones

delineated in the preceding section was evaluated for site-specific water and nitrogen management. Finally, the yield differences across management zones under uniform soil management were investigated to identify the potential production benefits from the proposed site-specific soil management practices.

Chapter 7 summarizes the general conclusions of this dissertation, and gives some recommendations for further research.

Chapter 2

Site-specific soil management: Literature review

2.1. Introduction

Being a relatively novel approach, the principles of site-specific soil management are still evolving. This is partly reflected by a range of definitions found in the literature with contrasting ideologies (McBratney et al., 2005). The key concepts of site-specific soil management are often misinterpreted (Taylor and Whelan, 2008). Moreover, the related research findings are being continually reported in peer reviewed journals and conference proceedings. In light of that, the objective of this chapter is to provide a conceptual basis for site-specific soil management with relevant research findings.

2.2. Site-specific soil management

Traditional soil management for crop production ignores the inherent within-field soil variability and considers the agricultural fields as homogenous units. Management practices such as tillage, irrigation and application of agrochemicals are undertaken according to so-called blanket recommendations, i.e. one application rate for an entire field or in some instances even for an entire region. The application rates are usually determined to meet the mean requirement of the field. However, when the within-field soil variation is substantial, such management may result in poor input use efficiencies due to the over-treatment in some parts of the field and under-treatment in others. This eventually leads to waste of inputs causing increased management costs, loss of net economical returns, waste of energy and more importantly environmental problems such as surface and ground water pollution (Robert, 1993). The increasing awareness about sustainable management of soil resources while enhancing its productivity and ecosystem health has strongly motivated to find alternative approaches for the traditional whole-field based soil management.

Site-specific soil management has been evolved as a potential alternative management strategy that markedly progressed since its inception in early 1990s. This allows growers to optimize the soil management practices according to the within-field level soil and crop spatial and temporal variation. For example, an

area of the field showing low levels of a given nutrient would receive higher than the average rate of fertilizer, while an area showing high nutrient levels would receive lower or no fertilizer input. The principle of tailoring soil management practices to the site-specific needs is far from new. When, soil management practices were carried out manually in smaller fields than the ones existing today, farmers had a considerable opportunity to understand the within-field soil variation. In these circumstances, fields were managed on site-specific basis, for example, little extra manure was added to the spots that looked infertile. However, with the enlargement of fields, intensive production and mechanization in the latter half of the last century, it was not possible to take within-field variation into account for soil management due to insufficient technology. Sylvester-Bradley et al. (1999) mentioned that the advances in technology in four main areas: global positioning systems for georeferencing, soil and crop sensing, computing and variable rate application of inputs are the main contributing factors for the initiation of site-specific soil management applicable for present day crop production.

Definitions of site-specific soil management are numerous. Often, definitions are provided within the context of precision agriculture, which encompasses the application of site-specific management practices for a range of agricultural enterprises such as dairy farming through viticulture to field crop production. Some of them not necessarily include soil management practices. McBratney (2005) provided a generic definition: “a kind of agricultural system that increases the number of (correct) decisions per unit area of land per unit time with associated net benefits”. In order to make it more applicable for site-specific soil management, this definition can be narrowed down to “matching resource application and agronomic practices with soil attributes as they vary across the field”. Site-specific soil management practices are called as the ‘differential’ management of within-field variation as opposed to the ‘uniform’ management undertaken in traditional management (Figure 2.1).

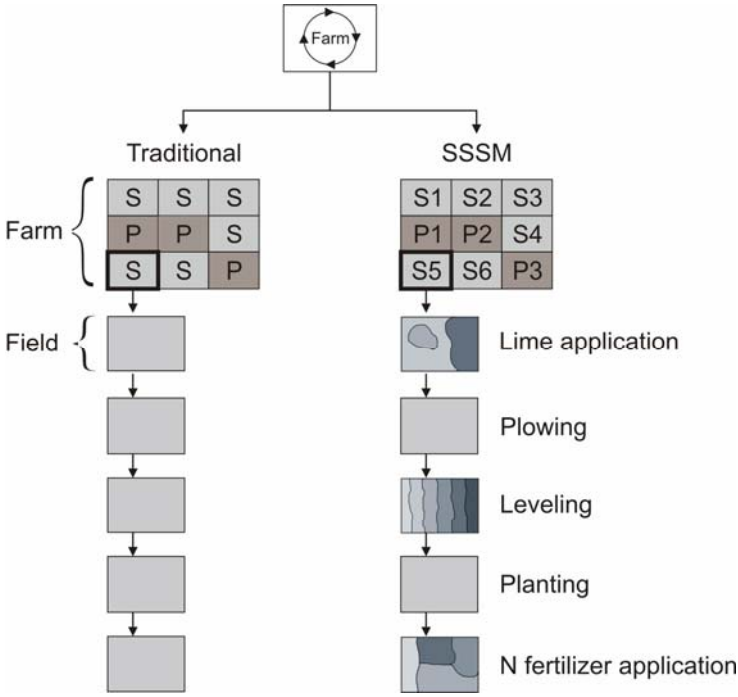

Figure 2.1. Site-specific soil management (SSSM) versus traditional soil management. In the traditional approach all fields planted to the same crop (e.g., sugar beet (S) or potato (P)) are managed uniformly, thus applications do not vary much between and within-fields (left side). In the site-specific approach, each field planted to the same crop may be treated differentially (e.g., P1 is different from P2). Also, some operations can be varied within-fields (right) (source: Dobermann et al., 2004).

2.2.1. Benefits of site-specific soil management

The success of any novel approach depends upon its benefits. Since site-specific soil management is still in its evolving phase, the progress depends on the scientifically validated evidences for the benefits claimed for the concept (Stafford, 2000). The benefits of site-specific soil management can be categorized into two areas: profitability for the producers and ecological and environmental benefits to the public. Mostly these benefits are inter-related. Dobermann et al. (2004) listed four requirements to be fulfilled to achieve the benefits of site-

specific soil management, namely (i) a significant spatial variation exists at the within-field scale that can be measured accurately, (ii) the influence of this variation on management practices is significant, predictable and less confounded by non-soil related factors, (iii) site-specific application of inputs can be done accurately, and (iv) the extra cost is kept low.

Profitability

Site-specific soil management allows farmers to change the application rate and timing of water, fertilizer and other agrochemicals within-field. Therefore, a profit increase can be originated from the higher yields with higher inputs for some parts of the field given the value of the extra yield outweighs the cost of the extra inputs and the technology, or where the cost savings in input exceed the reduced value of the yield either through the achievement of the same yield but with less inputs or a lower yield with less input. Site-specific application of lime has been proven to be successful in clay-pan soils of the United States (Wang et al., 2003). Raper et al. (2007) evaluated the site-specific tillage operation, where the depth of tillage was adjusted to match the depth of compaction. Site-specific sub-soiling practice produces corn and cotton yields equivalent to those produced by uniform deep tillage while saving the cost of fuel for the tillage operation. Alimardani et al. (2007) reported an energy saving of 50 % and a fuel saving of 30 % by site-specific tillage as compared to uniform-depth tillage in an agricultural filed dominated with loamy sand. Site-specific irrigation management is more likely to be economically viable for high-value crops. A field study carried out by King et al. (2006) demonstrated the economic benefits of site-specific irrigation management on potatoes, where it increased the total yield, marketable yield, and gross income relative to uniform irrigation management. The economical advantages of differential nitrogen fertilizer applications in Western Australia was reported by Robertson et al. (2007). The results of a long term (1996 to 2001) site-specific management project conducted in UK indicated a considerable efficiency of cereal production through the differential application of N (Godwin et al., 2003a). Depending upon field and the year, between 12 % and 52 % of the area

under the investigation responded positively, with an overall benefit of €36/ha. Maleki et al. (2008) reported a 336 kg ha^{-1} increment of maize yield through site-specific application of soil phosphorous.

Environment

Water pollution due to the excessive use of agrochemicals is increasingly becoming a major environmental concern among the general public. This has convinced legislators to establish directives in many countries including USA, Australia, UK, Germany and Belgium in order to force farmers to significantly reduce the usage of agrochemicals. Site-specific soil management allows farmers for precise and targeted application of agrochemicals, accurately record all field treatments and transfer of these recorded information with the harvested product (Stafford, 2000). Therefore, these practices not only reduce the environmental impacts from traditional agriculture but also assist in the enforcement of environmental legislations. Moreover, it is likely that through environmental legislations, levies will be introduced for chemical fertilizers and this would make site-specific soil management more attractive to gain profits. Numerous studies have shown the environmental benefits of site-specific management through reductions in nitrogen leaching (Godwin et al., 2003a; Whitley et al., 2000; Wong et al., 2005), run off loss of phosphorus (Lambert et al., 2006; Söderström et al., 2005) and herbicides (Gerhards and Christensen, 2003).

2.3. Site-specific soil management cycle

Site-specific soil management is a system approach which consists of three key components: (i) Monitoring of soil spatial and temporal variation, (ii) analysis of spatial data and (iii) managing variation (Figure 2.2). These components operate as a cycle for the functioning of site-specific soil management as a single system. A seasonal evaluation of the outcome is performed in relation to the specific objectives of the site-specific soil management, e.g., optimizing production efficiency and profits, improved product quality, energy conservation and surface

water and environmental protection. This is to fine tune the system by making necessary management changes.

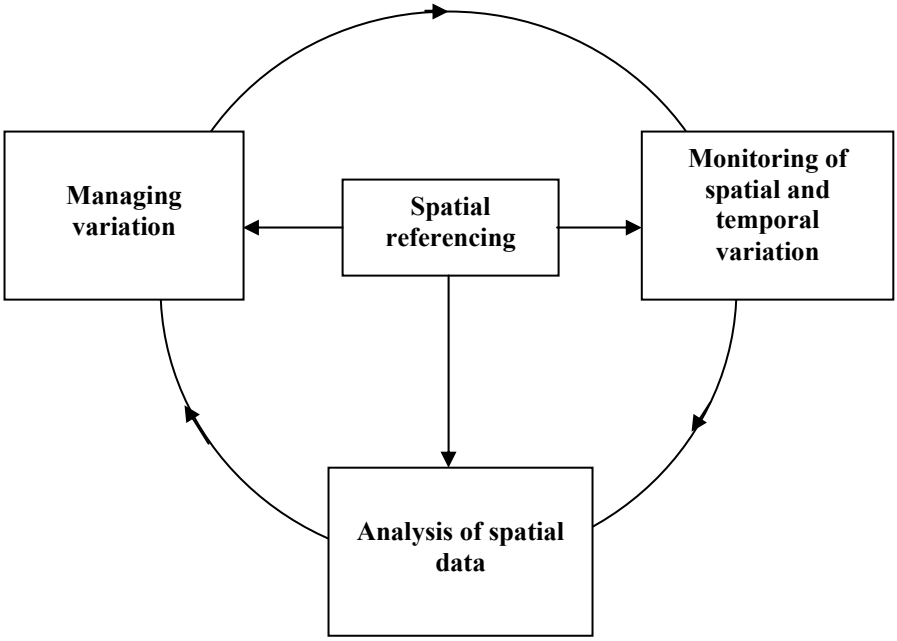

Figure 2.2. The components of site-specific soil management cycle.

The Global Positioning System (GPS) plays a central role in all site-specific soil management components by providing accurate information of the location. In the early days of site-specific soil management, use of GPS for geo-referencing was unreliable and expensive. The inaccuracies of measurements (with errors of ± 10 m horizontal and ± 30 m vertical spaces) were resulted by the intentional downgrading, also known as Selective Availability (SA) of satellite signals by the US Department of Defence (Langley, 1997). The SA was disabled in mid 2000, allowing the use of commercial GPS with an acceptable positioning accuracy. Since the year 2003, the satellite based GPS signal corrections became available. This includes the correction signals transmitted by three different satellite systems covering a large part of the earth: WAAS (Wide Area Augmentation System) by

US, EGNOS (European Geostationary Navigation Overlay Service) by the European Community and MSAS (Multi-Functional Satellite Augmentation System) by Japan and other Asiatic countries. These systems provide a GPS accuracy of 1 to 2 m for horizontal space free of charge enabling precise mapping of within-field variation and subsequent management. Moreover, the maturity of GPS hardware technologies have reduced the weight and prices of receivers dramatically.

2.3.1. Monitoring of the soil spatial and temporal variation

Monitoring of within-field spatial and temporal variability of soil properties is the initial and an essential step in the site-specific soil management. The national polygon-based soil maps are the commonly available sources of soil information. However, most of these maps are not at the appropriate level of accuracy and in sufficient detail as required for within-field level soil management. Therefore, compilation of detailed and quantitative soil data bases is usually a prerequisite to implement site-specific soil management.

On the basis of the frequency of sampling, Bouma et al. (1999) identified two types of soil information required for site-specific soil management (Figure 2.3). The first type represents the spatial variation of primary soil data and topographic data. This temporally stable information is usually characterized once for a particular field. The second type of soil information includes soil fertility and hydraulic data which are temporally unstable and required to obtain regularly to guide soil management decisions.

Initial studies on site-specific soil management were based on data acquired by grid sampling in the field. The optimum grid spacing is a function of spatial variability in the field, which is often unknown priori. This approach have had limited success due to the cost constraints and insufficient characterization of the spatial variability. For example, to map soil nutrient patterns accurately, Webster and Oliver (1992) recommended a sampling distance of less than 40 m. Sylvester-Bradley et al. (1999) argued that this entails over six times as many samples as the

sampling procedures generally adopted in the European countries. However, recent technological advances in soil and crop sensing have largely minimized field sampling and laboratory analysis procedures to acquire soil spatial information. At present a range of sensing methods are being used to characterize the within-field soil variation. These sensors are capable of providing either direct or indirect measurements of soil properties.

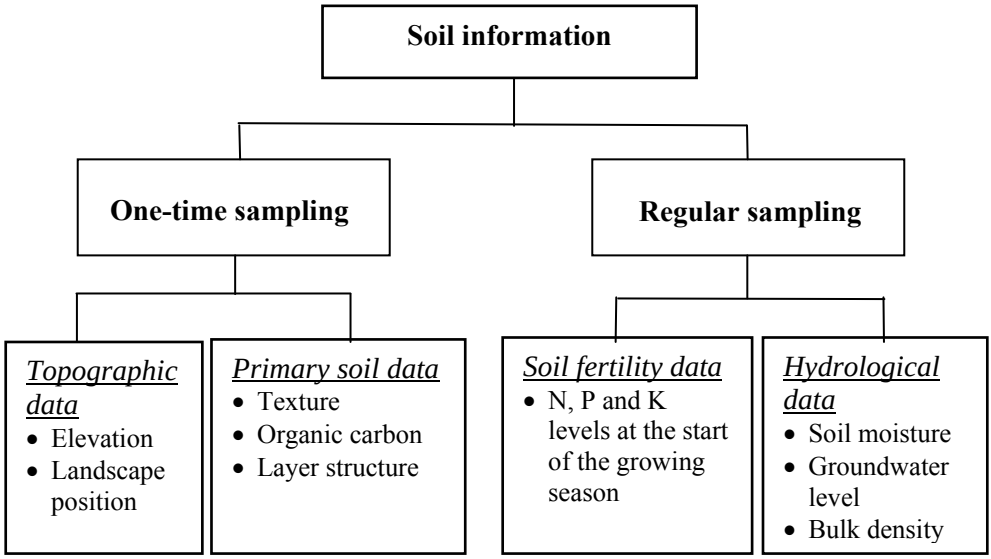

Figure 2.3. Soil information needs for site-specific soil management**.**

2.3.1.1. Invasive and non invasive soil sensors

Soil information obtained using invasive and non-invasive (proximal) sensors have proven to be useful for monitoring spatial and temporal variability of soil. Invasive methods require a direct contact with the soil to obtain measurements, whereas the non invasive methods provide estimates of soil properties at various depths without a direct contact. Both types of sensors can be inter-phased with a GPS receiver and attached to a tow-vehicle to obtain geo-reference measurements on-the-go. The main advantage of soil sensors lies in the fact that a large number of observations can be taken with little field sampling effort. Such exhaustive soil

information serves as a proper start for an accurate characterization of soil variation. Some of these sensors are capable of directly measuring the soil properties and others provide ancillary information (or secondary information) to estimate soil properties through (non) geostatistical techniques. Adamchuk et al. (2004) identified several types of soil sensors on the basis of their measurement principle:

- electrical and electromagnetic sensors measure the apparent electrical conductivity of the soil,
- optical and radiometric sensors make use of spectral scanners to detect the level of energy absorbed or reflected by the soil particles,
- mechanical sensors measure forces resulting from a tool engaged with the soil,
- acoustic sensors quantify the sound produced by a tool interacting with the soil,
- pneumatic sensors assess the ability to inject air into the soil,
- electrochemical sensors measure soil chemical properties.

These sensors are at various stages of development and commercialization. A comprehensive review about the current status of the soil sensors belong to each category is given by Adamchuk (2008; 2004).

Soil apparent electrical conductivity (EC_a) sensing is one of the widely applied techniques in site-specific soil management. Geospatial measurements of EC_a are reliable, quick, easy and cheap to obtain. Nevertheless, the commercialization of the EC_a measurement equipments has made it popular among researchers, agricultural planners and farmers. According to Corwin and Lesch (2003) three pathways of current flow inside the soil system contribute to the EC_a. These are: (1) via salts in the soil liquid phase occupying large pores (2) in moist soils via the exchangeable cations associated with clay minerals, and (3) via the solid phase through soil particles in direct and continuous contact with one another. The electrical conductivity of these pathways is largely influenced by a number of soil properties: soil salinity, clay content, cation exchange capacity, clay mineralogy,

pore size distribution, soil moisture content and temperature. This creates the potentiality of EC_a measurement to predict the soil property that dominantly influences the measurements. A number of studies have addressed the potential of EC_a to predict soil textural fractions (Domsch and Giebel, 2004; Vitharana et al., 2006; Weller et al., 2007). The suitability of EC_a as a surrogate for the available water capacity was explored by Brevik et al. (2006). Further, EC_a measurements were used indirectly to infer the exchangeable Ca and Mg, cation-exchange capacity (McBride et al., 1990), groundwater recharge (Cook and Kilty, 1992) and soil drainage class (Kravchenko et al., 2002). Anderson-Cook et al. (2002) and James et al. (2003) used EC_a to delineate soil type boundaries.

Two types of sensors are currently available for the field measurement of EC_a: electrical resistivity (ER) and electromagnetic induction (EMI) based sensors. Both techniques are well suited as a soil information gathering tool because their volume of influence covers the rooting depths of many crops. These measurements are less influenced by the very short scale soil variation (< 1 m) which is of little importance for management.

The basic configuration of ER based sensor is referred to as a Wenner array, which has four electrodes inserted into soil at equal distances. An electrical potential difference is applied to the two transmitter electrodes (current electrodes) and that results in an introduction of an electrical current in the soil. Subsequently, the EC_a is determined through the soil resistivity measured by two receiver electrodes (potential electrodes). The ER sensing concept forms the basis of a widely used commercial product, the Veris 3100 (Veris Technologies., Salina, USA). This mobile measuring system (Figure. 2.4a) uses six rolling coulters for electrodes and simultaneously generates shallow (0–30 cm) and deep (0–100 cm) measurements of EC_a (Lund et al., 1999). A non invasive ER sensor called OhmMapper (Geometrics Inc., San Jose, USA) is currently available, but its potentials for the prediction of soil properties are not well explored.

The EMI based sensor uses the principle of the propagation of alternating electromagnetic fields through the soil to measure EC_a. Therefore, there is no need

of direct contact between the soil and the sensor to obtain measurements. The most often used EMI based EC_a sensor is EM38 (Figure 2.4b) (Geonics Ltd., Mississauga, Ontario, Canada). The other commercialized EMI instruments include, EM31 and EM34 from the same manufacturer, the DUALEM instruments (DAULEM Inc., Milton, Ontario, Canada) and GEM instrument series (Geophex Ltd., Raleigh, NC, USA). Those sensors show differences in depth densities and physical construction, but the operating principle is common to all. Therefore, details of the operating principle of EMI sensor category is provided in the materials and methods chapter using the EM38 sensor as an example, which was used throughout this research.

Each of the commercial EC_a sensors has operational advantages and disadvantages. The Veris 3100 is a heavy equipment and requires a tractor or truck to pull it through the field limiting its use to firm and unplanted fields. This sensor is not suitable to obtain measurements in stony soils. The lightweight EMI based sensors require little power to pull through the field and make it possible to collect data under wet or dry soil conditions. Unlike the ER sensor, the instrument operation is not restricted by internal nature of soil materials. Also, it is possible to collect data even during crop growth. Generally, the EMI sensors require the user to complete a daily calibration procedure before use. However, the newest range of EMI sensors from DUALEM contains an automatic calibration procedure. Changes in ambient conditions such as air temperature, humidity, and atmospheric electricity (spherics) can affect the stability of EM38 measurements. Sudduth et al. (2001) reported a drift of EMI based EC_a measurements which was not consistently related to ambient conditions. They suggested that drift compensation be accomplished by a calibration transect or frequent recalibration of EMI sensors. In contrast, the ER sensor requires no user calibration and the measurements are less influenced by ambient conditions

A noticeable improvement can be seen in the development of on-the-go optical soil sensors that are capable of measuring top soil (0 – 20 cm) spectral reflectance at visible (VIS; 400-700 nm) near-infrared (NIR; 700-2500 nm) spectral ranges.

Viscarra Rossel et al. (2006) reported that the soil spectral reflectance at the mid-infrared range (MIR; 2500-25,000 nm) is capable of providing accurate predictions of soil properties such as pH, textural fractions, organic C and P. However, development of on-the-go MIR sensing systems has not been done to date, due to the complexities and expensiveness of the instrumentation. Investigations have revealed strong correlations between NIR reflections and organic C (Shonk et al., 1991), soil moisture, total C, total nitrogen, pH and Mehlich 1 Phosphorous (Christy et al., 2003; Maleki et al., 2008; Mouazen et al., 2007). An on-the-go NIR soil sensor has been commercially implemented (Figure 2.4c) mainly for the research purposes (Christy, 2008). The shank mounted spectrophotometer of this sensor measures the reflectance of soil at wavelengths ranging from 950 nm to 1650 nm and at a depth of approximately 7 cm below the soil surface. The high cost of the equipment, difficulty to operate the fragile sensor systems in fields with gravel or stones and also the need of tedious calibrations to predict soil properties are some of the drawbacks in the optical on-the-go soil sensors. However, attempts have been made to generate global (Brown et al., 2006) and regional level (Mouazen et al., 2007) models to predict range of soil properties using VIS and NIR sensing.

The proximal sensing of gamma radiation from the top 30 – 50 cm of soil has been tested for inferring the variation of soil properties. Viscarra Rossel et al. (2007) used hyperspectral gamma radiation measurement with on-the-go gamma-ray spectrometer to predict clay, coarse sand and Fe contents in the 0-15 cm soil layer and pH and coarse sand contents in the 15-50 cm soil layer.

The mechanical sensors also have been tested to acquire spatial information about soil mechanical resistance and compaction (Andrade-Sanchez et al., 2007; Mouazen et al., 2005; Sirjacobs et al., 2002). However, none of these devices are commercially available. Acoustic and pneumatic sensors have been investigated for determining several soil physical properties such as the structure and bulk density. Currently, these relationships are inadequately understood and additional research is needed. Several investigations have been conducted to use the soil

sensing systems with ion-selective electrodes or ion-selective field effect transistors in order to determine the soil nutrient availability and pH. Commercial introduction of the automated soil pH measurement system (Veris Technologies, Kansas, USA) is an outcome of the several years of research (Figure 2.4d). The sampling device of this sensor scoops a small amount of soil, presses it against an electrode to record the reading and then a cleaning mechanism rinses the system to prepare for the next sample.

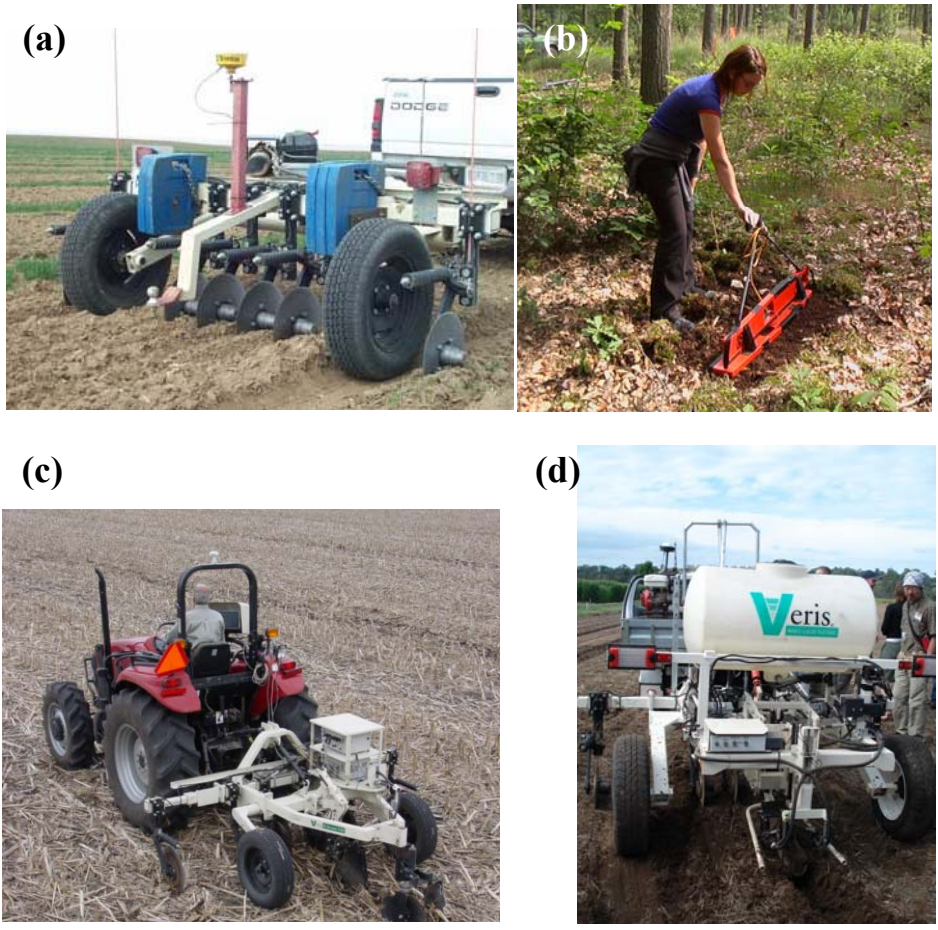

Figure 2.4. Soil sensors for site-specific soil management (a) electrical resistant based EC_a sensor (b) electromagnetic induction based EM38 sensor (c) NIR sensor and (d) pH sensor.

Adamchuk et al. (2007) concluded that the use of this sensor can significantly increase the accuracy of soil pH maps and therefore increase the profitability through site-specific lime application.

2.3.1.2. Yield monitoring

Monitoring of crop yield has become increasingly popular due to the commercialization of combine mounted yield sensors for grain crops. The spatial variation revealed by yield monitoring brings two messages: (a) substantial soil productivity differences exist within-field and (b) under or over utilization of the crop inputs in some parts of the field. These two pieces of information has convinced producers that uniform soil management for crop production may not always be appropriate. Therefore, yield maps are often considered as an eye opener to adopt site-specific soil management.

The yield monitors measure the volume or mass-flow rate of the harvested crop and then integrate this flow rate to generate a time-periodic yield (kg s^{-1}) record. By determining the area harvested by the combiner during a particular time interval (i.e. distance travelled x swath width), the onboard field computer records the yield in units of mass per unit area (e.g. kg ha^{-1}). The onboard GPS receiver provides location information. The operator can control the measurement density by regulating the driving speed and data recording frequency (Birrell et al., 1996). These data are processed to generate yield maps that depict the spatial patterns of production potential. The yield monitors for grain crops are now in a technologically very advanced status. Also, yield monitor systems for many other crops including cotton (Sui et al., 2004), peanut (Rains et al., 2005), potato (Persson et al., 2004), sugar cane (Magalhaes and Cerri, 2007), sugarbeet (Hennens et al., 2003) and tomato (Pelletier and Upadhyaya, 1999) have been researched.

Theoretically, yield maps could reflect partially the within-field soil variation. Therefore, numerous studies have used either single or multiple years of yield maps as a guide for site-specific soil management through the differential

application of crop inputs (Lark and Stafford, 1997; Stafford et al., 1996). Sudduth et al. (1996) observed that yield variation largely corresponds to landscape and soil physical properties related to water distribution and water availability rather than to the soil nutrient status. However, it is often highlighted that the relationship between the spatial variation of crop yield and soil productivity is complicated by other factors influencing yield, such as pest and weed infestations, the weather conditions that prevailed during a particular growing season and even the field management practices. Therefore, Boydell and McBratney (2002) advocated that at least five to seven years of yield maps are required to infer reliably the variability of soil properties through yield maps. However, such long sequences of yield maps are rarely available in European countries, where yield mapping is not a routine practice. On the other hand, the yield monitors can cause considerable errors in estimation of yield due to their improper calibration, mass or flow sensor errors, variations in combine speed, noise introduced by machine vibration and varying terrain. Therefore, a substantial pre-processing effort is required in order to extract information from yield monitor data (Simbahan et al., 2004).

2.3.1.3. Remote sensing

Remote sensing of electromagnetic radiation reflected by surface soil provides a great deal of information on the variation of the top few centimetres of soil. Thus, the images of bare soil, captured either from an aircraft or satellite platforms have been widely used to predict the soil variability (Moran et al., 1997). The majority of these studies have focused on the reflective region of the electromagnetic spectrum (300 – 2800 nm). Multispectral airborne (green, red, near infrared) and satellite images (SPOT and LandsatTM) have been used as covariates for predicting soil particle size distribution with varying levels of success (Barnes and Baker, 2000; Zhai et al., 2006). Several researchers have related soil organic carbon variation to soil reflectance data (Chen et al., 2005; Henderson et al., 1992; Sullivan et al., 2005). Remotely sensed microwave data (passive and active) have been employed to characterize the spatial distribution of soil moisture (Mattikalli et al., 1998; Simmonds and Burke, 1998). Microwave imagery has the strong

advantage of being able to penetrate clouds, which is extremely useful when images are captured from high altitude. Moreover, soil moisture has been correlated to visible and thermal infrared reflectance of bare soil fields (Scott et al., 2003). Despite the relations among soil reflectance and soil properties, the utility of remotely sensed images have shown limited success for site-specific soil management. The main reason is its inability to infer the soil variation throughout the root zone. Moreover, to characterize within-field soil variation, it needs images with high spatial resolution. Often such high resolution images are too costly to obtain. The changes in surface tillage condition, moisture content, atmospheric effects, observation conditions, vegetation cover and plant residue may influence the reflectance properties, thus weakening the spectral responses due to the target soil properties (Zhang et al., 2002). Therefore, timing of the acquisition of satellite images determines its usability. The user has little control over the timing of the satellite image acquisition.

2.3.1.4. Crop sensors

The response of crops to differences in soil conditions can also be used as indirect information to characterize within-field soil variation. The spatial variation of crop cover has been researched to predict the soil nutrient deficiencies, soil moisture availability and salinity (Moran et al., 1997). The advantage of this method over the bare soil imagery is that the crop response integrates the soil conditions of the entire root zone. Recently, a number of field vehicle mounted proximal crop sensors have been developed to deliver crop information on-the-go. The designing focus of the majority of these sensors was to provide crop information just before the soil nutrient applications. Recent commercialization of the tractor mounted Yara N-sensor (Yara International ASA, Norway) is a typical example. This sensor uses the leaf reflectance between the spectral range of 720-740 nm as an indicator of crop N status and relates to the N demand. Berntsen et al. (2006) reported promising benefits of N fertilizer management with the Yara N-sensor. Recently, an on-the-go mechanical sensor for measuring crop biomass has been

developed by Ehlert and Dammer (2006) and they used it to guide differential application of nitrogen. Evans et al. (2000) used an array of irrigation machine mounted infrared thermometers to measure the canopy temperature to control irrigation events. Recent developments of crop sensors are well documented in the proceedings of the Precision agriculture conferences held in the recent past and it is likely that some of them will reach the commercial market in the near future.

2.3.2. Analysis of spatial data

The first step of site-specific soil management generates large amounts of geo-referenced data. These data should be stored and analyzed in order to identify the within-field variation and to guide differential soil management practices. Therefore powerful data storing and processing tools play a crucial role in site-specific soil management. Geographical information systems (GIS) provide data base management tools to organize the data, both in spatial and attribute space, in a form which permits to be stored efficiently and retrieve quickly for updating and analysis. Data sets must also be subjected to an exploratory data analysis to identify outliers and measurement errors. Nevertheless, the spatial data gathered in different sampling densities are needed to be interpreted, compared and integrated to deduce information. This can be done only after bringing point data into continuous data layers or maps with a common grid configuration. This is accomplished by interpolating point data to a user defined grid using an appropriate prediction technique. Most GIS systems provide set of tools that can be used for spatial data analysis and integration (Burrough and McDonnell, 1998). The statistical techniques used in spatial data analysis will be discussed in the next chapter within the context of the research methodology.

2.3.3. Managing variation

Once the information about the within-field variation is known, the next steps are the use of this information to determine the appropriate site-specific management practices and their implementation. Decision supporting tools allow land managers

to decide on the appropriate site-specific management strategies. McBratney et al. (2005) identified that the development of decision support tools is one of the key areas in site-specific soil management needing lots of research input. A multidisciplinary team effort is a prime requirement in this regard. Currently available decision support systems such as WHEATMAN, COTTONLOGIC and APSIM are being used at within-field level assessment of decision. The potentials of crop models and scenario analysis have also been tested to identify optimal within-field management strategies (de Jonge et al., 2007; Miao et al., 2006; Thorp et al., 2007).

Managing the soil variability can be accomplished either by a sensor based or a map based approaches (Adamchuk et al., 2007; Morgan and Ess, 1997; Zhang et al., 2002). The sensor based approach (Figure 2.5a) measures the soil variation using a mobile sensor and controls the management practices like application rates of inputs simultaneously (in real time). By detecting and managing the within-field variation on-the-go, the need for a GPS is eliminated and post processing soil data for management decisions is greatly reduced. Generally, this approach is not popular because the sensing equipments are too expensive, not sufficiently accurate or not yet available (Chang et al., 2003). Nevertheless, the operator has less chance to detect erratic measurements and consequent management errors. The within-field variability and the application rate data are not essentially recorded in the sensor based approach. But, these data have a direct importance to evaluate the site-specific management process. Recently, Maleki et al. (2008) have successfully implemented a sensor based soil Phosphorus management system for the maize crop. Further, by comparing the uniform management, they have reported an improvement in the use efficiency of phosphorus fertilizers and also an increment of maize yield. The map based approach (Figure 2.5b) on the other hand, uses the spatial variation information obtained through field sampling or sensing techniques to delineate within-field subunits called management zones. Subsequently, the management options for each zone are defined on the basis of decision support systems. The result is a set of management maps, each providing application rates of different management inputs at every location of the field.

Finally, this information is fed to the data processor of the farm machinery employed with a variable rate applicator.

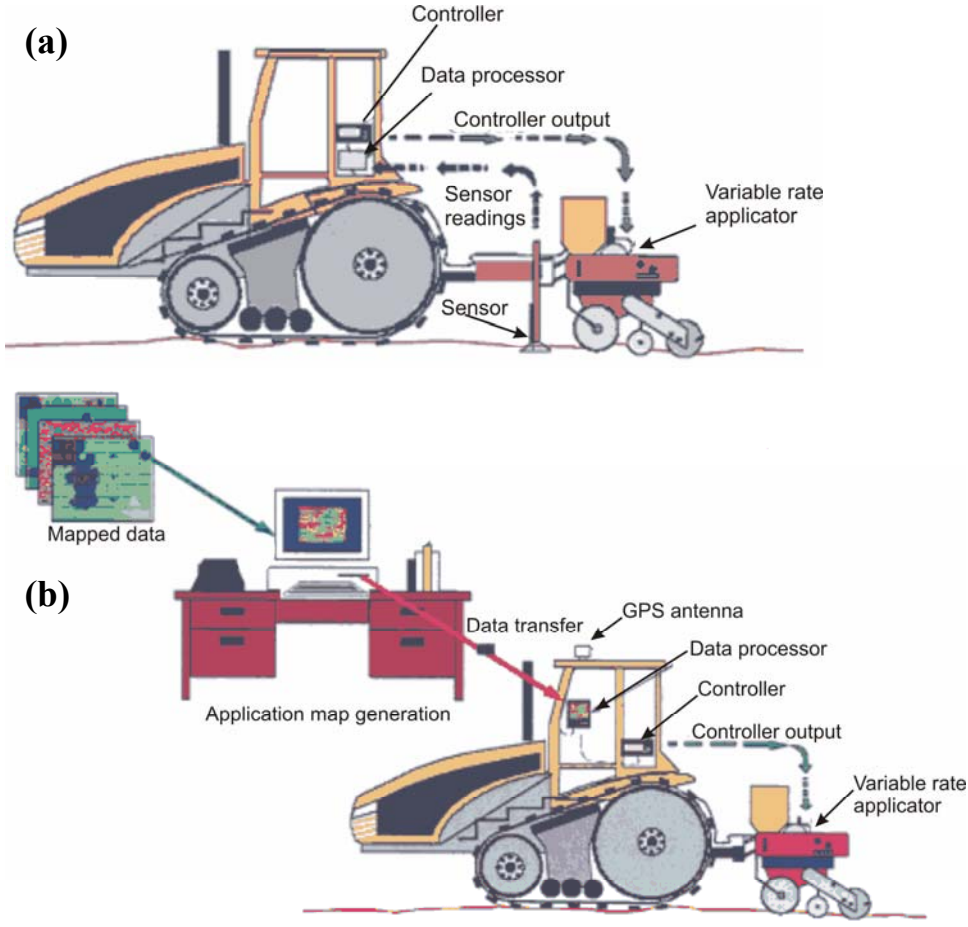

Figure 2.5. (a) The sensor based and (b) map based approaches for managing within-field soil variation.

In the map based approach, a GPS receiver is essential to synchronize the information available in the maps and the variable rate applicator in order to change the application of inputs on-the-go. Additionally, sub-meter accuracy

information about the application rates are recorded for the future use. The map based approach is currently the most evolved approach for site-specific soil management.

Management zones

Management zones are within-field subunits, each having relatively a homogenous combination of soil properties that identifies a single or range of management strategies. Bouma et al. (1999) recognized the management zones as areas of land acting significantly different in terms of the soil functions and solute movement. Therefore, management zones can be considered as decision units in site-specific soil management. Differential management strategies can be variable rates of fertilizer and amendments like lime, tillage or even sub soiling. Zhang et al. (2002) indicated that the information needed for the management zone delineation of a particular field may be different for different management practices.

"Management zone" and "management class" are often used in site-specific soil management research as interchangeable terms. According to Taylor et al. (2007) these terms are needed to be used with caution. They pointed out that a management class is the area to which a particular agronomic treatment may be applied, whereas a management zone is a spatially contiguous area to which a particular treatment may be applied. Therefore, a management class may consist of a number of zones, whereas a management zone can belong only to one management class.

A variety of data layers, including soil property maps, topographic attributes, soil drainage classes, proximally and remotely sensed soil information, yield maps and farmer's knowledge have been used with varying success to delineate management zones (Chang et al., 2003). Literature reports about three main approaches of management zone delineation in relation to the spatial information used. The first approach uses a single information layer such as a soil nutrient concentration or pH to identify management zones, targeting differential management of a single crop input. This approach demands a generation of variability maps at every

growing season. The second approach relies on a sequence of yield maps as the only information to delineate management zones (Boydell and McBratney, 2002; Brock et al., 2005; Lark, 1998). Kitchen et al. (2005) highlighted that terms "productivity zones" or "yield zones" may be more appropriate synonyms and that less management attention can be given to the poor yielding zones while optimally managing the medium to high yielding zones. Robertson et al. (2007) mentioned considerable financial gains through this approach. Further, some researchers have tried to find out soil factors underlying the within-field production potential in order to decide about best management practices (Cox and Gerard, 2007; Lark and Stafford, 1997; Ping et al., 2005). However, since the relationship between the spatial variability of crop yield and soil variability is often very complex (McBratney and Pringle, 1997), this approach often considers that the within-field yield variation occurs due to a single primary factor or several interacting factors. The main drawback of yield based management zone delineation is the need of multiple years of yield data (Dobermann et al., 2003) to delineate stable zones. Nevertheless, yield maps may not necessarily reflect soil variation since excessive application of crop inputs can mask the influence of soil variation on the yield. For example, within-field areas which are susceptible for nitrogen leaching may not appear in the yield maps when an excessive application of nitrogen has been applied. The third approach uses a combination of data layers, namely soil attributes, yield data and the topography to delineate management zones (Fraisse et al., 2001; Frogbrook and Oliver, 2007; Taylor et al., 2003; Vrindts et al., 2005). The selection of suitable data layers is often done on the basis of expert knowledge about the soil genesis of the area and their relevance to site-specific soil management.

Managing variability through the management zones should bring the expected objectives of site-specific soil management. Therefore, generally the delineated management zones are treated as potential management zones till their usability is evaluated and being confirmed.

Numerical methods for management zone delineation

A number of procedures have been tested to identify the boundaries of management zones based upon single or multiple layers of input data. These procedures range from the simple map overlaying (Kitchen et al., 1998) and hand drawing (Fleming et al., 2004) to the more widely used multivariate unsupervised cluster analysis (Boydell and McBratney, 2002; Vrindts et al., 2005). Unsupervised cluster analysis techniques recognize the natural grouping of input data in a multi-dimensional attribute space (Jensen, 1996). Fraisse et al. (2001) used the iterative self-organizing data analysis technique (ISODATA) to define management zones. To obtain better results with ISODATA, the data sets should have similar variances and follow an approximate normal distribution. These two requirements have restricted its popularity. The fuzzy *k*-means unsupervised classification has become very popular for management zones delineation due to its capability of handling data sets with different distributions. Moreover, it provides different indices to find out optimum number of classes suit for the data sets. A management zones delineation software called Management Zone Analyst (MZA) has been developed by Fridgen et al. (2004) on the basis of fuzzy *k*-means unsupervised classification algorithm. The next chapter provides a detailed description of the fuzzy *k*-means unsupervised classification.

2.4. Conclusions

This chapter provided the basic concepts of site-specific soil management. The whole management process can be summarized into a few steps: assessment of the within-field variation, identification of potential management zones and differential management of crop inputs across these zones. The potential and proven economic and environmental benefits have brought an expectation that most of the traditional cropping systems will gradually shift towards site-specific soil management. Moreover, environmental legislation with regard to the minimization and optimal use of inputs and the market pressures for traceability will force producers to seriously consider about site-specific management. Much

of the technology for the identification and the management of variation are in place. But, wide adoption of the site-specific soil management can only be expected upon the application of these technologies under different soil environments and farming conditions.

Chapter 3

Materials and methods

3.1. Introduction

The objective of this chapter is to present the spatial inventory techniques employed in this dissertation to characterise the within-field soil variation and subsequent delineation of the management zones. Firstly, soil sampling procedures, different types of soil information sources and the spatial analysis procedures used in this research are described. Next, an overview of the geology and the soil formation of Flanders is provided. This is to explain the potential causes of the within-field soil variability and also to formulate a basis of the selection of study fields for case studies presented in this dissertation. Finally, an introduction to the national soil map of Belgium is provided to present the currently available sources for the soil spatial information

3.2. Spatial sampling

To understand the within-field soil variability, it is necessary to conduct a spatial survey by taking soil samples at different locations. This section provides a discussion on the sampling schemes used in this research. However, in depth information about sampling procedures can be found in de Gruijter et al. (2006) and Yates (1981).

The term "support" is used in the spatial sampling literature to explain the area or volume of the physical sample on which the measurement is made (Burrough and McDonnell, 1998). For example, if three sub samples were collected and bulked within an area of 2 m x 2 m, the support would then be a square of the same dimensions. If the physical dimension of a sample is negligible compared to the size of the study area, samples can be referred to as point samples. In spatial sampling, it is advised to adhere to a constant support during the entire sampling campaign.

Simple random and grid sampling

When deciding on a sampling scheme for spatial studies, one must create a sampling configuration which satisfies two objectives: to accurately characterize

the spatial variation and to provide adequate information for the estimation (or interpolation) of the values of soil properties at unsampled locations. A distribution of sample locations at a range of distances (from few to some tens of meters) at all the directions is essential for an accurate characterization of the spatial variation (Webster and Oliver, 1990). Precise spatial estimations can only be guaranteed if the sample locations are spatially evenly distributed over the study area. Simple random sampling is one of the often used options, in which sampling locations are selected such that every location of the study area has an equal chance (probability) of being selected. This is achieved by randomly selecting *x* and *y* coordinate pairs using a table of random numbers or a random number generator software. Figure 3.1a shows such a random sampling scheme which consist of 49 samples. Although, this sampling scheme provides clusters of samples facilitating the characterizing of the short and long scale spatial variation, these clusters may be preferentially located in the field causing wrong conclusions on the overall spatial variation. Also, a uniform distribution of sampling locations can not be expected with random sampling. Alternatively, the use of a regular grid sample scheme provides a good spatial coverage, but to characterize the short scale variability the grid spacing should be very small, needing a large number of samples. Note also that the estimation of spatial variation by a regular grid sampling can be biased, if the sampling grid coincides with a regular pattern of land management such as drainage tubes.

Knowing the weaknesses and strengths of both strategies, we combined grid and random sampling schemes to obtain soil information for this research. This was achieved by firstly defining a grid by taking time, financial and laboratory limitations into account. To position the grid in a probabilistic way, the first sampling point was located randomly within the first grid cell. Subsequently, a random sample was added within each grid cell. This was done by superimposing a fine grid on each cell as a reference system and picking an *x* coordinate and a *y* coordinate randomly. This procedure was repeated till all grid cells are assigned with a random sample location. Figure 3.1b provides an example for a random plus a grid sampling scheme.

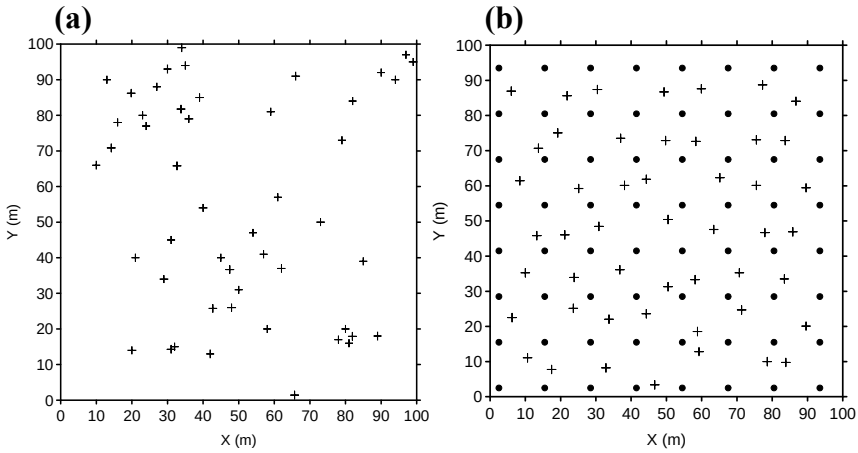

Figure 3.1. (a) Simple random sampling scheme of 49 locations and (b) grid sampling configuration (grid spacing of 14 m) with added couple random sample located within each grid cell (crosses and dots represent random grid samples, respectively)

Sampling for model calibration

In the site-specific soil management studies, it is often needed to obtain soil observations to establish the relationships between targeted soil variables and ancillary information like EC_a to use them as predictor variables. The potential management zones may also be sampled for further characterization to decide on management options. In both instances, the sample configuration should be decided in a way to represent the feature space of ancillary information, rather than optimizing the coverage of geographical space.

One of the approaches is the stratified random sampling (Webster and Oliver, 1990). Here, the study area is divided into few strata on the basis of the variation of the ancillary information and then within each stratum a number of sample locations are randomly identified. The potential management zones are then considered as different strata. However, this approach does not guarantee the full coverage of the attribute space. Consequently, the relationship established may not be adequately representing the data range of the ancillary information.

Purposive sampling is another widely used approach (Bianchini and Mallarino, 2002; Lund et al., 1999). A purposive sample is a sample which is selected by the researcher purposively or subjectively. The researcher attempts to obtain a sample that appears to be representative of the ancillary information and will try to ensure that the range of the variable values is included. The main advantages of this method are: sampling cost can largely be reduced by selecting a few but representative samples and the background knowledge about the field variability can be incorporated when the sampling configuration is decided upon. However, the use of this method is not convenient when samples have to be selected on the basis of several layers of ancillary information. Therefore, Minasny and McBratney (2006) introduced a sampling method called conditioned Latin hypercube sampling. This is a stratified random procedure that provides an efficient way of sampling variables from their multivariate distributions. This sampling approach considers that distributions of multiple variables (*p* variables) are represented as *p* dimensions of a Latin hypercube. Then a sample collection of size *n* from multiple variables is randomly drawn such that for each variable the sample is marginally maximally stratified. Also, this procedure ensures that the selected samples exist in the real world. A sample is maximally stratified when the number of strata equals the sample size *n* and when the probability of falling in each of the strata is n^{-1}. The conditioned Latin hypercube sampling procedure can also be used when only a single ancillary variable is available (see section 4.6.3.1).

3.3. Selection of soil variables and laboratory analysis

The within-field variation of four stable soil properties namely, texture, pH and organic C and $CaCO_3$ content were investigated in study areas chosen for this research. The relevance of these temporally stable soil attributes for site-specific soil management was the basis of their selection (Bouma et al., 1999). Soil texture is a physical property which has a direct effect on porosity, water, heat and nutrient fluxes, water and nutrient holding capacity and the soil structural form and stability. The organic C content represents the soil biological status and also interacts with soil texture influencing its related characteristics. Nevertheless the

within-field variation of organic C can considerably affect the inherent nutrient supply capacity of the soil. Thus, soil texture and organic C content are two key inputs of the decision support tools to determine the soil management practices such as nutrient application, irrigation and land preparation. Also information about the variation of $CaCO_3$ and pH is needed to evaluate the chemical status of a soil and direct site-specific lime applications.

3.3.1. Analysis of soil texture, organic carbon and $CaCO_3$ content

Soil textural analysis was performed using the pipette method following the procedure described by Gee and Bauder (1986). Twenty grams of air dried soil was treated with HCl to destroy carbonates. Subsequently, the organic materials were destroyed by heating the soil sample with H_2O_2 (30 %) at 70 ^{0}C until the reaction stops. The sample was washed with distilled water for three times to remove the excess HCl. After that, a mixture of sodium hexametaphosphate ($(NaPO_3)_6$) and sodium carbonate (Na_2CO_3) was added to disperse the soil particles. The sand fraction was separated by wet sieving through a 50 µm sieve and weighed after oven drying. The remaining clay and silt fractions (0 to 50 µm) were taken into a one-litre volumetric cylinder and volumerized using distilled water. Immediately after thoroughly shaking the soil solution, a suspended sample consisting of silt and clay fractions was pipetted out at room temperature and oven dry weight was determined. A sample of clay in the soil suspension was pipetted out after allowing the silt fraction to settle for 6 hrs and 31 minutes at 29 ^{0}C. The oven dry weight of the clay fraction in the pipetted sample was determined. The silt content was calculated by subtracting the weight of clay fraction from the dry weight of the firstly pipetted sample. Subsequently, the percentage sand, silt and clay fractions were calculated.

The organic C content was determined by the Walkley and Black method described by Nelson and Sommers (1996). One gram of the soil sample was treated with potassium dichromate ($K_2Cr_2O_2$) and H_2SO_4, in order to oxidize the organic matter. Upon completion of the oxidation phase, the unused or excess

dichromate ions ($Cr_2O_7^{-2}$) were determined to compute the organic C content. Therefore, the digestate was back titrated with ferrous sulphate ($FeSO_4$). Since the mean recovery of organic C by this method is 76 % (Walkley and Black, 1934), a correction factor of 1.33 was applied to calculate the organic C content (%). The calcium carbonate content was obtained by treating 1 g of soil with H_2SO_4, and subsequent back titration of the unused H_2SO_4 with NaOH.

3.3.2. pH-KCl

Soil pH-KCl was determined by mixing 10 g of air dried soil with 25 ml of 1M KCl. After 10 minutes pH-KCl was measured with pH meter.

3.4. Ancillary information

Two sources of ancillary information were consistently used in this research, namely EC_a and elevation. Therefore, the purpose of presenting the following sub sections is to provide a theoretical basis for their measurement principles and analysis procedures.

3.4.1. Apparent electrical conductivity measurement with EM38DD sensor

Electromagnetic induction based dual-dipole soil sensor, EM38DD was used to acquire EC_a data. The EM38DD sensor consists of two EM38 units fixed perpendicular to each other (see further). A schematic diagram of an EM38 sensor unit is presented in Figure 3.2 showing its construction and operating principle. This sensor unit consists of two electrical coils, a transmitter coil (*Tx*) and a receiver coil (*Rx*), which are embedded in a wooden frame with an inter-coil spacing (*S*) of one meter. Calibration controls and a digital display of EC_a measurements are included in the sensor. Analog data output is provided to allow the measurement to be recorded in a data logger or a field computer through a serial port.

During the operation, the *Tx* is energized with an alternating current with a frequency (*f*) of 14.6 kHz. This creates an alternating primary magnetic field (H_p)

around the *Tx*, which propagates into the soil generating electric fields according to the Faraday's law. McNeill (1980) mentioned that the resulted soil subsurface current flows take entirely horizontal pathways irrespective of the characteristics of the soil mass. Furthermore, the current flow at any point in the soil is independent of the current flow at any other point since the magnetic coupling between the current loops is negligible. These currents, in turn, induce a secondary magnetic field (H_s) in the soil. The induced field is superimposed on the primary field and both H_p and H_s are measured in the receiver coil. McNeil (1980) derived the instrument measurements of EC_a (S m^{-1}) as:

$$EC_a = \frac{4}{\omega \mu_0 S^2}\left(\frac{H_s}{H_p}\right) \qquad (3.1)$$

where H_s and H_p represent the intensities of the secondary and the primary magnetic fields at *Rx* (A m^{-1}), μ_0 is the magnetic permeability of air ($4\pi 10^{-7}$ H m^{-1}), *S* (m) is the inter-coil spacing and ω denotes the angular frequency (rad s^{-1}) of the instrument which equals to $2\pi f$ (operating frequency, f is expressed in Hz) . H_p is determined before the field EC_a surveying by calibrating the sensor in free space (2 m above ground), allowing the sensor to directly use H_s for the EC_a calculation.

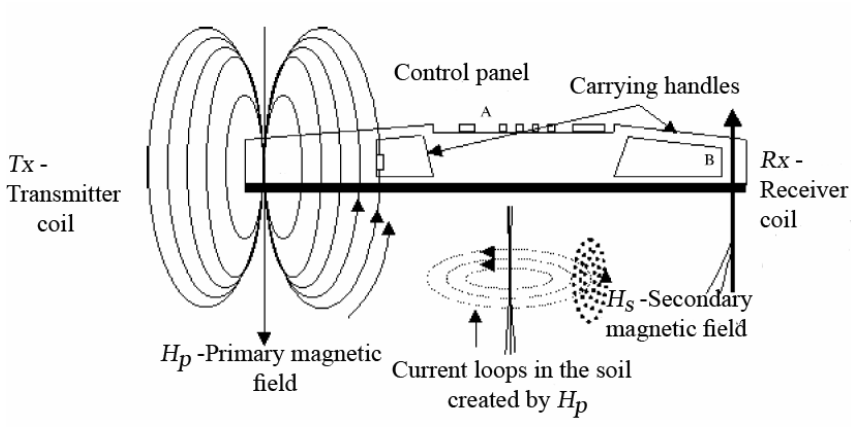

Figure 3.2. Diagram showing the operation of electromagnetic induction based EM38 sensor (source: Robinson et al., 2004).

The relationship given in the equation 3.1 is only valid for the conditions that the *EMI* instrument is operating at low induction number (β):

$$\beta = \frac{S}{\delta} = \frac{S}{\sqrt{\frac{2}{EC_a 2\pi f \mu_0}}} \tag{3.2}$$

where δ is the skin depth, defined as the depth at which the transmitted magnetic field strength decays to e^{-1} (i.e., 37 %) of its initial magnitude at a reference point. Equation 3.2 indicates that for an *EMI* sensor with fixed *f* and *S*, the only factor determining the magnitude of β is soil EC_a. McNeill (1980) asserted that the constraint of low β (<< 1) holds in soil environments where EC_a is ≤ 100 mS m^{-1}.

The EM38 sensor can be operated in two perpendicular orientations, with the transmitter and receiver coils in either vertical (Figure 3.2) or horizontal plane. Technically these two operating modes are referred to as vertical and horizontal dipole modes, respectively, on the basis of the orientations of magnetic dipoles. Importantly, these two different modes of operation produce different responses from soil material at different depths. According to McNeil (1980), the depth sensitivity functions for these modes are:

$$\Phi^V(z) = \left[4z/(4z^2+1)^{3/2}\right] \tag{3.3}$$

$$\Phi^H(z) = 2 - \left[4z/(4z^2+1)^{1/2}\right] \tag{3.4}$$

and respective EC_a measurements are given as:

$$EC_aV = \int_0^{\alpha} \Phi^V(z) EC_a(z) dz \tag{3.5}$$

$$EC_aH = \int_0^{\alpha} \Phi^H(z) EC_a(z) dz \tag{3.6}$$

where $\Phi^V(z)$ and $\Phi^H(z)$ refer to the relative contribution to the secondary magnetic field (or depth sensitivity) arising from a horizontal thin layer of soil (*dz*) at any depth *z* below the instrument, when the *EMI* sensor is operating at vertical and horizontal modes, respectively. Depth below the instrument is expressed as a

normalized depth; i.e. the depth divided by the inter-coil spacing. Since the EM38 sensor has an *S* of one meter, the normalized and actual depths are identical. The equations 3.1 to 3.6 suggest that the depth sensitivity of *EMI* sensing is not only dependent on the coil orientations but also on the *S*. An increase in depth can be obtained by increasing *S* (under the constraint of low induction number, equation 3.2). Since, *S* is fixed at 1 m, the EM38 sensor measurements mainly reflect the EC_a in the root zone. Electromagnetic induction sensors with larger *S* are available for a variety of applications (Hendrickx and Kachanoski, 2002). Figure 3.3 illustrates the depth sensitivity or relative response functions of the vertical and horizontal dipole modes of the EM38. It can be noted that when the sensor operates in the vertical dipole mode, soil material located at a 0.4 m gives the maximum contribution to the EC_a measurement but the contribution from the soil material at 1.5 m is still significant. Further, the near surface material makes a very small contribution to the measurement. On the other hand, the instrument is most sensitive to the conductivity of the near surface soil when it operates in the horizontal dipole mode.

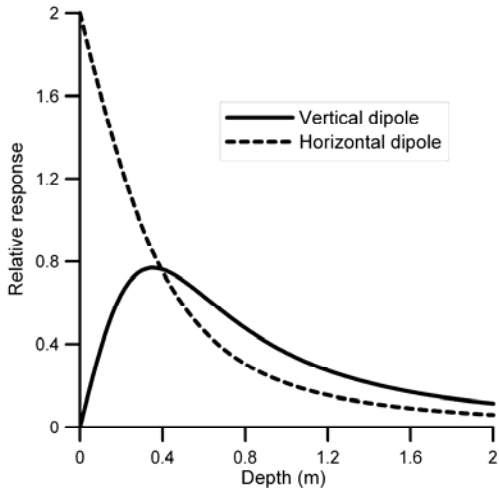

Figure 3.3. Comparison of depth sensitivity of the vertical and horizontal dipole modes of EM38 sensor.

Both EC_aV and EC_aH measurements are required for comprehensive characterizing of the top and the sub soil conductivities. Therefore, recently Geonics Ltd. developed a new version of EM38 sensor by coupling two individual sensors perpendicular to each other. This version is known as the EM38DD (Figure 3.4) and it allows obtaining simultaneous EC_a measurements in both horizontal and vertical dipole modes.

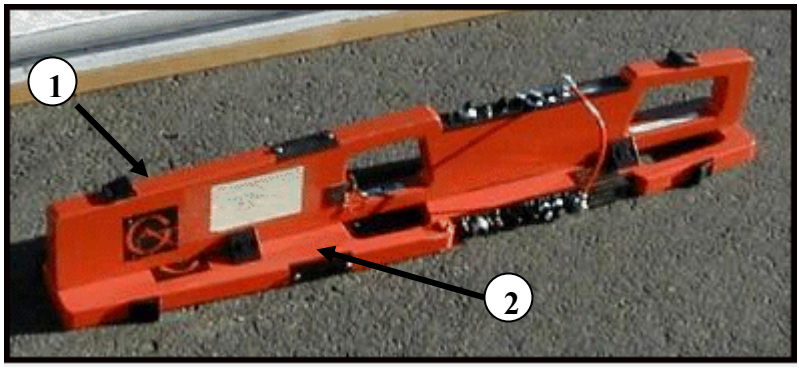

Figure 3.4. EM38DD sensor showing the vertical (1) and horizontal (2) dipole units.

Mobile EC_a measurement system

The EM38 sensor was originally designed to measure soil salinity by means of a hand held operation. Recently, mobilized systems were developed enabling the user to obtain a large number of field measurements within a small time. Figure 3.5 shows the mobile EC_a measurement system used in this research which was developed by the Research Group of Soil Inventory Techniques (Onderzoeksgroep Ruimtelijke Bodeminventarisatietechnieken - ORBit) of the Department of Soil Management. The mobile measurement system consists of five main components: the EM38DD sensor, a GPS receiver, a field computer, an All Terrain Vehicle (ATV) and a GPS based guidance system.

The EM38DD sensor is housed in a rugged non-metallic sled to make it possible to pull it by the ATV. The GPS receiver used in this system is a Trimble *A*gGPS®332

(Trimble Inc., Colorado, USA), which provides a positioning accuracy of < 10 cm with an OmniSTAR HP differential correction (OmniSTAR Inc., Texas, USA). The Allegro field computer unit (Juniper Systems Inc., Utah, USA) acts as the hardware interface to connect the EM38DD and the GPS receiver through two serial ports. The HGIS software (Starpal Inc., Colorado, USA) installed in the field computer combines the EC_a with the location data from the GPS and stores it in the hard disk drive. Moreover, this software provides an option to control the timing of data acquisition either at each second or at sub-second intervals. Generally, the mobile system is operated along transects separated by a predefined distance to obtain measurements in an approximate grid sampling configuration. The *Ag*GPS® EZ-Guide system (Trimble Inc., Colorado, USA) guides the operator to drive precisely along parallel tracks.

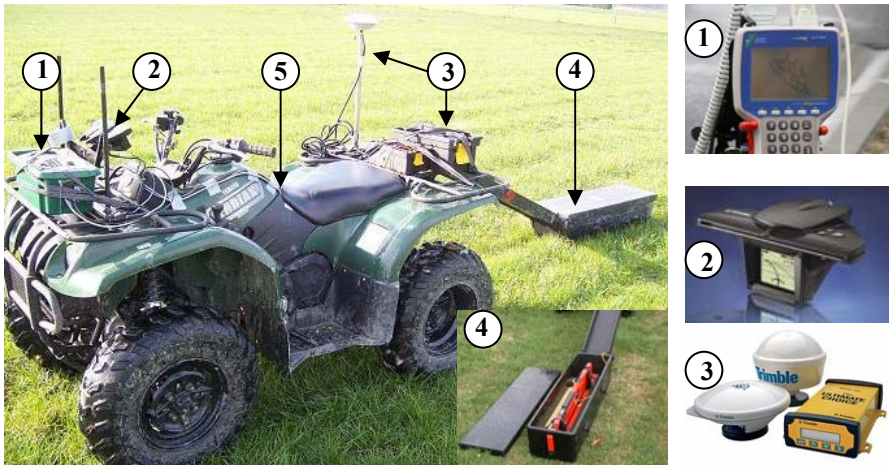

Figure 3.5. Mobile EC_a measurement system equipped with 1. Field computer, 2. *Ag*GPS EZ-Guide system, 3. GPS antenna and receiver, 4. EM38DD sensor housed in the sled and 5. All Terrain Vehicle (ATV).

Prior to the field measurements, the EM38DD sensor is calibrated according to the guidelines provided by the manufacturer. Corwin and Lesch (2003) highlighted that the changes in ambient conditions such as air temperature, humidity and

atmospheric electricity can affect the stability of the instrument. Therefore, after the calibration, the EC_a was measured at a reference point in the study field and this was repeated in hourly intervals to check the instrument stability. If considerable drift in the measurements were noticed, the equipment was recalibrated to assure the consistency of the measurements.

On the completion of field survey, the acquired data were transformed to a personal computer. The subsequent analysis involved two main steps. Firstly, the location data recorded in geographic coordinate system (according to WGS1984) were projected to Belgian Lambert72 coordinate system. Secondly, measurement anomalies resulting from interferences of metal objects were removed through an exploratory data analysis.

3.4.2. Digital Elevation Model

Topography is one of the major causes of soil heterogeneity (McBratney et al., 2003). Therefore, topographic attributes derived from square-grid digital elevation models (DEMs) have often been used as ancillary information for the spatial predictions of soil properties (Moore et al., 1993; Thompson et al., 2006) and also to delineate potential management zones (Parent et al., 2008). The source of elevation data for DEMs can be from the field measurements using theodolites, GPS receivers, stereo aerial photographs, scanner systems in satellites or aircrafts or digitizing of contour lines on paper maps (Burrough and McDonnell, 1998). Among them, the latter is not often favoured due to the fact that interpolating digitized contours to a regular grid can result in the creation of severe artefacts in the resulting DEM surface.

Elevation collected by airborne laser altimetry (Light Detection And Ranging - LiDAR) (OC-GIS Vlaanderen, 2003) was used in this research. These data have a measurement density of approximately one point measurement per each 16 – 20 m^2 and are characterized by very small average horizontal and vertical measurement errors, 0.14 and 0.20 m, respectively. Three key steps were followed to analyze elevation data: (1) Interpolation of elevation data and removal of pits,

(2) Delineation of catchment area (3) Calculation of primary and secondary topographic attributes.

3.4.2.1. Interpolation and removal of pits

The elevation data set which was used in this study was already pre-processed by the data provider. These data were interpolated with ordinary block kriging to generate square-grid DEMs. The grid interval was chosen to be compatible with the grids of other primary and secondary variables.

Digital elevation models may contain grid cells surrounded by neighbours that all have a higher elevation. These pits (or depressions) are often artefacts of the DEM gridding process, as opposed to few which are real (e.g. lakes). These local pits cause unrealistic terminations of surface water flow paths leading to an inaccurate estimations of specific catchment area (see further), thus the secondary topographic attributes. Therefore, it is advised to remove pits before proceed with topographic analysis (Burrough and McDonnell, 1998). Different pit removal algorithms are available. In this research the method published by Jenson and Domingue (1988) which made available in the Idrisi Kilimanjaro software (Clark labs, Worcester, MA, USA) was used. In this procedure, the cells contained in depressions are raised to the lowest elevation value on the rim of the depression.

3.4.2.2. Delineation of catchment area

Surface water flow processes that determine the soil spatial variation generally operate within a catchment scale (Hall and Olson, 1991). Therefore, the topographic attributes were calculated on the basis of the catchment area which envelopes the study area. The catchment delineation procedure developed by Jenson and Domingue (1988) was used. Idrisi Kilimanjaro software was used to implement this step. Generally, this important step is not followed when calculating topographic attributes (e.g. Moore et al., 1993) mainly due to limited availability of elevation data. However, access to a complete elevation data set made it possible to incorporate this step in the current research (see chapter 5).

3.4.2.3. Calculation of primary and secondary topographic attributes

A number of primary and secondary topographic attributes can be derived from a DEM. Primary attributes are computed directly from the DEM and the calculation of secondary attributes involves a combination of primary attributes. An extensive overview of these topographic attributes is provided by Moore et al. (1991), Burrough and McDonnell (1998) and Wilson and Gallant (2000). In this research, the most relevant topographic attributes for spatial prediction of soil variation were selected. These included, primary topographic attributes namely, slope (*Sl*) and specific catchment area (*As*) and secondary topographic attributes namely, wetness index (*WI*) and stream power index (*SPI*). These attributes were calculated using SimDTA software tool developed by Qin et al. (2007) .

Slope

Slope measures the rate of change of elevation in the direction of steepest decent (Wilson and Gallant, 2000). In this study, the slope in degrees was calculated locally for each grid cell (local slope) on the DEM from elevation values ($z(\mathbf{x}_\alpha)$) within a 3 x 3 cell window (Figure 3.6) moved over the surface.

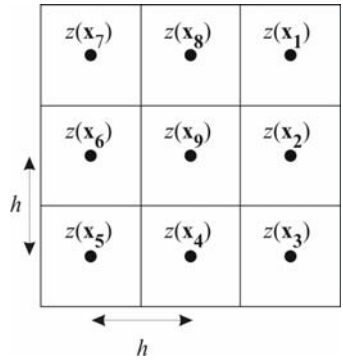

Figure 3.6. A 3 x 3 moving window for estimating the primary and secondary topographic attributes (h = grid spacing).

The Zevenbergen and Thorne (1987) formula was used for calculating the local slope of individual grid cells. This method uses the first order derivatives (z_x and x_y) estimated using centred finite differences (Wilson and Gallant, 2000). For example the slope angle of the centre grid cell $\mathbf{x}_9$ is calculated as:

$$Sl(\mathbf{x}_9) = \tan^{-1}\left(\sqrt{(z_x^2 + z_y^2)}\right) \tag{3.7}$$

where

$$z_x = \frac{\partial z}{\partial x} \approx \frac{z(\mathbf{x}_2) - z(\mathbf{x}_6)}{2h} \qquad \text{and} \qquad z_y = \frac{\partial z}{\partial y} \approx \frac{z(\mathbf{x}_8) - z(\mathbf{x}_4)}{2h}.$$

Specific catchment area

The specific catchment area ($m^2\ m^{-1}$) is the upslope area above a unit length of a contour. This attribute provides indications about the run off volume and the runoff rate at a particular location on the earth surface. In grid based DEMs, *As* is determined by taking the sum of the areas of grid cells in the upslope area that contributes to the water flow thorough a particular cell, i.e. upslope contributing area (*A* in meters), and dividing the same by contour length orthogonal to the direction of flow (*L* in meters). To compute *As*, the drainage topology or the flow direction of each grid cell to the downstream neighbour or neighbours should be determined. Two flow algorithms are available for determining *As*: single flow direction (SFD) and multiple flow direction (MFD) algorithm (Wolock and Mccabe, 1995). Both algorithms use 3 x 3 cells moving window approach to determine the flow direction of a particular grid cell. The basic idea of SFD algorithms is that water from a grid cell should flow only into one of the eight neighbouring cells and MFD allows the accumulated upslope contributing area for any one cell is to be distributed amongst all downslope directions. In this study, the MFD was preferred over the SFD algorithms due to its evident weaknesses; the inability to model divergence of flow and the production of parallel flow lines (Wilson and Gallant, 2000). The MFD algorithm developed by Qin et al. (2007) was used. This algorithm is an improved version of the MFD algorithm developed

by Quinn et al. (1991). The fraction (F) of the upslope contributing area of the central grid cell $\mathbf{x}_9$ (Figure 3.6) flow towards a neighbouring cell $\mathbf{x}_\alpha$ in the down slope direction (i.e. $F(\mathbf{x}_\alpha)$) is calculated as:

$$F(\mathbf{x}_\alpha) = \frac{\tan Sl(\mathbf{x}_\alpha)^p \cdot L(\mathbf{x}_\alpha)}{\sum_{\beta=1}^{n} \tan Sl(\mathbf{x}_\beta)^p \cdot L(\mathbf{x}_\beta)} \tag{3.8}$$

where $Sl(\mathbf{x}_\alpha)$ is slope angle from the central grid cell to neighbouring cell $\mathbf{x}_\alpha$, $L(\mathbf{x}_\alpha)$ is the contour length orthogonal to the direction of flow, which equals to $0.5h$ in cardinal directions and $0.35h$ in diagonal direction and p is the flow partition exponent ($p > 0$). Generally, p is set to a constant value, e.g. $p = 1$ (Quinn et al., 1991) or 6 (Holmgren, 1994) causing limitations to adopt the partition of flow according to local terrain conditions. The formula used in this study replaced the p by a varying flow-partition exponent which was determined through a flow-partition exponent function based on local terrain conditions identified through maximum slope gradiant (Qin et al., 2007). Note that β of the equation 3.8 (β = 1,…, n) indicate the number of neighbouring cells ($n \leq 8$) to which the upslope area for $\mathbf{x}_9$ is distributed.

By multiplying $F(\mathbf{x}_\alpha)$ by $A(\mathbf{x}_9)$ the amount of upslope contribution area that receives from the grid cell $\mathbf{x}_9$ to the cell $\mathbf{x}_\alpha$ can be calculated. So, by summing up the surface area of $\mathbf{x}_\alpha$ and contributing areas from its eight neighbours, $A(\mathbf{x}_\alpha)$ can be calculated. Finally, specific catchment area of $\mathbf{x}_\alpha$ can be calculated by:

$$As(\mathbf{x}_\alpha) = \frac{A(\mathbf{x}_\alpha)}{\sum L(\mathbf{x}_\alpha)} \tag{3.9}$$

where $\sum L(\mathbf{x}_\alpha)$ is the sum of contour lengths orthogonal to the direction of flow neighbouring to $\mathbf{x}_\alpha$.

Wetness index

The wetness index reflects the tendency of surface flow water to accumulate at any point in the catchment (Moore et al., 1988). It is defined as a ratio between the specific catchment area and the slope:

$$WI = \ln\left(\frac{As}{\tan Sl}\right) \tag{3.10}$$

where *Sl* is measured in degrees.

Stream power index

The stream power index is a measure of the erosive power of flowing water and calculated as (Wilson and Gallant, 2000):

$$SPI = As \times \tan Sl \ . \tag{3.11}$$

3.5. Methodology of spatial data analysis

The analysis of sampled soil data started with the exploratory data analysis. The objectives of this step were: to verify the correctness of the acquired data and also to get familiar with the different data sets and their quantitative relationships. The next step involved the characterization of the scale of spatial variation of variables and prediction (or interpolation) of values at un-sampled locations. The geostatistical interpolation techniques were used as a tool to proceed through this step. The resulting continuous surface maps helped to interpret the spatial patterns of different variables and their comparison. Finally, these map layers were integrated using a clustering procedure called fuzzy *k*-means to delineate the potential management zones.

3.5.1. Exploratory data analysis

Univariate description

This step involves the inspection of the data distribution of each variable and the computation of summery statistics. The data distributions were visualized by

means of histograms. The symmetry of a data distribution was inspected by means of a Kolmogorov-Smirnov test for normality and by calculating the coefficient of skewness.

Asymmetric distributions arise from a few extremely small or large values (outliers) which can affect the descriptive statistics and the characterization of spatial variation. Plotting the values of observations in a location map was used to verify whether extreme values are linked to the measurement errors or to several mixed populations within the study area. If the outliers resulted from measurement errors, corresponding samples were reanalyzed. If there was no sound basis to correct or discard the extremes, robust statistics such as the median were used to describe the samples in conjunction with the more conventional descriptive statistics (Goovaerts, 1997). The transformation of data, e.g. log-transformation (Webster and Oliver, 2001) is often performed in order to reduce the influence of extreme values on spatial analysis. However, considering the problems associated with back transformation (Goovaerts, 1997), the data transformations were not considered in this study.

The calculated summery statistics included: the median, mean, standard deviation and variance. The ratio of the standard deviation to the mean $(s/\bar{z})$ is the coefficient of variation (*CV*), which is usually presented as a percentage. It was useful for comparing the variation of different sets of observations of a single variable.

Bivariate description

This step of the exploratory data analysis was performed to find out the relationships between pairs of variables observed at the same location. If two random variables Z_i and Z_j are measured on n locations, $z_i(\mathbf{x}_\alpha)$, $z_j(\mathbf{x}_\alpha)$, $\alpha = 1,2,\ldots,n$, the relationship between these two variables can be visually examined in a scatter plot in which each data pair is plotted against one another.

The strength of the linear relationship between the two variables was determined by calculating the Pearson correlation coefficient (r_{ij}). This is the standardized form of the covariance (C_{ij}):

$$r_{ij} = \frac{C_{ij}}{s_i \cdot s_j} \qquad \in [-1,1] \tag{3.12}$$

where

$$C_{ij} = \frac{1}{n}\sum_{\alpha=1}^{n}(z_i(\mathbf{x}_\alpha) - m_i)\cdot(z_j(\mathbf{x}_\alpha) - m_j) \tag{3.13}$$

s_i and s_j are the standard deviations of Z_i and Z_j, respectively and m_i and m_j denote their arithmetic means.

The equivalent robust statistic for r_{ij} is the Spearman rank correlation (r_{ij}^R) which considers the relationship between the ranks of data $r(z_i(\mathbf{x}_\alpha))$ and $r(z_j(\mathbf{x}_\alpha))$:

$$r_{ij}^R = \frac{1}{n}\frac{\sum_{\alpha=1}^{n}[r(z_i(\mathbf{x}_\alpha)) - m_{Ri}]\cdot[r(z_j(\mathbf{x}_\alpha)) - m_{Rj})]}{s_{Ri}\cdot s_{Rj}} \tag{3.14}$$

where m_{Ri} and s_{Ri} represent the arithmetic mean and the standard deviation of n ranks of Z_i. A large deviation between r_{ij} and r_{ij}^R indicates a non-linear relationship between the two variables or the presence of marked asymmetry.

3.5.2. Geostatistical analysis

Geostatistics embodies a set of statistical tools to describe and model the spatial variation of the soil and crop variables and use this information to make unbiased predictions at un-sampled locations. It is based on the theory of regionalized variables introduced by the French scientist Matheron in the mid 1960s. Several text books provide excellent discussions on the currently available geostatistical tools (Goovaerts, 1997; Isaaks and Srivastava, 1989; Webster and Oliver, 2001).

Therefore, only a short description of a few selected geostatistical tools used in this research is presented below.

3.5.2.1. Characterizing the spatial variation by the variogram

The semivariance quantifies the degree of the spatial relationship or spatial correlation between two observations. The calculation of the semivariance is based on the intrinsic hypothesis proposed by Matheron (1965). The intrinsic hypothesis states that the expected difference between the values of a random variable Z observed at two places separated by a distance vector $\mathbf{h}$ (lag distance) is zero and does not depend on the position $\mathbf{x}$:

$$E[Z(\mathbf{x}) - Z(\mathbf{x}+\mathbf{h})] = 0\,. \tag{3.15}$$

Further, it also assumes that the variance of the differences depends on $\mathbf{h}$ and not on the absolute position:

$$Var[\{Z(\mathbf{x}) - Z(\mathbf{x}+\mathbf{h})\}] = E[\{Z(\mathbf{x}) - Z(\mathbf{x}+\mathbf{h})\}^2] = 2\gamma(\mathbf{h}) \tag{3.16}$$

where the quantity $\gamma(\mathbf{h})$ is known as the semivariance at lag $\mathbf{h}$. The average semivariance for any lag $\mathbf{h}$ can then be estimated by (Webster and Oliver, 1990):

$$\gamma(\mathbf{h}) = \frac{1}{2N(\mathbf{h})} \sum_{\alpha=1}^{N(\mathbf{h})} \{z(\mathbf{x}_\alpha) - z(\mathbf{x}_\alpha + \mathbf{h})\}^2 \tag{3.17}$$

where $z(\mathbf{x}_\alpha)$ and $z(\mathbf{x}_\alpha+\mathbf{h})$ are observations of Z at $\mathbf{x}_\alpha$ and $\mathbf{x}_\alpha+\mathbf{h}$, and $N(\mathbf{h})$ is the number of observation pairs separated by lag $\mathbf{h}$. A plot of the semivariances against the lag distances is known as the experimental variogram. The variogram serves as the central tool of geostatistics providing a description of the scale and pattern of the spatial variation. If the spatial variation is independent from direction, an omnidirectional experimental variogram can be calculated for the entire study area (Figure 3.7a).

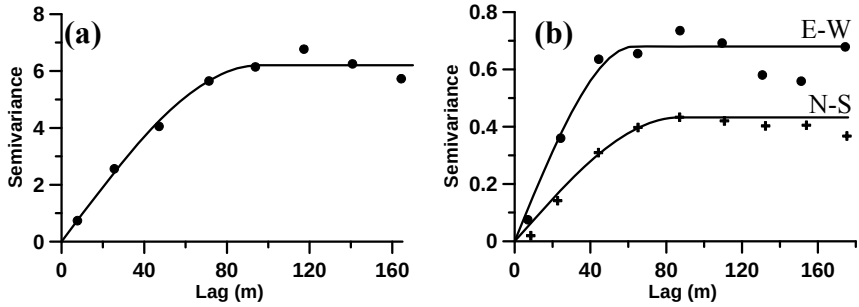

Figure 3.7. (a) Omnidirectional experimental variogram (dots) and (b) directional experimental variograms (dots east-west, crosses north south). The solid curves represent the fitted spherical models.

On the other hand, if the spatial variation is directionally dependent, a directional experimental variograms need to be calculated (Figure 3.7b). Data outliers can greatly affect the stability of the experimental variogram. Therefore, a temporary masking of outliers can be required to calculate the experimental variogram, otherwise the use of a robust variogram can be considered (Goovaerts et al., 1997). Webster and Oliver (2001) suggested that at least 50-100 data points are necessary to achieve a stable experimental variogram.

Typically, a variogram increases from the low values near to the origin to the larger values as h increases, reflecting that the dissimilarity between the observations increases with the increasing lag distance. The steeper the slope, the more the dissimilarity with increasing distance. The dissimilarly increases until it eventually reaches a maximum value of $\gamma(\mathbf{h})$ at which the variogram flattens. This is called the sill variance. The lag $\mathbf{h}$ at which the variogram reaches the sill variance represents the range of spatial correlation. The observations within the range are spatially correlated, but those greater than the range are considered as spatially independent. By definition, the semivariance at lag zero is itself zero, as depicted by Figures 3.7 a and b. But, often for soil data the variogram intercepts the ordinate at a positive semivariance value, the nugget variance. This represents the spatially correlated variation over distances less than the smallest sampling

interval, any measurement errors and any other random variation. Therefore the ratio of the nugget effect to the sill, or the relative nugget effect, (*RNE*, expressed in %) can be calculated to indicate the proportion of spatially unstructured variation in relation to the total variation. According to Cambardella et al. (1994), ratios from 0 % to 25 % indicate a strongly structured spatial dependence. Numbers ranging from 25 % to 75 % point to a moderately structured variability and ratios larger than 75 % are indicative of a weakly structured correlation coupled with a high degree of unexplained variability.

The geostatistical interpolation techniques use the variogram model to obtain unbiased predictions. Therefore, a continuous function or a theoretical model is fitted to the experimental variogram in order to obtain semivariance values at any possible lag **h**. Figure 3.8 shows three commonly used theoretical models (Goovaerts et al., 1997). These models are bounded in the sense that they reach a sill either at a particular range (spherical model) or asymptotically (exponential and Gaussian model):

$$\gamma(0) = 0 \qquad \text{for all models} \tag{3.18}$$

- Spherical model (Sph)

$$\gamma(h) = \begin{cases} C_0 + C_1 \left\{ \dfrac{3h}{2a} - \dfrac{1}{2}\left(\dfrac{h}{a}\right)^3 \right\} & \text{if } 0 < h \le a \\ C_0 + C_1 & \text{if } h > a \end{cases} \tag{3.19}$$

- Exponential model (Exp)

$$\gamma(h) = C_0 + C_1 \left\{ 1 - \exp\left(\frac{-h}{a} \right) \right\} \qquad \forall\ 0 < h \tag{3.20}$$

- Gaussian model (Gau)

$$\gamma(h) = C_0 + C_1 \left\{ 1 - \exp\left(\frac{-h^2}{a^2} \right) \right\} \qquad \forall\ 0 < h \tag{3.21}$$

where a is the range, h represents the lag distance, C_0 is the nugget variance and $C_0 + C_1$ equals the sill variance. For the exponential and Gaussian models, the practical range is defined as the distance at 95 % of the sill. Combinations of variogram models, known as a nested model can also be fitted to an experimental variogram.

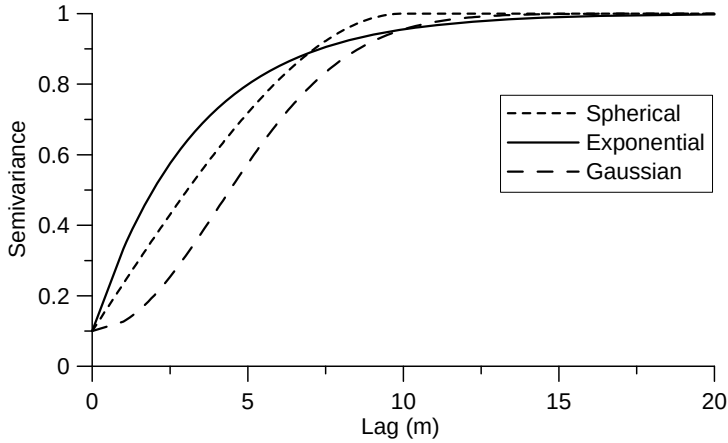

Figure 3.8. Spherical, exponential and Gaussian models with an identical nugget effect ($C_0 = 0.1$), range ($a = 10$ m) and sill ($C_1 = 1$).

There are different methods to select the most appropriate theoretical model, ranging from automatic to visual approaches where the model fitting is judged from a graphical point of view. In this research an intermediate approach was used where the model fitting was optimized by minimizing the weighted sum of squares (*WSS*) of the difference between experimental ($\hat{\gamma}(\mathbf{h}_k)$) and model ($\gamma(\mathbf{h}_k)$) semivariance values (Goovaerts, 1997):

$$WSS = \sum_{k=1}^{K} \omega(\mathbf{h}_k) \cdot [\hat{\gamma}(\mathbf{h}_k) - \gamma(\mathbf{h}_k)]^2 \qquad (3.22)$$

The weight, $\omega(\mathbf{h}_k)$ given to each lag $\mathbf{h}_k$ was calculated by dividing the number of data pairs that contribute to the estimate $\hat{\gamma}(\mathbf{h}_k)$ by the squared $\gamma(\mathbf{h}_k)$.

In this research, experimental variogram calculation was performed using the Variowin software (Pannatier, 1997).

3.5.2.2. Spatial prediction with kriging

Kriging is a geostatistical tool for the prediction of the value of a variable at an unsampled location on the basis of sample observations made in its neighbourhood. It is a weighted linear estimator where the weights are derived using the variogram ensuring an unbiased estimation with a minimum estimation error (Webster and Oliver, 1990). Therefore, in comparison to the other prediction methods, such as inverse distance interpolation and a Triangulated Irregular Network (TIN), kriging provides a Best Linear Unbiased Estimate (BLUE) (Burrough and McDonnell, 1998). A variety of kriging algorithms are available. Algorithms such as ordinary and simple kriging use the target (primary) variable to make predictions. On the other hand, techniques such as co-kriging use the joint spatial variation of the target variable and densely measured ancillary variables, such as EC_a, to improve the prediction accuracy. In this dissertation, ordinary kriging was used as a common methodology for the prediction of soil and crop variables. This section provides only a brief introduction on ordinary kriging. Other methods are discussed together with the related studies.

Consider a random variable Z that has been measured at n locations, $z(\mathbf{x}_\alpha)$, $\alpha = 1,\ldots,n$, the kriging estimator at an unsampled location $\mathbf{x}_0$ can be written as:

$$Z^*(\mathbf{x}_0) - m(\mathbf{x}_0) = \sum_{\alpha=1}^{n(\mathbf{x}_0)} \lambda_\alpha \cdot [Z(\mathbf{x}_\alpha) - m(\mathbf{x}_\alpha)] \qquad (3.23)$$

where $n(\mathbf{x}_0)$ is the number of neighbourhood measurements $z(\mathbf{x}_\alpha)$ used for estimating $Z^*(\mathbf{x}_0)$, λ_α are the weights assigned to data $z(\mathbf{x}_\alpha)$ which are considered to be a realization of the random variable Z, and $m(\mathbf{x}_0)$ and

$m(\mathbf{x}_\alpha)$ are the expected values (or means) of $Z^*(\mathbf{x}_0)$ and $Z(\mathbf{x}_\alpha)$, respectively. The weights are calculated by minimizing the estimation error variance:

$$s^2(\mathbf{x}_0) = E[\{Z^*(\mathbf{x}_0) - Z(\mathbf{x}_0)\}]^2 \qquad (3.24)$$

under the constraint of unbiasedness

$$E[Z^*(\mathbf{x}_0) - Z(\mathbf{x}_0)] = 0\,. \qquad (3.25)$$

Ordinary kriging

The ordinary kriging estimates correspond to the same support of the observations, even when the prediction results are displayed as a raster. Therefore, ordinary kriging is often referred to as ordinary point kriging. Ordinary kriging is applicable in situations where $m(\mathbf{x})$ of equation 3.23 is unknown. Therefore, it is assumed that $m(\mathbf{x})$ is stationary within the local neighbourhood. Accordingly, the ordinary kriging estimator is written as:

$$z^*_{OK}(\mathbf{x}_0) = \sum_{\alpha=1}^{n(\mathbf{x}_0)} \lambda_\alpha z(\mathbf{x}_\alpha) \qquad \text{with} \qquad \sum_{\alpha=1}^{n(\mathbf{x}_0)} \lambda_\alpha = 1\,. \qquad (3.26)$$

The ordinary point kriging weights are obtained by solving a set of equations deduced by minimizing the error variance under the constraint of unbiasedness. The resulting ordinary point kriging system is given as:

$$\begin{cases} \sum_{\beta=1}^{n(\mathbf{x}_0)} \lambda_\beta \gamma(\mathbf{x}_\alpha - \mathbf{x}_\beta) + \psi = \gamma(\mathbf{x}_\alpha - \mathbf{x}_0) & \alpha = 1,\ldots,n(\mathbf{x}_0) \\ \sum_{\beta=1}^{n(\mathbf{x}_0)} \lambda_\beta = 0 \end{cases} \qquad (3.27)$$

where $\gamma(\mathbf{x}_\alpha - \mathbf{x}_\beta)$ is the semivariance between the sampling locations $\mathbf{x}_\alpha$ and $\mathbf{x}_\beta$, and $\gamma(\mathbf{x}_\alpha - \mathbf{x}_0)$ is the semivariance between sampling location $\mathbf{x}_\alpha$ and the unsampled location $\mathbf{x}_0$, these can be obtained from the fitted variogram. The

quantity ψ is the Lagrange multiplier introduced to minimize the ordinary kriging variance under the constraint of unbiasedness. The most straightforward method to solve the ordinary kriging system is through matrix algebra:

$$[\boldsymbol{\lambda}] = [\mathbf{A}]^{-1}\,[\mathbf{B}] \tag{3.28}$$

where

$$[\boldsymbol{\lambda}] = \begin{bmatrix} \lambda_1 \\ \lambda_2 \\ . \\ . \\ \lambda_{n(\mathbf{x}_0)} \\ \psi \end{bmatrix},$$

$$[\mathbf{A}] = \begin{bmatrix} \gamma(\mathbf{x}_1 - \mathbf{x}_1) & \gamma(\mathbf{x}_1 - \mathbf{x}_2) & . & . & \gamma(\mathbf{x}_1 - \mathbf{x}_{n(\mathbf{x}_0)}) & 1 \\ \gamma(\mathbf{x}_2 - \mathbf{x}_1) & \gamma(\mathbf{x}_2 - \mathbf{x}_2) & . & . & \gamma(\mathbf{x}_2 - \mathbf{x}_{n(\mathbf{x}_0)}) & 1 \\ . & . & . & . & . & . \\ . & . & . & . & . & . \\ \gamma(\mathbf{x}_{n(\mathbf{x}_0)} - \mathbf{x}_1) & \gamma(\mathbf{x}_{n(\mathbf{x}_0)} - \mathbf{x}_2) & . & . & \gamma(\mathbf{x}_{n(\mathbf{x}_0)} - \mathbf{x}_{n(\mathbf{x}_0)}) & 1 \\ 1 & 1 & . & . & 1 & 0 \end{bmatrix}$$

and

$$[\mathbf{B}] = \begin{bmatrix} \gamma(\mathbf{x}_1 - \mathbf{x}_0) \\ \gamma(\mathbf{x}_2 - \mathbf{x}_0) \\ . \\ . \\ \gamma(\mathbf{x}_{n(\mathbf{x}_0)} - \mathbf{x}_0) \\ 1 \end{bmatrix}.$$

Ordinary kriging provides an error variance (kriging variance) which is computed as:

$$s^2_{\mathrm{OK}}(\mathbf{x}_0) = \sum_{\alpha=1}^{n(\mathbf{x}_0)} \{\lambda_\alpha \gamma(\mathbf{x}_\alpha - \mathbf{x}_0)\} + \psi\,. \tag{3.29}$$

The kriging variance value attached to each prediction can be used to evaluate the relative prediction precision in terms of the global variance modelled by the variogram. This helps to locate additional sampling locations to optimize the prediction.

Ordinary block kriging

Ordinary point kriging is an exact interpolator, i.e. the estimated value at a sampling site is identical to the observed value. Therefore, attribute maps constructed through ordinary point kriging often contain many sharp spikes or pits, which are of little relevance for the management. Ordinary block kriging provides a smooth attribute map by estimating average values over a certain area or grid cell, termed as a 'block' **B**. In the case of square blocks, the estimation procedure involves that the block B is discretized into N^2 number of points ($\varphi = 1,...,N^2$). The block kriging estimator can be written as:

$$z^*(\mathbf{B}) = \frac{1}{N^2}\sum_{\varphi=1}^{N^2} z^*(\mathbf{x}_\varphi)\,. \qquad (3.30)$$

The ordinary block kriging system is given as:

$$\begin{cases} \sum_{\beta=1}^{n(\mathbf{B})} \lambda_\beta \gamma(\mathbf{x}_\alpha - \mathbf{x}_\beta) + \psi = \bar{\gamma}(\mathbf{x}_\alpha - \mathbf{B}) \\ \sum_{\beta=1}^{n(\mathbf{B})} \lambda_\beta = 0 \end{cases} \qquad (3.31)$$

where $(\mathbf{x}_\alpha - \mathbf{B})$ is the average semivariance between block **B**, represented by N^2 number of points inside the block.

The ordinary block kriging system can also be represented as a matrix system, where [**A**] and [**λ**] remain identical as in the point kriging system. However, [**B**] changes to:

$$[\mathbf{B}] = \begin{bmatrix} \overline{\gamma}(\mathbf{x}_1 - \mathbf{B}) \\ \overline{\gamma}(\mathbf{x}_2 - \mathbf{B}) \\ . \\ . \\ \overline{\gamma}(\mathbf{x}_{n(\mathbf{B})} - \mathbf{B}) \\ 1 \end{bmatrix}.$$

Due to the merits of ordinary block kriging over the ordinary point kriging, attribute estimations to a common grid were done using block kriging throughout this dissertation. However, it is not recommended to use block kriging for attributes that can not be averaged linearly. Therefore, soil pH, defined as the logarithm of $[H^+]$ was predicted using ordinary point kriging.

Accuracy assessment of spatial prediction methods

Knowledge of the accuracy of spatial estimates is needed to allow their credible use. Spatial estimation procedures can be validated through two approaches: cross validation and independent validation. In cross validation (Isaaks and Srivastava, 1989), (also referred to as leave-one-out validation) one observation is removed and estimated with the remaining neighbourhood observations. Subsequently, the removed observation is added and another observation is removed. This process is repeated until all observations are estimated. Then the observations and corresponding estimates are compared to quantify the accuracy. The cross validation can not be treated as an independent validation procedure since all the observations are used to calculate the variogram. On the other hand, an independent validation uses an optional set of observations. The validation is performed by making estimations at validation sampling points. Let, $z(\mathbf{x}_\alpha)$ and $z^*(\mathbf{x}_\alpha)$, $\alpha = 1,\ldots,n$ denote n number of observations and corresponding estimations, respectively, a combination of validation indices can be used to assess the accuracy:

- Mean estimation error (*MEE*)

$$MEE = \frac{1}{n}\sum_{\alpha=1}^{n}(z^*(\mathbf{x}_\alpha) - z(\mathbf{x}_\alpha)) \,. \tag{3.32}$$

The *MEE* measures the bias of the estimation. The values near to zero inform unbiased estimations.

- Root mean squared estimation error (*RMSEE*)

$$RMSEE = \sqrt{\frac{1}{n}\sum_{i=1}^{n}(z^*(\mathbf{x}_\alpha) - z(\mathbf{x}_\alpha))^2} \,. \tag{3.33}$$

Generally, RMSEE is evaluated in comparison to the standard deviation of the data.

- Pearson correlation coefficient

The Pearson correlation calculated between $z(\mathbf{x}_\alpha)$ and $z^*(\mathbf{x}_\alpha)$ indicates the strength of the linear relationship.

In this research, geostatistical software, GSLIB (Deutsch and Journel, 1998) was used to perform spatial predictions.

3.5.3. Fuzzy *k*-means classification

The geostatistical analysis generates single or multiple layers of soil information, each with an identical grid configuration. The next step is to partition each grid cell ($\mathbf{x}_\alpha$), (or object) into a management zone by means of a uni- or multivariate classification algorithm. The classical approach is to classify each object into a crisp (hard) class on the basis of predefined class boundaries. However, geographical phenomena, like soil or topographic properties do not posses rigidly defined cut off boundaries, rather they vary gradually and continuously in a manner forming diffuse boundaries between classes (Dale et al., 1989). Classification of these variables in to crisp classes causes a considerable loss of

information (Burrough and McDonnell, 1998). Therefore, the classical classification approach was not preferred for management zones delineation.

The fuzzy *k*-means classification (Bezdek, 1974; Bezdek, 1981; McBratney and de Gruijter, 1992) developed upon the fuzzy set theory (Zadeh, 1965) was used in this research to delineate management zones. Fuzzy *k*-means classification overcomes the weakness of the classical approach by partitioning objects into continuous classes. This is accomplished by assigning partial memberships to objects. A membership value of 1 is assigned to the objects that exactly match the class centre (centroid), whereas other objects receive membership values depending on their degree of closeness to the class centroid. The membership assignment for each object is performed through a membership function developed for each class on the basis of the uni- or multiple attribute space. The membership function of a fuzzy set can take different forms: normal, log normal, rectangular, hyperbolic or Gausssian (McBratney and Odeh, 1997).

Consider a set of n grid cells ($z_i(\mathbf{x}_\alpha)$, $\alpha = 1,..., n$) each having p attributes ($i = 1,..., p$) grouped into k classes ($c = 1,\ldots, k$), the fuzzy *k*-means classification involves operations that satisfy three conditions:

$$\sum_{c=1}^{k} m_{\mathbf{x}_\alpha c} = 1 \qquad \alpha = 1,..., n \tag{3.34}$$

$$\sum_{i=1}^{n} m_{\mathbf{x}_\alpha c} \geq 0 \qquad c = 1,..., k \tag{3.35}$$

$$m_{\mathbf{x}_\alpha c} \in [0,1] \qquad \alpha = 1,..., n\ ;\ c = 1,..., k \tag{3.36}$$

where $m_{\mathbf{x}_\alpha c}$ indicates the membership of $\mathbf{x}_\alpha^{\text{th}}$ grid cell for the c^{th} class. The first condition indicates that the sum of memberships of individuals across all k classes sums to 1. The second condition ensures the absence of empty classes. The third condition allows the assignment of memberships between and including 1 and 0. The classification is achieved by minimizing the fuzzy *k*-means objective function

$J(\mathbf{M},\mathbf{C})$, which is the sum-of-square error as a function of each object by the centre of its class:

$$J(\mathbf{M},\mathbf{C}) = \sum_{\alpha=1}^{n} \sum_{c=1}^{k} m_{\mathbf{x}_\alpha c}^{\varphi} d^2(x_\alpha, c_c) \qquad (3.37)$$

where $\mathbf{M}$ is a n x k matrix of membership values, $\mathbf{C}$ is a k x p matrix of the class centroids, $x_\alpha = (z_1(\mathbf{x}_\alpha),...,z_p(\mathbf{x}_\alpha))^{\mathrm{T}}$ is the vector representing p variable values at the grid cell $\mathbf{x}_\alpha$, $c_c = (c_{c1},...,c_{cp})$ is the vector representing p centroids of class c, $d^2(x_\alpha, c_c)$ is the squared distance between x_α and c_c according to a chosen distance metric and φ is the fuzziness exponent which determines the degree of fuzziness of the classification (ranges between 1 and infinity, representing a crisp and a complete fuzzy classification, respectively). The choice of the distance metric and the fuzziness exponent directly influence the classification results. Two distance dependent metrics are commonly used:

- Euclidean distance

Euclidean distance gives equal weights to all measured attributes. Therefore it is insensitive to statistically dependent variables (Bezdek, 1981). The Euclidean distance is calculated as:

$$d^2(x_\alpha, c_c) = (x_\alpha - c_c)^T.(x_\alpha - c_c)\,. \qquad (3.38)$$

Euclidean distance is not recommended in situations where different variables consist of widely varying averages and standard deviations, since the classification can be biased towards the larger varying attributes.

- Mahalanobis distance

The Mahalanobis distance is calculated as:

$$d^2(x_\alpha, c_c) = (x_\alpha - c_c)^{\mathrm{T}} \sum{}^{-1} (x_\alpha - c_c) \qquad (3.39)$$

where $\sum$ denotes the variance-covariance matrix. Introduction of $\sum$ to the equation 3.38 standardizes the different attributes while taking the correlation

between variables into account. Therefore, the classification result is not much influenced by the distribution of the attributes and their statistical dependence.

There is no objective method to find out the optimum φ value. Odeh et al. (1992) suggested for soil data to set φ at 1.35 as a default value.

McBratney and de Gruijter (1992) summarized the fuzzy *k*-means algorithm as below:

1. Choose the number of classes *k*, with $1 < k < n$.
2. Choose a value for the fuzziness exponent φ, with $\varphi > 1$;
3. Choose a definition of distance in the variable-space;
4. Choose a value for the stopping criterion ε (ε =0.001 gives reasonable convergence);
5. Initialize the membership matrix $\mathbf{M} = \mathbf{M}_0$, with random memberships.
6. Start the iteration process (*it* = 1,2,3….) and continue till $\left\|\mathbf{M}_{it} - \mathbf{M}_{it-1}\right\| \leq \varepsilon$.

Identification of the optimal number of classes

The calculation of validity indices, fuzziness performance index (*FPI*) and the normalized classification entropy (*NCE*) allows finding out the optimum number of classes (*k*). *FPI* is a measure of the degree of the membership sharing between clusters which ranges between 0 and 1. An *NCE* value of 1 corresponds to the maximum fuzziness and a value of 0 indicates a non fuzzy classification. Roubens (1982) indicated *FPI* as below:

$$FPI = 1 - \frac{kF - 1}{F - 1} \tag{3.40}$$

where *k* is the number of classes and *F* is the partition coefficient:

$$F = \frac{1}{n} \sum_{\alpha=1}^{n} \sum_{c=1}^{k} m_{\mathbf{x}_\alpha c}^2 \ . \tag{3.41}$$

NCE is an estimate of the amount of disorganization created by a given number of classes, and it is also ranges between 0 and 1. *NCE* is mathematically given as below:

$$NCE = \frac{H}{\log k} \tag{3.42}$$

where *H* is the entropy function:

$$H = -\frac{1}{n}\sum_{\alpha=1}^{n}\sum_{c=1}^{k} m_{\mathbf{x}_\alpha c}^2 \times \log(m_{\mathbf{x}_\alpha c}) . \tag{3.43}$$

To find out the optimum number of classes, the classification was performed for a range of classes and the resulting *FPI* and *NCE* values were plotted against the number classes. The class number that minimizes *FPI* and *NCE* was considered as the optimum (Odeh et al., 1992).

In this research, fuzzy *k*-means classification was performed using FuzME software (Minasny and McBratney, 2002).

3.6. Geology and soils of Flanders

The Flanders region covers more than one third of the land area of Belgium (Figure 3.9). The present soil scapes of Flanders are mainly resulting from the geological processes which occurred during the Tertiary and the Quaternary periods (Table 3.1).

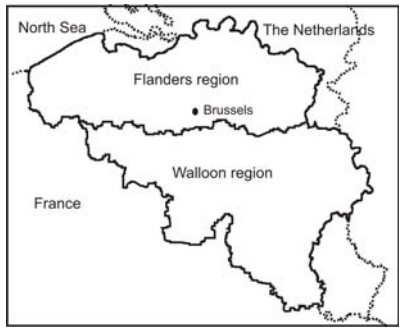

Figure 3.9. A map of Belgium showing the Flanders region.

Flanders was flooded by the sea during the Ypresian age of the early Eocene. During this marine period, a 100 m – 200 m thick glauconitic clay layer (Ieperiaan clay) was deposited. However, at the end of the Ypresian age, the sea level receded, resulting in the deposition of a sand layer. Above this "Ieperiaan sand", the "Paniseliaan" deposits (also belonging to the Ypresian age) can be found. It consists of a 100 m thick clay layer covered by a thinner sand layer.

Table 3.1. International geological time scale of the Tertiary and the Quaternary periods (Palmer, 1983).

Period	**Epoch**	**Age**	**Time (million years)**
Quaternary	Holocene		0.01 - present
	Pleistocene	Calabrian	1.0 - 0.01
Tertiary (Neocene)	Pliocene (Late)	Piacenzian	3.4 - 1.0
	Pliocene (Early)	Zanclean	5.3 - 3.4
	Miocene (Late)	Messinian	6.5 - 5.3
		Tortonian	11.2 - 6.5
	Miocene (Middle)	Serravallian	15.1 - 11.2
		Langhian	16.6 - 15.1
	Miocene (Early)	Burdigalian	21.8 - 16.6
		Aquitanian	23.7 - 21.8
Tertiary (Paleocene)	Oligocene (Late)	Chattian	30.0 - 23.7
	Oligocene (Early)	Rupelian	36.6 - 30.0
	Eocene (Late)	Priabonian	40.0 - 36.6
	Eocene (Middle)	Bartonian	43.6 - 40.0
		Lutetian	52.0 - 43.6
	Eocene (Early)	Ypresian	57.8 - 52.0
	Paleocene (Late)	Selendian	63.6 - 57.8
	Paleocene (Early)	Danian	66.4 - 63.6

The stratification and the sandwiched fossil fauna and flora suggest constant fluctuations of the sea level causing continental and marine phases. The last sea

intrusion in the Eocene took place in the Bartonian age. The sediments deposited during this period were rich in clay (Bartoon clay). After the Bartonian age, the entire Flanders region experienced a 30 million years long continental phase. The transgression in the Messinian age of the late Miocene was the last marine phase during the Tertiary period that submerged Flanders. The climatic fluctuations occurred during the Quaternary period are responsible for the formation of the present day soil cover and its characteristics. The Pleistocene epoch of the Quaternary period was dominated by four glacial periods, each separated by a warmer interglacial period. Intensive erosion processes occurred during these periods formed a ridge-and-valley landscape while resulting in the exposure of the different Tertiary strata. For example, Figure 3.10 shows the different Tertiary materials exposed on the slopes of hills in southern East-Flanders as a result of soil erosion.

During the youngest glacial epoch, the Weichselian (70000 -10000 years ago) the sea level was approximately 120 m - 70 m below the present level. Entire Flanders experienced a peri-glacial climate with a permafrost soil and tundra type of vegetation. The present North Sea was dry and it was covered by thick sediments deposited by the rivers of past glacials. The northern winds caused a massive eolian transport of soil materials from the North Sea towards Northern Europe.

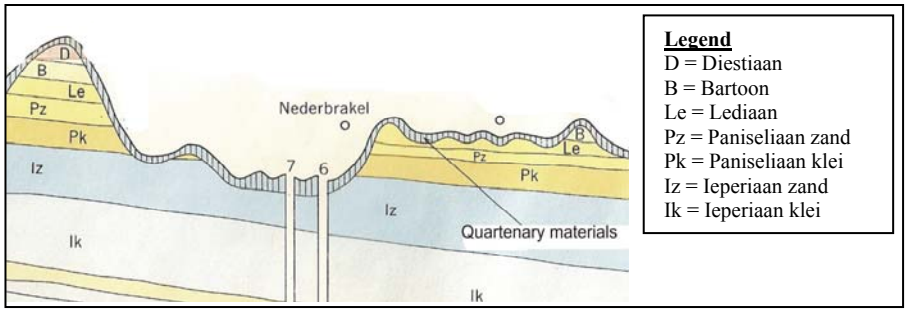

Figure 3.10. Tertiary materials exposed on the north facing slopes of southern East-Flanders, letters, D, B, Le, Pz, Pk, Iz and Ik indicate Tertiary layers (source: Province Oostvlaanderen, Geologische kaart).

The subsequent deposition pattern was mainly governed by the particle size. The largest particles were transported through saltation and deposited first in the low lands. Smaller particles like fine sand (50 μm – 200 μm) were transported by wind over longer distances and deposited in the northern part of Flanders. Silt (and to some extend clay) particles (< 50 μm) were transported in suspension (called loess material) over longer distances and to higher elevations. So they were deposited over the southern part of Flanders where the valley-and-ridge landscape was more prominent. Between the sand cover and the loess deposits a transition area is found with mixtures of sand and silt (silty sand to sandy silt). A general soil map (Figure 3.11) reflects this soil textural gradient along the north-south direction.

The surface topography (paleotopography) at the time of these aeolian deposition occurred, and the erosion processes thereafter, have greatly influenced the thickness of the Quaternary cover of the middle and the southern parts of Flanders. On the steep and convex slopes these layers are very shallow, or sometimes even absent exposing different Tertiary layers. These sediments are thick on gentle slopes with northern exposure and significantly thinner on the slopes facing towards the south. The aeolian sedimentation process stopped about 10000 years ago as the glacial period came to an end. Consequently, the sea level rose and the North Sea formed again separating the existed land bridge between the continent and the UK. The inland rivers were formed as the permafrost disappeared. The subsequent erosion and sedimentation processes largely influenced the current day soil spatial variability.

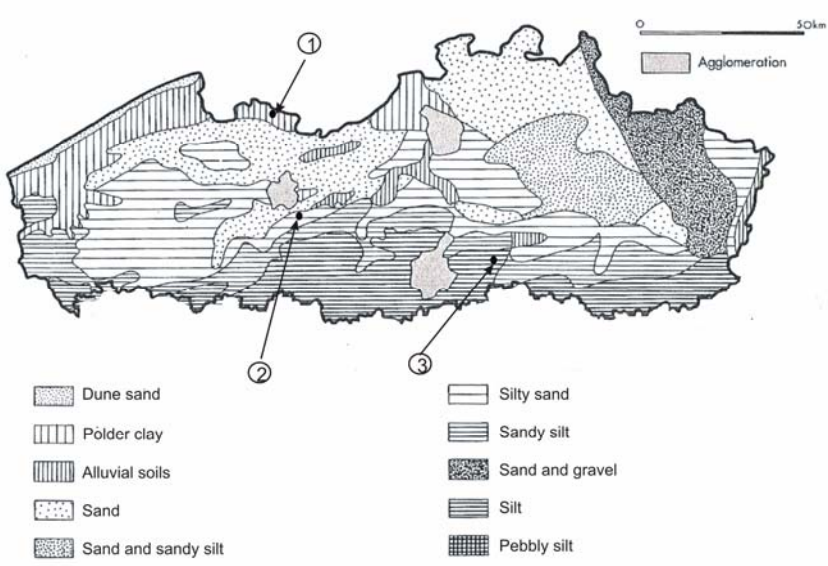

Figure 3.11. General soil map of Flanders and the locations of the three study areas (1) Watervliet (2) Melle and (3) Leefdaal (source: Flanders, a geographical portrait, geographical information and documentation centre, After R. Tavernier).

A series of sea intrusions that occurred during the warmer periods in the Holocene epoch has further modified the soils of the northern areas of Flanders. The first marine transgression called "Flandrian transgression" took place 7300 – 4300 years ago. After a regressive phase, the coast was flooded again in the 2nd, 4th and 11th centuries. These sea inundations caused a deposition of clay rich sediments over the Quaternary sand cover along the coast. From the 11th century onwards, the inhabitants of the coastal areas constructed dikes in order to protect their lands. The soils in these areas are known as "polder clay" (Figure 3.11).

3.7. Study area selection

The previous section explained why the soils of Flanders considerably change from the north to south. This large scale variation was taken into account during the study area selections. Three study areas, namely Melle, Leefdaal and Watervliet (Figure 3.11) were chosen for this research. The study area localized in

Melle represents the soils dominated with a sandy silt texture. The investigations conducted at the Leedaal field represent the silt textured loess region characterized with undulating topography caused by Tertiary layers. To represent the polder soils of the northern part, a study area was selected in the "Watervlietse" polders. The research findings at these locations are presented as case studies in the next chapters.

3.8. The national soil map of Belgium

The national soil survey of Belgium began in 1947 and aimed to facilitate the regional scale agricultural land use planning. The field work was conducted at a scale of 1:5000 which involved soil augering to a standard depth of 125 cm unless obstacles were encountered. The field observation density was approximately 1 – 1.5 locations for ha. Additionally, soil profile descriptions and horizon sampling have been conducted to support the soil survey. By 1989 the identification, classification and mapping of the soils of Belgium was complete. Presently, 373 out of 441 map sheets have been published at a scale of 1:20,000 with associated explanatory booklets.

The targeted user groups of the national soil map were the agricultural and rural land use planners. Therefore, the chosen map legend had to be easily understandable, not only for a soil scientist but also for a user having only a basic knowledge in soil science. The legend characterizes the soils at series level on the basis of top-soil textural classes, natural drainage classes and the nature of the profile development. These series are denoted by a code with three letters. The top-soil textural class is indicated by a first capital letter. They are identified according to the Belgian soil texture triangle (Figure 3.12a). These textural classes are: Z (zand – sand), S (lemig zand – silty sand), P (licht zandleem – light sandy silt), L (zandleem – sandy silt), A (leem – silt), E (klei – clay) and U (zware klei – heavy clay). The diameters of sand (50 µm – 200 µm), silt (2 µm – 50 µm) and clay (< 2 µm) are identical to the ones defined by the United States Department of Agriculture (USDA). However, the textural classes are markedly different

compared to the classes defined in the nowadays internationally used USDA textural triangle (Figure 3.12b). A large intra-class variation in classes like L, E and U is a main weakness of the Belgian textural triangle. Throughout this dissertation, the soil textural classes are referred to the Belgian texture triangle unless specifically mentioned.

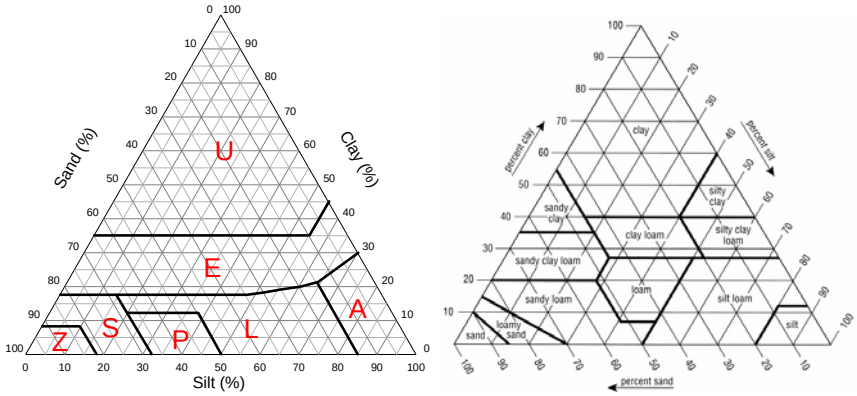

Figure 3.12. (a) Belgian and (b) USDA soil texture triangles.

The second letter specifies the soil drainage. The coding of the drainage class depends on the textural class and on the starting depths of mottling and permanent reductions features, e.g.

- .a.: very dry
  .
  .
- .i.: very wet for sandy textures (Z, S and A).

The third letter of the code indicates the level of the profile development. Some of the examples are:

- ..a: textural B (or Bt) horizon
- ..b: B horizon with an apparent colour or structural difference
- ..c: crushed, discontinuous or degraded Bt horizon
- ..g: humus and/or iron podzol B horizon
- ..h: crushed humus and/or iron podzol B horizon

Variants of soil series are identified on the basis of the presence of a substratum. Therefore, type and the depth of the substratum is denoted by a prefix letter. For example, the presence of a Tertiary clay substratum at different depths is denoted by:

- u…: at shallow depths (0 – 0.75 m)
- (u)…: at moderate depths (0.75 m – 1.25 m)
- u- …: at shallow to moderate depths.

Chapter 4

Utility of choropleth soil maps for site-specific soil management and map upgrading using proximal soil sensing

This chapter has been modified from the publication:

U.W.A. Vitharana, T. Saey, L. Cockx, D. Simpson, H. Vermeersch and M. Van Meirvenne. 2008. Upgrading a 1/20,000 soil map with an apparent electrical conductivity survey. Geoderma 148:107-112.

4.1. Introduction

Choropleth or polygon soil maps are the most prevalent source of soil information available for soil management decisions (Beckett and Webster, 1971; Dent and Young, 1981; Rossiter, 1996). Many countries posses nationwide soil maps produced during the 'golden-era' for soil survey (the 1950s and 1960s) and land evaluation (the 1970s and 1980s) (Manderson and Palmer, 2006). The density of field observations as well as the soil surveyors conceptual predictive models employed for classical soil surveying are not sufficient to predict the continuity of spatial variability (Heuvelink and Webster, 2001). Therefore, soil surveying typically predicts soil spatial variations by partitioning similar soils in the landscape into discrete entities called mapping units. On a soil map, these map units are shown as polygons across which the soil properties are considered to be significantly different and within which the properties are relatively homogenous (Dijkerman, 1974). Therefore, within a mapping unit average of a particular soil property is to serve as its soil map based prediction (Webster and Oliver, 2001).

The predictive quality of polygon soil maps is largely determined by the map scale which is defined as the ratio of the distance shown on the map to the corresponding distance on the ground. Intuitively, the predictions will be more accurate as soil surveying is done at a detailed scale. Concerning the data requirements of site-specific soil management, the map scale should be detailed enough to discern within-field variations. The minimum legible area, i.e. the smallest land area that can be legibly represented on the map at a given scale (Forbes et al., 1987), can be used as a basis for the scales of soil maps suitable for acquiring soil information for site-specific soil management. Table 4.1 shows minimum legible areas for some common polygon soil map scales. If we assume an average field size of 3 ha, the maps prepared at a scale larger than 1:25000 could be capable of providing some soil information needed for site-specific soil management.

Table 4.1. Minimum legible areas for some common map scales (source: Forbes et al., 1987).

Map scale	Minimum legible area (ha)
1:5000	0.1
1:10,000	0.4
1:15,000	0.9
1:20,000	1.6
1:25,000	2.5
1:50,000	10
1:100,000	40
1:200,000	160
1:250,000	250

Usually, soil mapping units are designated with qualitative terms which correspond to the level of soil classification. Therefore, map unit based prediction of quantitative soil data, which are needed for site-specific soil management, is not straight forward. One method of extracting quantitative soil information from soil maps is by consulting the survey report or memoir (Dent and Young, 1981), which gives the average soil properties within mapping units. These averages are reported on the basis of field or laboratory analysis of the properties of a representative profile(s) of the soil located within the mapping unit. The accuracy of this prediction depends on the variability within the mapping unit (Webster and Oliver, 2001) which is not essentially included in the soil survey report. Therefore, these predictions are subjected to an unknown degree of uncertainty and have only a small relevance on soil management decisions. Moreover, all required soil properties may not have been included in the map and thus in the accompanying survey report. As an alternative method, soil properties required can be measured at a number of locations within the mapping unit and their arithmetic means can be considered as map unit based predictions. Then, the estimated variances can be used to quantify the uncertainty in the prediction (Brus et al., 1992; Leenhardt et al., 1994; Webster and Oliver, 2001).

The predictive quality of soil maps in relation to the soil information needed for land use planning on a regional scale has been the focus of many researchers (Beckett and Webster, 1971; Leenhardt et al., 1994; Lin et al., 2005; Webster and Beckett, 1968). However, limited attention has been given to assess the potentials of choropleth soil maps for providing soil information needed for site-specific soil management. To address this research gap, the following research questions were answered in this chapter by means of a case study: (1) is the spatial variability of soil properties structured within a 14 ha field at the sandy silt region? (2) Are the 1:20,000 and more detailed 1:5000 soil maps suitable to provide soil information for site-specific soil management? and (3) Can EC_a information obtained with proximal sensing be used as an ancillary soil information to upgrade the 1:20,000 soil map with a minimum effort of invasive soil sampling?

4.2. Materials and methods

4.2.1. Study area and soils

The study area is located in Melle in East Flanders, with central coordinates: 50^o 58’ 42” N and 3^o 49’ 00” E (Figure 4.1). This 14.6 ha area is a part of the Ghent University agricultural research farm situated in the sandy silt region of Flanders and most of the lands of this region are used for crop cultivation. The soils of this region are formed from wind blown Pleistocene loess materials (sandy silt in texture) deposited during the Quaternary period. The loess material is underlain by clayey to sandy Tertiary marine sediments (Paniselian). The loess cover can have a substantial thickness in the depressions (5 m - 10 m), but it can diminish to some tens of centimetres on the ridges. Therefore, the spatial variation of the thickness of the loess cover has a very strong influence on both the water economy and on the development of the soil profile throughout the region. This study area was chosen because it is typical of the landform commonly found in the region. The topography of the study area comprises a long gentle slope along the north-east direction, while the highest position lies in the western corner.

Figure 4.1. Localisation of the study area.

The management history of the study area revealed that arable crop cultivation has been practiced in the western part while the eastern part has been used as pasture land for a half a century or more. For the arable part, there has been a regular rotation of crops namely maize, red clover, hay-grass, winter-wheat, summer-wheat, summer-barley, and fodder beets over time. These crops are usually harvested dry to serve as fodder for farm cattle.

4.2.1.1. National soil map (1:20,000)

The soils in the study area have been surveyed under the Belgian national survey (section 3.8). The published 1:20,000 map (Figure 4.2) has identified the presence of two soil series. Approximately two-third of the area belongs to the 'Ldc' series, which represents a sandy silt topsoil texture ('L'), moderately wet conditions (drainage class 'd') with a strongly degraded textural B-horizon (profile development type 'c'). The remaining part of the study area is characterized by the soil series 'Lcc', with a similar topsoil texture and profile development but with drier moisture conditions (drainage class 'c'). Both soil series inferred that there is no Tertiary material present within the top 1.25 m. These soil types correspond to

Albeluvisols according to the World Reference Base for Soil Resources (WRB) classification system (ISSS Working Group Reference Base, 1998).

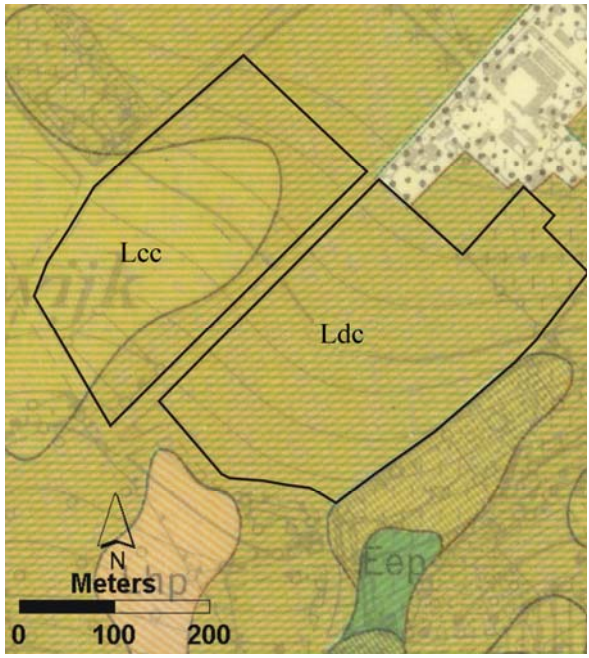

Figure 4.2. The 1:20,000 soil map of the study area.

4.2.1.2. Detailed soil map (1:5000)

The study area has been surveyed to a greater detail in 1951 by Dr. F. Moormann of the Soil Survey Centre of the Ghent University. The aim of this soil survey was to provide accurate soil information for agronomic research planning in the experimental farm. The mapping was done by taking auger observations down to a depth of 1.25 m. The average density of observations was 15 per ha, totalling approximately 210 observation within the study area. The outcome of the survey was a 1:5000 soil polygon map (Figure 4.3). It should be noted that such detailed soil maps are rarely available in Belgium. The soil series were delineated in a different manner compared with the legend used for the 1:20,000 map. The top (0 – 0.7 m) and subsoil (0.7 m – 1.25 m) texture and drainage condition have been

included in the map legend. In addition, three subtypes were identified on the basis of depth to the Tertiary material. The depth limits were slightly modified: 0.6 and 1.2 m instead of 0.75 and 1.25 m as used in the 1:20,000 map. The 1:5000 map shows (Figure 4.3) a more detailed description of the soil variability in the study area, and seven soil series and three subtypes can be observed.

Figure 4.3. The 1:5000 soil map of the study area.

4.3. Soil sampling and laboratory analysis

To investigate the spatial variability of the soil in the study area and to quantify the predictive quality of the two maps, soil samples were taken at 135 geo-referenced locations. This included 80 samples obtained at the nodes of a 50 m x 50 m grid and 55 random samples located within grid cells (Figure 4.4a). Samples were taken from two depths 0 - 30 cm and 50 - 80 cm, representing the top- and subsoil.

At each sampling point, three samples were taken by means of gauge auger within a 1 m radius and mixed to obtain a bulked sample. Air dried soil samples were analyzed for particle size distribution, organic C content and pH (in KCl).

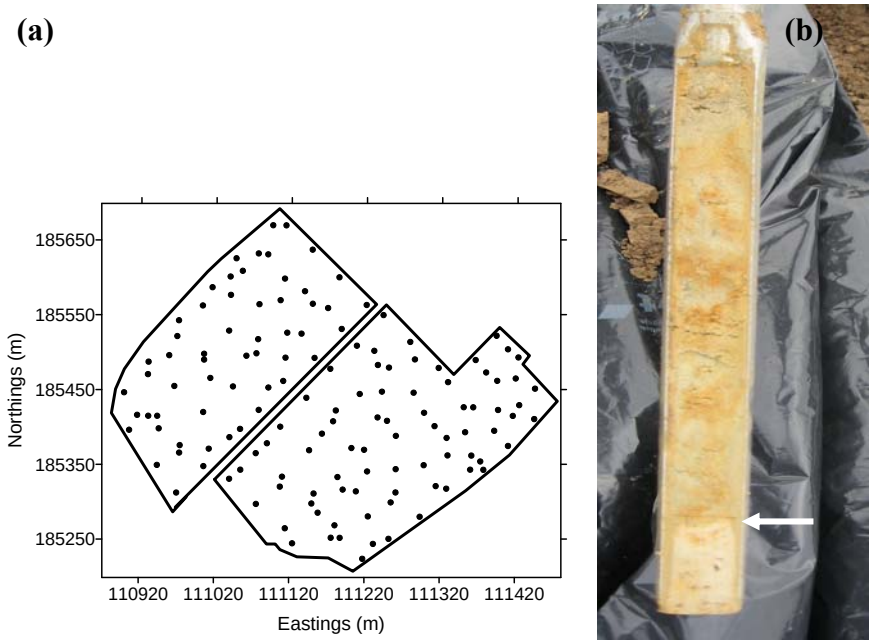

Figure 4.4. (a) The grid plus random sampling scheme showing 135 locations and (b) a depth observation showing the boundary (arrow) between loess material and the underlying Tertiary clay substratum.

Due to the practical difficulties associated with field observations, the depth to the Tertiary clay substratum (D_{ts}) was only determined at 60 locations. This includes the 55 random sampling locations and five additional positions located along the edges of the study area. At all locations a distinct and abrupt boundary was observed between the loess cover and the underlying Tertiary clay substratum (Figure 4.4b) within a depth of 3 m. Sometimes pebbles indicated the presence of a former erosion surface on top of the Tertiary substratum facilitating its identification.

4.4. Electrical conductivity measurements

An apparent electrical conductivity survey of the study area was conducted in April 2006. The mobile measurement system with EM38DD sensor (Figure 3.5) was driven at a speed of about 15 km h^{-1} along two 4 m spaced parallel lines. The measurements were recorded at a frequency of 1 Hz, and resulted in 9586 EC_aH and EC_aV measurements in the entire study area. The survey was conducted over two days. Initially, three quarters of the study area was surveyed. The remaining part was inaccessible and thus it was surveyed after two weeks. The two data sets were subjected to exploratory data analysis in order to remove measurement anomalies.

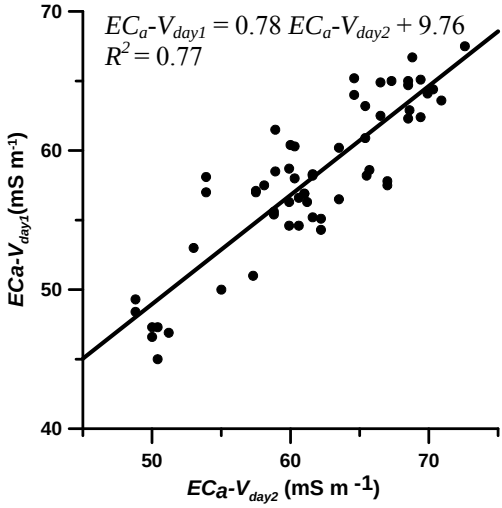

Figure 4.5. Scatter plot between the nearest neighbourhood observations of EC_aV of the surveying day 1 (EC_aV_{day1}) and day 2 (EC_aV_{day2}) and the fitted linear regression relationship.

Totally, 394 observations, having extremely large EC_a values due to the influence of the metal fence around and inside the study area, were removed from the two sets of data. Due to the different ambient conditions and soil moisture conditions prevailed during the two days of measurements, EC_a measurements needed to be

converted to a common basis. Therefore, the measurements taken on the second day were adjusted in order to be compatible with those of the first day. The adjustment procedure involved the pairing of all measurements made on the two survey days which lie within a distance of 4 m. Then, a regression relationship was fitted between them. Finally, this relationship was used to transform the measurements taken on the second day such that they are compatible with the measurements made on the first day. Figure 4.5 shows the scatter plot and the regression relationship calculated for EC_aV data (coefficient of determination, R^2 = 0.77). The EC_aH data also showed a similar strong linear relationship (R^2 = 0.73).

4.5. Data analysis

4.5.1. Spatial analysis

Before spatial analysis, soil data were subjected to exploratory analysis. Experimental variograms were computed and modelled to describe the structure of the spatial variation of soil properties. Subsequently, these soil properties were ordinary block kriged to a common grid (2.5 m x 2.5 m) in order to elucidate their spatial variations. However, due to the compositional nature of textural fractions (individual elements sum to 100 %), spatial prediction of three textural fractions with ordinary kriging was not straight forward. Any spatial prediction technique that is used to estimate the components of a composition should meet two basic requirements (de Gruijter et al., 1997):

1. estimated component of a composition must be non negative

$$z_i^*(\mathbf{x}_\alpha) \geq 0 \qquad i = 1,...p \tag{4.1}$$

where $z_i^*(\mathbf{x}_\alpha)$ denotes the estimate of the i^{th} component of a regionalized composition (with p components) at the location $\mathbf{x}_\alpha$.

2. at each location, the sum of the components must be a constant

$$\sum_{i=1}^{p} z_i^*(\mathbf{x}_\alpha) = 1 . \tag{4.2}$$

Unlike the other soil attributes, the elements of a composition are subject to non-stochastic constraints. This means, a regionalized composition with p components is not drawn from the p dimensional real space R^p, but from a p-1 dimensional simplex S^p embedded in the real space. As a result of this, ordinary kriging of separate components of a composition often fails to meet the second requirement. Consequently, this violates the unbiasedness constraint which is fundamental to kriging (Odeh et al., 2003). To deal with the restrictions associated with the analysis of compositional data, Aitchison (1986) proposed the transformation of S^p corresponding to the compositional data to the R^{p-1} through additive log-ratio transformation (ALR):

$$y_i(\mathbf{x}_\alpha) = \ln\left(\frac{z_i(\mathbf{x}_\alpha)}{z_k(\mathbf{x}_\alpha)}\right) \qquad i = 1,\ldots,p \tag{4.3}$$

where $y_i(\mathbf{x}_\alpha)$ is the ALR transformation of $z_i(\mathbf{x}_\alpha)$ and $z_k(\mathbf{x}_\alpha)$ is the k^{th} component of the composition. Pawlowsky-Glahn and Olea (2004) showed that the choice of the k^{th} component chosen for the denominator does not influence the analytical results (e.g. prediction results) of ALR transformed data. Therefore, the ALR transformation can be considered as order invariant.

Accordingly, the textural fractions were ALR transformed before spatial analysis. After performing variogram analysis and ordinary kriging of the ALR transformed data, predictions were back-transformed by means of additive generalized logistic transformation (Aitchison, 1986):

$$z_i(\mathbf{x}_\alpha) = \frac{\exp y_i(\mathbf{x}_\alpha)}{\sum_{i=1}^{p} \exp y_i(\mathbf{x}_\alpha)}. \tag{4.4}$$

4.5.2. Assessment of predictive quality of polygon maps

Consider a soil mapping unit k, which is sampled randomly at n_k locations, the prediction at any location within the same mapping unit is given by (Webster and Oliver, 2001):

$$z^*(\mathbf{x}_0) = \bar{z}_k = \sum_{i=1}^{n_k} \lambda_i z(\mathbf{x}_i) \tag{4.5}$$

in which

$$\lambda_i = \begin{cases} 1/n_k & \text{for } \mathbf{x}_i \in k, \\ 0 & \text{otherwise} \end{cases}$$

where $\bar{z}_k$ is the estimated mean of the mapping unit k and λ_i is the weight assigned to each observation. The mean squared error of prediction (MSE_k) is given as:

$$MSE_k = \sigma_k^2 (1 + \frac{1}{n_k}) \tag{4.6}$$

where σ_k^2 represents the variance within the mapping unit k. In classical soil mapping, surveyors try to maintain the same categorical level for all the mapping units in a particular survey, e.g. all soil series or all soil families (Webster and Oliver, 2001). Therefore, it can be assumed that the variance within mapping units is approximately the same for all. In these circumstances σ_k^2 in the above equation can be replaced by σ_w^2, the average or pooled within-mapping unit variance. This equation informs that the predictive accuracy of a polygon map is largely decided by the pooled within-mapping unit variance and therefore, can be used to estimate the predictive quality of a map (Leenhardt et al., 1994).

In light of the foregoing, the predictive quality of the two maps of differing scales were evaluated using an intra-class correlation ρ_i^2, which relates the pooled within-mapping unit variance to the total variance (Webster and Oliver, 1990):

$$\rho_i^2 = 1 - \frac{\sigma_W^2}{\sigma_T^2} \tag{4.7}$$

given that, $\sigma_T^2 = \sigma_W^2 + \sigma_B^2$

where σ_T^2 is the total variance and σ_B^2 denotes the variation among mapping unit means (between-mapping unit variance). For each soil property, one way analysis of variance (ANOVA) was used to compute s_T^2, s_B^2 and s_W^2, which estimate σ_T^2, σ_B^2 and σ_W^2, respectively. These were used to estimate the intra-class correlation (R_i^2) values of two polygon maps for all soil properties. The R_i^2 (constrained in the range $0 \leq R_i^2 \leq 1$) is the proportion of variance in the data explained by the classification and analogous to coefficient of determination (R^2) in regression analysis. Evidently, larger values of R_i^2 caused by larger values of s_B^2 and smaller values of σ_W^2, suggest a more precise delineation of map units and better predictive quality of a map. Among the different parameters that can be used to evaluate the predictive quality of soil maps, e.g. map purity and map bias (Van Meirvenne, 1998), the advantage of using R_i^2 is that it can be used to evaluate the predictive quality of a map for any soil property irrespective of the soil variables used in the map legend.

4.6. Results and discussion

4.6.1. Spatial variability of soil properties

The results of the exploratory and geostatistical analysis of the observed soil properties are presented in this section. The objective is the examination of the extent of within-field variability present in the study area. For clarity, the variations within the top and subsoils and the variation of the depth to the Tertiary clay substratum are presented under separate sections.

4.6.1.1. Descriptive statistics

Some descriptive statistics of the measured soil properties are given in Table 4.2. The Kolmogorov-Smirnov test for normality showed normal distribution (at 5 % level of probability) for all the properties except top and subsoil organic C (Figure

4.7) and subsoil clay content. This is further explained by their skewness coefficients given in Table 4.2. The mean particle size of the topsoil corresponds to sandy silt texture class as given by the 1:20,000 soil map. However, the *CV*s of textural fractions (16.2 – 20.7 %) implied a considerable variation.

Table 4.2. Descriptive statistics of sampled soil properties.

	Mean	Min	Max	Variance	*CV* (%)	Skewness
Topsoil (n = 135)						
Clay (%)	12.3	8.3	20.3	4.7	17.7	0.54
Sand (%)	49.7	31.8	69.3	64.5	16.2	0.32
Silt (%)	38.1	21.9	52.1	61.9	20.7	-0.41
Organic C (%)	1.74	1.06	3.2	0.21	26.46	0.80
pH-KCl	5.38	4.27	6.74	0.21	8.5	0.48
Subsoil (n = 135)						
Clay (%)	16.7	5.4	44	42	38.9	1.73
Sand (%)	49.5	13.7	82	249.9	31.9	0.04
Silt (%)	33.8	7.2	56.5	135.1	34.4	-0.22
Organic C (%)	0.2	0.04	0.51	0.01	44.1	0.91
pH-KCl	5.4	4.1	7.1	0.19	8	0.12
D_{ts} (m, n = 60)	1.6	0.5	2.9	0.42	41.1	0.18
EC_a (mS m^{-1}, n = 9192)						
EC_aV	47.2	22.2	78.0	141.6	25.3	0.07
EC_aH	38.9	20.8	64.4	59.3	19.8	0.15

The texture data of topsoil samples was superimposed on the Belgian textural triangle in Figure 4.6a, which classified 78 % of the observations into sandy silt and a majority of the remaining observations were classified to light sandy silt textural class. Therefore, 22 % of the topsoil samples had a different textural class than that predicted by the 1:20,000 soil map (sandy silt). The subsoil textural fractions showed much larger variability in comparison to the topsoil. This was clearly reflected by their *CV*s which were almost twice as large as the

corresponding topsoil fractions. Nevertheless, the textural classes were distributed over five textural classes (Figure 4.6b), silty sand (12.6 %), light sandy silt (8.9 %), sandy silt (48.9 %), clay and heavy clay (29.2 %) implying a larger heterogeneity of the texture of the subsoil

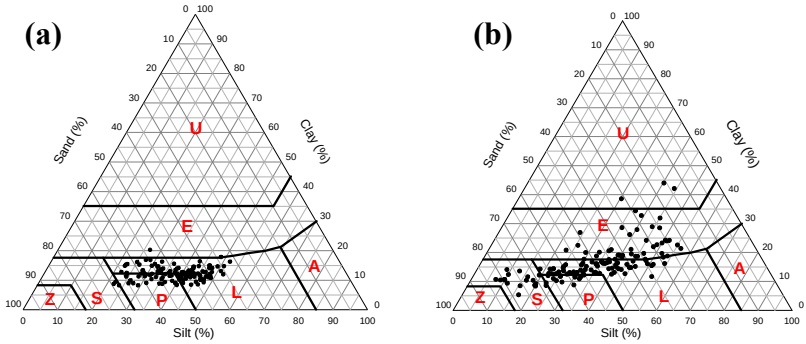

Figure 4.6. The distribution of (a) topsoil and (b) subsoil textural data on the Belgian textural triangle.

The organic C content of the topsoil was distinctively larger than that of the subsoil. The histogram of the topsoil organic C content showed sub populations (Figure 4.7a). However, this pattern was less pronounced in the histogram of the subsoil organic C content (Figure 4.7b).

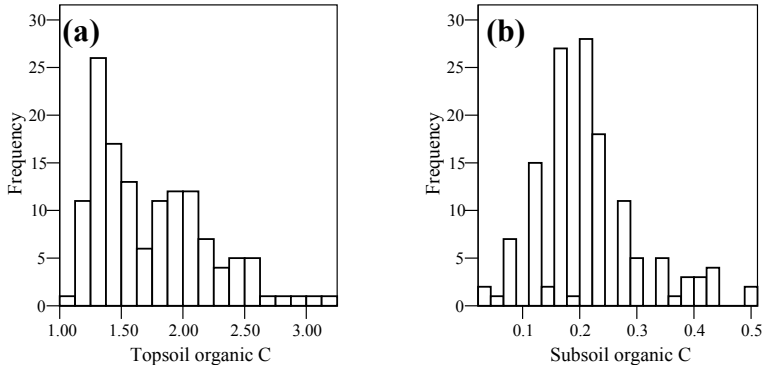

Figure 4.7. Histograms of (a) topsoil and (b) subsoil organic C (%) contents.

The distributions of the topsoil and subsoil pH values showed an equal level of variation (*CV* = 8 %) with similar mean values (pH = 5.4), being slightly acid.

The D_{ts} observations revealed the presence of the Tertiary clay substratum at very shallow (0.5 m) to deeper (2.9 m) depths across the study area (Table 4.2). Nevertheless, a large variation was evident when the *CV* was considered. Contrary to the D_{ts} predictions made by the 1:20,000 soil map (i.e. D_{ts} should be > 1.25 m in 100% of observations, see section 4.2.1.1.), 12 %, 28 % and 60 % of the observations belonged to the shallow (≤ 0.75 m), moderate (> 0.75 m and ≤ 1.25 m) and deep (> 1.25 m) depth classes, respectively.

4.6.1.2. Spatial variability of topsoil properties

The experimental variograms and models fitted for the topsoil properties are given in Figure 4.8 and the model parameters are listed in Table 4.3. The bounded variogram models (spherical and exponential) suggested the absence of spatial trends for the topsoil properties (Webster and Oliver, 2001). The ALR transformed clay content showed anisotropic variations along two principal directions: N22^{0}E and N68 ^{0}W. Directional variograms consisted of different sill and range parameter values implying the presence of a zonal anisotropy in the study area (Goovaerts, 1997). The sill variances indicated that clay content is spatially more heterogeneous in the direction of N68 ^{0}W. The ranges of directional variograms suggested that the spatial continuity of clay content measurements extend predominantly along the N68 ^{0}W direction (203.3 m). There were no prominent direction dependencies observed for the spatial variations of topsoil sand content, organic C content and pH value, thus omni-directional variograms were adequate to model their spatial variations. The small *RNE* values in the variograms (Table 4.3), indicated that the variations of topsoil properties are spatially strongly structured.

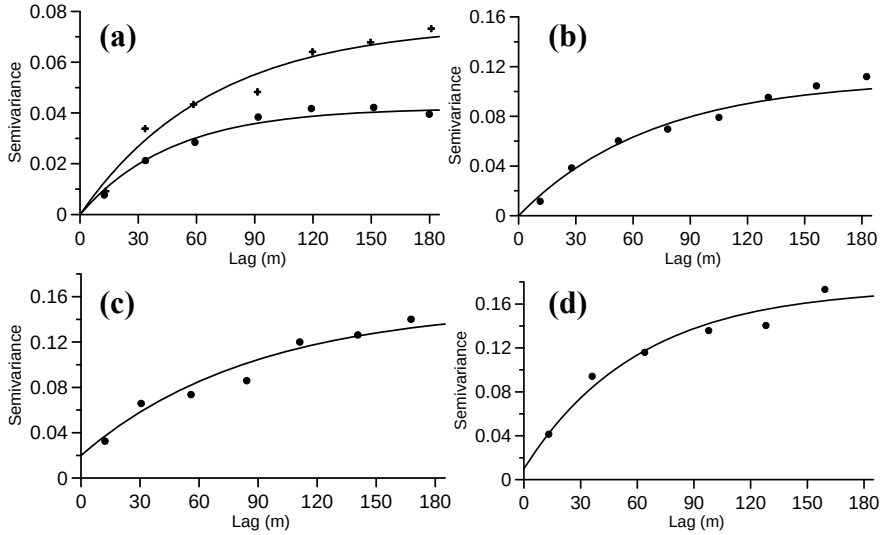

Figure 4.8. (a) Directional experimental variogram (dots: N22 ^{0}E and crosses: N68 ^{0}W direction) and fitted models (curves) for topsoil clay and omnidirectional experimental variograms and fitted models for (b) sand (c) organic C content and (d) pH.

Table 4.3. Model parameters of the fitted variogram models for the topsoil properties

Property	Direction	Model	Variogram parameters			*RNE* (%)
			Nugget	Sill	Range (m)	
Clay*	N22^{0}E	Exp	0.00	0.04	141.2	0.00
	N68^{0}W	Exp	0.00	0.08	203.3	0.00
Sand*	Omni	Exp	0.00	0.11	210.0	0.00
Organic C	Omni	Exp	0.02	0.15	263.9	13
pH	Omni	Exp	0.01	0.17	182.0	6

* Additive log ratio transformed

The zonal anisotropy of the topsoil clay content was incorporated into the ordinary kriging system employing the methodology described by Goovaerts (1997). The maps of kriged predictions for topsoil properties are shown in Figure 4.9. The topsoil sand map (Figure 4.9a), showed that the sand content is generally smaller (32 - 40 %) in the western part than in the eastern part of the study area (50 – 60 %). The reverse was true for the silt content. In contrast, the clay content map (Figure 4.9b) showed marked differences over short distances. Localized areas

with small and large clay contents could be found both in the western and eastern parts of the study area.

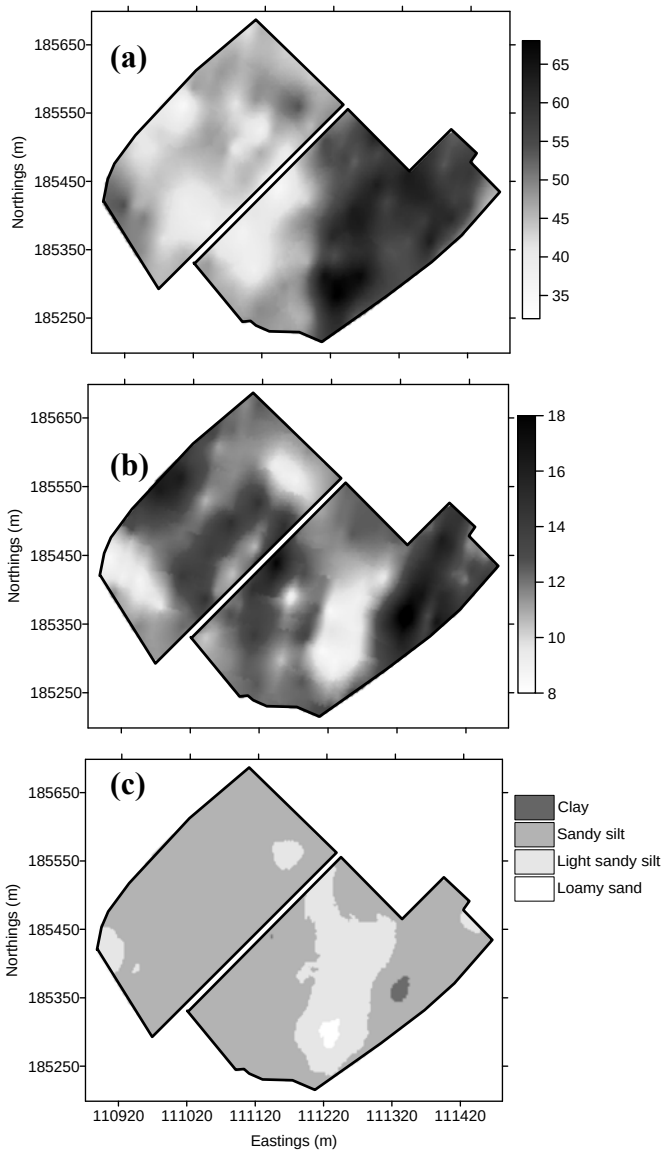

Figure 4.9. Kriged estimates of topsoil (a) sand (%), (b) clay (%), (c) texture classes, (d) organic C (%) and (e) pH.

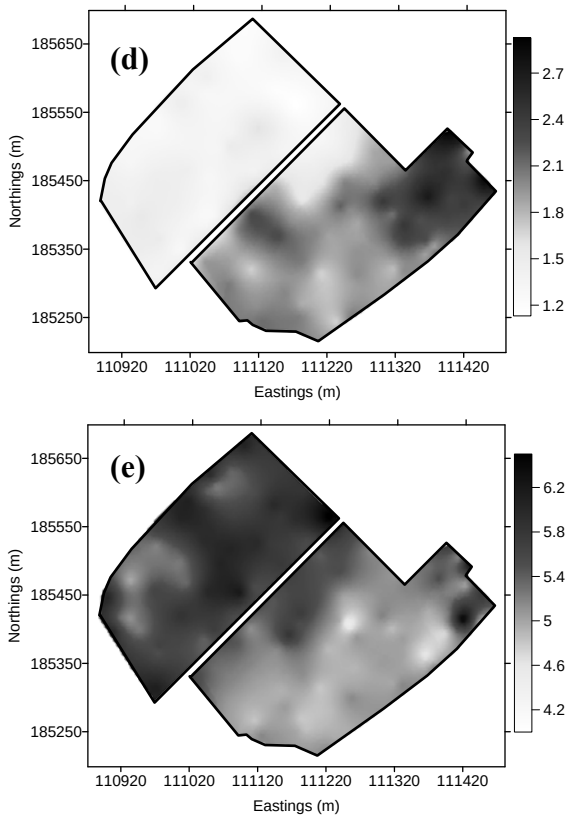

Figure 4.9. Continued…

Figure 4.9c shows the distribution of textural classes derived from the interpolated texture maps. The soil texture of a large part of the study area (11.8 ha) was sandy silt while a band covering a small area (2.7 ha) contained a light sandy silt soil. This indicated that the topsoil texture of a majority of the study area has been accurately classified (sandy silt texture) in the 1:20,000 soil map.

The spatial distribution of the topsoil organic C content (Figure 4.9d) was strongly influenced by the type of land use. The concentration of soil organic C content in pasture was approximately two times greater than that in arable field. This is confirmed by the distribution of organic C content on the two land uses shown by the box plot (Figure 4.10a). Such an enrichment of organic C content on pasture

lands is not uncommon (Dell and Sharpley, 2006). As Haynes et al. (2003) pointed out, the large turnover of the extensive, dense grass root system is the main cause of the enrichment of the organic C content in pasture fields even though above ground inputs in form of stem and leaf tissue and animal dung also occur. In contrast, in arable land, much of the plant material is removed for animal food and a relatively small amount is returned back to the soil. In addition, soil tillage aerates the soil and breaks up the organic residues, making them more susceptible to microbial decomposition. Nevertheless, a smaller variation of organic C content within the arable field (*CV* = 10 %) was observed in comparison to the pasture field (*CV* = 20 %). Contrary to the general spatial trend, a rectangular patch of low organic C content can be noticed in the north-western corner of the pasture land. It is likely that this part of the field might have been used for arable farming in the recent past.

The spatial distribution of pH also showed a clear relationship to land usage (Figure 4.9e). Generally, the pH values in the arable field was slightly larger than in the pasture field (Figure 4.10b).

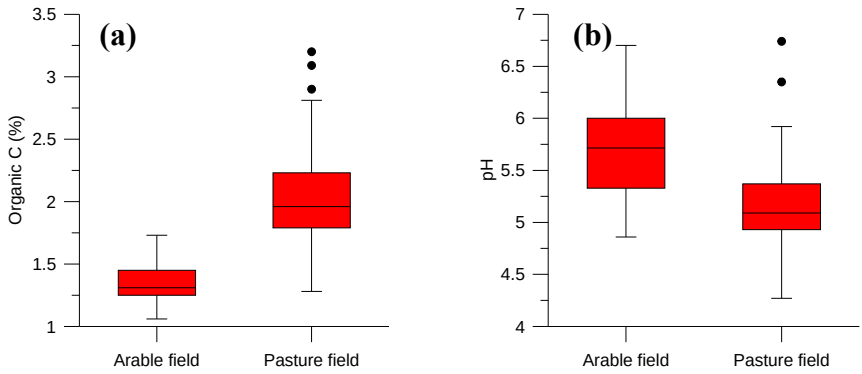

Figure 4.10. Box plots showing the variation of the topsoil (a) organic C and (b) pH in arable and pasture fields. The ends of bars indicate the 25th and 75th percentiles. The median is indicated by a line, and the symbols represent the data outliers.

The lower pH values observed in the pasture field can be related to higher microbial activities present in organic C rich soil environments. Therefore, the organic and inorganic acids produced by the enhanced microbial activity can have a strong influence on the lower pH in the pasture field.

The spatial variation of organic C content and pH highlights the fact that human-induced changes to the soil can have a strong influence on their within-field variability. Therefore, the information about the management history such as previous field allocations and the type of land use could be useful as categorical ancillary information for characterizing within-field soil spatial variability.

4.6.1.3. Spatial variability of subsoil properties

The experimental variograms for subsoil properties and the models fitted are shown in Figure 4.11 and Table 4.4 gives the model parameters.

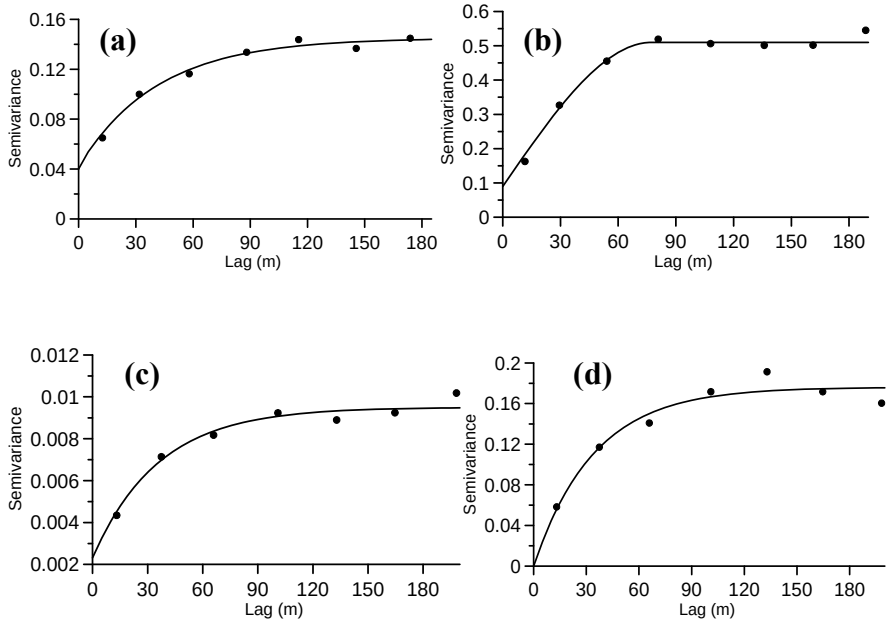

Figure 4.11. Omni directional experimental variograms (dots) and fitted models (curve) for subsoil (a) clay, (b) sand, (c) organic C and (d) pH.

Unlike in the topsoil, directional dependency was not evident for the spatial variation of subsoil clay content, therefore an experimental isotropic variogram was used. This emphasized that the variation of clay content in the top and subsoil layers are controlled by different processes. The patterns of variation of other soil properties were also fairly similar in all directions. The extent of the spatial continuity of all subsoil properties was generally smaller than their topsoil counterparts (compare range values in Tables 4.3 and 4.4). Moreover, the small *RNE* values of subsoil properties (> 25 %), except clay content (28.3 %), indicated that their spatial variations are strongly structured.

Table 4.4. Model parameters of the fitted variogram models for the subsoil properties.

Property	Direction	Model	Variogram parameters			*RNE* (%)
			Nugget	Sill	Range (m)	
Clay*	Omni	Exp	0.04	0.14	124.4	28.3
Sand*	Omni	Sph	0.09	0.51	77.5	17.6
Organic C	Omni	Exp	0.002	0.009	107.4	22.2
pH	Omni	Exp	0.00	0.176	103.4	0.0

* Additive log ratio transformed

The maps of kriged predictions for subsoil properties are shown in Figure 4.12. The sand content map (Figure 4.12a) showed that the values were vary to a greater extent in the western part of the study area. The larger sand contents distributed in the areas located at higher elevations, i.e. in the western corner, as well as on lower elevations, i.e. in the north eastern corner, suggested that the landscape processes have no relevance on its spatial distribution. The smaller values occurred on a relatively large area in the western part. The sand content was generally large and less variable in the eastern part. The spatial distributions of silt and clay contents (Figure 4.12b) were very similar to that of the sand content but opposite in magnitude. The subsoil texture classes map presented in Figure 4.12c captured largely the distributions of sand and clay contents. A major part of the study area (8.6 ha) belonged to sandy silt soils and the remaining area contains mainly clayey

soils (4.6 ha). Texture classes silty sand, light sandy silt and heavy clay were distributed on relatively smaller areas (< 0.8 ha). The individual textural fractions and textural classes resembled to large extent the D_{ts} map (see further).

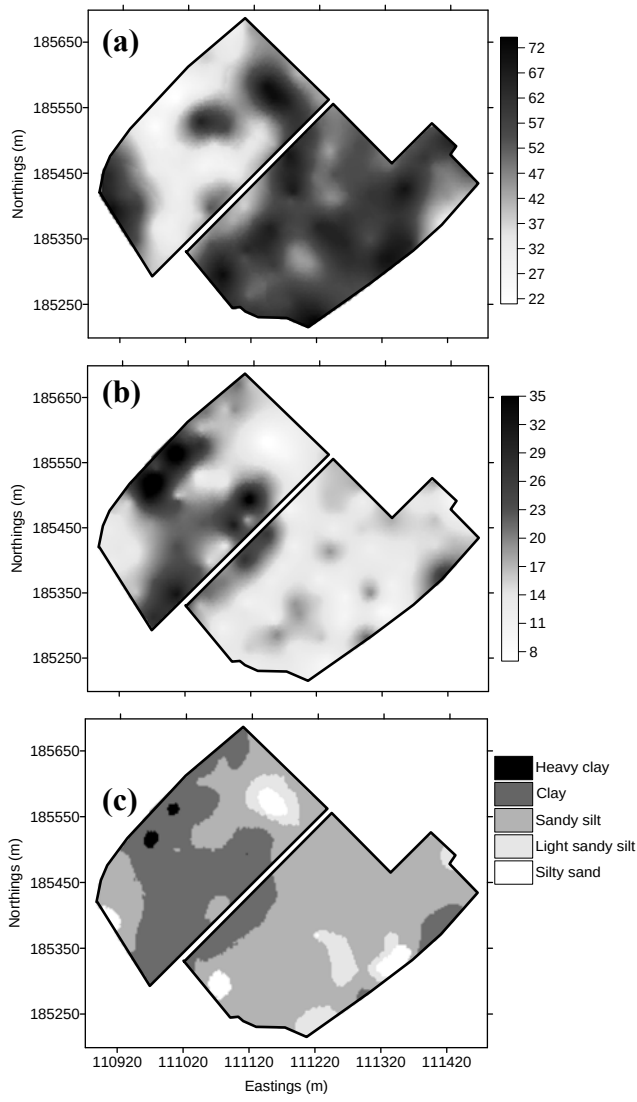

Figure 4.12. Kriged estimates of subsoil (a) sand (%), (b) clay (%), (c) texture classes, (d) organic C (%) and (e) pH.

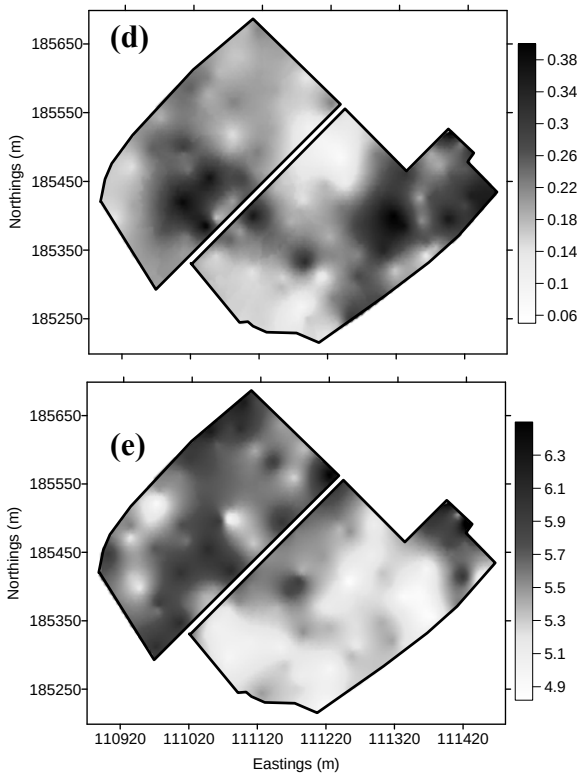

Figure 4.12. Continued…

The larger subsoil organic C (Figure 4.12d) was observed in the low lying north eastern area (pasture field) and in the western part (arable field) of the study area where high clay contents were observed (Figure 4.12b). Therefore, unlike the topsoil, the distribution of the subsoil organic C content did not have a distinct relationship with land use. Low lying landscape positions are known to accumulate organic materials due to lower microbial decomposition attributed to poor aeration as well as due to the deposition of eroded soil material. It is a well known fact that organic C content tends to increase with clay content because of the formation of clay-humus complexes that protect organic matter from degradation (Brady and Weil, 1999). The influence of land use could also be detected for the subsoil pH (Figure 4.12e), but not as prominently as in the topsoil.

4.6.1.4. Spatial variability of depth to the Tertiary clay substratum

The experimental variogram calculated for D_{ts} observations and the fitted spherical model (Figure 4.13a) showed a strong spatial structure (*RNE* = 15 %) and a spatial continuity extending up to 226.5 meters. The kriged estimates of D_{ts} are given in Figure 4.13b. It can be observed that the Tertiary clay substratum occurs quite deep (1.5 - 2.7 m) in the western corner of the study area, which coincided with the highest soil surface elevations within the study area. Importantly, shallow to moderate depths (0.4 - 1.50 m) were mapped over a large part of the western half of the study area. This shallow position of the substratum can be expected to influence crop performance and soil management through limiting soil drainage and the soil volume available for crop growth. In the eastern part, the substratum was predicted to occur at deep (1.5 - 3.0 m).

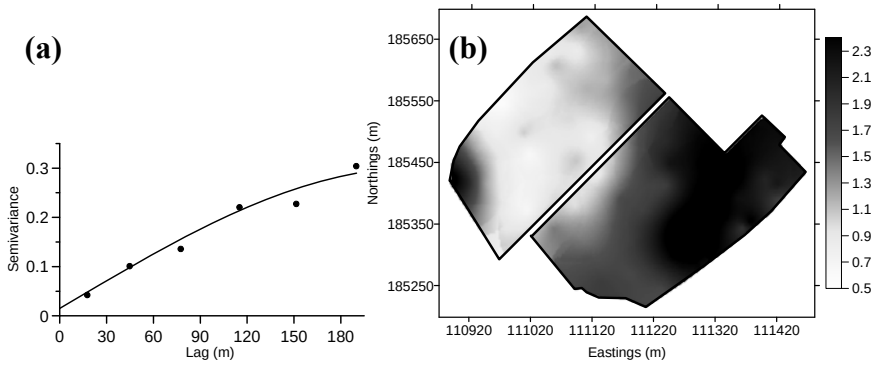

Figure 4.13. (a) Experimental variogram calculated for D_{ts} (dots) and fitted exponential model (curve, range = 226.5 m, sill = 0.3, nugget = 0.02 and *RNE* = 15 %), (b) kriged estimates of depth to the Tertiary substratum (m).

The within-field variation of D_{ts} obtained through the field observations disagreed considerably with that provided by the 1:20,000 soil map (Figure 4.2). However, the sub units of the more detailed 1:5000 map (Figures 4.3 and 4.14) resembled closely the observed spatial distribution of D_{ts}.

The spatial variation of D_{ts} strongly coincided with the spatial patterns of topsoil sand content (Figure 4.9a) as well as subsoil sand and clay contents (Figures 4.12a and b). This graphical interpretation was evident due to the strong correlations observed between D_{ts} (n = 60) and the corresponding observations of topsoil sand content (r = 0.74) and subsoil sand content (r = 0.57) and subsoil clay content (r = -0.60). These results suggested that the D_{ts}, has a direct influence on the particle size distribution of the overlying soil material. It is likely that the soil processes such as cryoturbation that occurred during the last glacial period has mixed the Tertiary clay with the aeolian material causing this variability. Although, the topsoil clay content distribution (Figure 4.9b) also showed some resemblance to the variation of D_{ts}, the clay contents at 60 observation points was poorly correlated with the D_{ts} (r = 0.15). Besides, the elevation showed a weak but a somewhat larger correlation to clay content (r = 0.29). It is likely that the variation of clay content is confounded by the influence of the Tertiary clay substratum as well as the geomorphic processes of erosion, transportation and deposition. This was further confirmed by the variogram analysis, which showed distinct differences in spatial variation along the direction of the main elevation gradient and its perpendicular direction.

4.6.2. Predictive quality assessment of polygon soil maps

4.6.2.1. Predictive quality of the 1:20,000 map

Two map units of the 1:20,000 map (Figure 4.2) were considered to calculate the R_i^2 for all the investigated soil properties. Table 4.5 lists their pooled within-class variances and R_i^2 values. For all soil properties, except subsoil organic C content and pH, the soil map has within-class variances smaller than the total variance (compare with Table 4.2). However, the reduction in total variance by the map units was not substantial. As a consequence, the R_i^2 values corresponding to both top and subsoil properties and D_{ts} were also small.

The intra-class correlation values for soil physical properties ranged from 0.02 (topsoil clay content) to 0.19 (D_{ts}) indicating a poor predictive quality of the 1:20,000 soil map.

Table 4.5. Within-class variances (s_W^2) and intra-class correlation values (R_i^2) of the 1:20,000 soil map.

	s_W^2	R_i^2
Topsoil		
Clay (%)	4.6	0.02
Sand (%)	56.0	0.13
Silt (%)	52.6	0.15
Organic C (%)	0.18	0.17
pH	0.19	0.09
Subsoil		
Clay (%)	37.1	0.12
Sand (%)	224.9	0.10
Silt (%)	127.8	0.05
Organic C (%)	0.01	0.00
pH	0.19	0.00
D_{ts} (m)	0.3	0.19

Subsoil organic C and pH showed no reduction in the total variance portioned by the two mapping units, thus the 1:20,000 soil map has no relevance for predicting their variability. Moreover, the same is true for topsoil organic C and pH, for which the map was only able to explain 9 % and 17 %, respectively, of the total variability. Webster and Beckett (1968) and Marsman and de Gruijter (1986) have also reported very poor predictive qualities of soil maps ($R_i^2 < 0.28$) for soil chemical properties.

The R_i^2 values of all measured soil properties indicated that their spatial prediction at a within-field scale, on the basis of mapping units will be subjected to a substantial prediction error. As Lin et al. (2005) pointed out, the prediction

accuracy of a particular map depends on the scale of spatial variation that needs to be resolved. Therefore, it should be emphasized that this poor prediction accuracy of the 1:20,000 map can not be generalized. Although it was not possible to accurately predict soil properties at a within-field scale level, its ability to predict soil properties at regional scale as shown by Van Meirvenne (1998) should not be undermined.

4.6.2.2. Predictive quality of 1:5000 soil map

The classification criteria of the 1:5000 soil map allowed for the derivation of three individual soil map layers detailing the variability of the topsoil (Figure 4.14a), the subsoil (Figure 4.14b) and the depth the Tertiary clay substratum (Figure 4.14c). These class delineations were used to calculate R_i^2 values of the corresponding soil properties (Table 4.6).

According to the variation of topsoil textural fractions, on the 1:5000 soil map three distinctive areas were identified. The soil surveyors have used a detailed version of Belgian soil texture triangle (16 classes) for map unit delineation, intending to minimize the within-class variation. However, Table 4.6 suggests that the reduction of total variation (compare with Table 4.2) achieved due to this partition was not as substantial as expected. As a consequence, the textural fractions, which were explicitly used for the classification showed small R_i^2 values ranging from 0.06 to 0.14. Surprisingly, the R_i^2 values of sand and silt contents were smaller than the values observed for the 1:20,000 map. The topsoil organic C content and pH values also showed small R_i^2 values. This suggested that no improvement in prediction accuracy of any of the topsoil properties has been achieved through the use of a detailed soil mapping.

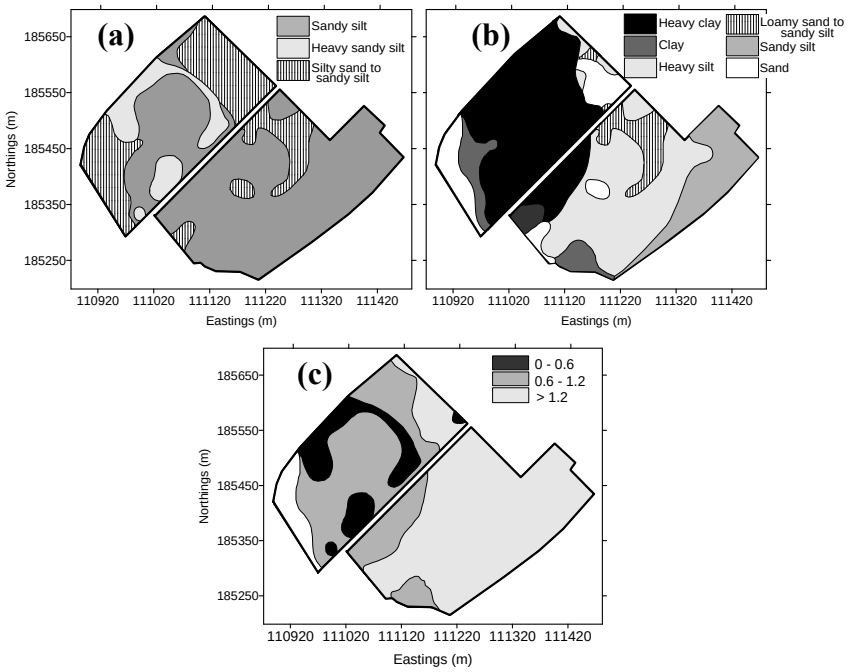

Figure 4.14. Mapping units of the 1:5000 soil map showing the variations of (a) topsoil and (b) subsoil texture and (c) depth to the Tertiary clay substratum (m).

The partition of variance by six subsoil classes showed the largest intra-class correlation values (> 0.30) for the soil textural fractions. The soil map is not useful with respect to the predictive quality of the organic C content and pH ($R_i^2 < 0.05$).

The inconsistency in predictive quality observed for the top and subsoil texture can be linked to the spatial variation in these two layers. It is evident that the soil surveys were able to partition the variation of highly varying subsoil textural fractions (Table 4.2) to a better manner compared to less varying topsoil texture. This clearly highlights the fact that the success of classical soil surveying is largely influenced by the variability of the soil environment. This statement is supported by the findings of Voltz and Webster (1990), who concluded that the partition of soil variation into map units becomes satisfactory where the soil changes abruptly, but not so well where the soil changes gradually.

Table 4.6. Within-class variances (s_W^2) and intra-class correlation values (R_i^2) of the 1:5000 soil map.

	s_W^2	R_i^2
Topsoil		
Clay (%)	4.1	0.14
Sand (%)	60.4	0.06
Silt (%)	57.7	0.07
Organic C (%)	0.16	0.24
pH	0.19	0.08
Subsoil		
Clay (%)	29.4	0.30
Sand (%)	166.4	0.33
Silt (%)	105.5	0.32
Organic C (%)	0.01	0.04
pH	0.18	0.05
D_{ts} (m)	0.2	0.62

The three depth classes of 1:5000 soil map (Figure 14.14c) explained a much larger proportion of the variance of D_{ts} ($R_i^2 = 0.62$) than it did for the other properties. This suggests that the major contributions to the variance are the changes across boundaries and these could be represented satisfactorily at 1:5000 soil map level. According to published values (Webster and Oliver, 1990) it is evident that the 1:5000 map is capable of accurately predicting D_{ts} in the study area.

4.6.3. Upgrading the Belgian national soil map using a EC_a data

The results presented above clearly demonstrated the requirement of upgrading the Belgian national soil map by incorporating accurate soil information. The traditional way to upgrade a soil map is to conduct a new survey, either at a similar scale but focussing on soil properties that have not been considered in the original soil survey (McGrath and Loveland, 1992), or at a more detailed scale to obtain a better representation of the spatial variability of the mapped soil properties (Dent

and Young, 1981). More recently, map upgrading attempts have been made by combining the predictions obtained by interpolating soil observations with predictions by soil polygon maps (Van Meirvenne et al., 1994). But these invasive methods require large field survey efforts and thus they are often limited by the cost and time constraints associated with intensive field sampling and laboratory analysis (Oberthür et al., 1996). Recent developments in proximal non-invasive soil sensing techniques including EC_a sensing, offer new opportunities to improve the accuracy of soil maps with considerable reductions in sampling effort (Adamchuk et al., 2004).

The focus of the subsequent sections of this chapter is to evaluate the potency of the use of EC_a to upgrade the soil map. Depth to the Tertiary clay substratum is selected as the target soil variable for map upgrading because of its dominant influence on soil properties such as hydraulic conductivity, lateral movement of soil water and agrochemicals and thus the site-specific soil management. Nevertheless, as seen in section 4.6.1.4 the composition of surface soil materials is also determined by D_{ts}. In previous work conducted in elsewhere, it has also been found that similar restrictive soil substrata have a direct influence on the variation of yield (Kitchen et al., 1999) as well as on management practices like nutrient and water management (Hummel et al., 1996; Thompson et al., 1991).

The map upgrading procedure adopted in this study involves three steps; (1) prediction of D_{ts} using densely measured EC_a, (2) replacement of incorrect D_{ts} information presented in the map with new information to generate an upgraded 1:20,000 soil map and (3) assessment of the achieved improvement in map accuracy in comparison with the 1:5000 soil map.

4.6.3.1. Spatial distribution of EC_a and its relationship with D_{ts}

On average, the 9192 EC_aV measurements were larger than the collocated EC_aH measurements (Table 4.2 in page 86), which indicated the presence of a more conductive subsoil underlying a topsoil of lower conductivity. The *CV* of the two measurements indicated a larger variation of EC_aV. However, both measurements

showed an approximately symmetric distribution, as shown by their near to zero coefficient of skewness. Moreover, a very strong correlation between both measurements (r = 0.98) and identical spatial patterns indicated a large degree of similarity in both measurements. Therefore, only the ordinary kriged map of EC_aV measurements is presented in Figure 4.15.

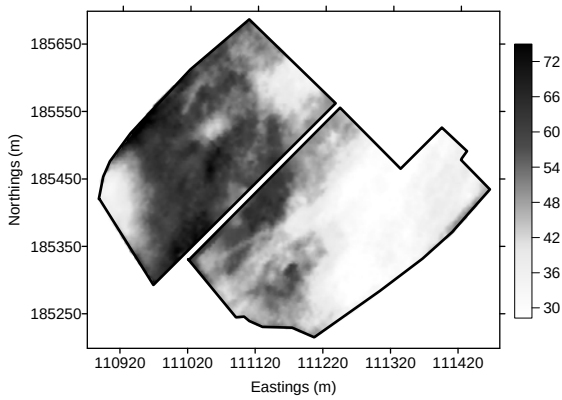

Figure 4.15. Kriged estimates of EC_aV (mS m^{-1})

The spatial distribution of the EC_aV data markedly resembled the ordinary kriged maps of subsoil textural fractions and depth to the Tertiary clay layer (Figures 4.12a to c and 4.13b, respectively). The lowest readings (i.e., < 40 mS m^{-1}) were observed in the western corner and in the eastern part of the field where the Tertiary clay layer was identified at relatively greater depth. The largest EC_aV (> 65 mS m^{-1}) values were distributed over the western part of the study area, where the clay layer was located at relatively shallow depths.

Strong negative correlations were found between D_{ts} and both EC_aV (r = -0.90) and EC_aH (r = -0.87). Considering the higher correlation and deeper sensing depth, the EC_aV measurements were preferred as an ancillary variable to predict D_{ts}. Several authors have reported a strong response of EC_a measurements to a range of subsoil features. This has enabled their use for estimating depth to permafrost (Kawasaki and Osterkamp, 1988), depth of sand deposition resulting

from flooding (Kitchen et al., 1996), mapping surface soil thickness (Boettinger et al., 1997; Bork et al., 1998) and for the evaluation of edaphic discontinuities (Saey et al., 2008; Stroh et al., 2001).

Figure 4.16 explains the reasons for the negative relationship observed between EC_a and D_{ts}. Recalling section 3.4.1, the response of EM38 sensor is an integration of soil conductivity with depth, as weighted by relative response function. When the Tertiary clay substratum appears near to the soil surface (low D_{ts}, Figure 4.16a), the highly conductive Tertiary clay materials occupy a large volume of the soil mass below the sensor. This results in the generation of large primary electrical current loops, as shown schematically by the thickness of the ellipses, thus giving rise to strong secondary magnetic fields at the receiver coil. Consequently, the sensor readings become large.

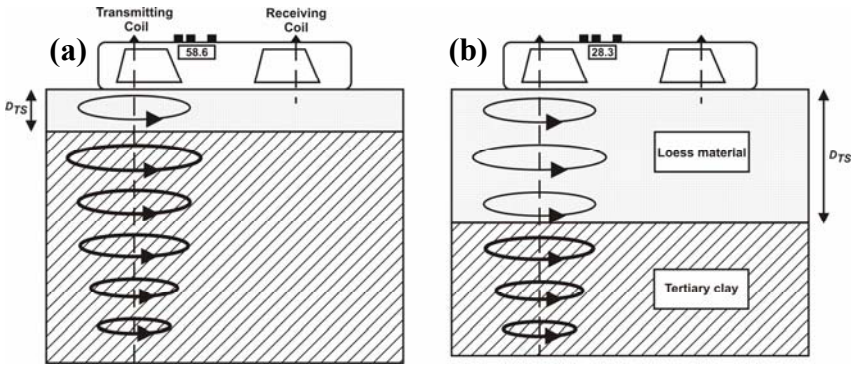

Figure 4.16. Schematic presentation showing the response of the EM38 sensor in vertical dipole mode when (a) the Tertiary clay substratum occurs at shallower and (b) at deeper depths.

On the other hand, the occurrence of the substratum at greater depths below the surface increases the contribution of loess materials for the overall EC_a values (Figure 4.16b). Consequently, the strength of the induced soil primary electrical

current loops and the resulting secondary magnetic fields at the receiver coil become low. The result is relatively low EC_a readings.

4.6.3.2. Spatial prediction techniques

A number of geostatistical interpolation techniques have been tested to predict sparsely measured primary soil variables supported by densely measured ancillary variable(s). For more descriptions of the theory and the applications opof these techniques, see McBratney et al. (2003). Among the different techniques, regression kriging has proven to be an accurate method, especially in circumstances where a strong empirical relationship can be established between the primary and ancillary variables (Hengl et al., 2004). It is important to note that the regression kriging procedure needs a considerable number of observations of the primary variable (> 60) in order to establish an empirical relationship and for subsequent interpolation of residuals (see further). Moreover, these samples should optimize both the attribute space of ancillary variables and geographical space. This requirement can greatly undermine the advantage of using ancillary information in circumstances where sampling of primary variables involves a lot of cost and time. The latter is especially true for D_{ts} observations. Therefore, as an alternative, a model derived on the basis of the depth sensitivity function of EM38 sensor (McNeill, 1980; Saey et al., 2008) can be used to directly transform the EC_a measurements to D_{ts}. We hypothesized that the number of observations of the primary variable can be considerably reduced employing this approach since the nature of the relationship between the primary and ancillary variables is known a priori. Therefore, having proposed two possible methods of predicting D_{ts}, this study considered the usability of these two approaches in relation to the prediction accuracy and required number of samples. The regression kriging procedure was adopted with all observations of the primary variable (60 points). The method based on the depth sensitivity function was tested for three different sample numbers: 60, 40 and 20.

The prediction accuracies of these methods were evaluated using 46 additional observations of D_{ts} and by calculating the *MEE*, *RMEE* and *r* for the observed and

the corresponding estimates. Observations along three transects were taken ensuring that both the smallest and the largest D_{ts} *values* predicted by EMI sensing and the 1:5000 map have been sampled.

Regression kriging

According to the regression kriging procedure outlined by Hengl et al. (2004), the methodology employed to estimate D_{ts} at any unsampled location ($z^*(\mathbf{x}_0)$) can be summarised in five steps: (1) interpolation of EC_aV to a 2.5 m x 2.5 m grid by the ordinary kriging procedure (2) establishment of a regression relationship between D_{ts} and EC_aV which is used to predict D_{ts} at all grid locations $\mathbf{x}_0$, yielding $D^*_{ts,r}(\mathbf{x}_0)$; (3) calculation of residuals $r(\mathbf{x}_\alpha)$ at the 60 locations where D_{ts} has been measured, $\mathbf{x}_\alpha$ ($\alpha = 1,\ldots, 60$) as:

$$r(\mathbf{x}_\alpha) = \{D_{ts}(\mathbf{x}_\alpha) - D^*_{ts,r}(\mathbf{x}_\alpha)\} \tag{4.8}$$

(4) interpolation of these residuals to all grid nodes $\mathbf{x}_0$ using simple kriging with a mean of zero and the variogram of the residuals and (5) estimation of D^*_{ts} at all grid nodes by taking the sum of $D^*_{ts,r}(\mathbf{x}_0)$ and the interpolated residuals $r^*(\mathbf{x}_0)$:

$$D^*_{ts}(\mathbf{x}_0) = D^*_{ts,r}(\mathbf{x}_0) + r^*(\mathbf{x}_0) \ . \tag{4.9}$$

Predictions based on the depth sensitivity function

Recall the depth sensitivity function of EC_aV measurement is provided by equation 3.3. The integral of the depth sensitivity function gives the cumulative response function of EC_aV measurements ($R_v(z)$) (McNeill, 1980):

$$R_v(z) = \int_z^\alpha \Phi_v(z)\mathrm{d}z \tag{4.10}$$

$R_v(z)$ provides the relative contribution for a EC_aV measurement from all the materials below a depth z (m). Specifically, the $R_v(z)$ function for the EM38 sensor can be written as:

$$R_v(z) = (4z^2 + 1)^{-0.5} \ . \tag{4.11}$$

This function is illustrated in Figure 4.17.

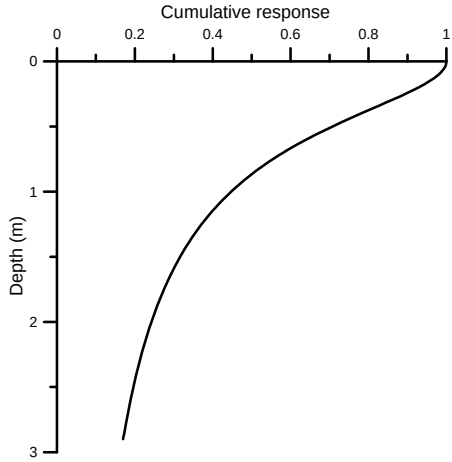

Figure 4.17. Cumulative response function of EM38 sensor for measurements taken in the vertical dipole mode in a homogenous material.

Equation 4.11 can be used to construct a relationship between EC_aV and D_{ts}. Consider the two-layered soil matrix observed in this area with loess on the surface and an underlying Tertiary clay layer. If we consider a location on the field $\mathbf{x}_\alpha$ where the Tertiary clay layer is measured at D_{ts}, the cumulative response arising from below this depth can be written as $R_v(D_{ts}(\mathbf{x}_\alpha))$, whereas the cumulative response from the loess material is given as 1- $R_v(D_{ts}(\mathbf{x}_\alpha))$. Assuming the electrical conductivities of Tertiary clay ($EC_{a,clay}$) and loess ($EC_{a,loess}$) are uniform, the instrument reading can be modelled as:

$$EC_aV(\mathbf{x}_\alpha) = [1 - R_v(D_{ts}(\mathbf{x}_\alpha))] \cdot EC_{a,loess} + [R_v(D_{ts}(\mathbf{x}_\alpha))] \cdot EC_{a,clay} . \quad (4.12)$$

Inversely, $R_v(D_{ts})$ at an unsampled location ($\mathbf{x}_0$) can be modelled if EC_aV ($\mathbf{x}_0$), $EC_{a,clay}$ and $EC_{a,loess}$ are known:

$$R_v(D^*_{ts}(\mathbf{x}_0)) = \frac{EC_aV(\mathbf{x}_0) - EC_{a,loess}}{EC_{a,clay} - EC_{a,loess}} . \quad (4.13)$$

The calculated cumulative response $R_v(D_{ts}^*)$ can be substituted into equation 4.11 to obtain the modelled $D_{ts}^*(\mathbf{x}_0)$:

$$D_{ts}^*(\mathbf{x}_0) = \left[\frac{1}{4 \cdot R_v(D_{ts}^*(\mathbf{x}_0))^2} - \frac{1}{4} \right]^{0.5} . \quad (4.14)$$

Direct conversion of EC_aV measurements to D_{ts} using the depth sensitivity function was not possible in this study, since $EC_{a,clay}$ and $EC_{a,loess}$ were unknown. Therefore, these unknown parameters were estimated iteratively on the basis of D_{ts} observations by minimizing the least squares function:

$$\sum_{i=1}^{n} \left[D_{ts}(\mathbf{x}_\alpha) - D_{ts}^*(\mathbf{x}_\alpha) \right]^2 = \min \quad (4.15)$$

where *n* indicates the number of calibration observations.

Ideally, for a successful calibration of a prediction model, samples should be selected in such a way as to represent the data distribution (or attribute space) of the ancillary variable (see section 3.2). Thus, to calibrate the model (equation 4.15) a representative subset of EC_aV measurements should be selected from the whole data set followed by the observations of corresponding D_{ts}. However, since the 60 D_{ts} observations were taken independent of the EC_a measurements, this sampling procedure could not be used to evaluate the prediction accuracy by decreasing the number of samples. Therefore, an alternative approach was used. This included two main steps: first, the EC_aV values corresponding to the 60 D_{ts} observations were recorded, then a Latin-hypercube sampling procedure (section 3.2) was used to pick subsets of samples of EC_aV (n = 40 and 20) and the corresponding D_{ts} measurements were taken for model calibration.

4.6.3.3. Performance of different prediction techniques

The relationship between EC_aV and D_{ts} was empirically fitted by an exponential regression (Figure 4.18a) with a coefficient of determination (R^2) of 0.80:

$$D_{ts} = 6.7 \exp(-0.03\ EC_aV). \quad (4.16)$$

An exponential relation can be expected since the response of EM38 measurements reduces non-linearly with an increasing depth (Figure 4.17).

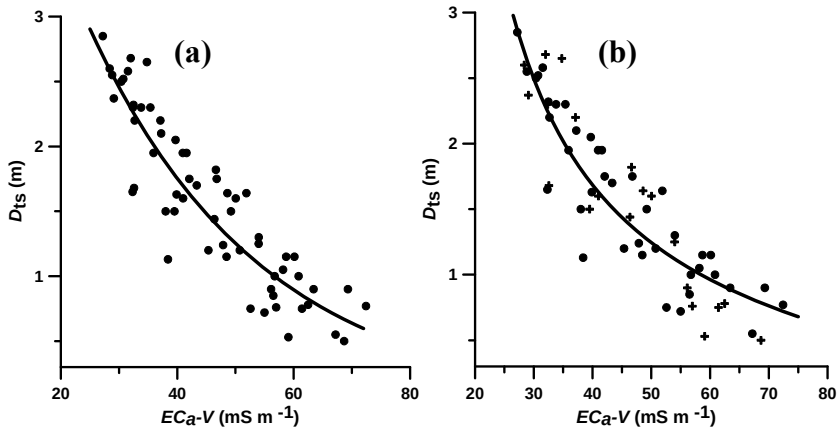

Figure 4.18. Depth to the Tertiary clay substratum (D_{ts}) as a function of apparent electrical conductivity in the vertical dipole mode (EC_aV) with (a) fitted empirical exponential regression and (b) depth sensitivity function calibrated with 20 samples (crosses: calibration samples; dots: remaining samples).

Non-linear empirical relationships between interface depths of contrasting soil layers and EC_a were reported by Doolittle et al. (1994) and Cockx et al. (2007). However, these relationships have generally been established for the layers located within the depth of exploration of the EMI sensor. This depth is defined as the soil depth that contributes for a 70 % of the instrument response and for EM38 sensor in the vertical dipole mode this is 1.5 m (Figure 4.17). The results of this study indicated that such relationships remain unchanged even for mapping materials located well below this depth.

An isotropic spherical variogram was found to represent best the spatial variation of the residuals (Figure 4.19). The absence of a nugget variance suggested a strong spatial structure of the residuals, indicating the potential of regression kriging.

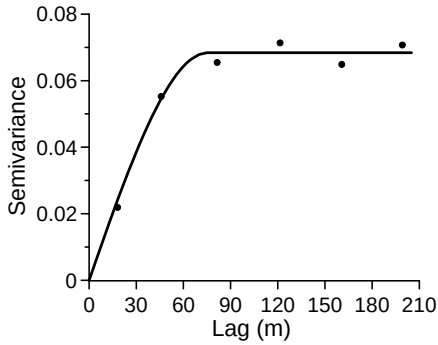

Figure 4.19. Experimental variogram (dots) calculated for residuals of D_{ts} and fitted spherical model (curve, range = 75.6 m, sill = 0.07, nugget = 0.0 and *RNE* = 0 %).

The predictions of D_{ts} obtained with regression kriging are given in Figure 4.20. The short scale variations of D_{ts} which were almost absent in the ordinary kriged estimates (Figure 4.13b), became apparent in the D_{ts} predictions by regression kriging.

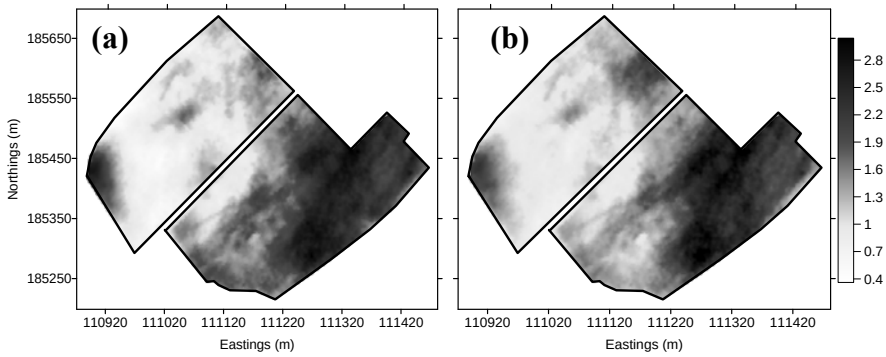

Figure 4.20. Predictions of D_{ts} made with (a) regression kriging and (b) the model based on the depth sensitivity function calibrated with 20 depth observations.

As expected, regression kriged D_{ts} (Figure 4.20a) resembled largely the EC_aV map (Figure 4.15) due to the strong dependency between these two variables. This also illustrates the risk that predictions of D_{ts} through regression kriging can be vulnerable to artefacts in the EC_a data. Therefore, the pre-processing of EC_a data is an essential step to enhance the credibility of the predictions.

The validation results of the different prediction methods are listed in Table 4.7. The *MEE* of regression kriging was close to zero (0.02 m) and this indicated the unbiasedness of prediction. This was further evident by the large *r* accompanied by the scatter plot of observed and predicted depths being aligned close to 1:1 line (Figure 4.21). An average prediction error (*RMEE*) of 0.24 m is highly acceptable given the standard deviation of this variable (0.65 m) and the measurement errors associated with auger observations in the field.

Table 4.7. Validation results of regression kriging (RK) and predictions based on the depth sensitivity function. (TM-60, TM-40 and TM-20 denote the models based on depth sensitivity function parameterized using 60, 40 and 20 calibration samples).

Prediction method	*MEE* (m)	*RMEE* (m)	*r*
RK	0.02	0.24	0.95
TM-60	0.09	0.32	0.91
TM-40	0.11	0.33	0.91
TM-20	0.08	0.32	0.91

The $EC_{a,loess}$ and $EC_{a,clay}$ calculated for the predictions based on the depth sensitivity function changed slightly with the number of calibration samples (Table 4.8). Thus, corresponding models also overlap considerably (e.g. Figure 4.18b). Equally larger R^2 values of all models (Table 4.8) showed that the models were capable of explaining more than three quarters of the total variation (> 76 %) of the D_{ts} measurements. These results bring us to the conclusion that the field sampling effort can greatly be reduced through an appropriate selection of calibration samples.

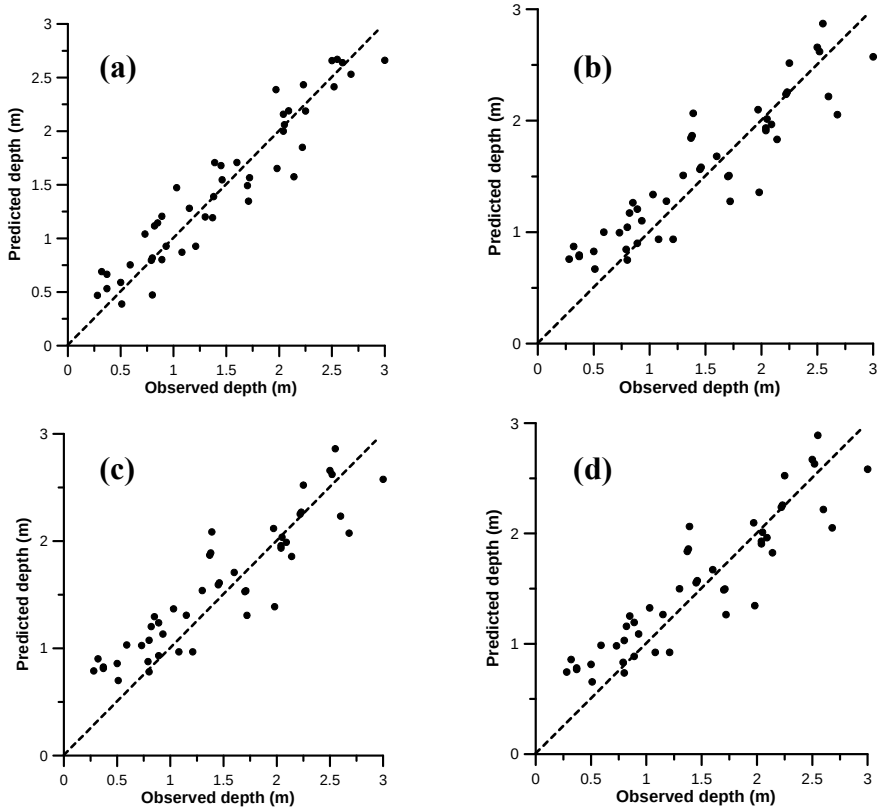

Figure 4.21. Scatter plots of observed depth versus predicted D_{ts} by (a) regression kriging and the depth sensitivity function using (b) 60, (c) 40 and (d) 20 calibration samples.

Table 4.8. Electrical conductivities (mS m^{-1}) of loess and clay layer calculated using the depth sensitivity function with varying number of calibration samples and coefficient of determination (R^2) values of the models.

calibration samples	$EC_{a,loess}$	$EC_{a,clay}$	R^2(*)
60	7.15	124.16	0.78
40	6.21	128.29	0.76
20	7.71	121.20	0.78

(*) calculated on the basis of 60 D_{ts} measurements.

No visible differences could be noticed between the maps of D_{ts} predicted based on the depth sensitivity function with varying number of calibration samples. Therefore, Figure 4.20 shows only the predictions made with the smallest number of calibration samples (20).

Table 4.7 lists the validation indices calculated with the depth sensitivity function based predictions. The similarity of the indices showed that the number of samples used for the calibration of the model had no influence on the accuracy of the predictions. The values of *MEE* pertaining to predictions were close to zero, but slightly larger than those of the regression kriging predictions. This overestimation of D_{ts} can also be observed in the scatter plots (Figures 4.21b to d). These further indicated that the over estimations were biased towards the smaller values of D_{ts}. The *RMSSE* and *r* values showed slightly lower prediction accuracy in comparison to regression kriging.

In conclusion, among the methods evaluated, regression kriging is the best choice for predicting D_{ts} using EC_a data if a large number of D_{ts} observations can be afforded. However, given the much lesser number of samples needed to ensure a reasonable accuracy of prediction, the depth sensitivity function based approach of predicting D_{ts} can also be considered as an appropriate approach with a limited number of D_{ts} observations.

4.6.3.4. Upgrading the 1:20,000 soil map

Given the higher accuracy of regression kriging, these estimates were used to upgrade the 1:20,000 soil map. The upgrading of the 1:20,000 choropleth soil map can be done either by incorporating the predicted D_{ts} information as a continuous layer into the 1:20,000 digitized soil map or by redefining the soil series based on this new information. Here we implemented the second approach in order to facilitate a comparison of the upgraded map with the two choropleth maps. Therefore, the D_{ts} predictions were classified according to the 1:20,000 map legend (Figure 4.22a) and subsequently these classes were also added to the soil

map. A few very small map units (< 0.1 ha) were omitted. The resulting upgraded 1:20,000 soil map is given in Figure 4.22b.

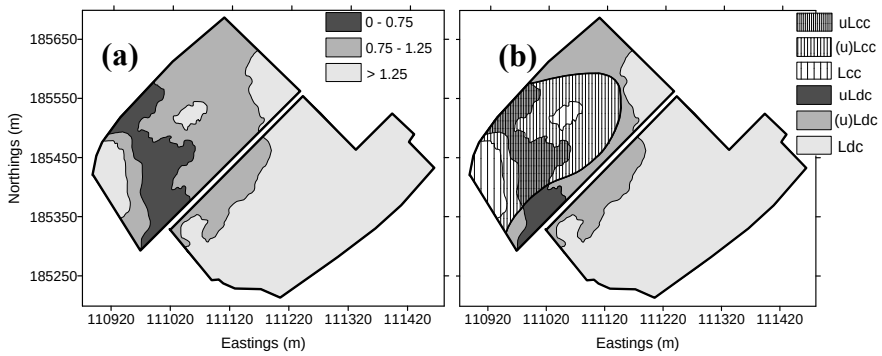

Figure 4.22. (a) Predicted D_{ts} classified according to the legend of the 1:20,000 Belgian national soil map and (b) the 1:20,000 soil map upgraded by incorporating predicted D_{ts}. The inner thick boundary separates the two soil series Lcc and Ldc.

The upgraded 1:20,000 soil map divided the two original soil series into six variants. The western half of the study area has been considerably modified when compared with the original map (Figure 4.2). Unlike the original map, nearly half of the upgraded map is covered with soil series denoting the presence of a shallow (prefix 'u') or a moderately deep (prefix '(u)') Tertiary clay substratum. The classification of the predicted D_{ts} map into substratum classes according to the conventional legend did not include D_{ts} classes below the lower limit of 1.25 m. Therefore, no modifications took place in the eastern part of the study area.

According to the upgraded map, the Tertiary clay layer occurs at depths of less than 1.25 m in about 6.2 ha of the study area. This considerably exceeds the minimum legible area of the 1:20,000 soil map (Table 4.1). Therefore, it is understandable that the poor map accuracy is not due to the scale of the soil map.

To determine the exact reasons, the original, 1:5000 scale field survey reports of the Belgian national soil survey (section 3.8) were consulted. These reports (more

than half a century old) are archived at the Department of Geology and Soil Science, Faculty of Sciences of the Ghent University. Figure 4.23a shows an extract of an original field survey report indicating the observations carried out in the study area. The total number of field observations made in the within our study area was 18. This represents a sample density of 1.2 observations for a hectare. The observed soil series were denoted using a 3 to 4 letter code (see section 3.8). The occurrence of a Tertiary clay substratum at a depth < 1.25 m was reported at five locations mainly in the western half of the field (encircled on Figure 4.23a). However, this information was not included for map unit delineation (Figure 4.23b). It is possible that the soil surveyors came to a conclusion that the shallow presence of the substratum was too erratic to allow mapping. So, neither on the 1:20,000 soil map nor the accompanying booklet, this information was mentioned.

4.6.3.5. Evaluation of the accuracy of the upgraded map

To evaluate the accuracy of the upgraded map with comparison to original 1:20,000 and 1:5000 maps, class predictions from each map were compared with the 46 validation observations. The result were summarised in a confusion matrix (Lillesand and Kiefer, 1994). Every element of this matrix (x_{lk}) represents the number of ground truth observations belonging to the depth class *k* which belong to class *l* of the soil map. The diagonal elements (x_{kk}) represent the agreement between the observations and map predictions. The overall map accuracy (θ_1) was calculated as:

$$\theta_1 = \frac{1}{n}\sum_{k=1}^{K} x_{kk} \qquad (4.17)$$

with *n* the total number of validation observations and *K* the number of classes.

All favourable θ_1 values do not implicate high map accuracies, because some classes may occupy much larger areas than other and thus dominate validation sample (Finke, 2007).

(a)

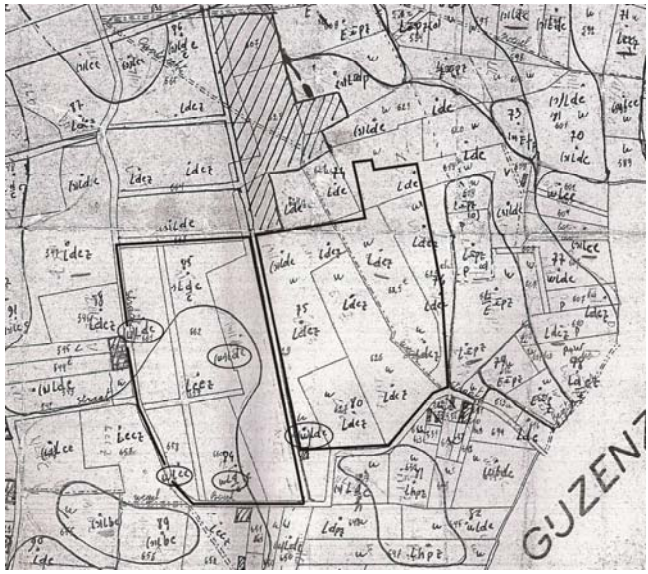

(b)

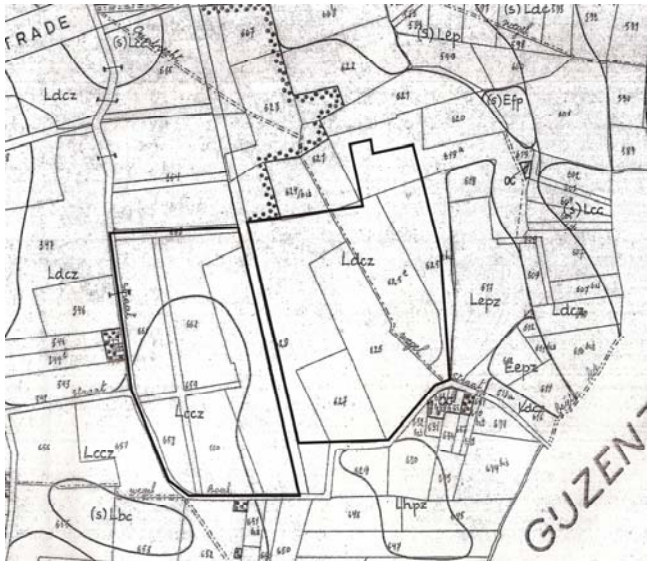

Figure 4.23. (a) Original 1:5000 field report of the Belgian national soil survey indicating the soil auger observations conducted in the study area, the encircled codes show the occurrences of Tertiary materials at a depth < 1.25 m, and (b) the manual delineations of soil series based on the field observations (the last letter z indicates the presence of subsurface sandy material). Note that the fields of the study area are indicated with bold lines.

Therefore, the interpretation of θ_1 needs to be supplemented with a kappa index of overall agreement (κ) obtained from (Cohen, 1960):

$$\kappa = \frac{\theta_1 - \theta_2}{1 - \theta_2} \tag{4.18}$$

given that $\theta_2 = \frac{1}{n^2}\sum_{k=1}^{K} x_{k\bullet} x_{\bullet k}$ with $x_{k\bullet}$ and $x_{\bullet k}$ the marginal sums of rows and columns respectively of the confusion matrix. This index provides an indication of the non-coincidental agreement between the observations and the predictions and ranges from -1 to 1. Landis and Koch (1977) divided this range into classes with the aim of providing an indication of the degree of correspondence: ≤ 0 = poor, 0.01 – 0.20 = slight, 0.21 – 0.40 = fair, 0.41 – 0.60 = moderate, 0.61 – 0.80 = substantial and 0.81 – 1 = almost perfect.

To quantify and compare the different map accuracies, both θ_1 and κ were calculated for the 1:20,000 (Figure 4.2), 1:5000 (Figure 4.3) and the upgraded soil map (Figure 4.22b). The 1:20,000 soil map, which did not indicate any variation in D_{ts}, had $\theta_1 = 0.60$ with $\kappa = 0$. Obviously these values indicated a poor map accuracy with respect to the prediction of D_{ts}. The 1:5000 soil map had a larger overall accuracy ($\theta_1 = 0.83$) and a kappa index of $\kappa = 0.70$, which represents a substantial correspondence between the observed and predicted depth classes. The upgraded map with the EMI sensor was found to be the most accurate, with $\theta_1 = 0.89$ and $\kappa = 0.82$.

4.7. Conclusions

The geostatistical analysis of soil variation addressed the first research question of this case study, i.e. is the variation of the soil properties spatially structured at a within-field scale? The variogram analysis showed that a large proportion of the total variation of all top and subsoil properties and D_{ts} (at least 71 %) were accounted for by the spatially structured component of the variogram model. Therefore, the random or unexplained variations of these properties were very small. The average spatial continuity of the top (200 m) and subsoil (100 m)

properties and D_{ts} (206.5 m) indicated that their spatial variation can be partitioned into within-field subunits (or potential management zones) which are large enough for the implementation of site-specific soil management decisions. Also, it became clear that the spatial distributions of the topsoil and subsoil texture were largely influenced by the underlying Tertiary clay substratum. Therefore, characterization of the spatial variation of D_{ts} is a key step for resolving the soil variation in the sandy silt region. The usefulness of classical soil-landscape models for characterizing the spatial variation of D_{ts} is doubtful due to the lack of correspondence between the existing topography and D_{ts}, which indirectly represents the paleotopography. The spatial variation of topsoil organic C and top and subsoil pH values emphasised the usefulness of categorical data on the history of land use when characterizing their spatial variations. These observations allowed to conclude that the spatial variation of the properties investigated, namely, top and subsoil textural fractions, organic C content, pH and D_{ts} are spatially well structured at a within-field scale.

Assessment of the predictive quality of soil maps allowed us to answer the second question, i.e. are the 1:20,000 and more detailed 1:5000 soil maps suitable to provide soil information for site-specific soil management? The low intra-class correlation values of the 1:20,000 soil map for all the investigated soil properties (< 0.19) clearly reflected the presence of a substantial within-map variation. Therefore, the prediction of soil properties based on the 1:20,000 mapping units will be erratic and not serve the detailed and accurate soil information needs for site-specific soil management. Thus, upgrading of this 1:20,000 soil map is a necessity to provide such detailed soil information. The same conclusion is valid for the 1:5000 soil map for all the properties investigated, except for D_{ts} ($R_i^2 = 0.62$). The large number of field observations (approximately 210 samples) undertaken in the study area allowed the surveyors to classify D_{ts} with a high accuracy. Thus, the information about D_{ts} provided by the 1:5000 map is useful for site-specific soil management.

The third research question addressed in this study was: can EC_a information obtained through proximal sensing be used as an ancillary source of soil information for upgrading the 1:20,000 soil map? The selected soil variable for map upgrading was the D_{ts}. Firstly, regression kriging which combined 60 D_{ts} observations and 9192 EC_aV observations to predict D_{ts}, resulted in the highest prediction accuracy. Nevertheless, almost a similar accuracy of prediction was achieved by calibrating the depth sensitivity function of the EM38 sensor with only 20 D_{ts} observations. Secondly, the upgraded 1:20,000 soil map using D_{ts} predictions obtained through regression kriging showed an almost perfect thematic accuracy. Interestingly, the accuracy was much better than of the 1:5000 soil map which was constructed using three times as many field observations. Therefore it is evident that EC_a measurements obtained through proximal soil sensing could be used as ancillary information to upgrade the 1:20,000 soil map in the sandy silt region by adding accurate information on the depth to the Tertiary clay substratum.

Chapter 5

Key soil and topographic properties to delineate potential management zones in the European loess area

This chapter is based on the publication:

Vitharana, U.W.A., M. Van Meirvenne, D. Simpson, L. Cockx, and J. De Baerdemaeker. 2008. Key soil and topographic properties to delineate potential management classes for precision agriculture in the European loess area. Geoderma 143:206-215.

5.1. Introduction

Soils derived from loess parent materials are recognized as among the most fertile of Europe. Consequently, they have been under intensive agriculture for centuries. A number of studies addressed the general fertility status (Brahy et al., 2000) and erodibility (Govers, 1991) of this soil material covering an undulating Tertiary landscape. Limited attention has been given to the within-field soil variability because loess soils are considered to be very homogeneous. Yet, Reyniers et al. (2006) observed important within-field variations in crop yield as a result of soil and landscape variability. However, they used only a one-year observation of crop yield. Although yield maps have been strongly promoted as a measure of crop productivity guiding the delineation of management zones for site-specific soil management (Jaynes et al., 2005), they often display a large temporal variation due to varying weather conditions, uneven management practices and influences of pest and diseases. To account for these variations, Lamb et al. (1997) and Boydell and McBratney (2002) suggested that more than five years of yield data are required to identify stable management zones.

Traditional general purpose soil maps, typically drawn on a scale between 1:20,000 and 1:200000, were made for regional land use planning and are therefore not suitable to provide detailed information about the within-field variability. Soil inventory by intensive soil sampling and subsequent interpolation is not a realistic alternative due to cost constraints. Thus there is a need for cost-effective, accurate and quantitative ways to inventorize soil information at a very detailed scale (Cook et al., 1996).

Recent advances in proximal and remote sensing and on-the-go soil and crop measurements have made available several types of ancillary information. Since these sources are capable of producing detailed spatial information, they offer a large potential to characterize the within-field soil and crop variation.

Nation-wide accurate elevation data are becoming accessible allowing the generation of DEMs. From these, several terrain attributes, for example slope properties or erosion indices (Wilson and Gallant, 2000) can be obtained, which

have a direct link with pedogenic processes. Franzen et al. (2002) delineated potential management zones on the basis of topographic information, and Fraisse et al. (2001) found that management zones were closely associated with yield variation attributed to soil water availability influenced by topography.

Another widely used source of ancillary information is the measurement of soil EC_a by either electromagnetic induction or electrical resistivity measurements. Mobile EC_a measurement systems, in conjunction with a GPS, are capable of producing a large number of georeferenced data in a short period of time. One system frequently used is the electromagnetic induction sensor EM38DD. Under non-saline conditions, EC_a is mainly related to clay, water and organic matter content (Corwin and Lesch, 2005b). Since these are very important properties for soil management, EC_a has been used frequently to delineate management zones (e.g. Cockx et al., 2005; Kitchen et al., 2005; Vitharana et al., 2006).

Due to the growing availability of all these information sources, and their derived products, there is a risk of over-information (Van Meirvenne, 2006). Although different ancillary information sources may reflect different levels of soil spatial variability, inter-correlations (i.e. partial duplication of information) between them are common. However, in spite of the large number of papers addressing the use of different ancillary information sources, little attention has been given to integrate such information.

This research aims at identifying the key soil and topographic properties required to delineate potential management classes in an agricultural field in the Loess belt of the Belgium. This area, having been cultivated since historical times and displays complex patterns of soil development due to the interaction of different types of soil parent material and slope processes. Data layers involved in this study were: (i) top- and subsoil textural fractions, organic C, $CaCO_3$ (%) and pH-KCl determined at 110 locations, (ii) EC_aV and EC_aH measurements obtained by an EM38DD sensor and (iii) a highly accurate and detailed DEM from which several topographic attributes were calculated. The crop productivity trends across

potential management classes were investigated using a three years sequence of grain and straw yield data.

5.2. Materials and methods

5.2.1. Study field

The investigated field was an 8 ha parcel located in Leefdaal (50º 50' 40" N, 4º 36' 35" E), in Flanders, Belgium. It is situated in the Belgian loess belt (Figure 5.1). The loess parent material is a Pleistocene aeolian sediment which originally had a thickness ranging from a few decimetres to approximately 10 m (see section 3.6). Around Leefdaal, these sediments were deposited on Tertiary glauconitic sands. The unweathered, loess was rich in $CaCO_3$ (10–20 %), but, decalcification has been active for approximately 10000 years. This acidification resulted in an eluviation of clay particles creating the typical horizon sequence of loess soils of Belgium: an acidic and clay eluviated plow layer Ap followed by E, a clay illuviated Bt, a decalcified C1, a $CaCO_3$ containing C2 (loess parent material) and the underlying Tertiary substrate 2C. Because of the high erodibility of the loess-derived silty soil, the topography plays a significant role in soil development through erosion and deposition (Desmet and Govers, 1995). On the slopes, most of the loess, or even all of it, may have been eroded, while in valley bottoms colluvial deposits with a mixed composition are found.

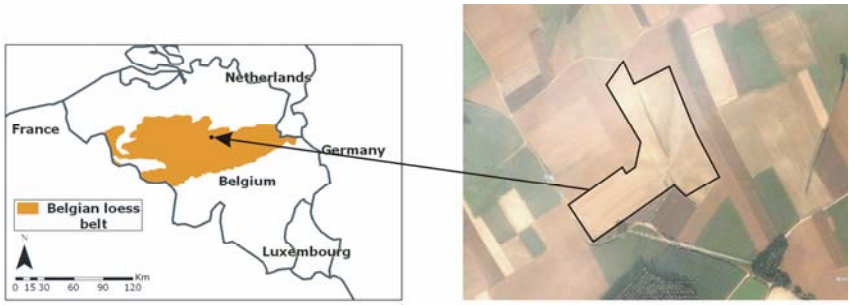

Figure 5.1. The location of the study field in the Belgian loess belt and the study field boundary demarcated on a satellite image.

The availability of multiple-year yield data (yield mapping is not yet a standard practice in Belgian agriculture) and the growing interest on the feasibility of site-specific soil management in this agriculturally important area, were the main reasons for selecting this field for the study. Moreover it displays an undulating topography, which is common in most parts of the European loess area. The field has been cultivated with winter wheat (*Triticum aestivum*), barley (*Hordeum vulgare*) and sugar beet (*Beta vulgaris*) in rotation for many years using conventional rain fed and under uniform management practices. Generally soils in this area are classified as Luvisols in the WRB (ISSS Working Group Reference Base, 1998). The Belgian soil map classified the study field as "Aba" soil series, which represents a silt topsoil texture ('A') and well drained conditions (drainage class 'b') with a argillic B horizon. In general, lime application is routinely performed in the loess region to minimize the influence of soil acidity on crop production.

5.2.2. Acquisition of spatial data layers

5.2.2.1. Soil sampling and EC_a measurements

In November 2004, soil samples were taken from 110 locations (Figure 5.2) at two depth intervals (0-30 cm and 50-80 cm). Half of the sampling locations were located on the nodes of a 40 m regular grid and the other half as a random pair associated to each grid node (see section 3.2). At each location a pooled sample was obtained from three augerings taken within a one meter radius. All sampling locations were georeferenced using a GPS receiver with a positional accuracy of 2 to 3 m and converted to the Belgium national coordinate system (Lambert72). Air dried samples were sieved through a 2 mm sieve and analyzed for a range of agronomically important stable soil properties closely linked with the pedogenesis of loess-derived soils. These included organic C (%), pH (in a 1 N KCl solution), $CaCO_3$ (%) and textural fractions.

To obtain EC_a measurements, the mobile measurement system with the EM38DD sensor was driven at a speed of about 15 km h^{-1} along 4 m spaced parallel lines. In

this way, georeferenced EC_a measurements were recorded on-the-go at 1 Hz yielding an approximate measurement density of one observation per 20 m^2. After the removal of measurement anomalies, the remaining 5534 EC_a measurements were used for further analysis.

After the exploratory data analysis, soil properties and EC_a measurements were geostatistically analyzed. Experimental variograms (omnidirectional in the absence of anisotropy, else directional) were computed and theoretical models were fitted to them. Interpolation to a 5 m grid was performed with ordinary kriging.

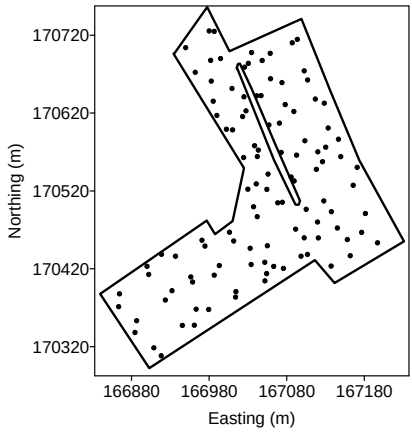

Figure 5.2. The grid plus random sampling scheme showing 110 locations.

5.2.2.2. DEM generation and topographic attributes calculation

Elevation data collected by airborne laser scanning (OC-GIS Vlaanderen, 2003) were used in this study (section 3.4.2). These data were interpolated to a 5 m grid using ordinary block kriging to generate the DEM of a large area (560 ha) within-which the study field is centrally located. The catchment area (drainage basin) of the study field was delineated from the DEM by using the algorithm of Jenson and Domingue (1988). The catchment had a surface area of 95 ha and its DEM (Figure 5.3a and b) showed that the major flow line (thalweg) of the catchment runs through the field which is located near to the catchment's outlet. The field

topography consists of two plateaus (in the east and west, the latter being the larger) gently sloping towards the narrow valley floor of the thalweg. A topographic discontinuity of almost 2 m height and 200 m length crosses the field (Figure 5.3c). This is most likely to be the remnant of a former hedge that might have reduced local erosion. The panoramic view of the study field presented in Figure 5.4 clearly visualizes this feature along with the undulating topography.

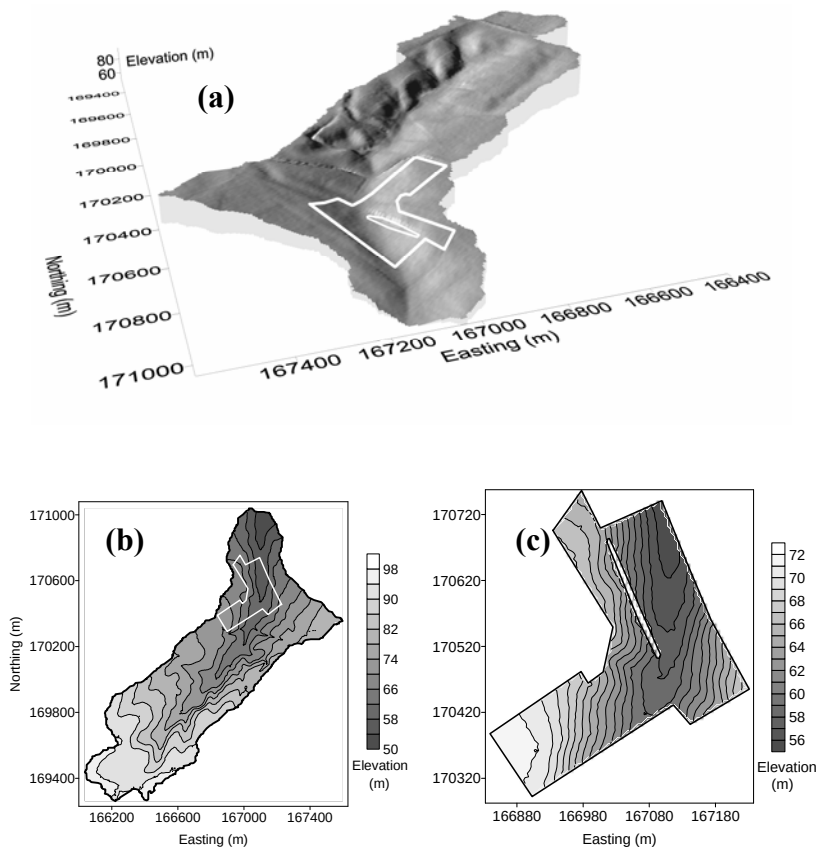

Figure 5.3. (a) Perspective view of the DEM of the catchment area, (b) contour map of the catchment area and the (c) DEM of the study field. The inner boundary of the field depicts the topographic discontinuity.

The primary (slope and specific catchment area) and secondary topographic attributes (*WI* and *SPI*) were calculated form the delineated catchment (refer to section 4.2 for details). Since, the field observations suggested that the topographic discontinuity is due to a former hedge row along the discontinuity, it needed to be included in the runoff modelling. Therefore, a height barrier along the discontinuity was defined in the catchment DEM before calculating the specific catchment area.

Figure 5.4. Panoramic view of the study field indicating the topographic discontinuity (arrow).

5.2.3. Identification of key information layers and delineation of management zones

Figure 5.5 outlines the data analysis steps involved in identifying key information layers and delineation of management zones. This analysis procedure consisted of two main steps: principal component analysis (PCA) and fuzzy *k*-means classification.

5.2.3.1. Principal component analysis

PCA was used to identify key variables which account for soil variability in the study field. PCA is a multivariate statistical method that is often used for dimension reduction of multivariate data sets. This is achieved by the

transformation of p dimensional original variables, Z_1, Z_2,…, Z_p to a fewer number of principal components (PCs) PC_1, PC_2,…, PC_q with a minimum loss of information. The details of PCA can be found elsewhere (Davis, 1986).

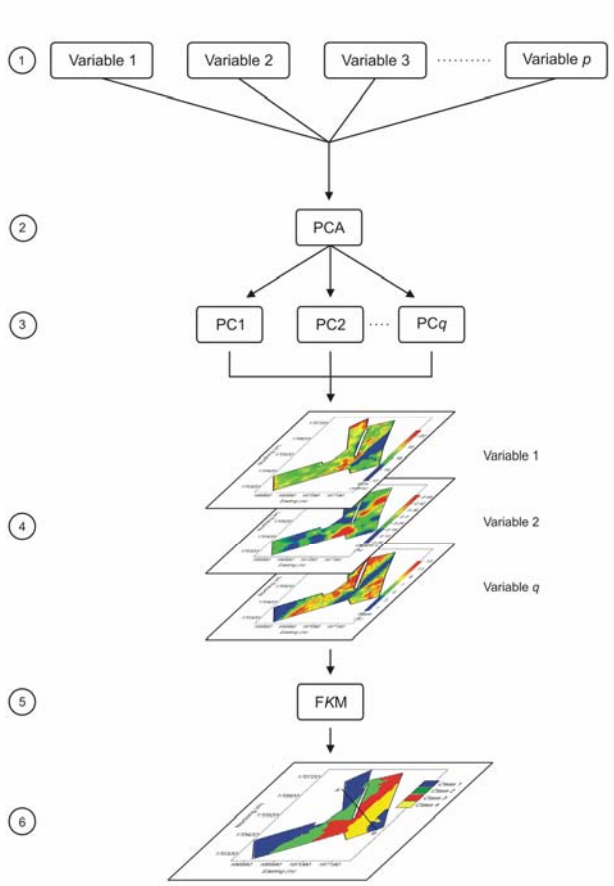

Figure 5.5. Data analysis procedure for the selection of key variables and delineation of management zones. Steps 1 – 2 show the insertion of p primary and ancillary variables for principal component analysis (PCA), step 3 represents the selection of q principal components (PCs) provided that $q < p$, step 4 indicates the selection of a q number of variables on the basis of loadings of extracted PCs and the management zone delineation using fuzzy *k*-means classification (F*K*M) is represented by steps 5 and 6.

The 110 top and subsoil properties and their collocated EC_a and topographic attributes extracted from interpolated maps were subjected to a PCA to identify the key variables. To avoid spurious correlations due to the compositional nature of the textural fractions, only the clay fraction was used as an input. The input data set for PCA consisted of 14 variables. Principal component analysis is sensitive to the scales (therefore the variances) on which the original observations are recorded. Since the different variables used in this study comprised of different units, their scales were standardized to ensure a standard deviations of one and a mean of zero. Thus, the correlation matrix, and not the covariance matrix, was used in the PC (or eigenvector) calculation.

Interpretable PCA results can only be expected when the input variables are reasonably correlated (Davis, 1986). Therefore, before the PCA, the adequacy of inter-correlations between variables was tested using Bartlett's test of sphericity. The Kaiser-Meyer-Olkin (KMO) measure of sampling adequacy was evaluated to ensure the applicability of the data set for a PCA. The KMO measure is an index for comparing the magnitudes of the observed correlation coefficients to the magnitudes of the partial correlation coefficients. A high KMO (between 0.5 and 1) is recommended for proceeding with PCA.

The selection of the number of retained PCs was based on the analysis of the explained variances by each PC represented by a scree plot (Catell, 1966). This is a plot of eigenvalues against the PC with which it is associated. Typically, the smaller eigenvalues representing random variations, tend to lie along a straight line.

To improve the interpretation of the retained PC's, a varimax rotation was applied. Finally, for each of the retained components, a representative key variable was identified based on the factor loadings, which represent the contribution of each original variable to the corresponding PC. All these calculations were performed using SPSS (v. 12.0, SPSS Inc., Chicago, IL).

5.2.3.2. Fuzzy *k*-means classification

Kriged maps of the selected *q* variables were classified into potential management classes using a fuzzy *k*-means classification procedure. Therefore, each map grid node (total 2969) with *q* variables were treated as objects for classification. The fuzziness exponent was fixed to the conventional value of 1.35 (Odeh et al., 1992) and the Mahalanobis' distance metric (equation 3.39) was used as it accounts for the differences in variances (Bezdek, 1981). The classification was repeated for a range of classes, i.e. *k* was set to a value between 2 and 8. The optimum *k*-value was identified on the basis of minimizing two cluster validity indices, the *FPI* and the *NCE*. The class number that corresponds to the largest membership value received by each grid cell was recorded and these values were mapped to produce the management zones map.

5.2.4. Crop productivity among potential management classes

Yield measurements were taken during the growing seasons of 2000, 2003 (in both years winter wheat was grown) and 2004 (barley) using a harvester mounted with the experimental grain, straw and moisture sensors of the Laboratory for Agricultural Machinery and Processing of the K.U.Leuven. The georeferencing of yield measurements taken at 1 m intervals was performed using a Trimble AgGPS132 DGPS system with sub-meter accuracy. The raw yield data were pre-processed to compensate for the systematic and random errors in this data (Reyniers, 2003). The data pre-processing procedure involved: removal of data with obvious positional errors, correction of measurement shifts caused by environmental factors and effects of noise on sensor signals and the removal of irrelevant data. The data acquisition and the pre-processing were conducted by Laboratory for Agricultural Machinery and Processing of the K.U.Leuven. Comprehensive details of the procedure can be found in Reyniers (2003). The grain (adjusted to 15 % reference moisture content) and straw yield maps were constructed using ordinary block kriging.

Due to the temporal instability of yield data, Stafford et al. (1996) and Colvin et al. (1997) suggested the use of the average of multiple years of yields to identify the productivity differences across management zones. Generally, this patio-temporal trend of yield is determined by averaging the yield at each grid cell over a sequence of yield maps. Since different grain crops were involved in this study, these simple averaging techniques could not be used to investigate the yield trends across potential management classes. Therefore the standardized yield at each grid cell for a given year was calculated as follows (Blackmore, 1999):

$$s_t(\mathbf{x}_\alpha) = \left(\frac{y_t(\mathbf{x}_\alpha)}{\bar{y}_t} \right) \times 100 \qquad (5.1)$$

where $s_t(\mathbf{x}_\alpha)$ is the standardised yield (%) at grid cell $(\mathbf{x}_\alpha)$ in the year t, $y_t(\mathbf{x}_\alpha)$ is the interpolated yield (t ha^{-1}) of the same grid cell and $\bar{y}_t$ is the average yield for the same year. Subsequently, an average standardized yield map was obtained by averaging the standardized yield at each grid cell over the three year period considered. These average standardized yield map was used to identify the productivity differences across management zones.

5.3. Results and discussion

5.3.1. Spatial distribution of topographic attributes

The spatial distribution of the slope across the study field is presented in Figure 5.6a. Confirming the field observations, a strip situated to the west of the thalweg had a relatively steeper slope (8 – 16 %). For the convenience of interpretation of the spatial variation, this area is hereafter referred to as the western slope of the field. The plateaus located in the NW and SW corners of the field can be clearly distinguished by the smaller slopes (1 - 6 %). Somewhat larger slopes were also present in the area located to the east of the thalwag which is referred to as the eastern slope of the field. The plateau located in the SE corner of the field is not clearly expressed by the slope map.

The *WI* map of the field (Figure 5.6b) derived from the DEM of the entire catchment (Figure 5.3a) showed large values in the valley floor. Since the major flow line of the catchment passes through this valley, this area is likely to be the wettest area of the field. The rest of the field showed intermediate to small *WI* values. However, larger *WI* values were observed along the eastern slope of the field in contrast to the western slope. Given similar slope gradients across both slopes, it is likely that the comparatively larger upslope area corresponding to the eastern slope (Figure 5.3a and b) has resulted in the higher values of *WI*. Importantly, this suggested that relatively wet soil conditions exist along the eastern slope of the field in comparison to the western slope and the plateaus.

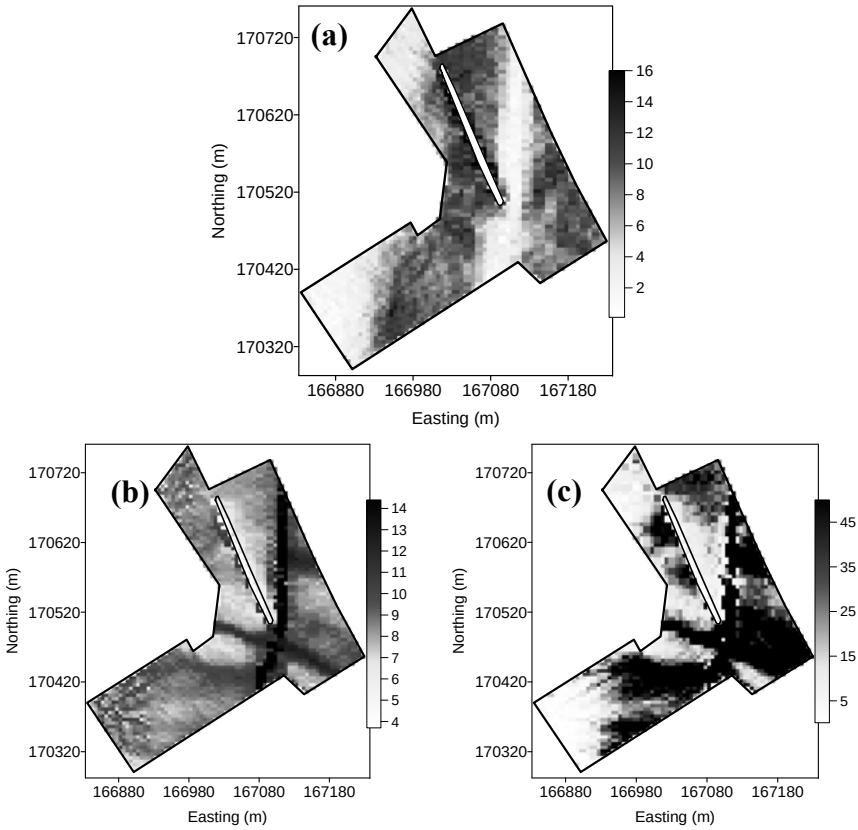

Figure 5.6. Spatial distribution of topographic attributes; (a) slope (%), (b) wetness index (*WI*) and (c) stream power index (*SPI*).

Large *SPI* values were found on both slopes (Figure 5.6c), which resulted from the combined effect of a large upslope contribution area and a steep slope angle (on both slopes the slope angle ranged between 8 and 16 %), reflecting a larger tendency for surface soil loss by runoff. However, on the western slope the topographic discontinuity caused smaller *SPI* values on downslope since it acted as a barrier for overland water flow. Naturally, on the plateau areas located in the NW and SW corners, the *SPI* values were smaller.

5.3.2. Spatial distribution of soil attributes

5.3.2.1. Exploratory data analysis

Descriptive statistics of the soil properties are given in Table 5.1. The Kolmogorov-Smirnov test for normality indicated non-normal distributions (at 5 % level of probability) associated with all the properties except topsoil organic C and pH, subsoil clay and pH and EC_a measurements. This is further reflected by the coefficients of skewness.

The median values of the textural fractions of the top and the subsoils were almost identical (about 16 % clay, 13.5 % sand and 69 % silt) resulting in the texture class, silt loam, which is typical of soils developed in loess (Govers, 1991). However, the sand fraction showed a large variability with a *CV* of 45 % in the topsoil and 65 % in the subsoil (ranging from 5.7 to 69.3 %). The organic C contents were small, ranging from 0.52 to 1.01 % in the topsoil (with a *CV* of 13 %) and from 0.04 to 0.69 % in the subsoil (with a much larger *CV* of 57 %).

A large variability was encountered for the pH. In this field, pH values ranged from 4.7 to 7.5 in the topsoil and from 4.7 to 7.7 in the subsoil. These differences in pH were remarkable, since this field has been under arable land use for a long period of time and good agricultural practice requires this soil property to be closely monitored. However, it is most likely that only average pH values (around 6.2) were considered by the advisory institution thus masking the within-field variability. Linked to the soil pH, the $CaCO_3$ content also varied largely, ranging from 0.0 to 5.8 % (*CV* of 167 %) in the topsoil and from 0.0 to 16.9 % in the

subsoil (*CV* of 189 %). This was an indication of the presence of decalcified loess and $CaCO_3$ rich loess parent material in the surface soil in different parts of the field.

Table 5.1. Summary statistics of sampled soil properties (n = 110) and EC_a (n = 5534).

	Mean	Median	Min	Max	Variance	*CV*	Skewness
Topsoil							
Clay (%)	15.6	16.2	8.4	19.1	5.2	14.7	-1.35
Sand (%)	15.2	13.4	8.2	46.1	46.9	45.1	2.80
Silt (%)	69.2	70.5	44.3	75.5	28.6	7.7	-2.97
Organic C (%)	0.77	0.76	0.52	1.01	0.01	13.0	-0.04
pH-KCl	6.19	6.00	4.73	7.49	0.54	11.90	0.25
$CaCO_3$ (%)	0.78	0.28	0.00	5.76	1.70	167.20	2.7
Subsoil							
Clay (%)	16.8	16.8	11.5	20.9	6.0	14.6	-0.38
Sand (%)	14.3	14.3	5.7	69.3	85.2	64.5	3.82
Silt (%)	68.8	68.8	15.5	78.0	72.7	12.4	-4.29
Organic C (%)	0.25	0.25	0.04	0.69	0.02	56.6	1.62
pH-KCl	6.23	6.23	4.69	7.72	0.71	13.50	0.28
$CaCO_3$ (%)	2.73	2.73	0.00	16.91	26.53	88.70	1.88
EC_a (mS m^{-1})							
EC_aV	16.6	16.6	8.2	23.8	4.0	12.0	0.33
EC_aH	11.9	11.9	5.7	18.6	3.6	16.0	0.33

5.3.2.2. Top and subsoil properties

Table 5.2 lists the Pearson and Spearman rank correlations between the top and subsoil properties. Moderate to strong correlations were observed between the top and subsoil for all properties except for the organic C content. Similar top- and subsoil spatial patterns were observed for all soil properties except organic C, which was quite uniform in the topsoil. Moreover, variability of subsoil organic C in loess landscapes is an important indication of colluvial deposits due to slope processes. It can also be beneficial to crop performance due to improved water and

nutrient holding capacity in the deeper layers. The $CaCO_3$ and pH strongly co-varied (Table 5.2), their spatial distributions were almost identical. Therefore, variogram analysis results and the ordinary kriged maps of only topsoil clay content, pH and subsoil organic C content are presented in this section.

Figure 5.7 shows the experimental variograms and the fitted theoretical models of selected soil properties. Model parameters are listed in Table 5.3. The semivariances of all properties except topsoil pH did not vary with the direction. Therefore, the spatial variations of these properties were represented by omnidirectional variograms. The directional variograms of topsoil pH showed greater spatial continuity and less variation along the N-S direction (range = 86.4 m and sill = 0.43) in comparison to the E-W direction (range = 63.0 m and sill = 0.68). This reflected the existence of a zonal anisotropy for soil pH which needed to be incorporated in ordinary kriging. The variograms of all selected soil variables had a zero nugget effect.

Topsoil clay (Figure 5.8a) was uniform over most of the area, with typical values for loess soil (15 - 16 %). However, across the eastern slope, an approximately triangular area with a decreased clay content (9 - 13 %), and consequently, an increased sand content, was found. The western border of this area was located next to the valley bottom (Figure 5.3c) and coincided with large *SPI* values (Figure 5.5c). Therefore it was likely that water erosion occurring in this part of the field may have completely removed the loess cover, exposing the underlying Tertiary sandy material (the 2C horizon). This was confirmed by the presence of surface gravel (with diameters of between 0.2 and 7.5 cm) in this part of the field. Moreover, it is commonly observed that N-W facing slopes have a thinner loess cover due to the prevailing N-W winds during the deposition period (Pleistocene).

Table 5.2. Pearson and sperman rank correlation (in brackets) between top (T) and subsoil (S) properties

	T_organic C	T_pH	T_$CaCO_3$	T_sand	T_silt	T_clay	S_organic C	S_pH	S_$CaCO_3$	S_sand	S_silt
T_pH	0.24										
	(0.29)										
T_$CaCO_3$	0.05	0.66									
	(0.31)	(0.77)									
T_sand	-0.03	-0.31	-0.21								
	(-0.01)	(-0.38)	(-0.26)								
T_silt	0.07	0.23	0.17	-0.96							
	(0.11)	(0.26)	(0.20)	(-0.88)							
T_clay	-0.08	0.39	0.26	-0.75	0.53						
	(-0.17)	(0.40)	(0.24)	(-0.60)	(0.21)						
S_organic C	0.44	-0.09	-0.25	0.25	-0.13	-0.44					
	(0.36)	(-0.15)	(-0.13)	(0.37)	(-0.14)	(-0.57)					
S_pH	0.15	0.82	0.59	-0.21	0.15	0.28	-0.11				
	(0.24)	(0.83)	(0.72)	(-0.26)	(0.16)	(0.27)	(-0.13)				
S_$CaCO_3$	-0.09	0.58	0.74	-0.20	0.13	0.29	-0..34	0.75			
	(0.11)	(0.54)	(0.60)	(-0.30)	(0.19)	(0.31)	(-0.23)	(0.74)			
S_sand	0.10	-0.20	-0.16	0.73	-0.73	-0.48	0.16	-0.17	-0.19		
	(0.05)	(-0.20)	(0.14)	(0.50)	(-0.42)	(-0.41)	(0.35)	(-0.14)	(-0.09)		
S_silt	-0.06	0.25	0.18	-0.68	0.71	0.36	-0.05	0.24	0.24	-0.97	
	(0.13)	(0.38)	(0.33)	(-0.53)	(0.63)	(0.26)	(-0.16)	(0.38)	(0.26)	(-0.77)	
S_clay	-0.16	-0.10	-0.04	-0.41	0.28	0.56	-0.42	-0.22	-0.10	-0.41	0.16
	(-0.25)	(-0.17)	(-0.21)	(-0.33)	(0.19)	(0.43)	(-0.36)	(-0.30)	(-0.22)	(-0.54)	(-0.02)

Over a large part of the field, the subsoil organic C content was low (< 0.25 %) (Figure 5.8b). But locally an increased level (> 0.45 %) was found, mainly along the valley floor. The possible reason for this was the deposition of eroded topsoil material from the slopes, together with reduced conditions for mineralization due to increased wetness (as indicated by the *WI*, Figure 5.6b).

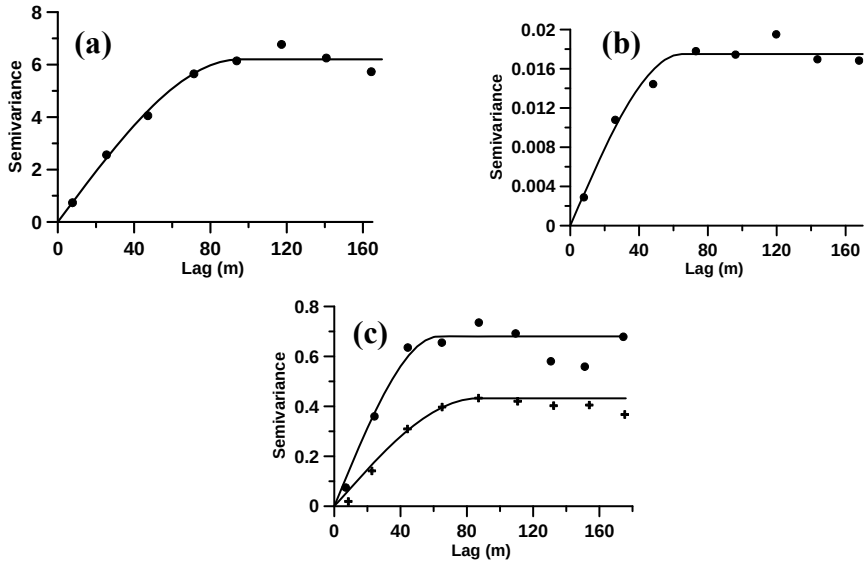

Figure 5.7. Omnidirectional experimental variogram (dots) and fitted models (curve) for (a) topsoil clay (b) subsoil organic C and directional experimental variograms and fitted models of topsoil (c) pH (crosses: N-S and dots: E-W directions).

Table 5.3. Model parameters of the fitted variogram models for the topsoil clay, pH, subsoil organic C and EC_aV.

Property	Direction	Model	Variogram parameters			*RNE* (%)
			Nugget	Sill	Range (m)	
Clay	Omni	Sph	0.00	6.2	95.2	0.00
Organic C	Omni	Sph	0.00	0.02	64.9	0.00
pH	E-W	Sph	0.00	0.68	63.0	0.00
	N-S	Sph	0.00	0.43	86.4	0.00
EC_aV	Omni	Exp	0.00	5.3	136.9	0.00

The map of topsoil pH (Figure 5.8c) showed a N-S oriented band of high pH values (> 6.6) over the western slope, more or less parallel to the valley bottom. Within this band, larger top- and subsoil $CaCO_3$ contents were found.

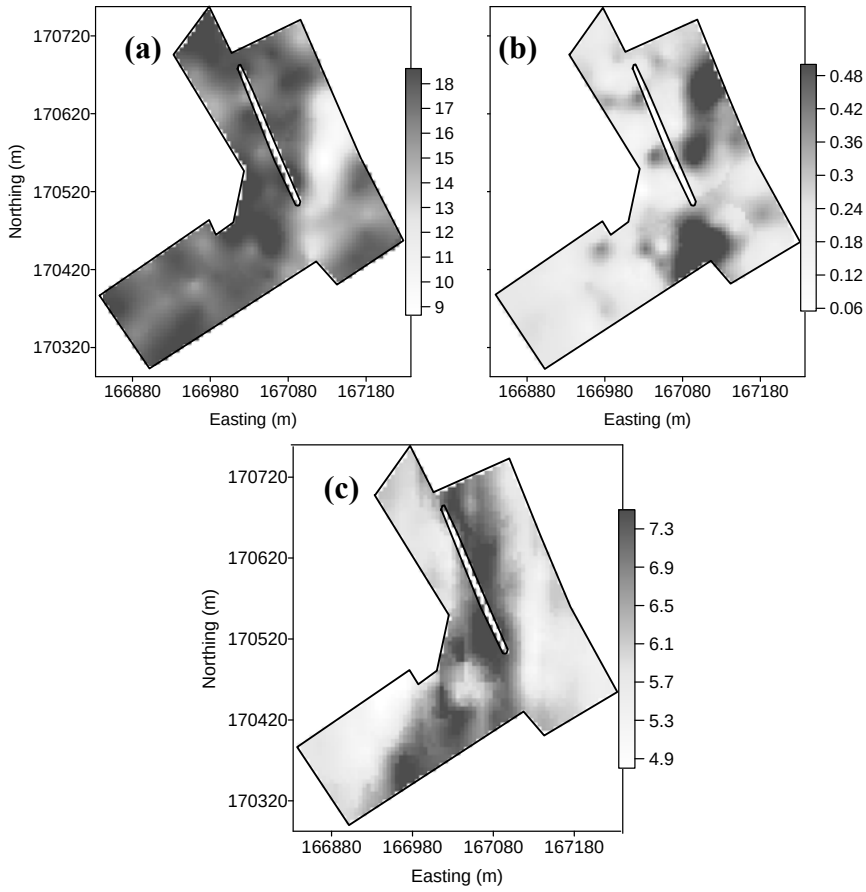

Figure 5.8. Maps of kriged estimates for (a) topsoil clay content (%), (b) subsoil organic C (%) and (c) topsoil pH.

This suggested that on this slope, the decalcified A_p, E, Bt and C1 horizons have been removed, exposing the $CaCO_3$ rich loess parent material (C2 horizon). This indicated less severe erosive conditions than on the eastern slope, where all loess material had been removed. The presence of a hedge in the past, which has

resulted in the topographic discontinuity, might have reduced the erosive power on this slope, as reflected by the reduced *SPI* values over this area (Figure 5.6c). Additionally, S-E facing slopes were originally covered by thicker loess layers. The rest of the field generally has a lower pH (< 5.8), with no $CaCO_3$ in the top or subsoil. This variability, obviously, has important implications for lime applications, which is a routine practice by the farmers in this area. In some areas in this field (along the plateaus and the eastern slope) liming is required, whereas in the western slope this is not so.

5.3.2.3. Apparent electrical conductivity

Table 5.1 shows the descriptive statistics of the measured EC_a values. The average EC_aV was 16.6 mS m^{-1} while the average EC_aH was 11.9 mS m^{-1}. The lower values of EC_aH indicated a lower topsoil conductivity which might have been the result of the somewhat drier state of the topsoil, compared to the subsoil. Both the variables had a similar variance and similar *CV* (12 % for EC_aV and 16 % for EC_aH), which indicated a moderate level of variability, compared to most of the other soil properties. A strong correlation (r = 0.90) was found between EC_aV and EC_aH. This is in addition to the similar omnidirectional variograms and spatial variation patterns of both the measurements. Therefore, only the variogram analysis results and the kriged map of EC_aV are reported in this section.

Figure 5.9a shows the experimental variogram calculated for EC_aV and the fitted exponential model. The absence of a nugget effect, thus zero relative nugget effect (Table 5.3) of the variogram reflected a strong spatial structure pertaining to the EC_aV measurements. The spatial continuity of EC_aV extended approximately 137 m in the field studied. The interpolated map of EC_aV (Figure 5.9b) shows low conductivity values on the eastern slope (< 14.5 mS m^{-1}), which coincides with the spatial pattern observed on the topsoil clay (Figure 5.8a) and sand maps. This was confirmed by the rather strong correlation that exists between EC_aV and topsoil clay (r = 0.7) and sand (r = -0.7). A number of studies (e.g. Corwin and Lesch, 2005b; Vitharana et al., 2006) reported similar relationships between EC_a and soil

textural fractions. The valley floor was distinct on the EC_a map, with large values (> 18.5 mS m^{-1}) reflecting the wetter soil conditions and the increased organic C content in the subsoil. The rest of the field was fairly homogeneous with moderate EC_a values.

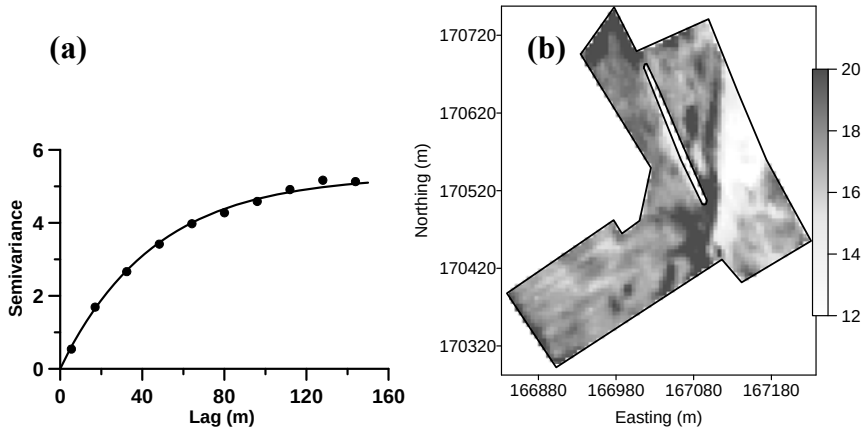

Figure 5.9. (a) Experimental variogram (dots) with the fitted exponential model (curve) and (b) the map of kriged estimates for EC_aV.

5.4. Identification of key variables

The Bartlett's test of sphericity indicated a significant correlation between the variables since the correlation matrix was statistically different from an identity matrix (χ^2 = 1192.5, $p < 0.05$). The KMO measure was 0.67, which exceeds the required value of 0.50 for principal component analysis. Both tests suggested that the multivariate data set with 14 variables is appropriate for PCA.

The scree plot from the PCA is given in Figure 5.10. It showed a typical declination of eigenvalues with increasing PC number; a typical sharp decrease for the first few (four in this case) factors, then levelling off. Cattell (1966) recommended the use of the PCs before the "elbow" (i.e. one less than the PC number at the point at which the curve bends) for further analysis. In Figure 5.10, PC4 coincides with the elbow of the curve and also contributes only a little to the

total variation_there onwards (< 7.7 %). Therefore, the first three PCs were retained and used in the further analysis by means of a varimax rotation.

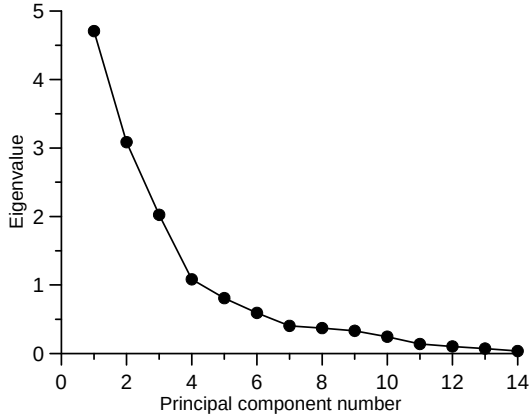

Figure 5.10. Scree plot for soil and topographic data.

The first 3 PCs accounted for 70.1 % of the total variance. Out of this, 33.6 % was accounted for by the first PC, while the second and third PCs accounted for 22 % and 14.5 % of the variation, respectively. Table 5.4 gives the communalities and loadings of the soil variables on the 3 rotated PCs. The communality of a particular variable gives the proportion of its variation represented by the extracted PCs. The smallest communality was 0.33, while most were larger than 0.55. This showed that the three retained PCs accounted for most of the variance in the original dataset.

Figure 5.11 gives the loading plots of the three principal components. The first PC (PC1) was strongly related to the top- and subsoil pH and $CaCO_3$ content, with subsoil pH having the largest loading on PC1 (0.877). Also the slope showed a strong association with this PC. The second PC which accounted for 21.3 % of the total variance, had the strongest contribution from the two EC_a variables (the largest loading on PC2 was for EC_aV: 0.949) and top- and subsoil clay content. The third component represented mainly top- and subsoil organic C (the largest

loading on PC3 was for subsoil organic C: 0.707), elevation and the *WI*. *SPI* was only weakly associated to the three PCs and appeared to be less informative.

Table 5.4. Factor loading of the rotated first three PC with labels (inside parenthesis) used in Figure 5.11.

Variable and label identification	Communality of first 3 PC's	Principal component loadings		
		PC1	PC2	PC3
Topsoil				
organic C (*1*)	0.55	0.048	0.187	0.714
pH (*2*)	0.88	0.820	0.368	0.260
$CaCO_3$ (*3*)	0.67	0.815	0.067	-0.041
Clay (*4*)	0.79	0.294	0.772	-0.334
Subsoil				
organic C (*5*)	0.73	-0.301	-0.119	0.789
pH (*6*)	0.83	0.877	0.101	0.222
$CaCO_3$ (*7*)	0.74	0.847	-0.059	-0.148
Clay (*8*)	0.59	-0.134	0.694	-0.303
EC_a and topographic attributes				
EC_aV (*9*)	0.91	0.046	0.949	0.098
EC_aH (*10*)	0.89	0.136	0.932	0.073
Elevation (*11*)	0.62	-0.246	0.340	-0.669
Slope (*12*)	0.55	0.698	0.040	-0.243
WI (*13*)	0.66	-0.418	-0.389	0.581
SPI (*14*)	0.33	-0.041	-0.511	0.263

The PCA results suggested an independent soil spatial behaviour along three major properties dominated by pH, EC_a and organic C. Currently, intensive observations of EC_aV and pH can be obtained by commercially available on-the-go sensors (Adamchuk et al., 2007, see section 2.3.11). On-the-go sensors suitable for organic C determinations (e.g. NIR sensor) are just becoming operational in practice. Therefore, elevation was selected as an easy-to-obtain surrogate for organic C,

since it had the second largest loading on PC3 after top- and subsoil organic C. However, Moore et al. (1993) observed a strong association between organic C and *WI* in a different landscape setting.

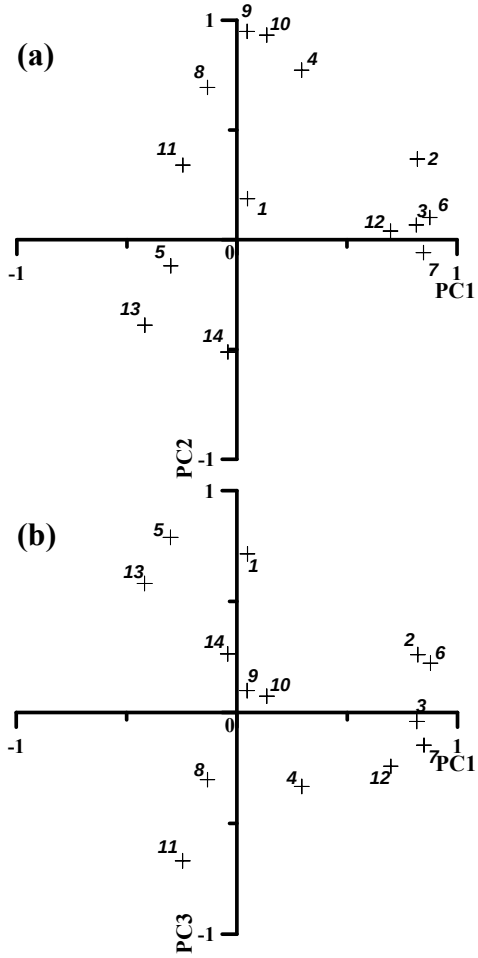

Figure 5.11. Rotated loading plots of the (a) first and second PC and (b) first and third PC. Label identifications and loading values are given in Table 5.4.

5.5. Delineation of potential management zones

As a result of the PCA, elevation, topsoil pH and EC_aV were identified as the key variables for characterizing the soil spatial variation in this field. Thus, ordinary

kriged values of these variables (Figures 5.3c, 5.8c and 5.9) were used as inputs for the fuzzy *k*-means classification. Consequently, the nodes of the grid cells (5 m x 5m) were treated as multivariate objects for classification.

Figure 5.12 shows the plot of the *FPI* and *NCE* performance indices (see section 3.5.3) against the number of classes. The optimum number of classes for each computed index exists when the index is minimum, representing the least number of members sharing (*FPI*) or the greatest amount of organization (*NCE*) as a result of this classification. It can be noticed that both *FPI* and *NCE* were minimized for four classes, i.e. $k = 4$. This means that the spatial variation in the study field can be optimally partitioned into four within-field units or management zones.

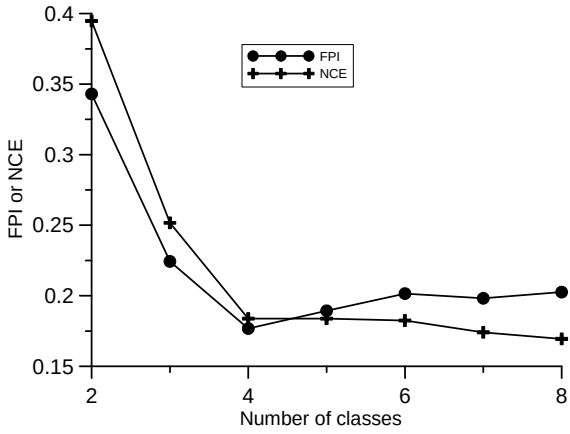

Figure 5.12. Fuzziness performance index (*FPI*) and normalized classification entropy (*NCE*) corresponding to different numbers of classes.

The classification did not produce contiguous classes that can directly be considered as potential management zones. Therefore, according to the recommendations made by Taylor et al. (2007) (see section 2.3.3) fuzzy *k*-means classes were referred to as potential management classes.

The map of the potential management classes shown in Figure 5.13a was obtained by a generalization of the fuzzy *k*-means class membership map by removing a few small island clusters which were not feasible for practical site-specific management purposes.

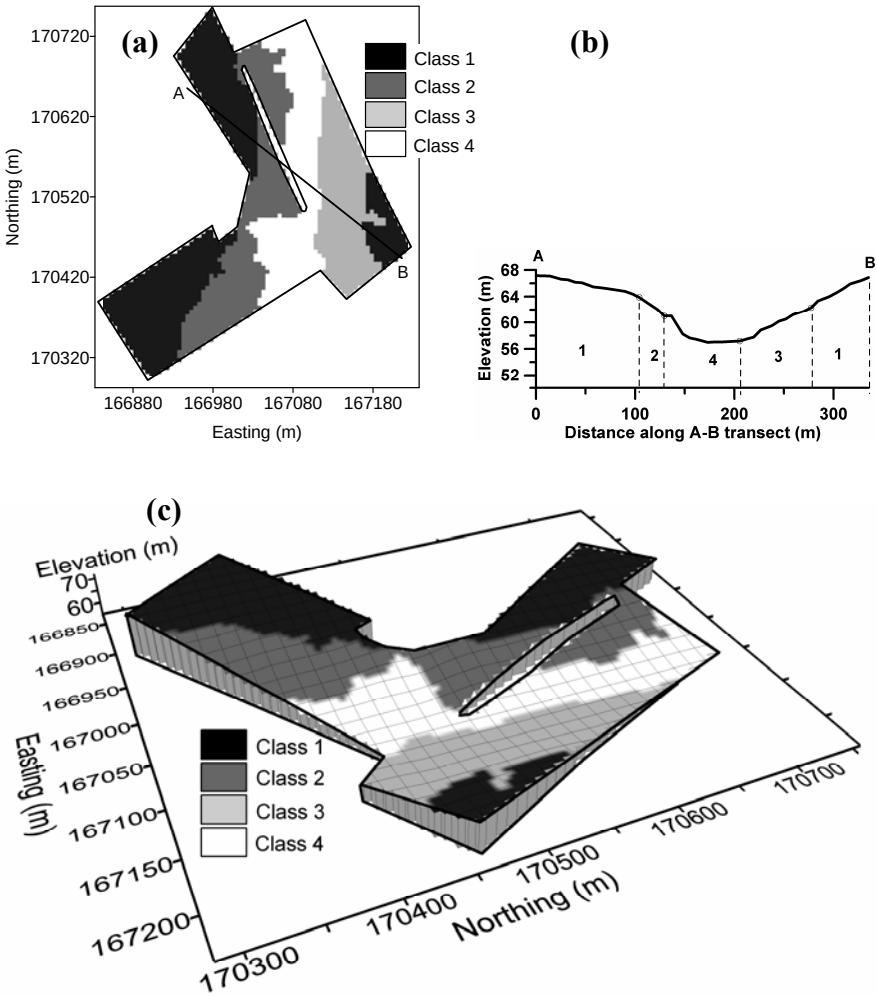

Figure 5.13. (a) Potential management classes delineated using topsoil pH, EC_aV and elevation, (b) elevation along A-B with indication of the potential management zones and (c) classes draped on the DEM.

A clear link between these management classes and the landscape position was visible when a cross-section of elevation across classes is used (Figure 5.13b) and the draping the management classes on the DEM (Figure 5.13c).

Class 1 occupied the southwest, northwest and southeast parts of the field and covered the largest area. Three zones of this class covered the highest plateau and upslope positions in the field, i.e. the areas least modified by slope processes. In this class the typical Ap-E-Bt-C1-C2-2C acidic silt loam soil of the loess area was found. This was confirmed by the average soil properties of the samples located within this class (Table 5.5). The average soil properties of class 1 were therefore used as a reference for comparing the properties of the other classes.

Class 2 coincided with the lesser eroded western slope where the $CaCO_3$ rich loess parent material was exposed (C2 layer), partially limited by the topographic discontinuity. Soil texture was similar to class 1, but class 2 had a higher pH and $CaCO_3$ content (Table 5.5).

Class 3 covered the severely eroded eastern slope, where the 2C sandy substrate is partially exposed. Due to tillage, this sand has been mixed with the remaining silt loam resulting in the doubling of the average sand content when compared to class 1, but pH and organic C remained similar (Table 5.5).

Class 4 represented the valley floor where texture, pH and $CaCO_3$ content were quite similar to class 1, but the organic C content was higher, especially in the subsoil (Table 5.5).

5.6. Crop productivity and potential management classes

The three-year (years 2000, 2003 and 2004) average standardized yield maps of grain and straw (%) are shown in Figures 5.14a and 5.14b. Visually, no strong relationship could be observed between grain yield and management class, but for straw there was a better correspondence between yield and management class. In particular, class 4 (the valley floor) had on average a higher straw productivity.

The three-year average standardized grain and straw yields were split according to management class and the results are given in Table 5.5. Straw yield was more variable than that of grain. The highest productivity occurred in class 4: 104.7 % for grain and 108.2 % for straw.

Table 5.5. Mean values of soil properties and yield data for each potential management class (with standard deviations between brackets).

	Mean			
	Class 1	Class 2	Class 3	Class 4
		Topsoil		
Clay (%)	16.2 (1.3)	16.8 (0.9)	12.5 (2.9)	15.0 (2.1)
Silt (%)	70.7 (1.8)	71.1 (1.9)	62.6 (9.5)	69.4 (3.3)
Sand (%)	13.0 (2.1)	12.0 (2.1)	24.7 (11.4)	15.5 (3.5)
pH	5.6 (0.4)	7.0 (0.4)	5.5 (0.4)	6.2 (0.5)
Organic C (%)	0.72 (0.08)	0.78 (0.12)	0.76 (0.09)	0.83 (0.12)
$CaCO_3$ (%)	0.16 (0.14)	1.90 (1.87)	0.30 (0.20)	0.38 (0.16)
		Subsoil		
Clay (%)	18.7 (1.2)	16.8 (1.7)	14.7 (2.8)	15.7 (2.6)
Silt (%)	70.0 (2.0)	72.4 (3.2)	59.2 (16.7)	69.7 (2.7)
Sand (%)	11.3 (1.8)	10.8 (3.1)	26.1 (16.9)	14.7 (4.3)
pH	5.5 (0.5)	7.1 (0.5)	5.9 (0.6)	6.1 (0.4)
Organic C (%)	0.2 (0.06)	0.19 (0.07)	0.27 (0.12)	0.40 (0.15)
$CaCO_3$ (%)	0.22 (0.27)	7.41 (6.81)	0.74 (1.25)	0.35 (0.24)
		Three-year average standardized yield		
Grain (%)	95.7 (7.1)	99.4 (8.5)	103.7 (7.6)	104.7 (7.7)
Straw (%)	94.4 (9.3)	98.7 (11.1)	102.9 (11.6)	108.2 (11.7)

The lowest yield was found in class 1: the plateau and upslope areas. Classes 2 and 3 had intermediate yield, with class 3 slightly above average and class 2 slightly below average. The sandy substrate of class 3 did not result in a yield decline during the three years considered. The relatively clay rich class 1 produced lower

yields, indicating that during those years, crop productivity did not fully reflect the general soil fertility variation in the field studied. However the yield trends represented to some degree the delineated management classes in relation to the landscape position (Figures 5.13b and c).

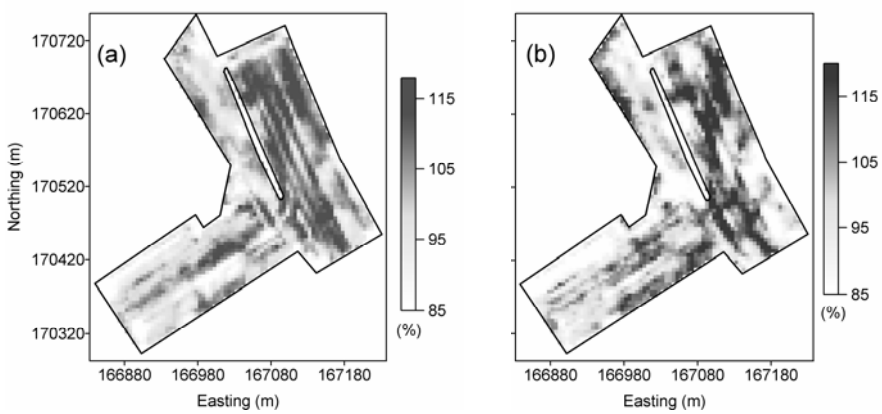

Figure 5.14. Three-year average standardized yield map of (a) grain and (b) straw.

Therefore, in the three years considered, crop productivity was likely driven by variations in the availability of moisture related to the landscape position. Weather records of these three growing seasons indicated that average (year 2000) to rather dry weather conditions (years 2003 and 2004) prevailed. So it is possible that the crop might have benefited from the wetter conditions prevalent along the valley floor and in the eastern slope while the reverse occurred in areas of higher elevations. However, it should be noted that under predominantly wet climatic conditions this relationship may be reversed. In the case of an extreme rain event, temporary flooding or fully saturated conditions might damage or even completely destroy the crop growing in the valley floor. As such, crop productivity in the valley floor is likely to vary much more greatly from year to year than at the other locations. Kaspar et al. (2003) and Reuter et al. (2005) made similar observations when investigating the relationships between landform units and yield potential.

5.7. Conclusions

A strongly structured spatial variation of several soil properties was found to be present at a within-field scale in a loess-derived soil with undulating topography. Although the overall soil texture was a homogeneous silt loam, on the eastern slope the soil texture was sandier, organic C increased in the subsoil of the valley and both $CaCO_3$ content and pH were much higher along a band on the western slope. These patterns originated, most likely, from different levels of soil erosion. These differences support the implementation of differential soil management practices at a field scale.

A PCA highlighted the importance of pH, EC_aV (as a surrogate for soil texture) and organic C content as key independent variables for characterizing the overall soil variation. Since on-the-go sensors for organic C are only just becoming operational, this parameter was replaced by elevation, which is the second most dominant variable on the principal component associated with organic C variation. In this way all three key properties could be investigated without intensive soil sampling and costly laboratory analyses.

These three key variables were used to identify and delineate four classes using a fuzzy *k*-means algorithm. Clear differences in top- and subsoil properties and landscape position were found between these classes. Furthermore, the three-year average standardised grain and straw yields were different across the four classes. The differences in yield were more due to differences in topography in the four classes and less due to the spatial variability of the soil properties.

The results indicated that the variability of pH, soil texture and organic C was suitable for the delineation of potential management classes. Since similar pedogenic processes have occurred in most parts of the undulating European loess landscape, it can be expected that these findings can be extended to a broader scale.

It can be concluded that in loess areas, with complex soil-landscape interactions, pH, EC_a and elevation can be defined as the key properties for the delineation of potential management classes for site-specific soil management.

Chapter 6

Delineation of potential management zones in a polder area and an investigation of their agronomic relevance

This chapter is based on the publications:

Part 1: U.W.A. Vitharana, M. Van Meirvenne, L. Cockx and J. Bourgeois. 2006. Identifying potential management zones in a layered soil using multiple sources of ancillary information. Soil Use and Management 22: 405-413.

Part 2: U.W.A. Vitharana, M. Van Meirvenne, D. Simpson, L. Cockx and G. Hofman. 2008. Agronomic consequences of potential management zones delineated on the basis of EM38DD measurements. Near Surface Geophysics 6(5): 289-296.

Part 1: Delineation of potential management zones in a polder area

6.1. Introduction

Site-specific soil management is the process of adjusting agricultural practices within-fields according to measured spatial variation. It has become an alternative to the traditional uniform management of agricultural fields to increase the profitability of crop production while reducing undesirable environmental impacts by regulating production inputs according to local needs (Godwin et al., 2003a). Identification of the within-field variability and division of a field into sub-units called management zones are therefore decision supporting steps in site-specific soil management (Sylvester-Bradley et al., 1999).

The Polder region of northwest East-Flanders, Belgium, extends over 6840 ha. This highly productive agricultural area with fairly large fields has received attention for possible implementation of site-specific soil management, to optimize yield and to minimize environmental impact from uniform application of agrochemicals. Investigating the spatial variation of soil texture of a 1 ha subfield within this area, Van Meirvenne and Hofman (1989) found a lithologic discontinuity between 40 and 50 cm depth and a more spatial variation in the subsoil texture than in the topsoil. However, existing soil maps or regional studies (e.g. Van Meirvenne et al., 1990) are not informative enough to reveal the detailed within-field variability of soil texture. Yet, soil textural variability is a major factor determining the yield variation (Earl et al., 1996; Stafford et al., 1996).

The production of detailed digital soil texture maps requires considerable sampling and laboratory analysis. Alternatively, spatial information on an easy-to-measure ancillary variable can reduce this effort through selection of a carefully designed sampling scheme (Lund et al., 1999). Further, such ancillary information can be used to improve soil texture prediction using multivariate (geo)statistical approaches. Many studies have addressed the usefulness of ancillary information for predicting soil texture usually based on Jenny's (1941) mechanistic model of soil development. Topographic attributes have been found to be very useful where

there are distinct topographic variations (e.g. Odeh et al., 1995). But, it has little relevance for accounting textural variability in a Polder region with nearly flat topography. Alternatively, Odeh and McBratney (2000) used remotely sensed data to map topsoil clay content. However, the use of remotely sensed data for textural mapping is not advantageous due to the inability to infer subsoil textural variation. For textural mapping of polder soils Van Meirvenne and Hofman (1989) used a cost-effective measurement based on gravimetric water content at a matric potential of -1.5 MPa ($\theta g_{(-1.5\ MPa)}$) (conventionally known as "wilting point"). Soil's apparent electrical conductivity (see section 2.3.1.1 and 3.4.1) has become one of the most reliable and frequently used ancillary information to resolve the spatial variability of soil texture (Corwin and Lesch, 2005a; Kitchen et al., 1999; Williams and Hoey, 1987). The practical utility of EC_a to map texture remains elusive because of the complex interactions between EC_a and range of soil physical and chemical properties (McCutcheon et al., 2006).

Co-kriging is a multivariate extension of kriging in which the ancillary information is incorporated in the estimation at unsampled locations. The unbiasedness of ordinary co-kriging is ensured by forcing the primary data weights to sum to one whereas the weights of each ancillary variable are constrained to sum to zero. This "traditional" co-kriging procedure has been often used for the prediction of a variety of soil variables (Triantafilis et al., 2001; Van Meirvenne and Hofman, 1989; Vauclin et al., 1983; Vaughan et al., 1995). However, Isaaks and Srivastava (1989) emphasized that under the unbiasedness constraints of traditional co-kriging most of ancillary data weights tend to be small restricting its influence. They proposed to use a single constraint that forces all primary and ancillary weights to sum to one. Deutsch and Journel (1998) used the term "standardized" co-kriging for this modified version since it ensures the unbiasedness of the estimator by rescaling all ancillary variables to the same mean as the primary variable. However, little evidence is available to justifying the comparative advantages of the two approaches (Goovaerts, 1998).

The objectives of the first part of this chapter are to explore the utility of EC_a sensing and the suitable co-kriging method to elucidate the soil textural variability in a polder area. To meet these objectives, three research questions are answered:

(1) Can EC_a measured with the EM38DD sensor be used as ancillary information to elucidate the spatial variability of soil texture in the Polder area?

(2) Can the prediction accuracy of soil texture be improved by means of traditional or standardized ordinary co-kriging?

(3) Is the within-field textural variation of the Polder area spatially structured enough to delineate potential management zones?

6.2. Materials and Methods

6.2.1. Study area

The study site was an 11.5 ha field in the polder area in northwest East-Flanders, Belgium (central coordinates: 51^o 16' 17" N, 3^o 40' 35" E, Figure 6.1). The West, East and Northern boundaries of Polder area share the border between the Netherlands and Belgium.

Figure 6.1. The polder area of northwest East-Flanders in Belgium (top left), the location of study field within this area (bottom left) and an aerial image of the study field (line shows the field boundary, right).

A series of marine transgressions following the last glaciation resulted in the deposits which form the parent material of these polder soils. Consequently the topsoil consists of Holocene alluvial silt to clay sediments deposited over Pleistocene aeolian material with a predominantly sandy texture. From the 11th century onwards dikes were constructed to protect this region against new marine invasions and later the land was reclaimed for agriculture by artificial drainage.

Soils in the polder area are classified as Fluvisols in WRB (ISSS Working Group Reference Base, 1998). According to the national soil map (scale 1:20,000), the study area is composed of one dominant soil series: sEdp, indicating a clayey topsoil texture (E) with a shallow sandy substrate (s) and a moderately wet soil (d) with little profile development (p). Rain-fed agriculture is practiced in the study field and typical crop rotation is potato (*Solanum tuberosum* L.), sugar beet (*Beta vulgaris* L.) and winter wheat (*Triticum aestivum* L.).

A digital elevation model indicated that the elevation of the study area ranges between 2.6 m to 4.0 m above the mean sea level. However, it can be observed in Figure 6.2 that the majority of the area is nearly flat with an elevation between 3.2 m and 3.8 m.

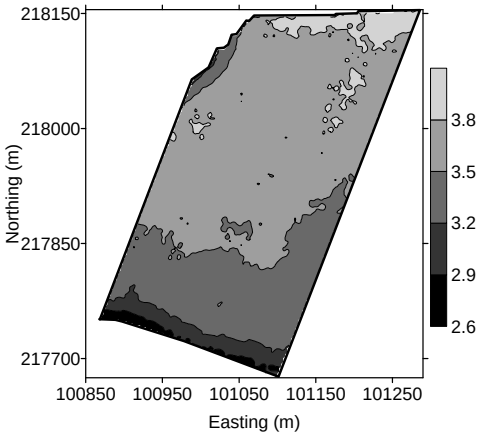

Figure 6.2. Digital elevation model of the study field (0.3 m contour intervals).

The maximum slope angle within the field is 1.8 degrees. Tang et al. (2002) emphasized that in areas where the slope if less than four degrees, the topographic attributes such as *WI* and *SPI* are not informative. Therefore, we considered the topographic indices to be of little relevance for modelling soil variation in this field.

6.2.2. Apparent electrical conductivity mapping and soil analysis

The apparent soil electrical conductivity of the field was measured on 17th November, 2003 with the dual dipole electromagnetic sensor EM38DD. Some studies suggest that EC_a and texture relations are more stable and prevalent at higher water contents (Auerswald et al., 2001; Godwin and Miller, 2003). Therefore, as recommended by Waine (1999) the measurements were taken when the soil moisture content was close to field capacity.

To obtain EC_a measurements, the mobile measurement system with EM38DD sensor (see section 3.4.1) was driven at a speed of about 15 km h^{-1} along 5 m spaced parallel lines. Georeferenced EC_a measurements were recorded every second yielding an approximate measurement configuration of 5 m by 4 m. After the removal of measurement anomalies through exploratory data analysis, 4048 EC_a measurements were retained for further analysis. The spatial distributions of both EC_aV and EC_aH were investigated by calculating the variograms and subsequently ordinary block kriging of measurements to a 2.5 m x 2.5 m grid.

6.2.3. Soil sampling and analysis

In order to investigate the relationships between EC_a and soil texture, a purposive sampling scheme with 63 sampling points was selected based on the EC_a pattern (Figure 6.3), so that spatial patterns such as the linear feature in the western part of the field were included. The geographical coordinates of the sample locations identified on the EC_aV map were uploaded to a GPS. At the field, these locations were tracked through GPS aided navigation. Topsoil (0 - 40 cm) and subsoil (50 - 80 cm) samples were taken at each sampling point, excluding any transition zone

between the two layers. Three soil samples within a one meter were pooled to obtain a bulked sample. Air dried samples were crushed and sieved through a 2 mm sieve for soil textural analysis by the pipette method after pre-treatment for organic residues and $CaCO_3$ removed. The $\theta g_{(-1.5\ MPa)}$ was measured for topsoil samples using a pressure plate apparatus. The measurements were made on disturbed samples since soil structure does not significantly influence the value of $\theta g_{(-1.5\ MPa)}$. The samples were placed on the porous plate of the apparatus. Then an air pressure of 1.5 MPa was applied above the porous plate and at the point of hydrostatic equilibrium, the gravimetric moisture contents of the samples were measured. As an optional variable the soil organic C content was determined by the conventional Walkley and Black method.

At this stage of sampling, it was hypothesized that the EC_aH and EC_aV measurements would be sufficient to predict both top and subsoil textural variability. On the basis of the EC_a results, the sampling procedure was extended to obtain an addition set of samples to measure the $\theta g_{(-1.5\ MPa)}$ (see further).

The EC_a at the 63 sampling points was not measured, but co-located EC_a data for cross-variogram calculations (see further) were estimated using punctual ordinary kriging to examine the relations between EC_a and other soil properties (Kerry and Oliver, 2003).

6.2.4. Spatial prediction of soil texture using ordinary co-kriging

Calculation and modelling of cross-variogram

The first step of co-kriging involves quantification of the spatial correlation of primary (Z_1) and densely measured ancillary variables (Z_2) through their experimental variograms, $\gamma_{11}(\mathbf{h})$ and $\gamma_{22}(\mathbf{h})$, respectively (section 3.5.2.1). Hereafter, these two variograms are referred to as "direct-variograms". Next, the joint spatial correlation (or co-regionalization) between the two variables is estimated through the calculation of experimental cross-variogram. Provided there

are samples where both Z_1 and Z_2 have been measured the cross-semivariance (γ_{12}) for lag **h** can be calculated as:

$$\gamma_{12}(\mathbf{h}) = \frac{1}{2N(\mathbf{h})} \sum_{i=1}^{N(\mathbf{h})} \{z_1(\mathbf{x}_\alpha) - z_1(\mathbf{x}_\alpha + \mathbf{h})\}\{z_2(\mathbf{x}_\alpha) - z_2(\mathbf{x}_\alpha + \mathbf{h})\} \quad (6.1)$$

where $N(\mathbf{h})$ is the number of pairs of comparisons at lag **h**, $z_1(\mathbf{x}_\alpha)$ and $z_1(\mathbf{x}_\alpha+\mathbf{h})$ are the measured values of the primary variable and $z_2(\mathbf{x}_\alpha)$ and $z_2(\mathbf{x}_\alpha+\mathbf{h})$ are the measured values of the ancillary variable at $\mathbf{x}_\alpha$ and $\mathbf{x}_\alpha+\mathbf{h}$, respectively. A plot of cross-semivariances against the lag distance is known as the experimental cross-variogram.

Modelling direct- and cross-variograms is much more difficult than in the univariate case. Difficulties lie in a condition imposed in describing the co-regionalization: any linear combination of variables is itself a regionalized variable and its variance must be positive or zero (Webster and Oliver, 2001). To ensure this condition, the matrix of direct- and cross-variograms must be positive semi-definite (Goovaerts, 1997). Therefore, the direct and cross variograms should be jointly modelled while fulfilling the Cauchy-Schwart inequality for all lags (Webster and Oliver, 2001):

$$\left|\gamma_{12}(\mathbf{h})\right| \le \sqrt{\gamma_{11}(\mathbf{h}) \cdot \gamma_{22}(\mathbf{h})} \quad (6.2)$$

In this study, a linear model of coregionalization (LMC) was used for direct- and cross-variogram model fitting (Goulard and Voltz, 1992). We used the FACTOR2D program developed by Pardo-Iguzquiza and Dowd (2002) to fit a LMC. Due to the limited number of soil samples taken in this study, the directional dependent spatial variation was not considered for experimental variogram calculations.

A plot of the hull of perfect correlation (Wackernagel, 1995) served as a visual check to describe the strength of the co-regionalization. This hull showed the boundary where the joint spatial correlation of two variables is perfect. The shape of the hull is similar to the direct- and cross- variograms and the model parameters are given as:

$$\pm C_{0,hull} = \sqrt{C_{0,11} \cdot C_{0,22}} \tag{6.3}$$

$$\pm C_{1,hull} = \sqrt{C_{1,11} \cdot C_{1,22}} \tag{6.4}$$

$$\pm a_{hull} = \sqrt{a_{11} \cdot a_{22}} \tag{6.5}$$

where $C_{0,hull}$, $C_{1,hull}$ and a are the nugget, scale and range values (see section 3.5.2.1) for the theoretical models that correspond to the hull.

Traditional versus standardized ordinary co-kriging

This study investigated the relative improvements of prediction accuracies of traditional and standardized versions of ordinary co-kriging. Similar to ordinary kriging, both versions of ordinary co-kriging assume that the means of primary and ancillary variables are locally stationary. For the case of a single ancillary variable (Z_2), the traditional ordinary co-kriging estimator of Z_1^* at $\mathbf{x}_0$ is given by:

$$Z_1^*(\mathbf{x}_0) = \sum_{\alpha_1=1}^{n_1(\mathbf{x}_0)} \lambda_{1\alpha_1} Z_1(\mathbf{x}_{\alpha_1}) + \sum_{\alpha_2=1}^{n_2(\mathbf{x}_0)} \lambda_{2\alpha_2} Z_2(\mathbf{x}_{\alpha_2}) \tag{6.6}$$

where $n_1(\mathbf{x}_0)$ and $n_2(\mathbf{x}_0)$ the number of observations of Z_1 and Z_2 used for the interpolation, respectively and $\lambda_{1\alpha_1}$ and $\lambda_{2\alpha_2}$ are the weights given to these observations. The estimator is unbiased under the following constraints on co-kriging weights:

$$\sum_{\alpha_1=1}^{n_1(\mathbf{x}_0)} \lambda_{1\alpha_1} = 1 \text{ and } \sum_{\alpha_2=1}^{n_2(\mathbf{x}_0)} \lambda_{2\alpha_2} = 0 \tag{6.7}$$

Weights of traditional ordinary co-kriging are obtained through solving the system of linear equations with two unbiasedness constraints (Goovaerts, 1997).

There are two shortcomings associated with the unbiasedness constraints imposed in traditional ordinary co-kriging: (1) some of the ancillary data weights become negative, thereby increasing the risk of getting inaccurate estimates (2) most of the weights of the ancillary variable tend to be small, thus reducing the influence of the ancillary information. These shortcomings lead to the development of

standardized (or rescaled) ordinary co-kriging (Deutsch and Journel, 1998; Isaaks and Srivastava, 1989), where the two unbiasedness constraints are replaced by a single constraint that requires all primary and ancillary data weights to sum to one:

$$\sum_{\alpha_1=1}^{n_1(\mathbf{x}_0)} \lambda_{1\alpha_1} + \sum_{\alpha_2=1}^{n_2(\mathbf{x}_0)} \lambda_{2\alpha_2} = 1 . \qquad (6.8)$$

Under the single constraint the unbiasedness of the ordinary co-kriging estimator is ensured by rescaling the ancillary variable so that its mean is equal to that of the primary variable. Therefore, the co-kriging estimator of standardized co-kriging is given by:

$$Z_1^*(\mathbf{x}_0) = \sum_{\alpha_1=1}^{n_1(\mathbf{x}_0)} \lambda_{1\alpha_1} Z_1(\mathbf{x}_{\alpha_1}) + \sum_{\alpha_2=1}^{n_2(\mathbf{x}_0)} \lambda_{2\alpha_2} [Z_2(\mathbf{x}_{\alpha_2}) - m_2 + m_1] \qquad (6.9)$$

where m_2 and m_2 denote means of primary and ancillary variables, respectively, are estimated by their sample means. The co-kriging weights are obtained by solving an ordinary co-kriging system with a single unbiasedness constraint (Goovaerts, 1997).

Evaluation of prediction accuracy

The topsoil and subsoil clay contents were predicted using ordinary kriging and the two co-kriging approaches mentioned above. The GSLIB programs (Deutsch and Journel, 1998) were used to implement all prediction methods. The prediction accuracies of different methods were assessed by cross-validation. The cross-validation results were interpreted using Pearson correlation between estimated and actual values, combined with two validation indices; the *MEE* and the *RMSE* (see section 3.5.2.2). The relative improvement of predictions (*RI* %) by traditional and standardized ordinary co-kriging over the ordinary kriging was calculated as:

$$RI = \frac{100(RMSE_{OK} - RMSE_p)}{RMSE_{OK}} \qquad (6.10)$$

where $RMSE_{OK}$ and $RMSE_p$ are root mean square errors for ordinary kriging and a given co-kriging method, respectively.

6.2.5. Management zones delineation

Kriged maps of top and subsoil textural fractions were classified into potential management zones using a fuzzy *k*-means classification procedure. Therefore, each map grid node with top and subsoil texture data was treated as object for the classification. The fuzziness exponent was fixed to the conventional value of 1.35 (Odeh et al., 1995). The classification was repeated for a range of classes, i.e. *k* was set to a value between 2 and 5. The optimum *k*-value was identified on the basis of minimizing two cluster validity indices, the *FPI* and the *NCE*. The class number that corresponds to the largest membership value received by each grid cell was recorded and these values were mapped to produce the management zones (or classes) map.

6.3. Results and discussion

6.3.1. EC_a measurements

The summary statistics for EC_a measurements are given in Table 6.1. The Kolmogorov-Smirnov test for normality indicated that both EC_aV and EC_aH data are not normally distributed (at 5 % level of probability). This is confirmed by the relatively large coefficients of skewness.

Table 6.1. Summary statistics of EC_a (mS m^{-1}) measurements (n = 4048).

	Mean	Median	Min	Max	Variance	*CV*	Skewness
EC_aV	26.7	26.1	18.5	46.9	20.7	17.0	1.39
EC_aH	21.4	20.7	12.2	36.4	14.1	17.6	1.02
EC_aGM	23.9	23.3	15.5	41.0	15.5	16.5	1.34

The measurements revealed that the large electrical conductivity observed mainly in the southern part of the field was the reason for the positively skewed data distribution. The EC_aV was larger than the simultaneously measured EC_aH. However, a strong overall correlation (r^R = 0.75 and r = 0.81) was found between these measurements. Despite the expected differences as a result of contrasts in soil texture between topsoil and subsoil, the ordinary kriged EC_aH and EC_aV maps showed similar patterns (Figure 6.3).

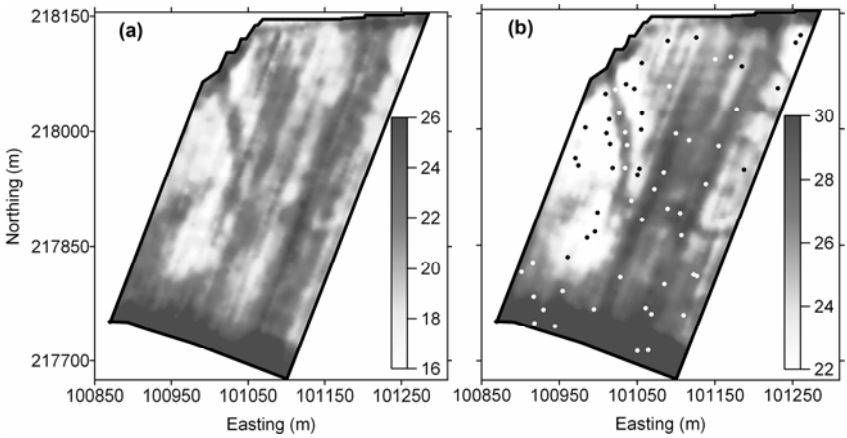

Figure 6.3. Interpolated values in mS m^{-1} for (a) EC_aH and (b) EC_aV with the 63 sampling locations shown as dots.

A distribution of larger and smaller EC_a values can be seen in the southern and western parts of the field. Two linear features with moderate EC_a values were observed on the EC_a maps, one diagonally dissecting the western part having smaller EC_a values and the other extending parallel to the eastern boundary of the field with narrow side branches. Given the overall similarity between the EC_aV and EC_aH data, we decided to pool the two signals for further analysis by taking the geometric mean (GM): $EC_aGM = (EC_aV \times EC_aH)^{0.5}$ which is more stable averaging operator for skewed distributions than the arithmetic mean (Corwin and Lesch, 2005a). Summery statistics of EC_aGM data are also presented in Table 6.1.

6.3.2. Soil textural variation and its relationship with EC_aGM

Because our sampling efforts focussed on the areas of greatest variation, care must be taken in using these data to describe the population. The purposive sampling might result in preferential selection of clusters of high or low values causing a bias towards estimates of population parameters. If an area is preferentially sampled, the bias of population estimates can be eliminated by declustering the data set (Isaaks and Srivastava, 1989). To detect preferential sampling, a cell declustering algorithm (Goovaerts, 1997) was applied. If preferential sampling has been done, there should be a considerable difference between the declustered and the original sample means. We found that neither the declustered mean (Table 6.2) nor the data distributions substantially changed for any of the soil properties. These results suggested that although the sampling was EC_a directed, it was not preferentially located in areas with higher or lower values of soil properties.

Table 6.2. Declustered and non-declustered means of top and subsoil properties.

	Clay (%)	Silt (%)	Sand (%)	Organic C (%)	$\theta g_{(-1.5\ MPa)}$ (%)
Topsoil					
Declustered	19.2	36.2	44.8	0.8	9.2
Non-declustered	19.1	36.3	44.6	0.9	9.4
Subsoil					
Declustered	10.2	20.6	69.1	0.2	-
Non-declustered	10.2	20.9	68.9	0.2	-

The exploratory analysis results of top and subsoil properties are reported in Table 6.3. All the subsoil properties showed slightly skewed distributions resembling the EC_a data whereas data on the topsoil properties were fairly symmetrically distributed. The Kolmogorov-Smirnov test for normality indicated that all soil properties were normally distributed (at 5 % level of probability).

The *CV*s of the topsoil properties varied between 11 and 22.6 %, whereas the *CV* was between 29.2 and 69.3 % for the subsoil properties. From the results it can be

concluded that the topsoil was more homogeneous than the subsoil. According to the Belgian soil texture classes (section 3.8) the sandy silt and clay were the dominant classes of topsoil (Figure 6.4a). However, subsoil texture was distributed over five textural classes ranging from sand to clay (Figure 6.4b).

Table 6.3. Summary statistics for topsoil and subsoil clay, silt, organic C (n = 63) and topsoil $\theta g_{(-1.5\ MPa)}$ (n = 117).

	Mean	Median	Min	Max	Variance	*CV*	Skewness
Topsoil							
Clay (%)	19.1	19.2	14.3	23.7	6.0	12.9	-0.03
Silt (%)	36.3	33.9	20.8	54.2	67.2	22.6	0.52
Sand (%)	44.6	46.8	23.4	64.8	96.8	22.0	-0.13
Organic C (%)	0.9	0.9	0.6	1.3	0.02	16.5	0.23
$\theta g_{(-1.5\ MPa)}$	9.4	9.4	6.6	13.8	1.1	11.0	0.37
Subsoil							
Clay (%)	10.2	8.5	3.2	26.5	33.5	56.6	1.14
Silt (%)	20.9	18.8	3.7	60.2	209.9	69.3	1.36
Sand (%)	68.9	72.8	13.6	92.9	404.9	29.2	-1.30
Organic C (%)	0.2	0.2	0.0	0.6	0.02	56.9	0.91

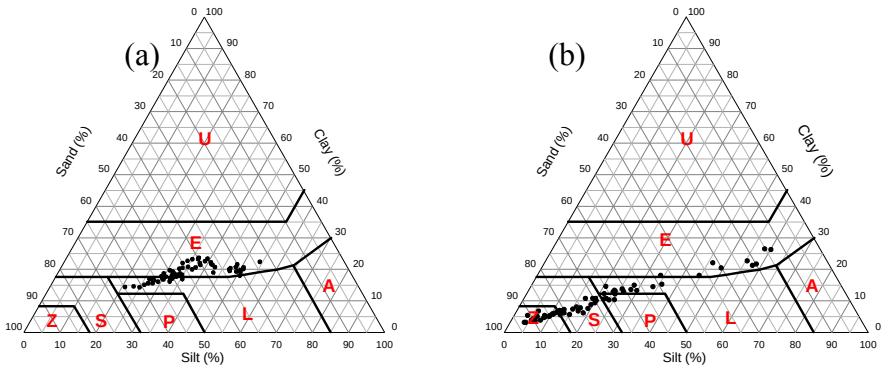

Figure 6.4. The distribution of (a) top and (b) subsoil texture according to the Belgian textural triangle.

Topsoil organic C content had a moderate to poor relationship with topsoil textural fractions (r = -0.42 for sand and 0.20 for clay). This was not true for subsoil organic C, which showed a strong correlation with subsoil textural fractions (r = -0.88 for sand and 0.89 for clay). The cross-variogram between topsoil organic C and clay (Figure 6.5a) was a pure nugget effect, indicating an absence of any structured spatial correlation between the two variables. In contrast, the experimental cross-variogram between subsoil organic C and clay content (Figure 6.5b) depicted a clear structure, indicating the presence of a spatial correlation between the two variables.

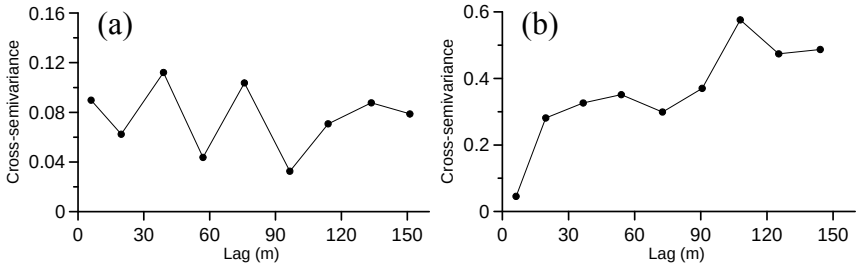

Figure 6.5. Experimental cross-variograms between (a) topsoil clay and organic C and (b) subsoil clay and organic C.

The poor relationship of topsoil textural fractions with organic C can be explained through two underlying reasons. First, incorporation of farm manure to the topsoil is routinely practiced in the polder region. This uniform application of organic C could mask its relationship with soil texture. Second, the variation of topsoil texture is not substantial as that of the subsoil (Table 6.3). Thus, the influence of the variation of soil texture might not be adequate to produce a clear relationship with organic C. The relationship between subsoil organic C and textural fractions agrees the observations made by Nichols (1984) and Burke et al. (1989). Brady and Weil (1999) explained the association between organic matter content and fine textured soils on the basis of three underlying reasons: (1) Restriction of aeration by micro pores causing a reduction of the rate of organic matter oxidation, (2)

Protection of the organic matter from degradation through the formation of clay-humus complexes. (3) Slowing down of organic matter degradation due to the poorly drained conditions created by the heavy soil texture. All these reasons can cause an accumulation of organic matter resulted in a positive relationship between organic C and increasing clay and silt contents.

Clay content can influence other soil physical-chemical properties such as water holding capacity, hydraulic properties and cation exchange capacity, and therefore the influence of subsoil clay content on overall soil functioning cannot be neglected. The ratio between subsoil and topsoil variances was the largest for the clay fraction and thus clay content was selected as the target variable to describe variations in soil texture for both layers. The correlations between top and subsoil clay contents and EC_a measurements are presented in Table 6.4. The EC_a measured with horizontal and vertical dipole modes, thus their geometric means exhibited strong correlations ($r \geq 0.80$) with subsoil clay content. However, both EC_aV and EC_aH exhibited a poor correlations ($r \leq 0.40$) with topsoil clay content.

Table 6.4. Pearson correlation between top- and subsoil clay (%) and EC_a (mS m^{-1}) and $\theta g_{(-1.5\ MPa)}$ (%) ($n = 63$).

	EC_aH	EC_aV	EC_aGM	$\theta g_{(-1.5\ MPa)}$
Topsoil Clay	0.44	0.36	0.40	0.96
Subsoil Clay	0.80	0.82	0.83	-

It is surprising to notice a weak correlation exhibited by EC_aH, which is theoretically more sensitive for the surface soil electrical conductivity. The depth sensitivity curve of EC_aH measurements (McNeill, 1980), presented in section 3.4.1 is helpful to explain the probable reasons for the poor correlation. It can be shown that top soil (0 - 40 cm) contributes to EC_a measurements by 50 %. This means that the subsoil material (> 40 cm) still has a considerable contribution to an EC_aH measurement. Because there is a much stronger variability of subsoil texture and organic C in comparison to the topsoil, it is likely that the measured EC_aH

patterns have been influenced by the variability of subsoil properties. This might have masked the relationship between EC_aH and topsoil texture. Further improvement of the relationship may be achieved through partitioning the depth intergraded EC_a measurements into top and subsoil conductivities. Researchers have tried complicated inversion processes like Tikhonov Regularization to construct such depth profiles of EC_a (Borchers et al., 1997; Hendrickx et al., 2002) with varying success. However, these methods were not considered in this study.

6.3.3. Mapping of topsoil clay content

Given the weak correlation, EC_aGM was considered as unsuitable ancillary information for mapping topsoil clay content and therefore the usefulness of another easy to obtain soil variable, $\theta g_{(-1.5\ MPa)}$, was investigated. In comparison to soil textural analysis by the pipette method, the $\theta g_{(-1.5\ MPa)}$ measurements conducted with a pressure plate apparatus are quicker and cheaper. A strong linear relationship (r = 0.96) was found between topsoil clay and $\theta g_{(-1.5\ MPa)}$. Therefore, we sampled the topsoil at 54 additional locations on a 50 m by 50 m grid over the field and determined $\theta g_{(-1.5\ MPa)}$ for these samples. The summery statistics of $\theta g_{(-1.5\ MPa)}$ measurements are provided in Table 6.3.

Figure 6.6 shows the omnidirectional experimental direct- and cross-variograms with fitted models. The model parameters are listed in Table 6.5. The relative nugget effect of the topsoil clay content indicated a strong spatial dependence. Also, the 72.5 % of joint variation between clay and $\theta g_{(-1.5\ MPa)}$ was accounted by its spatial component. The *RNE* of $\theta g_{(-1.5\ MPa)}$ slightly exceeded the 25 % boundary of strong spatial dependence given by Cambardella et al. (1994), thus $\theta g_{(-1.5\ MPa)}$ was moderately spatially dependent. The range of the cross-variogram indicated that the positive spatial correlation between $\theta g_{(-1.5\ MPa)}$ and topsoil clay content extends to a distance of 127.6 m.

To interpret the strength of the coregionalization, the hull of perfect correlation was plotted with the cross-variogram (Figure 6.6c dashed lines). Webster and Oliver (2001) emphasised that if the cross-variogram lies close to the hull then the

spatial correlation between the two variables is strong. The fitted cross-variogram model obtained with a LMC lies within and very close to this hull, indicating a strong coregionalization between topsoil clay and $\theta g_{(-1.5\ MPa)}$.

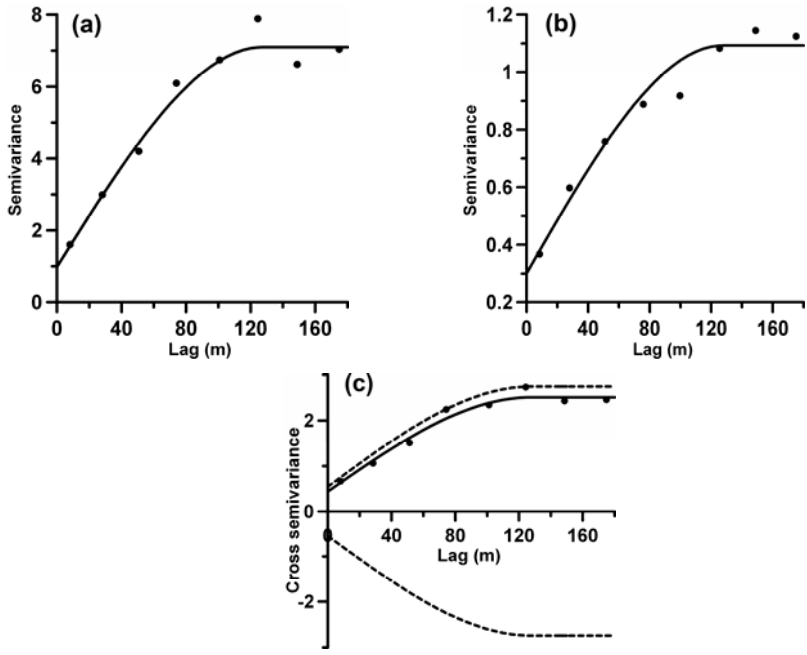

Figure 6.6. Experimental direct-variograms of (a) topsoil clay, (b) $\theta g_{(-1.5\ MPa)}$ and (c) the cross-variogram fitted with the linear model of coregionalization. The dashed lines on the cross-variogram represent the hull of perfect positive and negative correlation.

Table 6.5. Model parameters of the direct- variogram models for the topsoil clay and $\theta g_{(-1.5\ MPa)}$ and the cross-variogram.

Property	Direction	Model	Variogram parameters			*RNE*
			Nugget	Sill	Range (m)	(%)
Clay	Omni	Sph	0.99	7.09	127.6	14.00
$\theta g_{(-1.5\ MPa)}$	Omni	Sph	0.30	1.09	127.6	27.50
Clay x $\theta g_{(-1.5\ MPa)}$	Omni	Sph	0.44	2.51	127.6	17.5

The cross-validation results for topsoil clay prediction by the three kriging methods are given in Table 6.6. The *r* and *RMSEE* values indicated that the incorporation of ancillary information for topsoil clay mapping has slightly improved the prediction accuracy. The *RI* values suggested that, in comparison to the ordinary kriging, the standardized ordinary co-kriging improved the prediction accuracy by 4.3 % whereas the improvement by traditional ordinary co-kriging was 3.8 %. However, the improvement is small, possibly due to the limited number of additional samples of $\theta g_{(-1.5\ MPa)}$. The three prediction methods showed *MEE* values close to zero justifying the unbiasedness common to geostatistical interpolation techniques.

Table 6.6. Cross-validation indices between predicted and actual values of topsoil clay.

	MEE	*RMSEE*	*r*	*RI*
OK	0.0002	1.86	0.60	-
TOCK	0.485	1.79	0.71	3.8
SOCK	0.414	1.78	0.71	4.3

OK: ordinary kriging; OCK: ordinary cokriging. *r*: Pearson correlation coefficient; *MEE*: mean estimation error; *RMSEE*: root mean-squared estimation error and *RI*: relative improvement of prediction.

Figure 6.7a shows the topsoil clay content map constructed using standardized ordinary co-kriging based on 63 clay contents supplemented with 117 $\theta g_{(-1.5\ MPa)}$ measurements. This map illustrates the homogeneity of topsoil texture as revealed in the exploratory data analysis. The topsoil clay content ranges between 19 – 23 % over a large area of the field whereas only a small area in the north-western part of the field contains less clay (14 – 19 %).

6.3.4. Mapping of subsoil clay content

The strong correlation between subsoil clay and EC_aGM allowed the latter to be considered as ancillary information for subsoil clay mapping. We used the same

co-kriging methods as in topsoil clay mapping. The experimental direct- and cross-variograms fitted with the linear model of coregionalization are shown in Figure 6.8. A spherical function was fitted to the both direct- and experimental cross-variograms and the model parameters are given in Table 6.7.

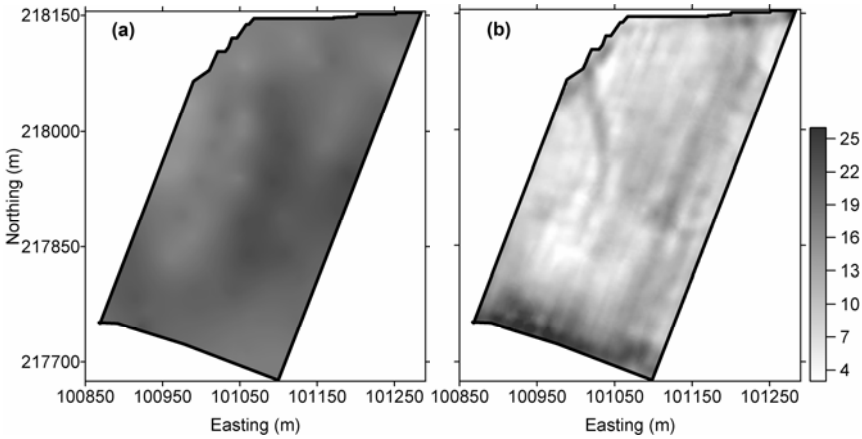

Figure 6.7. Predicted clay contents in % by standardized ordinary co-kriging for (a) topsoil (b) subsoil (maps are shown with the same legend to facilitate comparison).

The small relative nugget effect values (≤ 11.07 %) of both direct- and cross-variograms suggested the variation of individual properties and their joint variation are strongly spatially dependent. The cross-variogram model inferred that the coregionalization between subsoil clay and EC_aGM extended approximately 143.1 m. Moreover, this is a very strong coregionalization as evident from the fitted cross-variogram model that located within and close to the positive hull of perfect correlation (Figure 6.8c).

Cross-validation of subsoil clay prediction by the three methods (Table 6.8) showed that standardized ordinary co-kriging produced the most accurate predictions with the smallest *RMSEE* value and largest *r*. In comparison to the ordinary kriging, the standardized ordinary co-kriging improved the *RMSEE* by 12.6 % whereas the improvement of traditional ordinary co-kriging was 4.0 %.

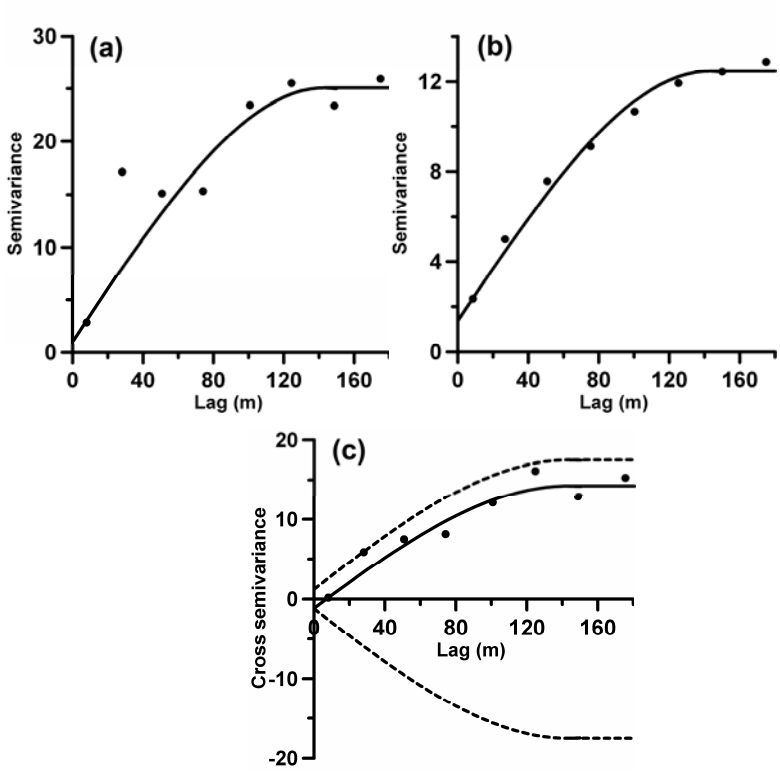

Figure 6.8. Experimental direct variograms of (a) subsoil clay, (b) EC_aGM and (c) cross-variogram with the fitted linear model of coregionalization. The dashed lines of the cross-variogram represent the hull of perfect positive and negative correlation.

Table 6.7. Model parameters of the direct-variogram models for the subsoil clay and EC_aGM and the cross-variogram.

Property	Direction	Model	Variogram parameters			*RNE*
			Nugget	Sill	Range (m)	(%)
Clay	Omni	Sph	1.02	25.07	143.1	4.00
EC_aGM	Omni	Sph	1.38	12.47	143.1	11.07
Clay x EC_aGM	Omni	Sph	-1.14	14.25	143.1	0

The relative improvement in prediction accuracy by standardized ordinary co-kriging is larger than in topsoil, possibly due to the large number of observations of EC_a. Clearly, the assignment of more weight to the ancillary information is an advantage, especially when dense ancillary information is available. Similar to topsoil clay mapping, all methods produced unbiased subsoil clay estimates with *MEE* values well below the standard deviation (5.8 %).

Table 6.8. Cross-validation indices between predicted and actual values of topsoil clay.

	MEE	*RMSEE*	*r*	*RI*
OK	-0.004	3.73	0.77	-
TOCK	0.148	3.58	0.79	4.0
SOCK	-0.030	3.26	0.81	12.6

OK, ordinary kriging; OCK, ordinary cokriging. *r*, Pearson correlation coefficient; *MEE*, mean estimation error; *RMSEE*, root mean-squared estimation error and *RI*, relative prediction improvement.

Figure 6.7b shows the subsoil clay content map constructed using standardized ordinary co-kriging based on 63 texture analyses combined with 4048 EC_aGM measurements. In contrast to the topsoil clay distribution a distinctive pattern of spatial variation in clay content is evident in the subsoil clay map and it fairly resembles the EC_a map. The western and northern parts of the field contain little subsoil clay ranging about from 4 to 8 %. A strip at the southern part of the field contains clayey subsoil (16 – 26 %). The other parts of the field and especially the linear features identified on the EC_a map consist of moderate subsoil clay ranging from 8 to 16 %. Most likely these linear features represent the branches of a creek network through which marine transgressions from the Schelder estuary occurred. The moderate clay contents observed in these creeks reflects clayey materials deposited as a consequence of the marine transgressions. A similar but still active creek network still remain at some locations of the Schelder estuary (Figure 6.9).

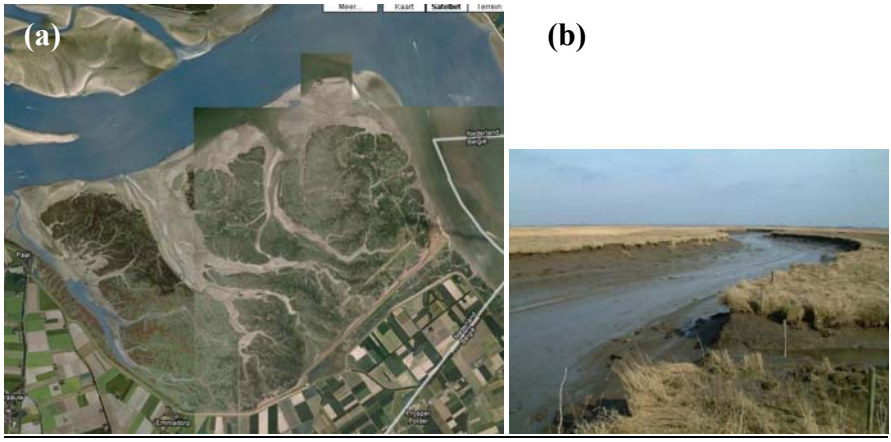

Figure 6.9. Unburied creek network in the (a) Schelder estuary and (b) a close view of a creek.

6.3.5. Delineation of potential management zones

The information on the spatial variation of top and subsoil clay could be used to support site-specific soil management by identifying classes showing clear clay content differences. We used the fuzzy *k*-means unsupervised classification scheme to identify classes showing differences in top and subsoil clay. Thus, standardized ordinary kriged top and subsoil clay contents (Figures 6.7a and b) were used as inputs for the fuzzy *k*-means classification. Therefore, the nodes of the grid cells (2.5 m x 2.5 m) were the multivariate objects for classification. The Euclidean distance that gives equal weight to all measured variables was used as the distance metric. The reasoning behind this selection was to enhance the influence of highly variable subsoil clay content on the overall classification.

Figure 6.10 shows the plot of the *FPI* and *NCE* performance indices (see section 3.5.3) against the number of classes. The optimum number of classes for each computed index is when the index is at the minimum, representing the least membership sharing (*FPI*) or greatest amount of organization (*NCE*) as a result of the classification. It can be noticed the minimizing of both *FPI* and *NCE* at three classes, i.e. $k = 3$. Figure 6.11a shows spatial distribution of the three classes. The

class centroids of the three classes had similar topsoil clay contents (class 1: 18.4 %, class 2: 20.5 % and class 3: 19.6 %). However, the subsoil clay contents varied more strongly: the smaller in class 1 (6.8 %), moderate in class 2 (11.0 %) and larger in class 3 (20.1 %).

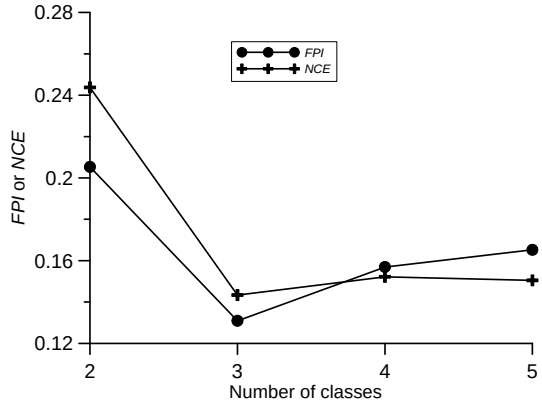

Figure 6.10. Fuzziness performance index (*FPI*) and normalized classification entropy (*NCE*) correspond to different number of classes.

The classes produced by the fuzzy *k*-means classification contained isolated small zones which are not very useful from a practical management point of view. Therefore, the fuzzy classes map was post-processed to obtain generalized potential management zones which are larger and spatially contiguous sufficient to allow site-specific management practices. First, an image filtering technique was applied to the classified image to smoothen the classes. We used a moving window (7 x 7 cells) to replace the value of a cell (i.e. the centre point of the moving window) based on the mode of the class values within the moving window. Then the remaining isolated small clusters were merged with the surrounding class. The resulted generalized potential management classes map is shown in Figure 6.11b.

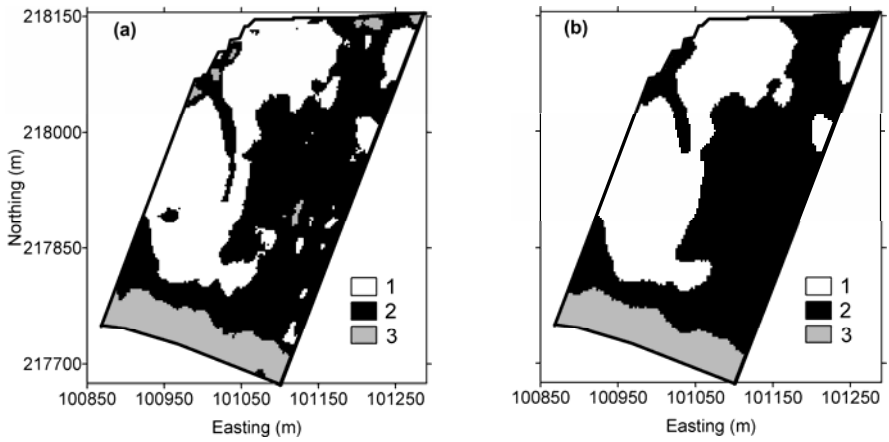

Figure 6.11. (a) Classes (1 to 3) obtained with Fuzzy *k*-means classification of top and subsoil clay contents (b) and generalized potential management classes.

Class 2 was the largest occupying an area of 5.9 ha, whereas class 1 and 3 covered 4.4 ha and 1.2 ha, respectively. The 63 soil samples (topsoil and subsoil) were attributed to the three management classes. Classes 1, 2 and 3 contained 28, 28 and 7 samples, respectively. Table 6.9 provides the mean values for each soil variable per class and the associated standard deviation values (between brackets). It is shown that the topsoil of the study field was quite homogeneous, in comparison to the subsoil. But the texture of class 1 was sandier than of the other two classes. Also, the differences of topsoil organic C across classes was limited. On the other hand, the subsoil was more heterogeneous: class 1 was dominated by very sandy soil, whereas class 3 remained rich in clay and silt and class 2 had an intermediate composition. This tendency was also reflected by organic C, the more clay the higher the values of organic C.

Given the textural differences between potential management classes, possible applications on the crop management can be suggested with respect to the influence of clay content on other soil physical-chemical properties. Water and nutrient management can be considered as key crop management practices to be

changed on the basis of delineated management zones to obtain the benefits of site-specific soil management.

Table 6.9. Mean values of soil textural fractions and organic C for each potential management class (with standard deviations between brackets).

	Mean		
	Class 1	Class 2	Class 3
Topsoil			
Clay (%)	18.4 (2.0)	20.5 (2.0)	19.9 (1.4)
Silt (%)	30.3 (4.5)	38.7 (6.1)	50.6 (1.8)
Sand (%)	51.2 (6.3)	40.8 (6.8)	29.5 (2.8)
Organic C (%)	0.81 (0.13)	0.86 (0.15)	0.94 (0.11)
Subsoil			
Clay (%)	5.6 (1.3)	11.8 (2.7)	22.7 (2.9)
Silt (%)	10.3 (4.5)	23.3 (5.7)	54.4 (6.3)
Sand (%)	84.1 (5.6)	64.9 (8.1)	23.0 (8.6)
Organic C (%)	0.24 (0.05)	0.27 (0.10)	0.47 (0.10)

Management strategies can only be defined after further investigation of the influence of soil textural differences across management zones on overall soil quality. However, the influence of variation in soil properties on crop behaviour can be qualitatively illustrated by an aerial photograph (Figure 6.12) which shows the sugar beet crop in July 1989.

The image closely resembles the spatial patterns observed on the EC_a maps, particularly the EC_aV map (Figure 6.3b). The vegetation in the sandy subsoil zone (class 1 of Figure 6.11b) appears in light grey whereas in the clayey subsoil area (classes 2 & 3 of Figure 6.11b) it is darker. These differences in vegetation clearly reflect the influence of subsoil texture on crop behaviour. The differences of crop behaviour across zones might have been originated by a single or a combination of factors that determine the crop growth. Kravchenko et al. (2003) found that subsoil

physical properties are of greater importance for understand the behaviour of crops and thus the crop yield when water availability is a leading yield-limiting factor.

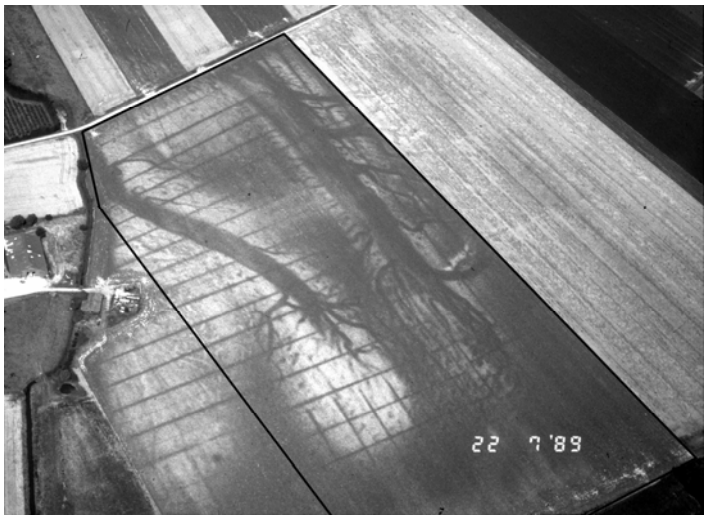

Figure 6.12. Oblique aerial image of the study field in July 1989 (© Dept. Archaeology and Ancient History of Europe, Ghent University, Belgium, Photo: J. Semey).

The linear features (creeks) identified on EC_a maps (Figure 6.3a & 6.3b) are also apparent in the aerial image. The narrow parallel linear features in the image represent the former drainage ditch network constructed at the time of land reclamation. These observations strengthen the utility of aerial images as an ancillary information source to resolve soil spatial variation. However, in practice, obtaining a geometrically accurate aerial images involves large costs. In contrast, obtaining an EC_a inventory as ancillary information for textural mapping is much more practicable and less dependent on weather or crop conditions.

6.4. Conclusions

This study can be considered as an extension to previous research to understand the soil variation in a polder-landscape. Invasive sampling was the only option

available in late 1980s to resolve the soil spatial variation in the polder area (e.g. Van Meirvenne and Hofman, 1989). Due to cost and labour constraints, previous studies were mainly restricted to small within-field blocks. Then the results had to be projected in the broader scale to explain the soil variation over the entire landscape. The results of the present study indicated that such a generalization of variation can result in a large uncertainty. For example, if a subfield experimental plot is accidentally located within a buried creek, the soil variation explanation from it may be largely deviated form the reality. This study clearly emphasised the fact that the technological improvements in proximal soil sensing and georeferencing have allowed researchers to change this classical way of exploring soil variation.

The correlation and co-regionalization analysis provided answers for the first research question "Can EC_a measured with EM38DD sensor and $\theta g_{(-1.5\ MPa)}$ be used as ancillary information to resolve the spatial variation of soil texture in Polder area?" Apparent electrical conductivity measured in both vertical and horizontal dipole orientations showed strong linear relationships with the subsoil clay content. Moreover, the cross-variograpy showed that this relationship was equally strong in the spatial context. This indicated that the EC_a measured with EM38DD sensor is a highly suitable ancillary information source for subsoil clay content mapping in this area. Although, this is not true for topsoil clay content mapping, the strong spatial relationship between the topsoil clay and the $\theta g_{(-1.5\ MPa)}$ indicated that the latter is a suitable ancillary variable to map topsoil clay content in the polder area. Having clearly recognized a larger subsoil textural heterogeneity in comparison to the topsoil and its relevance for site-specific crop management, one can solely rely on EC_a measurements to design an invasive soil sampling scheme and subsequently to characterize the within-field soil textural variation in this area. Moreover, these findings can be potentially extended for mapping the soils developed from alluvial and marine deposits. It is well known that the surface materials of these soil-scapes are generally homogenous and the subsoil variation is mainly determined by the topography existing at the time of flooding and sedimentation.

The second research question asked was “Can the prediction accuracy of soil texture be improved by means of traditional or standardized co-kriging?” The cross-validation results for both top and subsoil clay predictions indicated that two co-kriging methods are capable of improving the prediction accuracy. Nevertheless, these results also suggested that it is beneficial to use standardized ordinary co-kriging instead of traditional ordinary co-kriging.

Three findings allowed to investigate the third research question “Is the within-field textural variation of Polder area spatially structured enough to delineate potential management zones?” First, the classification of the top and subsoil clay allowed to delineate three relatively large management classes. Second, subsoil clay content was substantially different between these classes. Third, a clear visual resemblance between management classes and the aerial image of sugar beet crop indicated the potential relevance of management classes for crop performance. On the basis of these observations, it can be concluded that within-field textural variation of Polder area is spatially structured enough to delineate potential management zones.

Part 2: Agronomic relevance of potential management classes delineated in a polder area

6.5. Introduction

There is little doubt that drinking water contamination by NO_3^- is one of the environment issue of greatest concern for soil management (Keeney, 1982). The major human and animal health problems associated with consumption of excessive NO_3^- in drinking waters or foods are Methemoglobinemia in infants, carcinogenic effects from nitrous compounds and nitrate poisoning in livestock animals (Pierzynski et al., 2000). Moreover, nitrate enrichment in surface water bodies can contribute to the process of eutropication (Carpenter et al., 1998). Nitrogen is a key input in maximizing yield and economic returns to farmers thus its proper management is essential to improve farm profits. Site-specific management of soil N is found to be one of a pertinent strategies to improve the efficiency of N use in order to maximize profits while minimizing the associated environmental effects (Khosla et al., 2008; Larson et al., 1997; Mulla and Schepers, 1997). This has a particular importance for the polder area since the shallow (1.2 m) depth to the ground water level in the polder area (Van Meirvenne et al., 1990) enhances the risk of ground water pollution with NO_3^-. Nevertheless, the potential of NO_3^- leaching is largely influenced by the soil textural composition (Meisinger and Delgado, 2002) which is found to be highly variable in the polder soils. Therefore, it is very important to understand the effect of the management classes on the dynamics of soil nitrogen in order to evaluate the potential of site-specific N management in this area.

In rainfed agriculture, within-field variation of soil water availability can cause a significant influence on the crop growth in the different parts of a field and therefore the overall productivity (Kravchenko et al., 2005). The use efficiency of nutrients is also known to be influenced by the soil moisture availability (White, 1997). As a consequence, poor water management can also indirectly contribute to nutrient losses from the soil-crop system causing the contamination of ground and surface waters. Therefore, exploring the applicability of site-specific water

management in the study area is very important to optimize the productivity while minimizing negative environmental impacts. The improvement of crop yields and the net economic returns is the most convincing stimulant for farmers to adopt site-specific soil management practices (Lowenberg-DeBoer and Swinton, 1997). Therefore, Godwin et al. (2003b) stated that profitability analysis is an essential component in site-specific soil management research.

In line of this background literature, the second part of this research was intended to understand the agronomic relevance of management classes by providing answers to the following questions:

(1) Do soil water retention characteristics, nitrogen and water dynamics vary across potential management classes?

(2) Can variation of nitrogen and moisture contents across management classes affect the sugar beet yield and the farmers income?

6.6. Materials and methods

6.6.1. Land management practices

To evaluate soil and crop variables across management classes, the growing season of 2004 - 2005 was monitored. It started early October 2004, after the harvest of potatoes, when the farmer ploughed the field incorporating uniformly composted poultry manure at a rate of 11 Mg ha^{-1}. According to the information provided by the farmer the depth of fertilizer incorporation was 35 – 40 cm. Three samples of poultry manure were analysed for total N content by Kjeldahl method (Bremner and Mulvaney, 1982). The inorganic forms of N in these samples (NH_4-N and NO_3-N) were extracted using 2 M KCl solution and measured by steam distillation with MgO and Devarda's alloy (Keeney and Nelson, 1982). The analysis indicated an average total N content of 2.9 % and NO_3-N and NH_4-N contents of 0.07 % and 0.04 % respectively. Accordingly, the poultry manure application corresponds to an equivalent total nitrogen fertilization of 320 kg N ha^{-1}. On 28th and 29th March 2005 sugar beets were sown with an approximate spacing of 44 cm between and 20 cm within rows. According to

information provided by the farmer, the crop was not given any additional N-fertilization nor irrigation during the entire growing season. An intermediate application of fungicides was done as a precautionary measure. Harvesting of sugar beets was done in mid October 2005.

6.6.2. Field sampling scheme

To examine the nitrogen and moisture dynamics and yield differences across management classes, 10 monitoring (or sampling) points were established (Figure 6.13).

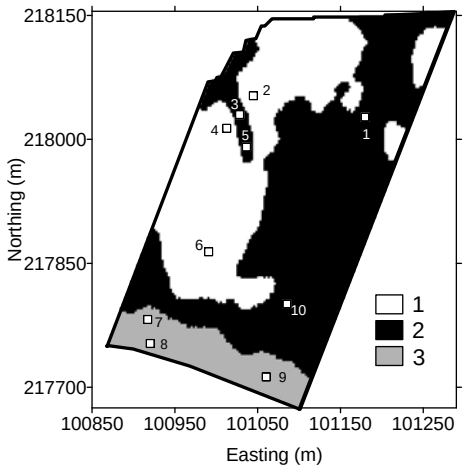

Figure 6.13. Ten monitoring points posted on the management class map.

Monitoring points were located purposively to represent three potential management classes, so they cannot be considered as pure random samples. This limited the possibilities for statistical processing of data, as discussed further. However, the choice of purposive sampling allowed us to locate samples to strengthen the interpretation of results. For example, the samples 2, 3 and 4 were located at a very close proximity but they still were distributed across two management classes. Therefore, differences of nitrogen content between these samples can easily be attributed to the differences in management classes. The

main reason for limiting this number of locations to 10 was the limited field accessibility granted by the farmer during the growing season.

6.6.3. Measurements of nitrogen and moisture

To measure soil nitrogen and moisture contents, samples were taken over two depth increments: 0 – 30 cm and 30 – 60 cm. At each sampling location three samples were taken within 1 m radius and these were mixed to obtain a bulked sample that corresponds to each depth interval. The soil sampling was carried out at five time events over the growing season. The monitoring dates were: 18th May, 20th June, 11th July, 14th August and 13th October 2005.

The analytical facilities available at soil laboratory of Department of Soil Management, Ghent University were used to determine inorganic N and soil moisture contents. To avoid microbial transformations of N, the samples were stored at -18^{0}C until the analysis of mineral nitrogen contents. The mineral forms of soil nitrogen were extracted with a 1 N KCl solution. The filtered extracts were analyzed for NH_4-N and NO_3-N with a continuous-flow auto analyser (ChemLab System 4). In this system, nitrate is transformed to nitrite using enzymatic reduction and the resulting nitrite is measured calorimetrically at 520 nm after reaction with sulphanilamide and N-(1-naphthyl)-ethylene diamine. The procedure to determine ammonium involved colorimetry at 650 nm after reaction with sodium salicylate and sodium dichloroisocyanurate. The gravimetric moisture content of samples was determined by putting a known weight of a soil sample in an oven at 108^{0}C till it reaches to a constant weight. The weight loss (soil moisture) was expressed as a percentage of the dry weight of the soil sample. Additionally, soil water retention characteristics of each management class were determined. Therefore, undisturbed core samples were taken from the mid point of the depth intervals at sampling locations 4, 1 and 8, representing management classes, 1, 2 and 3, respectively. The volumetric moisture contents of these samples were determined at eight soil-matric potential heads (-10 to -15300 cm) to

construct the soil water retention curves for each management class at two sampling depths.

6.6.4. Measurement of sugar beet yield

6.6.4.1. Leaves and roots biomass

On 13th October 2005, i.e. day before the harvesting date, samples were taken for the yield analysis. Above ground biomass (leaves and shoots) and root samples were collected manually from 2.25 by 3.5 m rectangular area located very near to the places where the soil was sampled for nitrogen and moisture analysis to avoid the inclusion of crop plants which were damaged during soil sampling. The weights of fresh beets (including soil attached to the beets) and of leaves were determined on the field. A sub sample of the beets from each monitoring point was taken to the Iscal sugar beet processing factory of Moerbeke, Belgium, to determine the net weight of samples and sugar content. Total biomass was obtained by adding the weight of the fresh leaves to the weight of the fresh roots without attached soil.

6.6.4.2. Income analysis

The sugar beet harvest of the study field was received by the CMS sugar factory in The Netherlands. Therefore, the income analysis was based on the pricing formula adopted by this factory. Net fresh weight of beets and sugar content were considered for pricing. Currently, the sugar extractability is not taken into account for pricing.

The standard price for sugar beet was determined for a sugar content of 16 %, which was 45 euro per Mg. The supplier was paid additional 9 % of the standard price for each 1 % increment in the sugar content. Similarly, a price reduction was applied if the sugar content was less than 16 % in a way that the value of the harvest sharply decreases as the sugar content drops (Table 6.10). The farmer also received 2.35 euros per Mg fresh beet as a compensation for the beet pulp. This pulp is a remnant of the sugar extraction process and is sold as organic manure.

Generally, the sugar content measurements are taken on a subsample taken from each batch received by the factory.

Table 6.10. Percentage of standard price (45 euro) added or deducted on the basis of sugar content.

Sugar content (%)	% price addition (+) or reduction (-)
17.1 - 18	+18
16.1 – 17	+9
16	0
16 – 15.1	-9
15 – 14.1	-19
14 – 13.5	-31
< 13.5	-51

6.6.4.3. Data analysis

The nitrogen and moisture dynamics, yield quality and quantity differences between three management classes were analyzed by comparing means and its standard error, $s_{e,i}$, obtained as:

$$s_{e,i} = \sqrt{\frac{s_i^2}{n_i}} \tag{6.11}$$

with s_i^2 the sample variance of class i, and n_i the number of observations in class i. The sampling scheme used in this study was not neither random nor independent. Therefore, statistical significant of the differences of means were not tested. In addition to the mean comparison, zone differences of biomass yield were further analyzed by calculating the intra-class correlation values (equation 4.7). Statistical analysis was performed with SPSS 15 software.

6.7. Results and discussion

6.7.1. Textural composition of monitoring points and soil moisture retention curves

The soil textural compositions of the monitoring points were averaged on the basis of management classes and are given in Table 6.11. The top (0 – 30 cm) and subsoil (30 – 60 cm) compositions of the management classes was similar to the composition calculated with the 63 samples (Table 6.9). Therefore, it is evident that the monitoring points adequately represented the soil texture of the management classes.

Table 6.11. Average values of the textural fractions and standard error of the mean (in brackets) per management class on the basis of 10 monitoring points.

	Mean		
	Class 1	Class 2	Class 3
0 – 30 cm			
Clay (%)	17.1 (0.4)	18.8 (0.9)	20.3 (1.1)
Silt (%)	29.8 (1.4)	36.4 (1.4)	51.3 (1.5)
Sand (%)	53.1 (1.5)	44.8 (4.1)	28.4 (2.5)
30 – 60 cm			
Clay (%)	5.8 (0.5)	12.4 (0.9)	22.0 (0.4)
Silt (%)	5.4 (0.9)	22.8 (1.1)	53.1 (3.5)
Sand (%)	88.8 (1.1)	64.8 (0.6)	24.9 (3.4)

For samples taken at three management classes, the volumetric moisture contents at different pressure heads (or matric potentials) are listed in Table 6.12. To these experimental data at each depth, the soil water retention curve was fitted using the Van Genuchten (1980) equation:

$$\theta = \theta_r + (\theta_s - \theta_r)\left[\frac{1}{1+(\alpha \cdot |h|)^n}\right]^m \qquad (6.12)$$

where θ is the volumetric water content (cm^3 cm^{-3}), *h* gives soil-matric potential head (cm), θ_s and θ_r represent saturated and residual water contents (cm^3 cm^{-3}). The symbols, α (cm^{-1}), *n* and *m* are empirical fitting parameters with their limitations being $\alpha > 0$, $n > 1$ and $0 < m < 1$. Between *m* and *n* the following relationship holds: $m = 1 - 1/n$.

Table 6.12. Volumetric water contents at different matric potential heads of soil samples taken in three management classes at two depth intervals.

Class	Depth (cm)	Volumetric water content (%) at matric potential head (cm)							
		-10	-30	-50	-70	-100	-330	-1020	-15300
1*	0 – 30	38.2	35.7	34.4	33.8	32.8	31.3	28.7	19.6
	30 – 60	38.4	36.7	34.7	32.5	29.4	14.2	11.4	8.6
2**	0 – 30	41.2	37.2	35.6	34.7	33.4	31.7	28.7	19.3
	30 – 60	41.6	39.1	37.1	35.7	33.5	23.6	21.7	14.1
3***	0 – 30	40.4	36.6	35.1	34.4	33.3	30.8	28.7	18.6
	30 – 60	39.7	37	35.8	35.2	34.2	33.7	31.2	19.1

Correspond to samples obtained at the monitoring points *4, **1 and ***8

The estimates of θ_s, θ_r and the Van Genuchten equation fitting parameters were obtained through an iterative procedure using the RETC software (US Salinity Laboratory, CA, USA). Table 6.13 lists these estimates and R^2 values of soil water retention curves. A good fit of the Van Genuchten equation for experimental data was indicated by large R^2 values (> 0.92). The curves and experimental values are presented in Figure 6.14 (note that pressure heads are expressed as pF values ($pF = \log_{10}|h|$)).

The structure and texture of a particular soil largely determines the shape of its water retention curve (Brady and Weil, 1999). A well structured soil has a larger total pore space resulting mainly from a greater amount of large pores in which water is held with little tenacity. As a consequence, the soil structure

predominantly influences the shape of the moisture retention curve in the portion where the pF values are between 0 and 3 (Koorevaar et al., 1983).

Table 6.13. Parameters and coefficient of determination (R^2) of the fitted Van Genuchten equation of the soil moisture retention curves.

Management class	Depth (m)	θ_s (%)	θ_r (%)	α (cm^{-1})	n	R^2
1	0 – 30	40.0	0.0	0.0703	1.0914	0.97
	30 – 60	38.0	9.0	0.0099	2.3070	0.99
2	0 – 30	44.3	0.0	0.1433	1.0981	0.97
	30 – 60	42.7	10.0	0.0205	1.3735	0.98
3	0 – 30	42.1	0.0	0.0823	1.1029	0.97
	30 – 60	40.0	0.0	0.0245	1.1063	0.92

The shape of the reminder of the curve generally reflects the influence of soil texture. This is mainly through the specific surface of the soil material. For example, a fined textured soil holds much more water at higher pF values than sand does and the water content gradually decreases as the pressure head increases.

The top soil water retention curves of the three management classes overlapped for pF values greater than 2.5 (Figure 6.14). However, slight differences in their shapes can be observed at lower pF values. The soil of class 1 has a steeper curve than the other two classes. It is likely that a comparatively better structure in classes 2 and 3 has caused a greater soil water retention at lower pF values. This is further confirmed by the density of the topsoil of class 1, which was higher (1663 kg m^{-3}) than of class 2 (1526 kg m^{-3}) and class 3 (1388 kg m^{-3}). The influence of the differences of subsoil texture on soil water is clearly evidenced by their water retention curves (Figure 6.14b). The water holding capacity throughout the entire range of pF values was smallest in the subsoil of management class 1, which is sandier in texture.

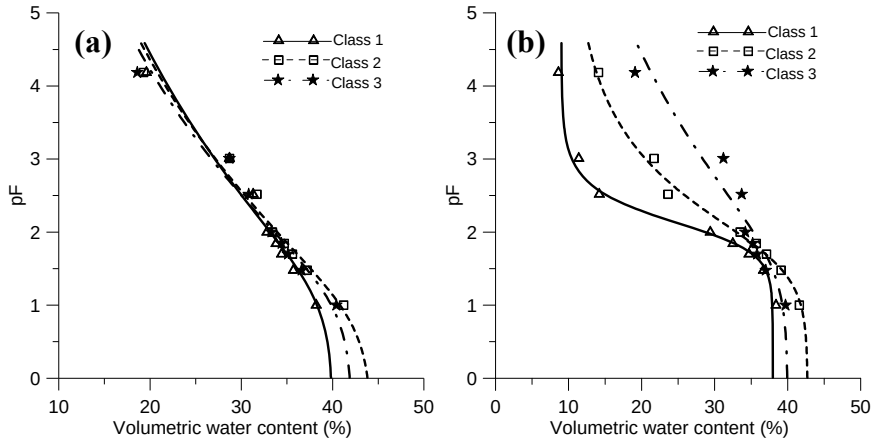

Figure 6.14. Soil water retention curves for soil depth intervals: (a) 0 – 30 cm and (b) 30 – 60 cm, of three management classes (symbols denote the experimental values).

Distinct differences of moisture retention can also be observed between the class 2 and 3, where the latter contains more clay and silt (Table 6.9) and showed the greatest water holding capacity. At lower pF values, differences of water retention narrowed due to abundance of macro pores in the subsoil of management class 1. These results indicated that the textural differences across management classes have a direct influence on the top and subsoil water retention characteristics. This can have implications on other hydraulic properties such as available water capacity and hydraulic conductivity. Therefore, differences in both water and solute balances across management classes can be expected in this study field.

6.7.2. Nitrogen and moisture dynamics across management classes

For the five monitoring dates, average and associated $s_{e,i}$ values of the top and subsoil NO_3-N contents across potential management classes and associated standard errors are presented in Figure 6.15. At the start of the growing season (18th May), marked differences of NO_3-N contents were noticed in both top and subsoil. The NO_3-N content of the topsoil layer of fine textured management

classes 2 (198 kg ha^{-1}) and 3 (203 kg ha^{-1}) were similar but much larger than in the sandier class 1 (110.3 kg ha^{-1}). The associated $s_{e,i}$ values further explain these differences. On average class 2 and 3 had 80 and 84.5 % more NO_3-N content in comparison to class 1.

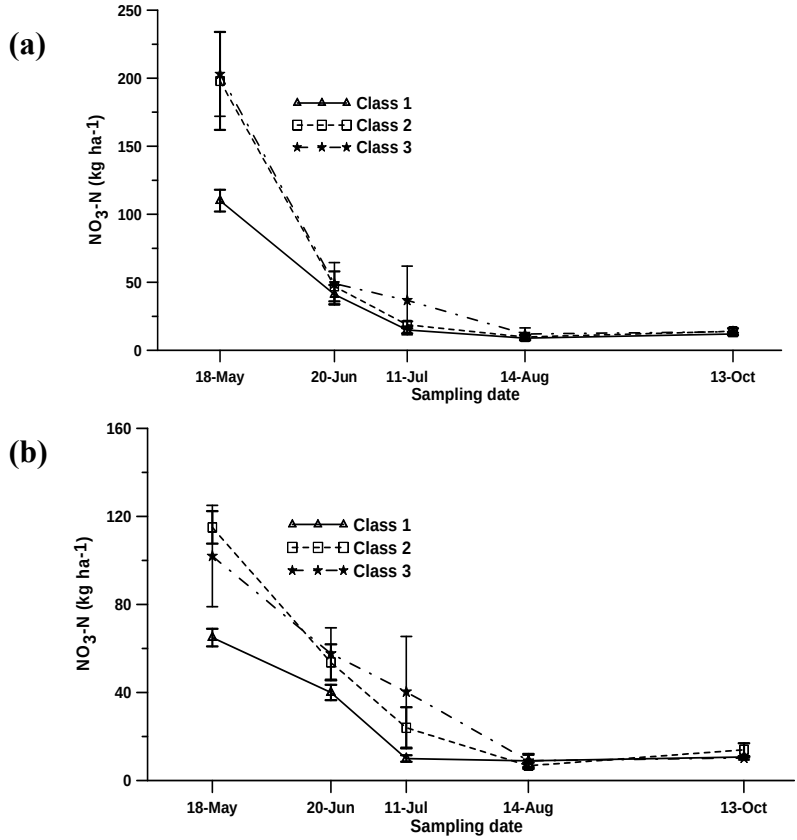

Figure 6.15. Average NO_3-N content in soil depth intervals (a) 0 – 30 cm and (b) 30 – 60 cm for each monitoring date across potential management classes. Vertical error bars show the ± standard error of sampling means.

For the subsoil layer, a similar trend of the average NO_3-N contents was observed across management classes. The average NO_3-N contents of class 2 (115 kg ha^{-1}) and class 3 (101 kg ha^{-1}), were 77 and 55 % larger as compared with class 1

(64.7 kg ha^{-1}). It is interesting to notice marked differences of NO_3-N contents in the monitoring points 2, 4 and 3 which were located very close to each other but they represent two management classes (see Figure 6.13). For example, the subsoil of monitoring points 2 and 4 located in the class 1 contained 75 and 59 kg ha^{-1} NO_3-N, whereas the monitoring point 3 in the class 2 had 136 kg ha^{-1} of NO_3-N. This particular observation stressed that fact that the observed differences of means have no association with manure application.

The differences in mean NO_3-N suggested that a considerable amount of uniformly applied N-fertilizer and residual mineral N of the previous crop was lost during the winter and early spring in class 1. In cropped fields, the loss of mineral nitrogen forms mainly occur as gaseous, erosional and leaching losses (Follett and Delgado, 2002). However, the method of manure application and the prevailing soil conditions namely neutral pH and well drainage conditions do not favour the gaseous loss of N as NH_3 or N_2O. Moreover, due to the flat topography, the contribution of soil erosion for the loss of NH_4-N or NO_3-N is also negligible. Therefore, NO_3-N leaching can be considered as the main cause of the loss of nitrogen in the study area. In general, any downward movement of water through the soil profile will cause leaching of NO_3-N, with the magnitude of the N loss proportional to the concentration of NO_3^- in the soil solution and the volume of leaching water (Pierzynski et al., 2000). It is well known that sandy soils are more susceptible for nitrogen leaching in comparison to finer textured soil (Delgado, 2001; Juergens-Gschwind, 1989). This was further justified by the differences of mean NO_3-N observed across texturally different three management classes. This allows us to confirm that management class 1 with sandy textured subsoil is highly sensitive area for nitrogen leaching, especially during the winter due to the absence of crop uptake of N. This implies that particularly class 1 should be given a careful attention in fertilizer application to avoid losses of NO_3-N to the ground water during the winter.

One month after the first sampling (20th June), most of the NO_3-N was disappeared from the soil (Figure 6.15), most likely it mainly taken up by the sugar beets. As a

consequence, the average topsoil NO_3-N content of class 1 (41 kg ha^{-1}, $s_{e,i}$ = 7 kg ha^{-1}), 2 (47 kg ha^{-1}, $s_{e,i}$ = 11 kg ha^{-1}) and 3 (49 kg ha^{-1}, $s_{e,i}$ = 16 kg ha^{-1}) were almost equal. However, a slight difference could be observed in the average subsoil NO_3-N contents between class 1 (40 kg ha^{-1}, $s_{e,i}$ r = 3 kg ha^{-1}) and class 2 (54 kg ha^{-1}, $s_{e,i}$ = 8 kg ha^{-1}) and 3 (58 kg ha^{-1}, $s_{e,i}$ = 12 kg ha^{-1}). The rapid decline of soil nitrogen levels could be expected, as Armstrong et al. (1986) reported that sugar beet plants might need to take up as much as 5 kg N ha^{-1} day^{-1} for rapid leaf expansion during early stages of its vegetative phase. The same pattern of NO_3-N was observed by 11th July. At the latter stages of the growing period (14th August and 13th October) very low NO_3-N contents were observed and top and subsoil averages of the three classes were almost identical.

Very low top and subsoil NH_4-N contents were observed during the entire growing season. This is a normal observation in most well drained agricultural lands where NH_4^+ formed during the organic matter mineralization are quickly converted to NO_3^- through microbial processes (Pierzynski et al., 2000).

Figure 6.16 summarises top and subsoil moisture dynamics across the potential management classes. Throughout the growing period of sugar beet, both the top and subsoil of class 1 contained a lower average moisture content compared to the other two classes. These differences were more distinct in the subsoil where the soil texture differs greatly, indicating possible limitations of soil moisture availability for crop growth.

On most monitoring days except on 13th October, the topsoil moisture content of class 2 had a similar average moisture content as class 3 with overlapping standard error intervals. However, this was quite different in the subsoil, where marked differences of moisture content were observed between these two classes except on 20th June. These differences of moisture contents across classes suggested the potential of site-specific water management practices in the polder area for optimizing crop productivity.

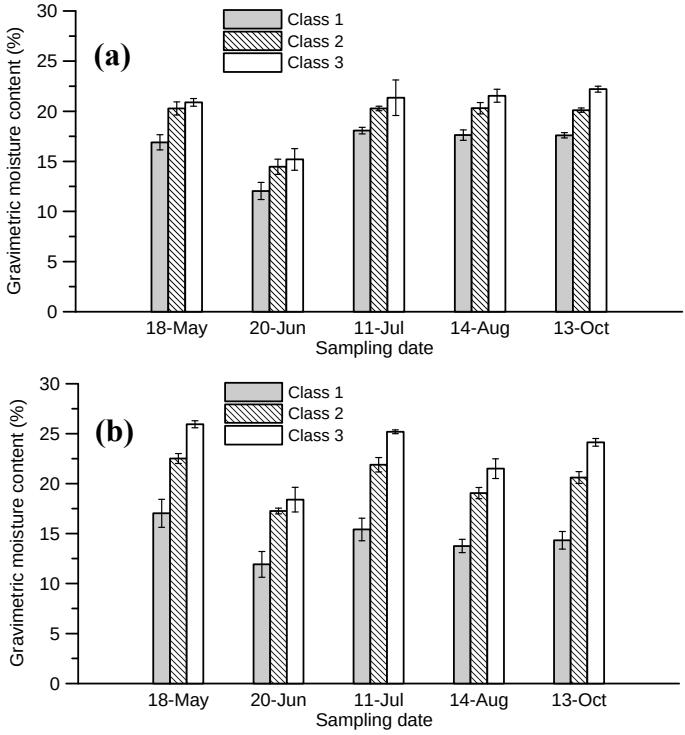

Figure 6.16. Average gravimetric moisture content in soil depth intervals (a) 0 –30 cm and (b) 30 – 60 cm for each monitoring date across potential management classes. Vertical error bars show the ± standard error of sampling means.

6.7.3. Crop yield and farm income across management classes

The average crop biomass (roots plus leaves) of class 1 was distinctly smaller than that of class 2 and 3: 105 Mg ha^{-1}, 147 Mg ha^{-1} and 150 Mg ha^{-1}, respectively (Table 6.14). The results of an ANOVA revealed a large intra-class correlation (R_i^2 = 0.89) of the crop biomass (Table 6.15). As a consequence, the delineation of potential management classes was very successful in differentiating biomass production within this field. It is likely that the less available soil nitrogen and moisture in class 1 has caused a lower biomass yields. This argument agrees with the observations of Milford (2006), who stressed that nitrogen and moisture availability at the early stages of sugar beet growth are key factors determining total biomass production.

An inverse relationship was found for the sugar content: on average it was 17.2 % for class 1, 16.3 % for class 2 and 15.7 % for class 3, with very small standard errors and a R_i^2 of 0.69. It is well known that crops that are well supplied with nitrogen tend to produce a larger yield of beets containing a lower concentration of sugar (Draycott and Christenson, 2003). This is further explained in Figure 6.17 which relates the response of sugarbeet to increasing nitrogen fertilizer amounts. Sugar content remains almost constant until close to the optimal dose and after which it decreases more rapidly. Therefore, it is very likely that the larger nitrogen levels in the soil of class 2 and 3 (Figure 6.15) has caused the lower concentrations of sugar in the beets. The larger moisture availability might have further enhanced this effect (due to water retention in tap root) resulting in a lower sugar contents.

Class 1 had the smallest root weights, which are generally the richest in sugar content. The opposite was found in classes 2 and 3. As a result the sugar yield was more homogeneous, it ranged from 13 Mg ha^{-1} for class 1 to 14.2 Mg ha^{-1} for class 2 which was almost the same for class, and R_i^2 dropped to 0.23.

The financial income obtained by the farmer reflected this compensation effect. Although the delineation of management zones was not able to differentiate the income between the classes (with R_i^2 of 0.07 and relatively large standard errors), there still was a considerable difference in average income of 287 € ha^{-1} between class 1 and 2. Between class 1 and 3 the difference in average income was 159 € ha^{-1}.

Table 6.14. Mean values of crop yield (sugar beets) variables per management class and, between brackets, the standard error of the mean.

Class	Biomass (Mg ha^{-1})	Sugar content (%)	Sugar yield (Mg ha^{-1})	Income (€ ha^{-1})
1	105.5 (2.5)	17.2 (0.3)	13.0 (0.3)	3958 (72)
2	147.0 (4.1)	16.3 (0.3)	14.2 (0.4)	4245 (151)
3	150.3 (4.3)	15.7 (0.2)	14.0 (0.2)	4117 (172)

Table 6.15. Results of the ANOVA on the crop yield (sugar beets) variables based on the 3 management classes.

	Biomass (Mg ha^{-1})	Sugar content (%)	Sugar yield (Mg ha^{-1})	Income (€ ha^{-1})
s_T^2	472.2	0.59	0.72	56786
s_W^2	50.3	0.18	0.55	52828
R_i^2	0.89	0.69	0.23	0.07

It should be added that the similarity in income between classes was obtained through a completely different soil-crop interaction, notwithstanding the uniform management. In class 1 both the NO_3-N and moisture content were the lowest, resulting in small beets with high sugar contents.

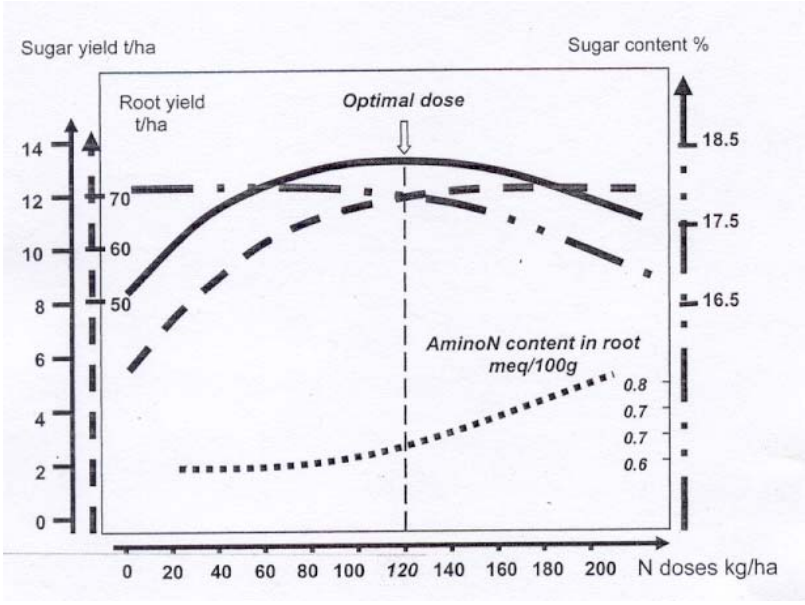

Figure 6.17. Response of sugar beet to increasing nitrogen fertilizer amounts. Example for a 120 kg N ha^{-1} optimum application (source: Cariolle and Duval, 2005).

In class 3 the beets were the largest, but with the lowest sugar content. Class 2 had intermediate values for both variables, resulting in the largest financial income. This indicates that if the three management zones would have received a different N-fertilization, with N-fertilization split into several applications for class 1 and a single but smaller N-application for class 3, both classes could have an increased sugar production resulting in an overall increased income. Also, a proper water management in class 1 could benefit the crop growth, especially in early growing conditions.

6.8. Conclusions

The focus of this research was to recognize the agronomic relevance of potential management classes delineated in section 1 of this chapter. In this context, the first research question formulated was "Do the soil water retention characteristics, Nitrogen and moisture dynamics under uniform soil management vary across potential management classes?" As explained by the soil water retention curves, the water retention of the sub soil is highly different across potential management classes. However, the same is not true for the comparatively homogenous topsoil, where slight differences of water retention between classes were only observed for pF values > 2.5. Despite that, during the growing period clear differences of top soil moisture contents were evident between the coarse textured class 1 and the other two classes. The differences of soil moisture contents in the subsoil were substantial between all three classes. Three potential management classes were found to reflect clear differences in dynamics of NO_3-N during the growing season of 2005 and the preceding winter. The soil of class 1 contained less available NO_3-N at the start of the growing season than the other classes, notwithstanding the more or less uniform application of N-fertilization in the previous autumn. Through these observations it can be highlighted that soil water retention characteristics, nitrogen and moisture dynamics under uniform soil management substantially vary across potential management classes.

The second research question was "Can the variation of nitrogen and moisture contents across management classes affect on the sugar beet yield and farmers income?". The differences between management classes had an impact on the sugar beets. The beets grown in class 1 produced clearly less biomass (beet roots and leaves), which was compensated by a larger sugar content. As a consequence, relatively small differences were found between the zones for the sugar yield and the sugar related income by the farmer. However, it should be noted that the relatively small differences in income (of about 287 € ha^{-1}) are the result of strongly different growing conditions and compensation effects between total biomass and sugar accumulation under uniform input application. Consequently there is a clear opportunity to optimize the yield while reducing the environmental implications by nitrate losses. A different management for the three classes is recommended. Class 1, with its permeable sandy subsoil, would benefit from a fertilization scheme split into different applications, whereas class 2 and 3 could suffice with a single, and probably smaller, N-application. Also, differences in water management could be considered.

As a general conclusion it can be stated that EC_a measurements are able to provide a stable and relevant basis for delineating agronomically relevant management zones.

Chapter 7

General conclusions and future research

7.1. Introduction

In this dissertation, the potential use of two types of ancillary information: EC_a and elevation data was evaluated for the detailed mapping of soil variability with a minimum effort of invasive field sampling. Through this objective, attempts were made to fulfil the soil information needs for site-specific soil management.

In this chapter, the major contributions of this research to understand and inventorize the soil variability in support of site-specific soil management are summarized. Then, some prospects for future research are mentioned.

7.2. General conclusions

National choropleth soil maps remain the major soil information available in most countries. However, assessment of the potentials and weaknesses of these soil information inventories in relation to current needs of soil information is essential to improve their usability. Through the case study conducted at the Melle site (chapter 4), we investigated the adequacy of the 1:20,000 soil map of Belgium to provide soil information needed for site-specific soil management. The study clearly demonstrated the general weakness of this map in accurately predicting soil properties at a within-field scale. Therefore, an upgrading of it by incorporating detailed soil information was required. The traditional way to upgrade a choropleth soil map is to conduct a new survey, either at a similar scale but focussing on other soil properties, or at a more detailed scale with the same soil properties to obtain a better representation of their spatial variability. It was a unique opportunity for us to assess the second upgrading option using a more detailed 1:5000 choropleth soil map of the same area. In comparison to the 1:20,000 soil map, the 1:5000 map was able to characterise the within-field variability of depth to the Tertiary clay substratum (D_{ts}) with a high accuracy. Therefore the past solution to improve the map predictions by increasing the map scale and taking more observations proved to be successful for D_{ts}. However, it must be realized that this high accuracy was gained through approximately 210 soil augerings. In addition, even with a dense

invasive soil sampling, the 1:5000 map failed to characterize the within-field variation of soil texture with a sufficiently high accuracy.

Modern technology, however, allows to proceed a step further in the upgrading of soil maps. More than nine thousand EC_a observations obtained with the EM38DD sensor provided abundant information which could be strongly linked to the D_{ts}. By combining a strategic sampling scheme, i.e. Latin-hypercube sampling, with a prediction model derived on the basis of the depth sensitivity function of the EM38 sensor, we were able to make accurate predictions of D_{ts} only with 20 soil augerings. These predictions can be further improved by employing regression kriging with some extra samples. For example, the upgraded soil map using EC_a data and 60 soil augerings showed a better accuracy than the 1:5000 map. It can be concluded that proximal soil sensing using the EM38DD sensor is a useful step to upgrade the regional scale soil map by adding accurate information on the depth to a texturally contrasting subsoil layer.

The study conducted at the Leefdaal field (chapter 5) revealed a strongly structured within-field soil variability present in the European loess area. The variations of relatively stable soil properties, such as pH, organic C and soil texture are mainly linked to the pedogenic processes as well as slope processes. Though loess soils are generally considered to be spatially very homogenous, the findings of this research allowed us to disregard this perception. New opportunities were opened for site-specific management of loess soils. Elevation, EC_aV and soil pH were found to be the key variables to characterize the within-field variation and ultimately to delineate potential management zones. Among these, elevation and EC_aV represent easy to acquire surrogates for organic C and texture, respectively. Necessity of invasive soil samples to detect the variation of pH in this area can be avoided by using a commercially available pH sensor. Moreover, terrain attributes, namely slope angle and stream power index, provided a logical basis to explain the variations of soil texture and pH through a visualization of soil erosion and sedimentation patterns present in this area. Therefore, if sensors for EC_a and pH measurements would not be available, topographic attributes could be

useful to design an optimum sampling scheme to acquire information on texture and pH. This research allowed us to highlight three essential spatial inventory steps suitable in support of site-specific soil management: (1) acquisition of elevation, EC_aV and on-the-go pH measurements, (2) classification of these data layers, and (3) characterization of texture and organic C contents of each class using a few soil samples obtained within each class.

The research reported in chapter 6 identified a well structured soil textural variation in the polder soils of northwest East-Flanders, which had been inadequately identified before. The highly heterogeneous subsoil can cause a substantial variation of crop performance and therefore, it is a key information to be included in the soil spatial inventories in support of site-specific soil management. Since the present day flat landscape has no link to the subsurface variability, the classical surveying procedure would require large numbers of field observations to inventorize this variability. However, we found a strong spatial relationship between the EC_a measurements and the subsoil clay content. This allowed us to accurately map the variation of subsoil clay with a limited number of soil textural analysis. The delineated management zones showed substantial differences in nitrogen and moisture dynamics and ultimately differences in crop yield. Therefore, there is a clear opportunity to practice site-specific management in the polder area in order to optimize the yield while reducing the environmental implications by nitrate losses. The findings reported in this chapter confirmed that the electromagnetically sensed EC_a is a promising and cost effective source of ancillary information for detailed mapping of the heterogeneous subsoil of the polder soils. The mapped subsoil variation has a direct relevance for the site-specific management of soil water and nitrogen. These findings can be applicable for many soils formed in either marine or alluvial deposits.

7.3. Future research issues

This research reported on the spatial inventory techniques to map within-field variation of relatively stable soil properties like, soil textural fractions, pH, organic

C and depth to subsurface compacted soil layers. It became evident that the recent advances in soil sensing and data processing techniques have opened new possibilities to accurately map the variation of these properties with a minimum effort of field sampling. The way forward is to use this soil information to determine the appropriate site-specific management decisions. Process based simulation modelling can be proposed as a suitable approach to achieve this target. With this approach, the influence of these stable soil properties on agriculturally important soil qualities such as availability of soil moisture, soil nutrient status and nitrogen leaching potential could be quantified. Thereafter a proper scenario analysis could be used to determine the best site-specific soil management practise to gain expected goals of site-specific soil management.

The three case studies presented in this dissertation consistently showed that proximal soil sensing of EC_a is a very satisfactory method for elucidating the soil variability at a within-field scale. It should be noted that its applicability is equally valid for soil mapping at a regional scale and also upgrading of the existing coarse-scale soil maps. These two are priorities in the developing countries as well as in many developed countries for the sustainable use of soil resources through proper land use planning. However, up to now, the adoption of proximal sensing of soil EC_a has not been introduced to developing countries. This is mainly due to the high cost[1] of equipments and the lack of expertise to operate soil sensing systems and analyze and interpret the data. The ample evidences for the utility of proximally sensed EC_a for soil mapping however are sufficiently convincing that such an such investment is worthwhile.

[1] Currently, the EM38DD sensor is no longer production. The upgraded version of this sensor, EM38-MK2 is available and its quoted price was $ 17,200 as at June 2008.

References

Adamchuk, V.I. 2008. Development of on-the-go soil sensor systems Proceedings of 1st global workshop on high resolution digital soil sensing and mapping (CD-ROM), Sydney, Australia, 5-8 February 2008.

Adamchuk, V.I., J.W. Hummel, M.T. Morgan, and S.K. Upadhyaya. 2004. On-the-go soil sensors for precision agriculture. Computers and Electronics in Agriculture 44:71-91.

Adamchuk, V.I., E.D. Lund, T.M. Reed, and R.B. Ferguson. 2007. Evaluation of an on-the-go technology for soil pH mapping. Precision Agriculture 8:139-149.

Aitchison, J. 1986. The statistical analysis of compositional data. Chapman and Hall, London.

Alimardani, R., Y. Abbaspour-Gilandeh, A. Khalilian, A. Keyhani, and S.H. Sadati. 2007. Energy Savings with Variable-Depth Tillage "A Precision Farming Practice". American-Eurasian Journal of Agricultural & Environmental Science 2:442-447.

Anderson-Cook, C.M., M.M. Alley, J.K.F. Roygard, R. Khosla, R.B. Noble, and J.A. Doolittle. 2002. Differentiating soil types using electromagnetic conductivity and crop yield maps. Soil Science Society of America Journal 66:1562-1570.

Andrade-Sanchez, P., S.K. Upadhyaya, and B.M. Jenkins. 2007. Development, construction, and field evaluation of a soil compaction profile sensor. Transactions of the ASABE 50:719-725.

Armstrong, M.J., G.F.J. Milford, T.O. Pocock, P.J. Last, and W. Day. 1986. The dynamics of nitrogen uptake and its re-mobilization during the growth of sugar beet. Journal of Agricultural Science 107:145-154.

Auerswald, K., S. Simon, and H. Stanjek. 2001. Influence of soil properties on electrical conductivity under humid water regimes. Soil Science 166:382-390.

Baligar, V.C., N.K. Fageria, and Z.L. He. 2001. Nutrient use efficiency in plants. Communications in Soil Science and Plant Analysis 32:921-950.

Barnes, E.M., and M.G. Baker. 2000. Multispectral data for mapping soil texture: Possibilities and limitations. Applied Engineering in Agriculture 16:731-741.

Beckett, P.H.T., and R. Webster. 1971. Soil variability: a review. Soils and Fertilisers 34:1-15.

Berntsen, J., A. Thomsen, K. Schelde, O.M. Hansen, L. Knudsen, N. Broge, H. Hougaard, and R. Horfarter. 2006. Algorithms for sensor-based redistribution of nitrogen fertilizer in winter wheat. Precision Agriculture 7:65-83.

Bezdek, J.C. 1974. Numerical taxonomy with fuzzy sets. Journal of Mathematical Biology 1:57-71.

Bezdek, J.C. 1981. Pattern recognition with fuzzy objective function algorithms. Plenum Press, NY.

Bianchini, A.A., and A.P. Mallarino. 2002. Soil-sampling alternatives and variable-rate liming for a soybean–corn rotation. Agronomy Journal 94:1355-1366.

Birrell, S.J., K.A. Sudduth, and S.C. Borgelt. 1996. Comparison of sensors and techniques for crop yield mapping. Computers and Electronics in Agriculture 14:215-233.

Blackmore, S. 1999. The interpretation of trends from multiple year maps. Computers and Electronics in Agriculture 26:37-51.

Boettinger, J.L., J.A. Doolittle, N.E. West, E.W. Bork, and E.W. Schupp. 1997. Nondestructive assessment of rangeland soil depth to petrocalcic horizon using electromagnetic induction. Arid Soil Research and Rehabilitation 11:375-390.

Borchers, B., T. Uram, and J.M.H. Hendrickx. 1997. Tikhonov regularization of electrical conductivity depth profiles in field soils. Soil Science Society of America Journal 61:1004-1009.

Bork, E.W., N.E. West, J.A. Doolittle, and J.L. Boettinger. 1998. Soil depth assessment of sagebrush grazing treatments using electromagnetic induction. Journal of Range Management 51:469-474.

Bouma, J., J. Stoorvogel, B.J. van Alphen, and H.W.G. Booltink. 1999. Pedology, precision agriculture, and the changing paradigm of agricultural research. Soil Science Society of America Journal 63:1763-1768.

Boydell, B., and A.B. McBratney. 2002. Identifying potential within-field management zones from cotton-yield estimates. Precision Agriculture 3:9-23.

Brady, N.C., and R.R. Weil. 1999. The nature and properties of soils. 12 ed. Prentice Hall, NJ.

Brahy, V., J. Deckers, and B. Delvaux. 2000. Estimation of soil weathering stage and acid neutralizing capacity in a toposequence Luvisol-Cambisol on loess under deciduous forest in Belgium. European Journal of Soil Science 51:1-13.

Bremner, J.M., and C.S. Mulvaney. 1982. Nitrogen-Total, p. 595-624, *In* A. L. Page, ed. Methods of soil analysis. Part 2: Chemical and microbiological properties, 2 ed. Agronomy Monograph 9, American Society of Agronomy, Madison, WI.

Brevik, E.C., T.E. Fenton, and A. Lazari. 2006. Soil electrical conductivity as a function of soil water content and implications for soil mapping. Precision Agriculture 7:393-404.

Brock, A., S.M. Brouder, G. Blumhoff, and B.S. Hofmann. 2005. Defining yield-based management zones for corn-soybean rotations. Agronomy Journal 97:1115-1128.

Brown, D.J., K.D. Shepherd, M.G. Walsh, M. Dewayne Mays, and T.G. Reinsch. 2006. Global soil characterization with VNIR diffuse reflectance spectroscopy. Geoderma 132:273-290.

Brus, D.J., J.J. Degruijter, and A. Breeuwsma. 1992. Strategies for updating soil survey information - a case-study to estimate phosphate sorption characteristics. Journal of Soil Science 43:567-581.

Burke, I.C., C.M. Yonker, W.J. Parton, C.V. Cole, K. Flach, and D.S. Schimel. 1989. Texture, Climate, and Cultivation Effects on Soil Organic-Matter Content in Us Grassland Soils. Soil Science Society of America Journal 53:800-805.

Burrough, P.A., and R.A. McDonnell. 1998. Principles of geographical information systems. Oxford University Press Inc., NY.

Cambardella, C.A., T.B. Moorman, J.M. Novak, T.B. Parkin, D.L. Karlen, R.F. Turco, and A.E. Konopka. 1994. Field-scale variability of soil properties in central Iowa soils. Soil Science Society of America Journal 58:1501-1511.

Cariolle, M., and R. Duval. 2005. Nutrition - Nitrogen, p. 169-189, *In* A. P. Draycott, ed. Sugar Beet. Blackwell Publishing, Oxford.

Carpenter, S.R., N.F. Caraco, D.L. Correll, R.W. Howarth, A.N. Sharpley, and V.H. Smith. 1998. Nonpoint pollution of surface waters with phosphorus and nitrogen. Ecological Applications 8:559–568.

Catell, R.B. 1966. The scree test for the number of factors. Journal of Multivariate Behavioral Research 1:245-276.

Chang, J.Y., D.E. Clay, C.G. Carlson, S.A. Clay, D.D. Malo, R. Berg, J. Kleinjan, and W. Wiebold. 2003. Different techniques to identify management zones impact nitrogen and phosphorus sampling variability. Agronomy Journal 95:1550-1559.

Chen, F., D.E. Kissel, L.T. West, D. Rickman, J.C. Luvall, and W. Adkins. 2005. Mapping surface soil organic carbon for crop fields with remote sensing. Journal of Soil and Water Conservation 60:51-57.

Christy, C. 2008. Real-time measurement of soil attributes using on-the-go near infrared reflectance spectroscopy. Computers and Electronics in Agriculture 61:10-19.

Christy, C., P. Drummond, and D. Laird. 2003. An on-the-go soil strength profile sensor for soil. Papar No. 03-1044, ASAE, St. Joseph, Michigan.

Cockx, L., M. Van Meirvenne, and G. Hofman. 2005. Characterization of nitrogen dynamics in a pasture soil by electromagnetic induction. Biology and Fertility of Soils 42:24-30.

Cockx, L., M. Van Meirvenne, and B. De Vos. 2007. Using the EM38DD soil sensor to delineate clay lenses in a sandy forest soil. Soil Science Society of America Journal 71:1314-1322.

Cohen, J. 1960. A coefficient of agreement for nominal scales. Educational and Psychological Measurement 20:37-46.

Colvin, T.S., D.B. Jaynes, D.L. Karlen, D.A. Laird, and J.R. Ambuel. 1997. Yield variability within a central Iowa field. Transactions of the ASAE 40:883-889.

Cook, P.G., and S. Kilty. 1992. A helicopter-borne electromagnetic survey to delineate groundwater recharge rates. Water Resource Research 28:2953-2961.

Cook, S.E., R.J. Corner, G. Grealish, P.E. Gessler, and C.J. Chartres. 1996. A rule-based system to map soil properties. Soil Science Society of America Journal 60:1893-1900.

Corwin, D.L., and S.M. Lesch. 2003. Application of soil electrical conductivity to precision agriculture: Theory, principles, and guidelines. Agronomy Journal 95:455-471.

Corwin, D.L., and S.M. Lesch. 2005a. Apparent soil electrical conductivity measurements in agriculture. Computers and Electronics in Agriculture 46:11-43.

Corwin, D.L., and S.M. Lesch. 2005b. Characterizing soil spatial variability with apparent soil electrical conductivity: I. Survey protocols. Computers and Electronics in Agriculture 46:103-133.

Cox, M.S., and R.D. Gerard. 2007. Soil management zone determination by yield stability analysis and classification. Agronomy Journal 99:1357-1365.

Daily, G., P. Dasgupta, B. Bolin, P. Crosson, J. du Guerny, P. Ehrlich, C. Folke, A.M. Jansson, B.O. Jansson, N. Kautsky, A. Kinzig, S. Levin, K.G. Maler, P. Pinstrup-Andersen, D. Siniscalco, and B. Walker. 1998. Policy forum: Global food supply - Food production, population growth, and the environment. Science 281:1291-1292.

Dale, M.B., A.B. McBratney, and J.S. Russell. 1989. On the role of expert systems and numerical taxonomy in soil classification. Journal of Soil Science 40:223-234.

Davis, J.D. 1986. Statistics and data analysis in Geology. 2 ed. John Wiley & Sons, N.Y.

de Gruijter, J.J., D.J.J. Walvoort, and P.F.M. vanGaans. 1997. Continuous soil maps - A fuzzy set approach to bridge the gap between aggregation levels of process and distribution models. Geoderma 77:169-195.

de Gruijter, J.J., D. Brus, M.F.P. Bierkens, and M. Knotters. 2006. Sampling for natural resource monitoring. Springer, Berlin.

de Jonge, K.C., A.L. Kaleita, and K.R. Thorp. 2007. Simulating the effects of spatially variable irrigation on corn yields, costs, and revenue in Iowa. Agricultural Water Management 92:99-109.

Delgado, J.A. 2001. Use of simulations for evaluation of best management practices on irrigated cropping systems, p. 355 - 381, *In* M. J. Shaffer, et

al., eds. Modeling Carbon and Nitrogen dynamics for soil management. Lewis Publishers, USA.

Dell, C.J., and A.N. Sharpley. 2006. Spatial variation of soil organic carbon in a northeastern US watershed. Journal of Soil and Water Conservation 61:129-136.

Dent, D., and A. Young. 1981. Soil survey and land evaluation. George Allen & Unwin, London.

Desmet, P.J.J., and G. Govers. 1995. Gis-based simulation of erosion and deposition patterns in an agricultural landscape - a comparison of model results with soil map information. Catena 25:389-401.

Deutsch, C.V., and A.G. Journel. 1998. GSLIB: geostatistical software library and user's guide. 2 ed. Oxford University Press, NY.

Dijkerman, J.C. 1974. Pedology as a science - role of data, models and theories in study of natural soil systems. Geoderma 11:73-93.

Dobermann, A., S. Blackmore, S.E. Cook, and V.I. Adamchuk. 2004. Precision farming: challenges and future directions. New directions for a diverse planet. Proceedings of the 4th International Crop Science Congress (CD-ROM), Brisbane, Australia, 26 September – 1 October 2004.

Dobermann, A., J.L. Ping, V.I. Adamchuk, G.C. Simbahan, and R.B. Ferguson. 2003. Classification of crop yield variability in irrigated production fields. Agronomy Journal 95:1105-1120.

Domsch, H., and A. Giebel. 2004. Estimation of soil textural features from soil electrical conductivity recorded using the EM38. Precision Agriculture 5:389-409.

Doolittle, J.A., K.A. Sudduth, N.R. Kitchen, and S.J. Indorante. 1994. Estimating Depths to Claypans Using Electromagnetic Induction Methods. Journal of Soil and Water Conservation 49:572-575.

Draycott, A.P., and D.R. Christenson. 2003. Nutrients for sugar beet production: soil plant relationships. CABI publishing, Wallingford.

Earl, R., P.N. Wheeler, B.S. Blackmore, and R.J. Godwin. 1996. Precision farming: the management variability. Landwards 51:18-23.

Ehlert, D., and K.H. Dammer. 2006. Widescale testing of the crop-meter for site-specific farming. Precision Agriculture 7:101-115.

Evans, D.E., E.J. Sadler, C.R. Camp, and J.A. Millen. 2000. Spatial canopy temperature measurements using center pivot mounted IRTs. Proceedings of 5th International Conference on Precision Agriculture (CD-ROM), Bloomington, MN, USA, 16-19 July 2000.

Finke, P.A. 2007. Quality assessment of digital soil maps: producers and users perspective, p. 523-541, *In* P. Lagacherie, et al., eds. Digital soil mapping: An introductory perspective, Development in soil science 31. Elsevier, Amsterdam.

Fleming, K.L., D.F. Heermann, and D.G. Westfall. 2004. Evaluating soil color with farmer input and apparent soil electrical conductivity for management zone delineation. Agronomy Journal 96:1581-1587.

Follett, R.F., and J.A. Delgado. 2002. Nitrogen fate and transport in agricultural systems. Journal of Soil and Water Conservation 57:402-408.

Forbes, T., D. Rossiter, and A. Van Wambeke. 1987. Guidelines for evaluating the adequacy of soil resource inventories, p. 1-3, SMSS Technical Monograph 4. Cornell University Department of Agronomy, Ithaca, NY.

Fraisse, C.W., K.A. Sudduth, and N.R. Kitchen. 2001. Delineation of site-specific management zones by unsupervised classification of topographic attributes and soil electrical conductivity. Transactions of the ASAE 44:155-166.

Franzen, D.W., D.H. Hopkins, M.D. Sweeney, M.K. Ulmer, and A.D. Halvorson. 2002. Evaluation of soil survey scale for zone development of site-specific nitrogen management. Agronomy Journal 94:381-389.

Fridgen, J.J., N.R. Kitchen, K.A. Sudduth, S.T. Drummond, W.J. Wiebold, and C.W. Fraisse. 2004. Management Zone Analyst (MZA): Software for subfield management zone delineation. Agronomy Journal 96:100-108.

Frogbrook, Z.L., and M.A. Oliver. 2007. Identifying management zones in agricultural fields using spatially constrained classification of soil and ancillary data. Soil Use and Management 23:40-51.

Gee, G.W., and J.W. Bauder. 1986. Particle size analysis, p. 383-411, *In* A. Clute, ed. Methods of soil analysis, part 1. Physical and mineralogical methods. Agronomy monograph 9. American Society of Agronomy, Medison, WI.

Gerhards, R., and S. Christensen. 2003. Real-time weed detection, decision making and patch spraying in maize, sugarbeet, winter wheat and winter barley. Weed Research 43:385-392.

Godwin, R.J., and P.C.H. Miller. 2003. A review of the technologies for mapping within-field variability. Biosystems Engineering 84:393-407.

Godwin, R.J., G.A. Wood, J.C. Taylor, S.M. Knight, and J.P. Welsh. 2003a. Precision farming of cereal crops: a review of a six year experiment to develop management guidelines. Biosystems Engineering 84:375-391.

Godwin, R.J., T.E. Richards, G.A. Wood, J.P. Welsh, and S.M. Knight. 2003b. An economic analysis of the potential for precision farming in UK cereal production. Biosystems Engineering 84:533-545.

Goovaerts, P. 1997. Geostatistics for natural resources evaluation. Oxford University Press, NY.

Goovaerts, P. 1998. Ordinary cokriging revisited. Mathematical Geology 30:21-42.

Goovaerts, P., R. Webster, and J.P. Dubois. 1997. Assessing the risk of soil contamination in the Swiss Jura using indicator geostatistics. Environmental and Ecological Statistics 4:31-48.

Goulard, M., and M. Voltz. 1992. Linear Coregionalization Model - Tools for Estimation and Choice of Cross-Variogram Matrix. Mathematical Geology 24:269-286.

Govers, G. 1991. Rill erosion on arable land in central belgium - rates, controls and predictability. Catena 18:133-155.

Hall, G.F., and C.G. Olson. 1991. Predicting variability of soils from landscape models, p. 9-38, *In* M. J. Mausbach and L. P. Wilding, eds. Spatial variabilities of soils and landforms, SSSA Special publication 28, SSSA, Madison, WI.

Haynes, R.J., C.S. Dominy, and M.H. Graham. 2003. Effect of agricultural land use on soil organic matter status and the composition of earthworm communities in KwaZulu-Natal, South Africa. Agriculture Ecosystems & Environment 95:453-464.

Henderson, T.L., M.F. Baumgardner, D.P. Franzmeier, D.E. Stott, and D.C. Coster. 1992. High dimensional reflectance analysis of soil organic-matter. Soil Science Society of America Journal 56:865-872.

Hendrickx, J.M.H., and R.G. Kachanoski. 2002. Indirect measurement of solute concentration: Nonintrusive electromagnetic induction, p. 1297-1306, *In* J. H. Dane and G. C. Topp, eds. Methods of soil analysis, SSSA Book Ser. 5. Soil Science Society of America, MA.

Hendrickx, J.M.H., B. Borchers, D.L. Corwin, S.M. Lesch, A.C. Hilgendorf, and J. Schlue. 2002. Inversion of soil conductivity profiles from electromagnetic induction measurements: Theory and experimental verification. Soil Science Society of America Journal 66:673-685.

Hengl, T., G.B.M. Heuvelink, and A. Stein. 2004. A generic framework for spatial prediction of soil variables based on regression-kriging. Geoderma 120:75-93.

Hennens, D., J. Baert, B. Broos, H. Ramon, and J. De Baerdemaeker. 2003. Development of a flow model for the design of a momentum type beet mass flow sensor. Biosystems Engineering 85:425-436.

Heuvelink, G.B.M., and R. Webster. 2001. Modelling soil variation: past, present, and future. Geoderma 100:269-301.

Holmgren, P. 1994. Multiple flow direction algorithms for runoff modeling in grid based elevation models - an empirical-evaluation. Hydrological Processes 8:327-334.

Hummel, J.W., L.D. Gaultney, and K.A. Sudduth. 1996. Soil property sensing for site-specific crop management. Computers and Electronics in Agriculture 14:121-136.

Isaaks, E., and R. Srivastava. 1989. An introduction to applied geostatistics. Oxford University Press, NY.

ISSS WorkingGroupReferenceBase. 1998. World reference base for soil resources: keys to reference soil groups of the world. World Soil Resource Report No84, FAO, Rome.

James, I.T., T.W. Waine, R.I. Bradley, J.C. Taylor, and R.J. Godwin. 2003. Determination of soil type boundaries using electromagnetic induction scanning techniques. Biosystems Engineering 86:421-430.

Jaynes, D.B., T.S. Colvin, and T.C. Kaspar. 2005. Identifying potential soybean management zones from multi-year yield data. Computers and Electronics in Agriculture 46:309-327.

Jenny, H. 1941. Factors of soil formation: a system of quantitative pedology McGraw-Hill, NY.

Jensen, J.R. 1996. Introductory digital image processing: A remote sensing perspective Prentice Hall, Upper Saddle River, NJ.

Jenson, S.K., and J.O. Domingue. 1988. Extracting topographic structure from digital elevation data for geographic information-system analysis. Photogrammetric Engineering and Remote Sensing 54:1593-1600.

Johnson, R.K., and P. Robert. 1998. A new methodology for developing applied soil surveys for precision agriculture. Agronomy Abstracts, Baltimore, MD.

Juergens-Gschwind, S. 1989. Ground water nitrates in other developed countries (Europe) -relationships to land use patterns, p. 75 - 138, *In* R. F. Follett, ed. Nitrogen management and ground water protection. Elsevier, Amsterdam.

Kaspar, T.C., T.S. Colvin, D.B. Jaynes, D.L. Karlen, D.E. James, D.W. Meek, D. Pulido, and H. Buttler. 2003. Relationship between six years of corn yields and terrain attributes. Precision Agriculture 4:87-101.

Kawasaki, R.G., and T.E. Osterkamp. 1988. Mapping shallow permafrost by electromagnetic inductive methods - practical considerations. Cold Regions Science and Technology 15:279-288.

Keeney, D.R. 1982. Nitrogen management for maximum efficiency and minimum pollution, p. 605-649, *In* Stevenson, ed. Nitrogen in agricultural soils. American Society of Agronomy, Madison, WI.

Keeney, D.R., and D.W. Nelson. 1982. Methods of soil analysis. Part 2: Chemical and microbiological properties, p. 643-698, *In* A. L. Page, ed., 2 ed. Agronomy Monograph 9, American Society of Agronomy, Madison, WI.

Kerry, R., and M.A. Oliver. 2003. Co-kriging when the soil and ancillary data are not co-located, p. 303-308, *In* J. V. Stafford and A. Werner, eds. Precision agriculture '04. Proceedings of the 5th European Conference on Precision Agriculture, Berlin, Germany, 15-19 June 2003. Waganingen Academic.

Khosla, R., D. Inmam, D.G. Westfall, R.M. Reich, M. Frasier, M. Mzuku, B. Koch, and A. Hornung. 2008. A synthesis of multi-disciplinary research in precision agriculture: site-specific management zones in semi-arid western Great Plains of the USA. Precision Agriculture 9:85-100.

King, B.A., J.C. Stark, and R.W. Wall. 2006. Comparison of site-specific and conventional uniform irrigation management for potatoes. Applied Engineering in Agriculture 22:677-688.

Kitchen, N.R., K.A. Sudduth, and S.T. Drummond. 1996. Mapping of sand deposition from 1993 midwest floods with electromagnetic induction measurements. Journal of Soil and Water Conservation 51:336-340.

Kitchen, N.R., K.A. Sudduth, and S.T. Drummond. 1998. An evaluation of methods for determining site specific management zones, p. 133-139, *In* M. Dak, ed. Proceedings of North Central Extension Industry Soil Fertility Conference, Potash and Phosphate Institute, St. Louis, Missouri, 11-12 November 1998.

Kitchen, N.R., K.A. Sudduth, and S.T. Drummond. 1999. Soil electrical conductivity as a crop productivity measure for claypan soils. Journal of Production Agriculture 12:607-617.

Kitchen, N.R., K.A. Sudduth, D.B. Mayers, S.T. Drummond, and S.Y. Hong. 2005. Delineating productivity zones on claypan soil fields using apparent soil electrical conductivity. Computers and Electronics in Agriculture 46:285-308.

Koorevaar, P., G. Menelik, and C. Dirksen. 1983. Elements of soil physics Elsevier, Amsterdam.

Kravchenko, A.N., G.A. Bollero, R.A. Omonode, and D.G. Bullock. 2002. Quantitative mapping of soil drainage classes using topographical data and soil electrical conductivity. Soil Science Society of America Journal 66:235-243.

Kravchenko, A.N., K.D. Thelen, D.G. Bullock, and N.R. Miller. 2003. Relationship among crop grain yield, topography, and soil electrical conductivity studied with cross-correlograms. Agronomy Journal 95:1132-1139.

Kravchenko, A.N., G.P. Robertson, K.D. Thelen, and R.R. Harwood. 2005. Management, topographical, and weather effects on spatial variability of crop grain yields. Agronomy Journal 97:514-523.

Lal, R. 1991. Soil structure and sustainability. Journal of Sustainable Agriculture 4:67-92.

Lamb, J.A., R.H. Dowdy, J.L. Anderson, and G.W. Rehm. 1997. Spatial and temporal stability of corn grain yields. Journal of Production Agriculture 10:410-414.

Lambert, D.M., and J. Lowenberg-DeBoer. 2000. Precision farming profitability review [Online]. Available by Site-Specific Management Center, Purdue University, West Lafayette, IN, USA. www.purdue.edu/ssmc (verified 25th February 2008).

Lambert, D.M., J. Lowenberg-DeBoer, and G.L. Malzer. 2006. Economic analysis of spatial-temporal patterns in corn and soybean response to nitrogen and phosphorus. Agronomy Journal 98:43-54.

Landis, J.R., and G.G. Koch. 1977. Measurement of observer agreement for categorical data. Biometrics 33:159-174.

Langley, R.B. 1997. The GPS error budget. GPS world 6:26-35.

Lark, R.M. 1998. Forming spatially coherent regions by classification of multivariate data: an example from the analysis of maps of crop yield. International Journal of Geographical Information Science 12:83-98.

Lark, R.M., and J.V. Stafford. 1997. Classification as a first step in the interpretation of temporal and spatial variation of crop yield. Annals of Applied Biology 130:111-121.

Larson, W.E., and P.C. Robert. 1991. Farming by soil, p. 103-112, *In* R. Lal and F. J. Pierce, eds. Soil management for sustainability. Soil and Water Conservation Society, Ankeny, IA, USA.

Larson, W.E., J.A. Lamb, B.R. Khakural, R.B. Ferguson, and G.W. Rehm. 1997. Potential of site-specific management for nonpoint environmental protection, *In* F. J. Pierce and E. J. Sadler, eds. The State of Site-specific Management for Agriculture. ASA,CSSA and SSSA, Madison WI, USA.

Leenhardt, D., M. Voltz, M. Bornand, and R. Webster. 1994. Evaluating Soil Maps for Prediction of Soil-Water Properties. European Journal of Soil Science 45:293-301.

Lillesand, T.M., and R.W. Kiefer. 1994. Remote sensing and image interpretation John Wiley & Sons, NY.

Lin, H.S., D. Wheeler, J. Bell, and L. Wilding. 2005. Assessment of soil spatial variability at multiple scales. Ecological Modelling 182:271-290.

Lowenberg-DeBoer, J., and S.M. Swinton. 1997. Economics of site-specific management in agronomic crops, p. 369-396, *In* F. J. Pierce and E. J. Sadler, eds. The State of Site-Specific Management for Agriculture. ASA, CSSA, SSSA, Madison, WI.

Lund, E.D., C. Christy, and P. Drummond. 1999. Practical applications of soil electrical conductivity mapping, p. 771-779, *In* J. V. Stafford, ed. Precision Agriculture '99, Proceedings of the 2nd European Conference on Precision Agriculture, Odense, Denmark, 11-15 july 1999. Sheffield Academic Press, UK.

Magalhaes, P.S.G., and D.G.P. Cerri. 2007. Yield monitoring of sugar cane. Biosystems Engineering 96:1-6.

Maleki, M.R., A.M. Mouazen, B. De Ketelaere, H. Ramon, and J. De Baerdemaeker. 2008. On-the-go variable-rate phosphorus fertilisation based on a visible and near-infrared soil sensor. Biosystems Engineering 99:35-46.

Manderson, A., and A. Palmer. 2006. Soil information for agricultural decision making: a New Zealand perspective. Soil Use and Management 22:393-400.

Marsman, B.A., and J.J. De Gruijter. 1986. Quality of soil maps. A comparison of survey methods in a sandy area. Soil Survery Papers No.15. Netherlands Soil Survey Institute, Wageningen.

Matheron, G. 1965. Regionalized variables and their estimation (in French). Editions Masson, Paris.

Mattikalli, N.M., E.T. Engman, T.J. Jackson, and L.R. Ahuja. 1998. Microwave remote sensing of temporal variations of brightness temperature and near-surface soil water content during a watershed-scale field experiment, and its application to the estimation of soil physical properties. Water Resources Research 34:2289-2299.

McBratney, A.B., and J.J. de Gruijter. 1992. Continuum approach to soil classification by modified fuzzy k-means with extragrades. Journal of Soil Science 43:159-175.

McBratney, A.B., and I.O.A. Odeh. 1997. Application of fuzzy sets in soil science: Fuzzy logic, fuzzy measurements and fuzzy decisions. Geoderma 77:85-113.

McBratney, A.B., and M.J. Pringle. 1997. Spatial variability in soil-implications for precision agriculture, p. 3-32, *In* J. V. Stafford, ed. Precision Agriculture '97. Proceedings of the 1st European Conference on Precision Agriculture, Warwick University, UK, 8-10 September 1997.

McBratney, A.B., M.L.M. Santos, and B. Minasny. 2003. On digital soil mapping. Geoderma 117:3-52.

McBratney, A.B., B.M. Whelan, T. Ancev, and J. Bouma. 2005. Future directions of precision agriculture. Precision Agriculture 6:7-23.

McBride, R.A., A.M. Gordon, and S.C. Shrive. 1990. Estimating forest soil quality from terrain measurements of apparent electrical conductivity. Soil Science Society of America Journal 54:290-293.

McCutcheon, M.C., H.J. Farahani, J.D. Stednick, G.W. Buchleiter, and T.R. Green. 2006. Effect of soil water on apparent soil electrical conductivity and texture relationships in a dryland field. Biosystems Engineering 94:19-32.

McGrath, S.P., and P. Loveland. 1992. The soil geochemical atlus of England and Wales. Blackie Academic and Professional, Glasgow.

McNeill, J.D. 1980. Electromagnetic terrain conductivity measurement at low induction numbers, Technical Note TN-6. Geonics Ltd., Mississauga, ON.

Meisinger, J.J., and J.A. Delgado. 2002. Principles for managing nitrogen leaching. Journal of Soil and Water Conservation 57:485-498.

Miao, Y., D.J. Mulla, W.D. Batchelor, J.O. Paz, P.C. Robert, and M. Wiebers. 2006. Evaluating management zone optimal nitrogen rates with a crop growth model. Agronomy Journal 98:545-553.

Milford, G.F.J. 2006. Plant structure and crop physiology, p. 34-36, *In* A. P. Draycott, ed. Sugar Beet. Blackwell publishing, Oxford.

Minasny, B., and A.B. McBratney. 2002. FuzME Version 3 [Online]. Available by Australian Centre for Precision Agriculture The University of Sydney NSW 2006 Australia http://www.usyd.edu.au/su/agric/acpa/fkme/program.html (verified 15th January 2007).

Minasny, B., and A.B. McBratney. 2006. A conditioned latin hypercube method for sampling in the presence of ancillary information. Computers and Geosciences 32:1378-1388.

Moore, I.D., G.J. Burch, and D.H. Mackenzie. 1988. Topographic effects on the distribution of surface soil water and the location of ephemeral gullies. Transactions of ASAE 31:1383-1385.

Moore, I.D., R.B. Grayson, and A.R. Ladson. 1991. Digital terrain modelling: A review of hydrological, geomorphological and biological applications. Hydrological Processes 5:3-30.

Moore, I.D., P.E. Gessler, G.A. Nielsen, and G.A. Peterson. 1993. Soil attribute prediction using terrain analysis. Soil Science Society of America Journal 57:443-452.

Moran, M.S., Y. Inoue, and E.M. Barnes. 1997. Opportunities and limitations for image-based remote sensing in precision crop management. Remote Sensing of Environment 61:319-346.

Morgan, M.T., and D.R. Ess. 1997. The Precision Farming Guide for Agriculturists John Deere Publishing, Moline, IL.

Mouazen, A.M., J. De Baerdemaeker, and H. Ramon. 2005. On-the-go sensor for measurement of dry bulk density referring to soil compaction, p. 521-528, *In* J. V. Stafford, ed. Precision agriculture '05. Proceedings of the 5th European Conference on Precision Agriculture, Uppsala, Sweden, 8-11 June 2005 Waganingen Academic.

Mouazen, A.M., M.R. Maleki, J. De Baerdemaeker, and H. Ramon. 2007. On-line measurement of some selected soil properties using a VIS-NIR sensor. Soil & Tillage Research 93:13-27.

Mulla, D.J., and A.R. Schepers. 1997. Key processes and properties for site-specific soil and crop management, p. 1-18, *In* F. J. Pierce and E. J. Sadler, eds. The state of site-specific management for agriculture. ASA,CSSA and SSSA, Madison WI, USA.

Nelson, D.W., and L.E. Sommers. 1996. Total carbon, organic carbon, and organic matter, p. 961-1010, *In* A. L. Page, ed. Methods of Soil Analysis, Part 2. Chemical and Microbiological Properties. American Society of Agronomy, Medison, WI.

Nichols, J.D. 1984. Relation of Organic-Carbon to Soil Properties and Climate in the Southern Great Plains. Soil Science Society of America Journal 48:1382-1384.

Oberthür, T., A. Dobermann, and H.U. Neue. 1996. How good is a reconnaissance soil map for agronomic purposes? Soil Use and Management 12:33-43.

OC-GIS_Vlaanderen. 2003. Digitaal hoogtemodel Vlaanderen, Nieuwsbrief GIS-Vlaanderen 16 (in Dutch). VLM, Brussel.

Odeh, I.O.A., and A.B. McBratney. 2000. Using AVHRR images for spatial prediction of clay content in the lower Namoi Valley of eastern Australia. Geoderma 97:237-254.

Odeh, I.O.A., A.B. McBratney, and D.J. Chittleborough. 1992. Soil pattern recognition with fuzzy-c-means: application to classification and soil-landform Interrelationships. Soil Science Society of America Journal 56:505-516.

Odeh, I.O.A., A.B. Mcbratney, and D.J. Chittleborough. 1995. Further Results on Prediction of Soil Properties from Terrain Attributes - Heterotopic Cokriging and Regression-Kriging. Geoderma 67:215-226.

Odeh, I.O.A., A.J. Todd, and J. Triantafilis. 2003. Spatial prediction of soil particle-size fractions as compositional data. Soil Science 168:501-515.

Palmer, A.R. 1983. The decade of North American geology geologic time scale: Geological Society of America Map and Chart Series MC-50.

Pannatier, Y. 1997. VARIOWIN: software for spatial data analysis in 2D. Springer, NY.

Pardo-Iguzquiza, E., and P.A. Dowd. 2002. FACTOR2D: a computer program for factorial cokriging. Computers & Geosciences 28:857-875.

Parent, A.C., M.C. Belanger, L.E. Parent, R. Santerre, A.A. Viau, F. Anctil, M.A. Bolinder, and C. Tremblay. 2008. Soil properties and landscape factors affecting maize yield under wet spring conditions in eastern Canada. Biosystems Engineering 99:134-144.

Pawlowsky-Glahn, V., and R.A. Olea. 2004. Geostatistical Analysis of Compositional Data. Oxford University Press, NY.

Pelletier, G., and S.K. Upadhyaya. 1999. Development of a tomato load/yield monitor. Computers and Electronics in Agriculture 23:103-117.

Persson, D.A., L. Eklundh, and P.A. Algerbo. 2004. Evaluation of an optical sensor for tuber yield monitoring. Transactions of the ASAE 47:1851-1856.

Pierzynski, G.M., J.T. Sims, and G.F. Vance. 2000. Soil nitrogen and environmental quality, p. 97-153. Soils and environmental quality, 2 ed. CRC Press, FL.

Ping, J.L., C.J. Green, K.F. Bronson, R.E. Zartman, and A. Doermann. 2005. Delineating potential management zones for cotton based on yields and soil properties. Soil Science 170:371-385.

Plant, R.E. 2001. Site-specific management: the application of information technology to crop production. Computers and Electronics in Agriculture 30:9-29.

Qin, C., A.X. Zhu, T. Pei, B. Li, C. Zhou, and L. Yang. 2007. An adaptive approach to selecting a flow-partition exponent for a multiple-flow-direction algorithm. International Journal of Geographical Information Science 21:443-458.

Quinn, P., K. Beven, P. Chevallier, and O. Planchon. 1991. The Prediction of Hillslope Flow Paths for Distributed Hydrological Modeling Using Digital Terrain Models. Hydrological Processes 5:59-79.

Rains, G.C., C.D. Perry, and G. Vellidis. 2005. Adaptation and testing of the Agleader cotton yield sensor on a peanut combine. Applied Engineering in Agriculture 21:979-983.

Raper, R.L., D.W. Reeves, J.N. Shaw, E. van Santen, and P.L. Mask. 2007. Benefits of site-specific subsoiling for cotton production in Coastal Plain soils. Soil and Tillage Research 96:174-181.

Reuter, H.I., A. Giebel, and O. Wendroth. 2005. Can landform stratification improve our understanding of crop yield variability? Precision Agriculture:521-537.

Reyniers, M. 2003. Precision farming techniques to support grain crop production. PhD thesis. Faculty of Agricultural and Applied Biological Sciences, Katholieke Universiteit Leuven, Leuven.

Reyniers, M., K. Maertens, E. Vrindts, and J. De Baerdemaeker. 2006. Yield variability related to landscape properties of a loamy soil in central Belgium. Soil & Tillage Research 88:262-273.

Robert, P. 1993. Characterization of soil conditions at the field level for soil specific management. Geoderma 60:57-72.

Robert, P.C. 2002. Precision agriculture: a challenge for crop nutrition management. Plant and Soil 247:143-149.

Robertson, M., B. Isbister, I. Maling, Y. Oliver, M. Wong, M. Adams, B. Bowden, and P. Tozer. 2007. Opportunities and constraints for managing within-field spatial variability in Western Australian grain production. Field Crops Research 104:60-67.

Robinson, D.A., I. Lebron, S.M. Lesch, and P. Shouse. 2004. Minimizing drift in electrical conductivity measurements in high temperature environments using the EM-38. Soil Science Society of America Journal 68:339-345.

Rossiter, D.G. 1996. A theoretical framework for land evaluation. Geoderma 72:165-190.

Rossiter, D.G. 2005. Digital soil mapping: Towards a multiple-use soil information system. Análisis Geográficos (Revista del Instituto Geográfico "Augusín Codazzi") 32:7-15.

Roubens, M. 1982. Fuzzy clustering algorithms and their cluster validity. European Journal of Operational Research 10:294-301.

Saey, T., D. Simpson, U.W.A. Vitharana, H. Vermeersch, J. Vermang, and M. Van Meirvenne. 2008. Reconstructing the paleotopography beneath the loess

cover with the aid of an electromagnetic induction sensor. Catena 74:58-64.

Scott, C.A., W.G.M. Bastiaanssen, and M.U.D. Ahmad. 2003. Mapping root zone soil moisture using remotely sensed optical imagery. Journal of Irrigation and Drainage Engineering 129:326-335.

Seelan, S.K., S. Laguette, G.M. Casady, and G.A. Seielstad. 2003. Remote sensing applications for precision agriculture: A learning community approach. Remote Sensing of Environment 88:157-169.

Shonk, J.L., L.D. Gaultney, D.G. Schulze, and G.E. Vanscoyoc. 1991. Spectroscopic sensing of soil organic-matter content. Transactions of the ASAE 34:1978-1984.

Simbahan, G.C., A. Dobermann, and J.L. Ping. 2004. Screening yield monitor data improves grain yield maps. Agronomy Journal 96:1091-1102.

Simmonds, L.P., and E.J. Burke. 1998. Estimating near-surface soil water content from passive microwave remote sensing - an application of MICRO-SWEAT. Hydrological Sciences Journal-Journal Des Sciences Hydrologiques 43:521-534.

Sirjacobs, D., B. Hanquet, F. Lebeau, and M.F. Destain. 2002. On-line soil mechanical resistance mapping and correlation with soil physical properties for precision agriculture. Soil & Tillage Research 64:231-242.

Söderström, M., A. Nyberg, C. Anderson, and B. Lindén. 2005. A key indicator for the assessment of spatially variable phosphorus fertilisation, p. 977-983, *In* J. V. Stafford, ed. Precision agriculture '05. Proceedings of the 5th European Conference on Precision Agriculture, Uppsala, Sweden, 8-11 June 2005. . Waganingen Academic.

Stafford, J.V. 2000. Implementing precision agriculture in the 21st century. Journal of Agricultural Engineering Research 76:267-275.

Stafford, J.V., B. Ambler, R.M. Lark, and J. Catt. 1996. Mapping and interpreting the yield variation in cereal crops. Computers and Electronics in Agriculture 14:101-119.

Stroh, J.C., S. Archer, J.A. Doolittle, and L. Wilding. 2001. Detection of edaphic discontinuities with ground-penetrating radar and electromagnetic induction. Landscape Ecology 16:377-390.

Sudduth, K.A., S.T. Drummond, and N.R. Kitchen. 2001. Accuracy issues in electromagnetic induction sensing of soil electrical conductivity for precision agriculture. Computers and Electronics in Agriculture 31:239-264.

Sudduth, K.A., S.T. Drummond, S.J. Birrell, and N.R. Kitchen. 1996. Analysis of spatial factors influencing crop yield, p. 129-140, *In* P. C. Robert, et al., eds. Proceedings of 3rd International Conference on Precision Agriculture, Minneapolis, USA, 23–26 June 1996.

Sui, R., J.A. Thomasson, R. Mehrle, M. Dale, C. Perry, and G. Rains. 2004. Mississippi cotton yield monitor: beta test for commercialization. Computers and Electronics in Agriculture 42:249-260.

Sullivan, D.G., J.N. Shaw, D. Rickman, P.L. Mask, and J.C. Luvall. 2005. Using remote sensing data to evaluate surface soil properties in Alabama ultisols. Soil Science 170:954-968.

Sylvester-Bradley, R., E. Lord, D.L. Sparkes, R.K. Scott, J.J.J. Wiltshire, and J. Orson. 1999. An analysis of the potential of precision farming in Northern Europe. Soil Use and Management 15:1-8.

Tang, G., W. Shi, and M. Zhao. 2002. Evaluation of the accuracy of hydrologic data derived from DEMs of different spatial resolution, p. 204-213, *In* G. J. Hunter and L. Kim, eds. Proceedings of the 5th International Symposium on Spatial Accuracy Assesment in Natural Resources and Environmental Sciences, Melbourne, Australia, 10-12 July 2002.

Taylor, J.A., and B.M. Whelan. 2008. A General Introduction to Precision Agriculture. available at www.usyd.edu.au/su/agric/acpa/GRDC/Intro.pdf, last accessed 5th February 2008.

Taylor, J.A., A.B. McBratney, and B.M. Whelan. 2007. Establishing management classes for broadacre agricultural production. Agronomy Journal 99:1366-1376.

Taylor, J.C., G.A. Wood, R. Earl, and R.J. Godwin. 2003. Soil factors and their influence on within-field crop variability, part II: Spatial analysis and determination of management zones. Biosystems Engineering 84:441-453.

Thompson, A.L., C.J. Gantzer, and S.H. Anderson. 1991. Topsoil Depth, Fertility, Water Management, and Weather Influences on Yield. Soil Science Society of America Journal 55:1085-1091.

Thompson, J.A., E.M. Pena-Yewtukhiw, and J.H. Grove. 2006. Soil-landscape modeling across a physiographic region: Topographic patterns and model transportability. Geoderma 133:57-70.

Thorp, K.R., W.D. Batchelor, J.O. Paz, A.L. Kaleita, and K.C. DeJonge. 2007. Using cross-validation to evaluate CERES-Maize yield simulations within a decision support system for precision agriculture. Transactions of the ASABE 50:1467-1479.

Triantafilis, J., A.I. Huckel, and I.O.A. Odeh. 2001. Comparison of statistical prediction methods for estimating field-scale clay content using different combinations of ancillary variables. Soil Science 166:415-427.

Van Genuchten, M.T. 1980. A Closed-Form Equation for Predicting the Hydraulic Conductivity of Unsaturated Soils. Soil Science Society of America Journal 44:892-898.

Van Meirvenne, M. 1998. Predictive quality of the Belgian soil survey information. Pedologie 5:71-74.

Van Meirvenne, M. 2006. Soil inventory in transition: from too few to too many geo-data?, p. 142-144, *In* A. Hartemink, ed. The Future of Soil Science. IUSS, Wageningen.

Van Meirvenne, M., and G. Hofman. 1989. Spatial variability of soil texture in a polder area. II. Cokriging. Pedologie 39:209-226.

Van Meirvenne, M., G. Hofman, J. Van Hove, and M. Van Ruymbeke. 1990. A continuous spatial characterization of textural fractions and CaCO3 content of the topsoil of the polder region of NorthWest East-Flanders, Belgium. Soil Science 150:710-716.

Van Meirvenne, M., K. Scheldeman, G. Baert, and G. Hofman. 1994. Quantification of soil textural fractions of Bas-Zaire using soil map polygons and or point observations. Geoderma 62:69-82.

Vauclin, M., S.R. Vieira, G. Vachaud, and D.R. Nielsen. 1983. The Use of Cokriging with Limited Field Soil Observations. Soil Science Society of America Journal 47:175-184.

Vaughan, P.J., S.M. Lesch, D.L. Corwin, and D.G. Cone. 1995. Water-Content Effect on Soil-Salinity Prediction - a Geostatistical Study Using Cokriging. Soil Science Society of America Journal 59:1146-1156.

Viscarra Rossel, R.A., H.J. Taylor, and A.B. McBratney. 2007. Geophysical tools and digital elevation models: Tools for understanding crop yield and soil variability. European Journal of Soil Science 58:343-353.

Viscarra Rossel, R.A., D.J.J. Walvoort, A.B. McBratney, L.J. Janik, and J.O. Skjemstad. 2006. Visible, near infrared, mid infrared or combined diffuse reflectance spectroscopy for simultaneous assessment of various soil properties. Geoderma 131:59-75.

Visschers, R., P.A. Finke, and J.J. de Gruijter. 2007. A soil sampling program for the Netherlands. Geoderma 139:60-72.

Vitharana, U.W.A., M. Van Meirvenne, L. Cockx, and J. Bourgeois. 2006. Identifying potential management zones in a layered soil using several sources of ancillary information. Soil Use and Management 22:405-413.

Voltz, M., and R. Webster. 1990. A Comparison of Kriging, Cubic-Splines and Classification for Predicting Soil Properties from Sample Information. Journal of Soil Science 41:473-490.

Vrindts, E., A.M. Mouazen, M. Reyniers, K. Maertens, M.R. Maleki, H. Ramon, and J. De Baerdemaeker. 2005. Management zones based on correlation between soil compaction, yield and crop data. Biosystems Engineering 92:419-428.

Wackernagel, H. 1995. Multivariate geostatistics: An introduction with applications. Springer, Berlin.

Waine, T.W. 1999. Non invasive soil property measurement for precision farming. EngD Thesis. Cranfield University, Cranfield.

Walkley, A., and I.A. Black. 1934. An examination of the Degtjareff method for determining organic carbon in soils: Effect of variations in digestion conditions and of inorganic soil constituents. Soil Science 63:251-263.

Wang, D., T. Prato, Z. Qiu, N.R. Kitchen, and K.A. Sudduth. 2003. Economic and environmental evaluation of variable rate nitrogen and lime application for claypan soil fields. Precision Agriculture 4:35-52.

Webster, R., and P.H.T. Beckett. 1968. Quality and usefulness of soil maps. Nature 219:680-682.

Webster, R., and M.A. Oliver. 1990. Statistical methods in soil and land resource survey. Oxford University Press, NY.

Webster, R., and M.A. Oliver. 1992. Sample adequately to estimate variograms of soil properties. Journal of Soil Science 43:177-192.

Webster, R., and M.A. Oliver. 2001. Geostatistics for environmental scientists John Wiley and Sons, Chichester.

Weller, U., M. Zipprich, M. Sommer, W.Z. Castell, and M. Wehrhan. 2007. Mapping clay content across boundaries at the landscape scale with electromagnetic induction. Soil Science Society of America Journal 71:1740-1747.

White, R.E. 1997. Principles and practice of soil science. 3 ed. Black Science, University Press, Cambridge.

Whitley, K.M., J.R. Davenport, and S.R. Manley. 2000. Difference in nitrate leaching under variable and conventional nitrogen fertilizer management in irrigated potato systems Proceedings of 5th International Conference on Precision Agriculture (CD-ROM), Bloomington, MN, USA 2000.

Williams, B.G., and D. Hoey. 1987. The Use of Electromagnetic Induction to Detect the Spatial Variability of the Salt and Clay Contents of Soils. Australian Journal of Soil Research 25:21-27.

Wilson, J.P., and J.C. Gallant. 2000. Digtal terrain analysis, p. 1-27, *In* J. P. Wilson and J. C. Gallant, eds. Terrain analysis: principles and applications. John Wiley & Sons, Inc. NY.

Wollenhaupt, N.C., D.J. Mulla, and C.A.G. Crawford. 1997. Soil sampling and interpolation techniques for mapping spatial variability of soil properties, p. 19-53, *In* F. J. Pierce and E. J. Sadler, eds. The state of site-specific management for agriculture. ASA,CSSA and SSSA, Madison WI, USA.

Wolock, D.M., and G.J. Mccabe. 1995. Comparison of single and multiple flow direction algorithms for computing topographic parameters in Topmodel. Water Resources Research 31:1315-1324.

Wong, M.T.F., S. Asseng, and H. Zhang. 2005. Precision agriculture improves efficiency of nitrogen use and minimizes its leaching at within-field to farm scale, p. 969-976, *In* J. V. Stafford, ed. Precision agriculture '05. Proceedings of the 5th European Conference on Precision Agriculture, Uppsala, Sweden, 8-11 June 2005. Waganingen Academic.

World_Resources_Institute. 1998. World resources: A guide to the global environment. Oxford University Press, New York, USA.

Yates, F. 1981. Sampling methods for censuses and surveys. 3 ed. Charles Griffin & Co., London.

Zadeh, L.A. 1965. Fuzzy sets. Information and Control 8:338-353.

Zevenbergen, L.W., and C.R. Thorne. 1987. Quantitative analysis of land surface topography. Earth Surface Processes and Landforms 12:47-56.

Zhai, Y.S., J.A. Thomasson, J.E. Boggess, and R.X. Sui. 2006. Soil texture classification with artificial neural networks operating on remote sensing data. Computers and Electronics in Agriculture 54:53-68.

Zhang, N.Q., M.H. Wang, and N. Wang. 2002. Precision agriculture - a worldwide overview. Computers and Electronics in Agriculture 36:113-132.

Curriculum Vitae

Personal Data:

Name	Wellewatte Arachchige Udayakantha Vitharana
Address	No 28, Andangama, Pearadeniya, Sri Lanka.
Phone	+94812384356
Email	u.vitharana@live.com
Place of Birth	Kandy (Sri Lanka)
Date of Birth	February 13, 1971
Nationality	Sri Lankan

Education:

2002 – 2004	M.Sc. in Physical Land Resources Ghent University, Belgium. Thesis title: Evaluation of Pedometrical Techniques to Delineate Potential Management Zones at Within-field Scale Promoter: Prof. dr. ir. Marc Van Meirvenne
1994 – 1999	B.Sc. in Agriculture University of Peradeniya, Sri Lanka. Thesis title: In-vitro Mutagenesis of *Hosta sieboldiana* Promoter: Prof. S. E. Peiris

Professional Experience:

2001 – to date	Lecturer Department of Soil Science University of Peradeniya, Peradeniya, Sri Lanka.
1999 – 2001	Plantation Monitoring Officer Ministry of Plantation Industries, Vauxhall Lane, Colombo 02.

Scientific Publications:

Publications in international journals[2] with peer review

Vitharana, U.W.A., T. Saey, L. Cockx, D. Simpson, H. Vermeersch, and M. Van Meirvenne. 2008. Upgrading a 1/20,000 soil map with an apparent electrical conductivity survey. Geoderma 148:107-112.

Vitharana, U.W.A., M. Van Meirvenne, D. Simpson, L. Cockx, and G. Hofman. 2008. Agronomic consequences of potential management zones delineated on the basis of EM38DD measurements. Near Surface Geophysics 6:289-296.

Vitharana, U.W.A., M. Van Meirvenne, D. Simpson, L. Cockx, and J. De Baerdemaeker. 2008. Key soil and topographic properties to delineate potential management classes for precision agriculture in the European loess area. Geoderma 143:206-215.

Cockx, L., M. Van Meirvenne, U.W.A. Vitharana, L.P.C. Verbeke, and F.M.B. Van Coillie. 2008. A neural network approach to clay prediction using an EMI-based soil sensor. Soil Science Society of America Journal (submitted).

Saey, T., D. Simpson, U.W.A. Vitharana, H. Vermeersch, J. Vermang, and M. Van Meirvenne. 2008. Reconstructing the paleotopography beneath the loess cover with the aid of an electromagnetic induction sensor. Catena 74:58-64.

Balasooriya, B.L.W.K., R. Samson, F. Mbikwa, U.W.A. Vitharana, P. Boeckx, and M. Van Meirvenne. 2008. Biomonitoring of urban habitat quality by anatomical and chemical leaf characteristics. Environmental and Experimental Botany (in press).

Vitharana, U.W.A., M. Van Meirvenne, L. Cockx, and J. Bourgeois. 2006. Identifying potential management zones in a layered soil using multiple sources of ancillary information. Soil Use and Management 22:405-413.

Publications in national journals with peer review

Vitharana, U.W.A., and S.E. Peiris. 2002. An investigation of in vitro mutagenesis of *Hosta sieboldiana*. Sri Lankan Journal of Agricultural Science 39:94-101.

[2] All journals belong to A1 category according the classification of scientific journals by the Ghent University, Belgium.

Conference and workshop Proceedings

Vitharana, U.W.A., Van Meirvenne, M., Amakor, X.N.C, Saey, T. and Vermeersch, H. 2008. Use of proximal soil sensing to improve the thematic accuracy of a soil-polygon map. Geophysical Research Abstracts, Vol.10, file: EGU2008-A-09214. EGU General Assembly 13-18th April 2008, Vienna, Austria (on CD).

Saey, T., Simpson, D., Vitharana, U.W.A., Vermeersch, H., Vermang, J., Van Meirvenne, M. 2008. Reconstructing the paleotopography at the beginning of the Weichselian glacial stage using electromagnetic induction. Geophysical Research Abstracts, Vol.10, file: EGU2008-A-00121. EGU General Assembly 13-18th April 2008, Vienna, Austria (on CD).

Cockx L., Van Meirvenne M. and Vitharana U.W.A. 2008. Extracting topsoil information from high resolution EM38DD sensor data using contexual neural networks. In: R. Viscarra Rossel, First Global Workshop on High Resolution Digital Soil Sensing & Mapping, 5-8 February, 2008, Sydney, Australia, 8 pgs.

Vitharana, U.W.A., M. Van Meirvenne, X.N.C. Amakor, T. Saey and D. Simpson. 2007. Potency of proximal soil sensing to upgrade the soil map of Belgium: test case UGent experimental farm at Melle. Thematic Day 2007: Soil resources in Belgium - Current and future issues Soil Science Society of Belgium, 6th December 2007. Brussels, p. 10.

Vitharana U.W.A., M. Van Meirvenne, X.N.C. Amakor, D. Simpson and L. Cockx. 2007. Evaluating two scales of polygon soil maps and an electrical conductivity Survey in Characterizing Within-field Soil Textural Variability. Pedometrics 2007, 27-30 August 2007. Tübingen, Germany, p.41.

Van Meirvenne M., Vitharana U.W.A. and Cockx L. 2006. Developments in soil sampling and proximal sensing with applications in precision agriculture. In: Langouche D. & Van Ranst E. (Eds.) New Waves in Physical Land Resources, Gent 3-9 September 2006, pp. 226-227, ISBN: 9789076769950.

Vitharana U.W.A., Van Meirvenne M., Simpson D., Cockx L. and De Baerdemaeker J. 2006. Influence of the topography on the within-field soil variability in the Loess region in Belgium. In: 2nd Global Workshop on Digital Soil Mapping: book of abstracts, Ed.: Mendonça-Santos M. et al., Rio de Janeiro, Brazil, 4-7 July 2006, p. 56. ISBN: 85-85864-21 (on CD).

Simpson D., Van Meirvenne M., De Baerdemaeker J., Vitharana U,W.A. and Cockx L. 2006. Soil-crop-landscape relationships within an agricultural field in the loess region of Belgium. Day of the Young Soil Scientists, Belgian Soil Science Society, 22 February 2006. Brussels, p. 10.

Vitharana U.W.A., Simpson D., Van Meirvenne M. and Cockx L. 2005. Evaluation of multiple ancillary information to support potential management zones delineation: case study in the loess region of Belgium. In: "Monitoring space-time dynamics of soil chemical properties to improve soil management and environmental quality", edited by: L. Cockx et al. Proceedings of a workshop held in Ghent (8-9 December 2005) in the framework of a Bilateral Co-operation between Flanders and Hungary. pp. 57-69. ISBN: 90-5989-097-3

Van Meirvenne M., Cockx L. and Vitharana U.W.A. 2005. Pedometrics in transition: from too few to too many data? Pedometrics 2005: Frontiers in Pedometrics, Naples, USA. 12-14 September 2005, Abstract book p. 81-82.

Vitharana W.A.U., Van Meirvenne M. and Cockx L. 2005. Using secondary information sources to improve the within-field soil textural mapping in a layered alluvial soil. Day of the Young Soil Scientists, Belgian Soil Science Society, 23 February 2005. Brussels, p. 5.

Vitharana W.A.U., Van Meirvenne M. and Cockx L. 2005. Using secondary information sources to improve the within-field soil textural mapping in a layered alluvial soil. In: Stafford J. (Ed.), Precision Agriculture '05. Wageningen Academic Publishers, pp. 425-432. ISBN: 9076998698.

Oral Presentations

Vitharana, U.W.A., Van Meirvenne, M., Amakor, X.N.C, Saey, T. and Vermeersch, H. 2008. Use of proximal soil sensing to improve the thematic accuracy of a soil-polygon map. EGU General Assembly 13-18th April 2008, Vienna, Austria.

Vitharana, U.W.A., M. Van Meirvenne, X.N.C. Amakor, T. Saey and D. Simpson. 2007. Potency of proximal soil sensing to upgrade the soil map of Belgium: test case UGent experimental farm at Melle. Thematic Day 2007: Soil resources in Belgium - Current and future issues Soil Science Society of Belgium, 6th December 2007. Brussels, Belgium.

Vitharana U.W.A., M. Van Meirvenne, X.N.C. Amakor, D. Simpson and L. Cockx. 2007. Evaluating two scales of polygon soil maps and an electrical conductivity Survey in Characterizing Within-field Soil Textural Variability. Pedometrics 2007, 27-30 August 2007. Tübingen, Germany.

Vitharana U.W.A., Van Meirvenne M., Simpson D., Cockx L. and De Baerdemaeker J. 2006. Influence of the topography on the within-field soil variability in the Loess region in Belgium. 2nd Global Workshop on Digital Soil Mapping, 4-7 July 2006: Rio de Janeiro, Brazil.

Vitharana U.W.A., Simpson D., Van Meirvenne M. and Cockx L. 2005. Evaluation of multiple ancillary information to support potential management zones delineation: case study in the loess region of Belgium. Workshop on monitoring space-time dynamics of soil chemical properties to improve soil management and environmental quality, 8-9 December 2005, Ghent University, Ghent, Belgium.

Vitharana W.A.U., Van Meirvenne M. and Cockx L. 2005. Using secondary information sources to improve the within-field soil textural mapping in a layered alluvial soil. Day of the Young Soil Scientists, Belgian Soil Science Society, 23 February 2005. Brussels, Belgium.

Vitharana W.A.U., Van Meirvenne M. and Cockx L. 2005. Using secondary information sources to improve the within-field soil textural mapping in a

layered alluvial soil. 5th European Conference on Precision Agriculture, 8-11 June 2005, Uppsala, Sweden.

December 11, 2008